

Development and application of modern pure shift NMR techniques and improved HSQC/HSQMBC experiments

Laura Castañar Acedo

Doctoral Thesis
Ph.D. in Chemistry
Chemistry Department
Faculty of Sciences

2015

Supervisors: Teodor Parella Coll Albert Virgili Moya



Chemistry Department Faculty of Sciences

Memòria presentada per as _l	pirar al Grau de Doctor per	Laura Castañar Acedo
Vist i plau,		
Dr. Teodor Parella Coll	Dr. Albert Virgili Moya	Laura Castañar Acedo
Bellaterra, 21 de Mayo de 20	015	

TABLE OF CONTENTS

ACKNOWLEDGEMENIS	IX
LIST OF ACRONYMS	XI
THESIS OUTLINE	XIII
. INTRODUCTION	
1. INTRODUCTION	1
1.1. Pure shift NMR spectroscopy	1
1.1.1. Homodecoupling NMR building blocks	3
1.1.1.1. BIRD-based elements	6
1.1.1.2. Frequency-selective pulses	8
1.1.1.3. Spatial encoding	9
1.1.2. Homodecoupling acquisition modes	13
1.1.2.1. Historical review	13
1.1.2.2. Pseudo-2D Zangger-Sterk experiment	15
1.1.2.3. Real-time ZS experiment	17
1.1.3. Homodecoupled NMR experiments and applications	20
1.2. 2D HSQC and HSQMBC NMR experiments	21
1.2.1. The HSQC experiment	22
1.2.1.1. Basic HSQC pulse scheme	22
1.2.1.2. HSQC with PEP: improved sensitivity	29
1.2.1.3. Measurement of heteronuclear ${}^{1}\mathcal{L}_{CH}/{}^{1}\mathcal{T}_{CH}$ coupling constants	31
1.2.2. The HSQMBC experiment	38
1.2.2.1. Basic HSQMBC pulse scheme	39
1.2.2.2. Improvements in HSQMBC experiments	41
2. OBJECTIVES	49

3. RESULTS AND DISCUSSION	51
Publication 1 Simultaneous multi-slice excitation in spatially encode experiments	53 d NMR
■ Introduction ■ Original Research Paper	55 57
Publication 2	87
Full sensitivity and enhanced resolution in homodecompand-selective NMR experiments	oupled
IntroductionOriginal Research Paper	89 91
Publication 3	103
Measurement of T_1/T_2 relaxation times in overlapped r from homodecoupled ¹ H singlet signals	regions
IntroductionOriginal Research Paper	105 107
Publication 4	129
Enantiodifferentiation through frequency-selective pur 1H nuclear magnetic resonance spectroscopy	re shift
IntroductionOriginal Research Paper	131 133
Publication 5	147
Simultaneous ¹ H and ¹³ C NMR enantiodifferentiation highly-resolved pure shift HSQC spectra	n from
IntroductionOriginal Research Paper	149 151
Publication 6	171
Implementing homo- and heterodecoupling in region-selective HSQMBC experiments	
IntroductionOriginal Research Paper	173 175

	Publication 7	183
	Disentangling complex mixtures of compounds with near-identical ¹ H and ¹³ C NMR spectra using pure shift NMR spectroscopy	
	Introduction	185
	Original Research Paper	187
	Publication 8	215
	Pure in-phase heteronuclear correlation NMR experiments	
	Introduction	217
	■ Original Research Paper	219
	Publication 9	255
	Suppression of phase and amplitude J _{HH} modulations in HSQC experiments	
	Introduction	257
	Original Research Paper	259
	Publication 10	273
	Recent advances in small molecule NMR: improved HSQC and HSQMBC experiments	
	Introduction	275
	Original Research Paper	277
4.	SUMMARY AND CONCLUSIONS	347
5.	APPENDIX	351
	Publication 11	353
	P.E. HSQMBC: Simultaneous measurement of proton-proton and proton-carbon coupling constants	
	Introduction	355
	Original Research Paper	357

Publication 12	363
Straightforward measurement of individual ${}^1\mathcal{L}_{CH}$ and ${}^2\mathcal{L}_{HH}$ in diastereotopic CH_2 groups	
Introduction	365
Original Research Paper	367
Publication 13	385
Broadband ¹ H homodecoupled NMR experiments: Recent developments, methods and applications	
Introduction	387
Original Research Paper	389
PULSE PROGRAMS AND DATA SET EXAMPLES	417

ACKNOWLEDGMENTS

I would like to thank the financial support for this research provided by the following institutions:

- Universitat Autònoma de Barcelona and Chemistry Department for giving me a PIF (Personal Investigador en Formació) grand to carry out this doctoral thesis.
- Project: "Nuevas metodologías en Resonancia Magnética Nuclear (part IV)" CTQ2012-32436. MINECO, IP: Dr. Teodor Parella Coll

I would also like to thanks for all the grants received from GERMN (*Grupo Especializado de Resonancia Magnética Nuclear*) to attend to different scientific meetings and courses along this doctoral thesis.

En primer lugar quiero dar las gracias a mis directores de tesis, Albert y Teo. Muchas gracias por la confianza depositada, por vuestra ayuda, consejos, entrega y dedicación. No me puedo sentir más afortunada. Recuerdo perfectamente el día que vine a hacer la entrevista. Llegué nerviosa, asustada y con mil preguntas en mi cabeza pero tenía una cosa clara: quería aprender RMN. Tras casi cuatro años con vosotros estoy convencida de que aquel día tomé una de las mejores decisiones de mi vida. He tenido la gran suerte de aprender de los mejores, de empaparme no sólo de vuestros conocimientos científicos sino también de vuestra manera de hacer las cosas, de trabajar y de organizaros en el día a día. Todo el trabajo realizado habría sido imposible sin vosotros y por eso todos los reconocimientos recibidos en los últimos meses no son míos, son nuestros. Albert, gracias por tantos buenos momentos, por esas increíbles paellas de grupo (a las que me apuntaré cuando ya me haya ido), por los abrazos y achuchones recibidos y por ayudarme cuando lo he necesitado. Teo, gracias por esas interminables y divertidas conversaciones de la vida, la ciencia, el futbol, la política y la "historia natural". Gracias por todos los buenos momentos vividos, los consejos dados y las risas compartidas.

En segundo lugar he de hacer una mención especial a una persona que ha sido indispensable para mí en estos cuatro años: Miquel. Sin él mi nivel de desesperación con todo lo que tiene que ver con la electrónica/tecnología habría sido increíble. Seguramente habría quemado la sonda, apaleado la IPSO o tirado el ordenador por la ventana. Pero no, porque ahí está Miquel siempre para ayudarme. Mil millones de gracias Miquel por toda la ayuda, por todo el tiempo dedicado y la paciencia invertida. Y como no mencionar a alguien realmente importante para mí durante todo este tiempo...Pau. Tú fuiste la persona con la que di mis primeros pasos en este mundo de la RMN, la que me enseñó cómo funcionaba todo y como arreglarlo cuando no funcionaba. Me has ayudado con cada problema, me has respondido a cada una de las mil preguntas hechas y hasta hemos aprendido juntos! Pero nuestra relación ha ido más allá de los imanes, te has convertido en un gran amigo que espero que forme parte siempre de mi vida.

Muchas gracias también a todos los compañeros del Servei y del laboratorio: Eva, Silvia, Miriam, Josep, Albert, Eduard, Nuria, André, Ana, Marta y Josep. Gracias a todos por haberme recibido con los brazos abiertos, por vuestra ayuda y por hacer que el día a día sea más ameno. Muchos de vosotros os habéis convertido en algo más que compañeros de trabajo y sé que aquí tendré unos amigos para toda la vida. También me gustaría dar las gracias a todos los doctorandos del Departament con los que he compartido grandes momentos, fiestas, viernes de birras, calçotadas y barbacoas varias. Gracias Joseju, Silvia, Cris, Marc, Carme, Sergio, Asli, Rubén, Roser, Mery, Marc, Julen. Y como no, he de hacer una mención especial a todos aquellos con los que he compartido mi vida en estos últimos cuatro años: Laurita, Pau, Joseju, Josep, Carol, Alba, Albert, Couso, Silvia, Katia y Alba. Mil gracias por haber hecho que me sienta en Barcelona como en casa, os habéis convertido en mi pequeña familia catalana!

Y a ti, Diego, mi inseparable compañero de aventuras, mi otra mitad. Mil millones de gracias por tu apoyo incondicional, por tu cariño, por tu paciencia y comprensión. Mil gracias por embarcarte conmigo en esta aventura y en las que vendrán para que pueda cumplir una parte de mis sueños. Sin ti nada de esto habría sido posible, sin ti nada de esto tendría sentido. Mil millones de gracias mon amour!

Finalmente me gustaría darle las gracias a las personas más importantes de mi vida: mis abuelos, mis padres y mi hermana. En los últimos años cientos de kilómetros me separan de vosotros, pero a pesar de la distancia siempre habéis estado a mi lado y siempre me habéis apoyado en todos mis proyectos e ilusiones. Por eso, todos los éxitos que tenga en la vida sin duda serán también vuestros porque sin vosotros habrían sido imposibles!

LIST OF ACRONYMS

AP Anti-Phase

ASAP Acceleration by Sharing Adjacent Polarization

BASHD BAnd-Selective Homonuclear Decoupling

BIRD Bllinear Rotation Decoupling

CLAP **CL**ean **A**nti-**P**hase

CLIP CLean In-Phase

COSY COrrelation SpectroscopY

CPD Composite Pulses Decoupling

CPMG Carr-Purcell-Maiboom-Gill pulse sequence

CSAs Chiral Solvating Agents

CTP Coherence Transfer Pathway

DIPSI Decoupling In Presence of Scalar Interactions

DOSY Diffusion-OrderedSpectroscopY

DQ Double Quantum

DQC Double Quantum Coherence

E/A Echo/Anti-echo

FID Free Induction Decay

HMBC Heteronuclear MultipleBond Correlation

HMQC Heteronuclear Multiple Quantum Correlation

HOBB **HO**modecoupled **B**road**B**and

HOBS **HO**modecoupled **B**and-**S**elective

HSQC Heteronuclear Single Quantum Correlation

HSQMBC Heteronuclear Single Quantum Multiple-Bond Correlation

INEPT Insensitive Nuclei Enhanced by Polarization Transfer

IP In-Phase

IPAP In-Phase Anti-Phase

IR Inversion Recovery

ME **M**ultiplicity-**E**dited

MQ Multiple Quantum

MQC Multiple QuantumCoherence

MRI Magnetic Resonance Imaging

NMR Nuclear Magnetic Resonance

NOESY Nuclear Overhauser Effect Spectroscopy

NUS Non-Uniform Sampling

PEP Preservation of Equivalent Pathways

PFG Pulse Field Gradient

PO **Product Operators**

PROJECT Periodic Refocusing Of JEvolution by Coherence Transfer

PS Pure Shift

PSYCHE Pure Shift Yielded by CHirp Excitation

RE-BURP REfocusing Band-selective Uniform-Response Pure-phase

RESET Reducing nuclEar Spin multiplicitiEs to singuleTs

RDC Residual Dipolar Coupling

ROESY Rotating-frame Overhauser Effect SpectroscopY

SA **S**pectral **A**liasing

SAPS Spectral Aliased Pure Shift

SNR Signal to Noise Ratio

SPFGE Single PulsedField Gradient Echo

SQ Single Quantum

SQC Single Quantum Coherence

SS Slice Selective

TOCSY TOtal Correlation SpectroscopY

ZQ Zero Quantum

ZQC Zero Quantum Coherence

ZQF Zero Quantum Filter

ZS **Z**angger-**S**terk

THESIS OUTLINE

This thesis is presented as a compendium of publications. All the results here exposed have already been evaluated and analyzed by expert researchers in the fields of the *Nuclear Magnetic Resonance* (NMR) spectroscopy and Chemistry, and published in prestigious peer-reviewed international scientific journals. The complete list is:

1. Title: Simultaneous multi-slice excitation in spatially encoded NMR experiments.

Authors: L. Castañar, P. Nolis, A. Virgili and T. Parella.

Reference: Chem. Eur. J., 2013, 19, 15472-15475.

DOI: 10.1002/chem.201303272

2. Title: Full sensitivity and enhanced resolution in homodecoupled band-selective NMR experiments.

Authors: L. Castañar, P. Nolis, A. Virgili and T. Parella.

Reference: Chem. Eur. J., 2013, 19, 17283-17286.

DOI: 10.1002/chem.201303235

3. Title: Measurement of T_1/T_2 relaxation times in overlapped regions from homodecoupled ¹H singlet signals.

Authors: L. Castañar, P. Nolis, A. Virgili and T. Parella.

Reference: J. Magn. Reson., 2014, 244, 30-35.

DOI: 10.1016/j.jmr.2014.04.003

4. Title: Enantiodifferentiation through frequency-selective pure-shift ¹H Nuclear Magnetic Resonance spectroscopy.

Authors: L. Castañar, M. Pérez-Trujillo, P. Nolis, E. Monteagudo, A. Virgili and T. Parella.

Reference: ChemPhysChem., 2014, 15, 854-857.

DOI: 10.1002/cphc.201301130

5. Title: Simultaneous ¹H and ¹³C NMR enantiodifferentiation from highly-resolved pure shift HSQC spectra.

Authors: M. Pérez-Trujillo, L. Castañar, E. Monteagudo, L. T. Kuhn, P. Nolis, A. Virgili,

R. T. Williamson and T. Parella.

Reference: Chem. Comm., 2014, 50, 10214-10217.

DOI: 10.1039/C4CC04077E

6. Title: Implementing homo- and heterodecoupling in region-selective HSQMBC experiments.

Authors: L. Castañar, J. Saurí, P. Nolis, A. Virgili and T. Parella.

Reference: J. Magn. Reson., 2014, 238, 63-69.

DOI: 10.1016/j.jmr.2013.10.022

7. Title: Disentangling complex mixtures of compounds with near-identical ¹H and ¹³C NMR spectra using pure shift NMR spectroscopy.

Authors: L. Castañar, R. Roldán, P. Clapés, A. Virgili and T. Parella.

Reference: Chem. Eur. J., 2015, 21, 7682-7685.

DOI: 10.1002/chem.201500521

8. Title: Pure in-phase heteronuclear correlation NMR experiments.

Authors: L. Castañar, J. Saurí, R. T. Williamson, A. Virgili and T. Parella.

Reference: Angew. Chem. Intl. Ed., 2014, 53, 8379-8382.

DOI: 10.1002/anie.201404136

9. Title: Suppression of phase and amplitude J_{HH} modulations in HSQC experiments.

Authors: L. Castañar, E. Sistaré, A. Virgili, R. T. Williamson and T. Parella.

Reference: Magn. Reson. Chem., 2015, 53, 115-119.

DOI: <u>10.1002/mrc.4149</u>

10. Title: Recent advances in small molecule NMR: Improved HSQC and HSQMBC experiments.

Authors: L. Castañar and T. Parella.

Reference: Annu. Rep. NMR Spectrosc., 2015, 84, 163-232.

DOI: <u>10.1016/bs.arnmr.2014.10.004</u>

The research work carried out during this doctorate (October 2012 – May 2015) is framed within the NMR field, more specifically in the design of new NMR methodologies. The starting point was the prior knowledge and experience of our research group in the development of modern NMR methodologies, with special emphasis in methods to measure homo- and heteronuclear coupling constant through HSQC and HSQMBC-type experiments. One of the two parts of the present thesis is framed in this line of research and the other part is centered on the design and application of new pure shift NMR methodologies, which is a new research topic started in our group during this Ph.D.

This thesis has been organized in five sections:

- 1. **Introduction**. This section contains a brief general explanation of the most important NMR concepts needed to understand the work carried out.
- 2. Objectives. Here the main specific goals that led to the development of this thesis are described.
- 3. Results and Discussion. This section is the main part of the thesis. Here, all the new developed NMR methods and their applications are presented as Original Research Papers (Publications). Since every published paper has gone through a peer-review process by NMR experts, not much attention is devoted to the discussion of the results beyond discussed in each publication. Nevertheless, a little introduction is presented for each one of published papers.
- **4. Summary and Conclusions**. Finally, a brief summary with the main conclusions extracted from the experimental results is exposed.
- 5. Appendix. Additionally, some results obtained during this doctoral thesis which have not could be used as Publication are included in this last section.

1. INTRODUCTION

1.1. Pure shift NMR spectroscopy¹

Nuclear Magnetic Resonance (NMR) spectroscopy is one of the most powerful tools for determining structural, dynamics, chemical and physical properties of small and medium-size molecules under a great variety of sample conditions. The most significant aspects that determine the quality of NMR spectra are sensitivity and spectral resolution. Advances in sensitivity have been occurring over the years by a multitude of different techniques intended to improve NMR data acquisition and processing. The development and the improvements in NMR instrumentation have also played a key role to enhance sensitivity, with a particular emphasis in the technical design of cryogenically cooled probes or higher magnetic fields. On the other hand, spectral resolution is also improved inherently in higher magnetic fields, which disperse the chemical shifts over a wider frequency range, although the effects of signal overlap can still be a limiting factor when analyzing complex NMR spectra. The continuous development of new pulse sequences and the improvement of the existing ones have been another very important factor to understand the enormous potential of the NMR spectroscopy. Additionally, the incorporation of multiple-frequency dimensions achieves a tremendous qualitative and quantitative leap, particularly when it comes to improving signal dispersion.

The associated benefits of decoupling through-bond interactions for the apparent simplification of scalar coupling constant splittings are easily understood when analysing a typical ¹³C spectrum, which is routinely recorded under broadband heteronuclear ¹H decoupling during data acquisition.² In a standard 1D ¹³C{¹H} spectrum, all signals appear as singlet lines providing excellent signal dispersion, allowing the knowledge of the number of signals that are present and also measuring accurate chemical shift values in a very straightforward way. In contrast, despite using high magnetic fields, 1D ¹H NMR spectra often suffer of low signal resolution and severe signal overlap due to the limited range of ¹H chemical shifts (~10-15 ppm) and also to the additional proton-proton scalar coupling (J_{HH}) splittings observed in each proton resonance. The analysis of the fine multiplet structure contains valuable structural information such as the number and the

^[1] Introduction about pure shift NMR has been adapted from the recently published review: L. Castañar, T. Parella, *Mag. Reson. Chem.*, **2015**, *53*, 399.

^[2] a) M. H. Levitt, R. Freeman, T. Frenkiel, J. Magn. Reson., 1982, 47, 328. b) A. J. Shaka, J. Keeler, T. Frenkiel, R. Freeman, J. Magn. Reson., 1983, 52, 335. c) A. J. Shaka, P. B. Barker, R. Freeman, J. Magn. Reson., 1985, 64, 547. d) E. Kupče, R. Freeman, J. Magn. Reson., 1995, 115, 273. e) R. Fu, G. Bodenhausen, Chem. Phys. Lett., 1995, 245, 415.

nature of neighbouring spins or dihedral angle constraints. However, in many cases, signal overlap hampers a definitive multiplet analysis or the accurate extraction of chemical shifts, which are also fundamentals in the analysis and interpretation of NMR spectra. On the other hand, scalar coupling constant (*J*) information can become redundant when multidimensional NMR spectra are analyzed, because only the correlation between chemical shifts is usually of interest for assignment purposes.

Signal resolution in ¹H NMR spectra could be significantly enhanced if all signals could be converted into singlets. This is the aim of broadband homodecoupled NMR techniques, also referred to as "pure shift NMR spectroscopy". The advantages of obtaining pure shift ¹H NMR spectra have been extensively recognized for years, although there is no easy and general solution to achieve this goal. Only as an example of the potential of this approach, Figure 1 shows how the simplified *J* multiplet structures achieved for all resonances in a small molecule like progesterone is a clear proof of the excellent complementarity between the homodecoupled and the standard 1D ¹H spectra. The absence of coupling splittings improves signal dispersion, facilitates and accelerates chemical shift recognition, and simplifies the analysis and assignment of complex regions, as observed for the overlap signals resonating around 1.6 and 2.0 ppm.

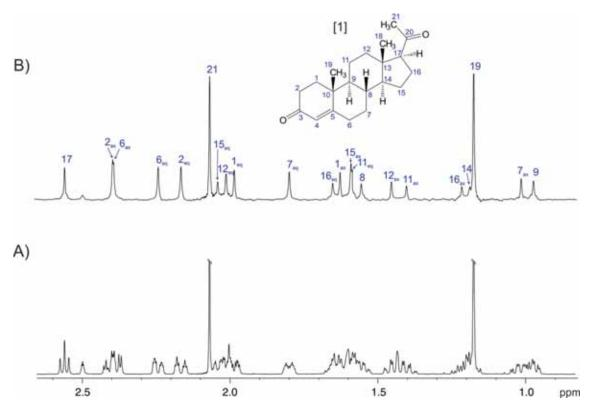


Figure 1: 600 MHz A) conventional and B) broadband homodecoupled 1D 1 H NMR spectra of the steroid progesterone [1] in DMSO-d₆. Note how all simplified singlet resonances at their chemical shift frequencies can be distinguished in the pure shift spectrum.

In the last few years, there has been a revival in the development of pure shift NMR techniques. Several strategies have been suggested being the experiments based on the original *Zangger-Sterk* (ZS) methodology³ the most widely used. This introduction aims to describe the fundamental key points for understanding the principles of modern broadband homodecoupled ¹H NMR experiements.

1.1.1. Homodecoupling NMR building blocks

The development and implementation of new homodecoupling building blocks into specific pulse schemes is nowadays an expanding area of research. Efforts are mainly concentrated in the design of methodologies that guarantee a routine use involving a simple and non-extended acquisition set-up, a standard and non-sophisticated data processing procedure, and a general applicability on a wide range of NMR experiments.

The most widely used pure shift experiments are based on the refocusing of the homonuclear coupling evolution. To achieve it, several \mathcal{L} refocused pulse sequence elements can be used in the middle of a given evolution time. These elements divide the available spins into two subsets: (i) active spins, which provide the final detected signal, and (ii) passive spins, which are decoupled but not observed. The effects of a pair of NMR elements are combined: a non-selective 180° pulse and a selective inversion element that affects only the active spins (Figure 2). Some basic selective elements that perform such specific perturbation have been proposed: (i) a $^{12}\text{C}/^{13}\text{C}$ isotopic *Bllinear Rotational Decoupling* (BIRD)⁴ module (Figure 2A), (ii) frequency- or region-selective 180° pulses (Figure 2B-D), and (iii) spatially-resolved elements consisting of a selective or adiabatic 180° pulse applied simultaneously to a weak *Pulsed Field Gradient* (PFG) (Figure 2E-H). In all these cases, the passive spins experience a 180° pulse whereas the active spins are unperturbed because they undergo an overall rotation of 360° . In practical terms, this means that chemical shift of active nuclei will not be affected and therefore it will evolve, while all homonuclear $J_{\text{Hoassive-Hactive}}$ couplings will be efficiently refocused.

^[3] K. Zangger, H. Sterk, J. Magn. Reson., 1997, 124, 486.

^[4] a) J. P. Garbow, D. P. Weitekamp, A. Pines, *Chem. Phys. Lett.*, **1982**, *93*, 504. b) D. Uhrín, T. Liptaj, K. E. Kövér, *J. Magn. Reson.*, **1993**, *101*, 41.

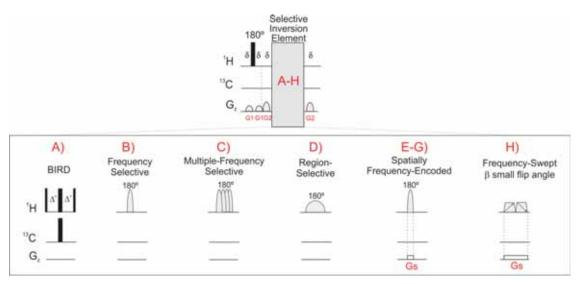


Figure 2 Basic NMR building blocks to perform homonuclear decoupling, consisting of a non-selective 180° pulse and a selective inversion element: A) BIRD^x cluster to selectively invert $^{1}\text{H}_{-}^{-13}\text{C}$ VS $^{1}\text{H}_{-}^{-12}\text{C}$ protons; B-D) frequency-selective 180° pulses designed to invert/refocus a single or specific groups of signals; E-G) slice-selective element to achieve spatial frequency-encoding along the *z*-axis thanks to the simultaneously application of an encoding $G_{\rm s}$ gradient and a single-, multiple- or region-selective 180° pulse; H) spatially-selective element using a pair of small flip angle frequency-swept adiabatic pulses jointly with an encoding $G_{\rm s}$ gradient. The use of gradients $G_{\rm 1}$ and $G_{\rm 2}$ flanking each inversion element can be optionally applied to remove improper refocusing/inversion.

This double effect on active and passive spins can be analyzed using the *Product Operator* (PO) formalism⁵. Consider the simplest situation:

- A weakly coupled spin system comprising an active spin (I_a) and a passive spin (I_p) with $J_{I_aI_p}$.
- A NMR building block consisting of " τ_1 hard 180° selective 180° τ_1 " element, where a selective 180° pulse (Figure 2B) is applied on I_a .

Initially, the active spins arrive as *In-Phase* (IP) magnetization, $-I_{ay}$, prior to τ_1 . During the first delay (τ_1) , the magnetization evolves freely under the effects of the chemical shift (Ω_a) and the homonuclear coupling with the passive spin $(J_{I_aI_p})$:

$$\begin{split} -I_{ay} &\xrightarrow{\Omega_a \tau_1} -I_{ay} \cos(\Omega_a \tau_1) + I_{ax} \sin(\Omega_a \tau_1) \xrightarrow{\pi J_{IaI_p} \tau_1} -I_{ay} \cos(\Omega_a \tau_1) \cos(\pi J_{IaI_p} \tau_1) \\ &+ 2I_{ax} I_{pz} \cos(\Omega_a \tau_1) \sin(\pi J_{IaI_p} \tau_1) \\ &+ I_{ax} \sin(\Omega_a \tau_1) \cos(\pi J_{IaI_p} \tau_1) \\ &+ 2I_{ay} I_{pz} \sin(\Omega_a \tau_1) \sin(\pi J_{IaI_p} \tau_1) \end{split}$$

Eq.1.1

^[5] O. W. Sorensen, G. W. Eich, M. H. Levitt, G. Bodenhausen, R. R. Ernst. *Prog. Nucl. Magn. Reson. Spectrosc.*, **1983**, *16*, 163.

Next, a broadband 180° pulse is applied followed by a selective 180° pulse on active spins:

$$+I_{ay}\cos(\Omega_{a}\tau_{1})\cos(\pi J_{I_{a}I_{p}}\tau_{1}) -I_{ay}\cos(\Omega_{a}\tau_{1})\cos(\pi J_{I_{a}I_{p}}\tau_{1})$$

$$-2I_{ax}I_{pz}\cos(\Omega_{a}\tau_{1})\sin(\pi J_{I_{a}I_{p}}\tau_{1}) -2I_{ax}I_{pz}\cos(\Omega_{a}\tau_{1})\sin(\pi J_{I_{a}I_{p}}\tau_{1})$$

$$+I_{ax}\sin(\Omega_{a}\tau_{1})\cos(\pi J_{I_{a}I_{p}}\tau_{1}) +I_{ax}\sin(\Omega_{a}\tau_{1})\sin(\pi J_{I_{a}I_{p}}\tau_{1})$$

$$+2I_{ay}I_{pz}\sin(\Omega_{a}\tau_{1})\sin(\pi J_{I_{a}I_{p}}\tau_{1}) -2I_{ay}I_{pz}\sin(\Omega_{a}\tau_{1})\sin(\pi J_{I_{a}I_{p}}\tau_{1})$$

Eq.1.2

Finally, the system evolves again for a time au_1 under both Ω_a and $J_{I_aI_p}$ effects:

$$-l_{ay}\cos^{2}(\Omega_{a}\tau_{1})\cos(\pi J_{lal_{p}}\tau_{1}) \\ +l_{ax}\cos(\Omega_{a}\tau_{1})\sin(\Omega_{a}\tau_{1})\cos(\pi J_{lal_{p}}\tau_{1}) \\ +l_{ax}\cos(\Omega_{a}\tau_{1})\sin(\Omega_{a}\tau_{1})\cos(\pi J_{lal_{p}}\tau_{1}) \\ -2l_{ax}J_{pz}\cos^{2}(\Omega_{a}\tau_{1})\sin(\pi J_{lal_{p}}\tau_{1}) \\ +l_{ax}\cos(\Omega_{a}\tau_{1})\sin(\Omega_{a}\tau_{1})\sin(\pi J_{lal_{p}}\tau_{1}) \\ +l_{ax}\cos(\Omega_{a}\tau_{1})\sin(\Omega_{a}\tau_{1})\sin(\Omega_{a}\tau_{1})\sin(\pi J_{lal_{p}}\tau_{1}) \\ +l_{ax}\cos(\Omega_{a}\tau_{1})\sin(\Omega_{a}\tau_{1})\cos(\Omega_{a}\tau_{1})\sin(\pi J_{lal_{p}}\tau_{1}) \\ +l_{ax}\sin(\Omega_{a}\tau_{1})\cos(\Omega_{a}\tau_{1})\cos(\pi J_{lal_{p}}\tau_{1}) \\ +l_{ax}\sin^{2}(\Omega_{a}\tau_{1})\cos(\pi J_{lal_{p}}\tau_{1}) \\ -2l_{ax}J_{pz}\sin^{2}(\Omega_{a}\tau_{1})\cos(\Omega_{a}\tau_{1})\sin(\pi J_{lal_{p}}\tau_{1}) \\ -2l_{ax}J_{pz}\sin^{2}(\Omega_{a}\tau_{1})\sin(\pi J_{lal_{p}}\tau_{1}) \\ +2l_{ax}J_{pz}\sin^{2}(\Omega_{a}\tau_{1})\sin(\pi J_{lal_{p}}\tau_{1}) \\ +2l_{ax}J_{pz}\sin^{2}(\Omega_{a}\tau_{1})\cos(\pi J_{lal_{p}}\tau_{1}) \\ +2l_{ax}J_{pz}\sin^{2}(\Omega_{a}\tau_{1})\sin(\pi J_{lal_{p}}\tau_{1}) \\ +2l_{ax}J_{pz}\sin^{2}(\Omega_{a}\tau_$$

Eq.1.3

Regrouping the terms according some basic trigonometric identities, the magnetization components are reduced to:

$$\begin{split} -I_{ay}\cos^2(\Omega_a\tau_1)\left[\cos^2\left(\pi J_{I_aI_p}\tau_1\right) + \sin^2(\pi J_{I_aI_p}\tau_1)\right] \\ +I_{ay}\sin^2(\Omega_a\tau_1)\left[\cos^2\left(\pi J_{I_aI_p}\tau_1\right) + \sin^2(\pi J_{I_aI_p}\tau_1)\right] \\ +I_{ax}\cos(\Omega_a\tau_1)\sin(\Omega\tau_1)\left[\cos^2(\pi J_{I_aI_p}\tau_1) + \sin^2(\pi J_{I_aI_p}\tau_1)\right] \\ & \qquad \qquad \downarrow \cos^2\theta + \sin^2\theta = 1 \\ -I_{ay}\left[\cos^2(\Omega_a\tau_1) - \sin^2(\Omega_a\tau_1)\right] + I_{ax}\cos(\Omega_a\tau_1)\sin(\Omega_a\tau_1) \\ & \qquad \qquad \downarrow \cos^2\theta - \sin^2\theta = \cos 2\theta \\ & \qquad \qquad \downarrow \cos^2\theta + \sin 2\theta \\ & \qquad \qquad -I_{ay}\cos(2\Omega_a\tau_1) + I_{ax}\sin(2\Omega_a\tau_1) \end{split}$$

Eq.1.4

These results demonstrate that with this building block Ω_a evolves during the period $2\tau_1$ while $J_{I_aI_p}$ is fully refocused. The choice of the selective inversion element is dependent on the sample analyzed and on the information required. Importantly, the amount of active spins being inverted is typically much smaller than the passive spins, entailing some cost in sensitivity that must be carefully evaluated in each case.

1.1.1.1 BIRD-based elements

A simple way to perform homonuclear decoupling in heteronuclear spin systems is using the BIRD module,^{4b} which is based on a different isotopic 12 C/ 13 C behavior. Mainly, two different BIRD blocks are available: BIRD^x and BIRD^y (Figure 3):

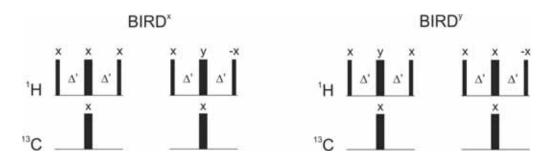


Figure 3: Different implementations of the BIRD^x (right) and BIRD^y (left) NMR building blocks. Δ' is adjusted according to $1/(2^1 J_{CH})$.

The BIRD^y block inverts ¹²C-bound protons while keep the magnetization of protons bound to ¹³C unchanged (Figure 4). Starting with 90° ¹H excitation, the magnetization of ¹³C-bound protons evolves under the effect of the one-bond coupling to the directly-attached carbon (${}^{1}J_{CH}$) during the Δ' periods (where Δ' is adjusted to $1/(2^{1}J_{CH})$). ¹H chemical shift evolutions for both ¹H-¹³C and ¹H-¹²C components are not considered because all they will be refocused by the central 180° ¹H pulse (spin-echo). The final 90° pulse rotates the magnetization of ¹³C-bound protons onto the +*z*-axis and ¹²C-bound protons onto –*z*-axis producing the desired selective inversion of the ¹H-¹²C resonances. The BIRD^x block works in the reverse mode.

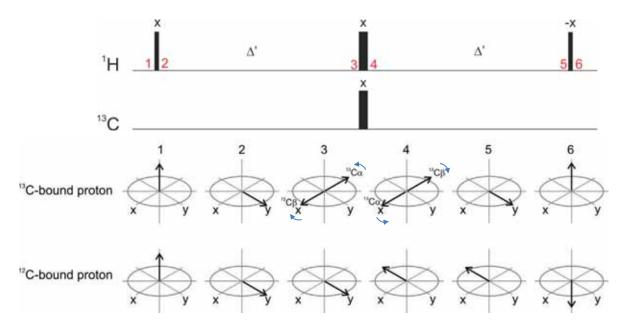


Figure 4: Pulse sequence of the BIRD⁹ element used to invert the magnetization of ¹²C-bound protons while leaving the magnetization of ¹³C-bound protons essentially unaffected. The fates of the ¹³C- and ¹²C-bound protons magnetizations are shown in the vector representation. The spin state of the bound ¹³C nucleus is also indicated.

BIRD-based homodecoupling was introduced by Garbow and coworkers more than thirty years ago. ^{4a} The basic homodecoupling block consists of the combination of a hard 180° ¹H pulse followed by a BIRD^x element (Figure 2A), and the net effect is therefore a 360° rotation of protons directly ¹³C bounded and a 180° rotation of the protons attached to ¹²C. The main features of the success use of BIRD homodecoupling are as follows:

- i. Problems associated to strong $J_{\rm HH}$ coupling effects are minimized.
- ii. The geminal ${}^2J_{HH}$ interaction between diastereotopic protons is retained because the BIRD element cannot distinguish between protons directly bound to the same 13 C nucleus. As a practical consequence, BIRD-based pure shift spectra will show doublets for non-equivalent methylene protons. Recently, novel concepts based on

constant-time BIRD⁶ or perfect BIRD⁷ elements have been proposed to remove such $^2J_{HH}$ effects.

- iii. The ideal behavior expected for spins during the BIRD block can be compromised in real situations because of the single delay Δ' (optimized to $1/(2^1J_{CH})$) that may not simultaneously satisfy the heteronuclear couplings arising for different spins of the molecules and because of imperfect inversions for 13 C sites spanning up to 200 ppm in their chemical shift ranges. Either of these two deviations can affect the behaviour expected for the 13 C-bonded protons, leading to artefacts. In practice, a suitable compromise value of Δ' can be found to minimize the J_{CH} -derived artefacts whereas the use of adiabatic-shaped 180° 13 C pulses eliminates off-resonance effects. 8
- iv. The price to pay for applying BIRD-based homodecoupling is sensitivity. Natural abundance of ¹³C is approximately 1,1%, and therefore, an unavoidable sensitivity loss of about 99% is obtained after using a BIRD filter. This sensitivity penalty is avoided in experiments that preselect ¹H-¹³C magnetization, as carried out in pure shift HSQC experiments.⁹
- v. BIRD fails for fully 13 C-labeled compounds because of J_{CC} evolution.

The BIRD-based homodecoupling method has been further refined and adapted for pure shift 1D^{8,10} and 2D HSQC experiments,^{9,11} and recently applied in a variety of structural problems.^{6,12}

1.1.1.2 Frequency-selective pulses

The use of a frequency-selective 180° pulse is a simple option to achieve selective inversion on a single or multiple ¹H signals (Figure 2B-D). The performance is under the

^[6] T. Reinsperger, B. Luy, J. Magn. Reson., 2014, 239, 110.

^[7] L. Kaltschnee, A. Kolmer, I. Timári, V. Schmidts, R. W. Adams, M. Nilsson, K. E. Kövér, G. A. Morris, C. M. Thiele, *Chem. Commun.*, **2014**, *50*, 15702.

^[8] A. Lupulescu, G. L. Olsen, L. Frydman, J. Magn. Reson., 2012, 218, 141.

^[9] L. Paudel, R. W. Adams, P. Király, J. A. Aguilar, M. Foroozandeh, M. J. Cliff, M. Nilsson, P. Sándor, J. P. Waltho, G. A. Morris, *Angew. Chem. Int. Ed.*, **2013**, *52*, 11616.

^[10] J. A. Aguilar, M. Nilsson, G. A. Morris, *Angew. Chem. Int. Ed.*, 2011, 50, 9716.

^[11] P. Sakhaii, B. Haase, W. Bermel, J. Magn. Reson., 2009, 199, 192.

^[12] a) I. Timári, L. Kaltschnee, A. Kolmer, R. W. Adams, M. Nilsson, C. M. Thiele, G. A. Morris, K. E. Kövér, J. Magn. Reson., 2014, 239, 130. b) Y. Liu, M. D. Green, R. Marques, T. Pereira, R. Helmy, R. T. Williamson, W. Bermel, G. E. Martin, Tetrahedron Lett., 2014, 55, 5450. c) J. A. Aguilar, G. A. Morris, A. M. Kenwright, RSC Adv., 2014, 4, 8278. d) K. J. Donovan, L. Frydman, Angew. Chem. Int. Ed., 2014, 54, 594.

control of the NMR user by an appropriate choice of the duration and shape of the selected 180° pulse that defines the effective bandwidth of the selective excitation. Several options are feasible, including single frequency (Figure 2B), multiple-frequency (Figure 2C) or band-selective (Figure 2D) excitation covering a specific region of the proton spectrum. The only requirement for a proper homodecoupling is that this selective pulse must not affect to mutually J coupled protons to avoid the evolution of this mutual coupling.

These building blocks were initially used to significantly increase the spectral resolution in the indirect F1 dimension of 2D experiments, by collapsing J_{HH} multiplets to singlets by BAnd-Selective Homonuclear Decoupling (BASHD) techniques. This strategy can be combined with other homodecoupling techniques along the detected F2 dimension in order to obtain ultra-high resolution in both dimensions of fully homodecoupled 2D spectra.

1.1.1.3 Spatial encoding

Conventional NMR experiments involve the nonspecific excitation and detection of the NMR signal in the entire detector coil (Figure 5A). The incorporation of the spatial encoding concept, traditionally used in *Magnetic Resonance Imaging* (MRI) applications, into high-resolution NMR spectroscopic techniques is attracting an increasingly larger interest. Several strategies have been developed to perform spatial encoding into an NMR tube:

i. Data collection is focused on a specific *z*-slice along the NMR sample (Figure 5B). Spatially resolved NMR applications have been reported for the analysis and characterization of heterogeneous samples, for instance, to study biphasic systems, ¹⁴ to detect and quantify sample inhomogeneities and spatial distribution in different alignment media such as gels or liquid crystals, ¹⁵ to investigate solvation and diffusion of CO₂ in ionic liquids, ¹⁶ to perform fast titrations and *in situ* reaction monitoring for obtaining information about reaction mechanisms and detecting

^[13] a) R. Brüschweiler, C. Griesinger, O. W. Sørensen, R. R. Ernst, *J. Magn. Reson.*, 1988, 78, 178. b) V. V. Krishnamurthy, *Magn. Reson. Chem.*, 1997, 35, 9.

^[14] a) W. Kozminski, *Pol. J. Chem.*, **2000**, *1189*, 1185. b) B. T. Martin, G. C. Chingas, O. M. McDougal, *J. Magn. Reson.*, **2012**, *218*, 147. c) C. Mantel, P. A. Bayle, S. Hediger, C. Berthon, M. Bardet, *Magn. Reson. Chem.*, **2010**, *48*, 600.

^[15] a) P. Trigo-Mouriño, C. Merle, M. R. M. Koos, B. Luy, R. R. Gil, *Chem. Eur. J.*, **2013**, *19*, 7013. b) A. C. Pöppler, S. Frischkorn, D. Stalke, M. John, *Chemphyschem*, **2013**, *14*, 3103.

^[16] J. Allen, K. Damodaran, Magn. Reson. Chem., 2015, 53, 200.

- intermediates¹⁷ or to avoid *z*-gradient imperfections in diffusion NMR experiments.¹⁸
- ii. Achievement of a selective and simultaneous signal perturbation, where each proton frequency is excited at different z positions (Figure 5C). This is the basis of the original ZS experiment,³ and it has also been applied in single-scan \mathcal{T}_1 relaxation time measurements,¹⁹ to measure coupling constants,²⁰ or for the efficient diagonal peak suppression in 2D experiments.²¹

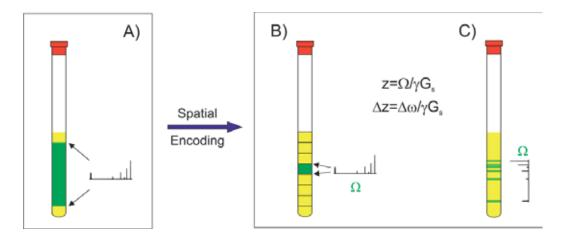


Figure 5: Different strategies to induce spatial selection along the *z*-axis of a NMR tube: A) Standard excitation/detection over the entire coil; B) Single-slice selection; C) Frequency-selective spatial selection.

Most of the reported slice-selective applications have been implemented in conventional liquid-state NMR spectrometers equipped with a basic hardware configuration; this is a direct or indirect detection probe incorporating a gradient coil that can delivers maximum gradient strengths around 50-60 G/cm along the z-axis. Experimentally, spatial frequency encoding is achieved by simultaneous application of a frequency-selective 90° or 180° pulses and a weak spatial-encoding PFG (G_s) both with the same duration (Figure 2E-G).

When a PFG is applied along the *z*-axis, the B_0 field is made spatially inhomogeneous by varying linearly along the applied dimension. Thus, during the application of a PFG, different parts of the sample experience a different magnetic field strength depending of their *z*-position, leading to a spatial-dependent frequency shift across the sample volume. Figure 6 compares the effects to apply a hard 90° pulse, a frequency-selective 90° pulse

^[17] T. Niklas, D. Stalke, M. John, Chem. Commun., 2014, 51, 1275.

^[18] a) B. Antalek, Concepts Magn. Reson., 2002, 14, 225. b) K. D. Park, Y. J. Lee, Magn. Reson. Chem., 2006, 44, 887.

^[19] N. M. Loening, M. J. Thrippleton, J. Keeler, R. G. Griffin, J. Magn. Reson., 2003, 164, 321.

^[20] a) N. Giraud, L. Béguin, J. Courtieu, D. Merlet, *Angew. Chem. Int. Ed.*, **2010**, *49*, 3481. b) M. E. Di Pietro, C. Aroulanda, D. Merlet, *J. Magn. Reson.*, **2013**, *234*, 101.

^[21] S. Glanzer, E. Schrank, K. Zangger, J. Magn. Reson., 2013, 232, 1.

and a simultaneous frequency-selective 90° pulse/gradient element. In the conventional ¹H spectrum, all signals from any part of the NMR tube into the active detector coil contribute to the observed signal (Figure 6A). In the selective experiment, only those signals experiencing the selective pulse contribute to the detected data; although the maximum sensitivity for these signals is retained (Figure 6B). In the slice-selective experiment, a complete ¹H spectrum can be obtained using optimized pulses and gradients, but each individual signal exclusively comes from a different part of the tube along the *z*-dimension (Figure 6C). As an obvious consequence, a decrease of overall sensitivity is always associated with any slice-selective experiment, which is proportional to the number of generated *z*-slices.

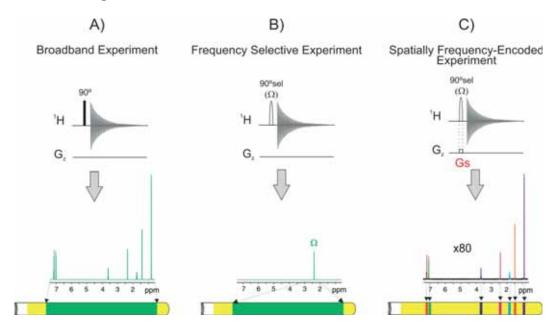


Figure 6: General illustration to understand slice-selective excitation: A) conventional acquisition scheme to obtain a 1 H spectrum; B) selective excitation using a frequency-selective 90° pulse; C) slice selection consisting of the simultaneous application of a 90° frequency-selective pulse and a weak encoding gradient (G_s). In the latter case, the full spectrum is obtained thanks to the spatial-dependent Z-position of each individual resonance along the NMR tube.

Experimentally, the range of sampled frequencies (SW_G) which include the entire chemical shift of interest is defined by the strength of G_S according to:

$$SW_{\rm G} = \gamma LG_{\rm S}$$
 Eq.1.5

where γ is the gyromagnetic ratio of the spatially-encoded nucleus and L is the active volume coil length. On the other hand, the carrier frequency (Ω) and the selective pulse bandwidth ($\Delta\omega$) determine the Z-position of each nuclear spin (Z) and the slice thickness (Δz) according to these two expressions, respectively:

$$z = \Omega / (\gamma G_S)$$
 Eq. 1.6
 $\Delta z = \Delta \omega / (\gamma G_S)$ Eq. 1.7

The Signal to Noise Ratio (SNR) in slice-selective experiments depends on the active slice thickness because the detected signal only comes from a selected Z-slice. As shown, Δz depends both on the strength of G_S (which is proportional to SW_G) and on the selectivity of the pulse (which should not exceed the smallest chemical shift difference expected between any coupled proton pairs). For instance, a typical 20 ms Gaussian shaped 180° pulse (bandwidth of 60.7 Hz) applied simultaneous with a gradient G_S of 0.74 G/cm splits the sample height (L=1.8 cm) into around 94 slices along the Z axis, defining a Δz of about 0.019 cm and covering an SW_G of 5694 Hz (9.5 ppm in a 600 MHz spectrometer). Thus, under these general conditions, the single-slice selection procedure would afford only about 1% of the sensitivity of a conventional 1 H spectrum.

Another fundamental aspect when optimizing and applying slice-selection in homodecoupling experiments it is the presence of strong couplings. Slice selection works well for weakly coupled spin systems, but it can fail for strongly coupled signals. If the chemical shift difference ($\Delta\delta$) of coupled spins is less than the selective pulse bandwidth

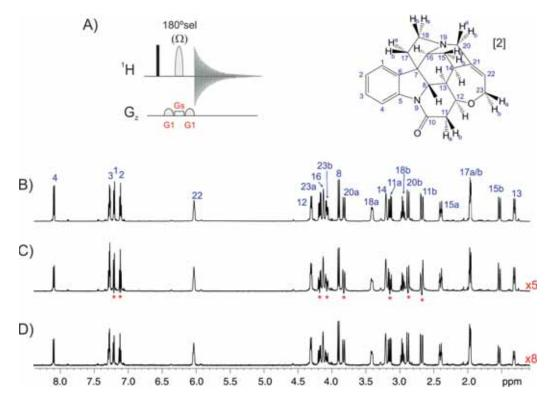


Figure 7: A) Pulse scheme of the ss-SPFGE experiment. B) 600 MHz 1 H NMR spectrum of strychnine [2] in CDCl₃; C,D) ss-SPFGE spectra acquired with an encoding strength of 1.1 G/cm and with a selective 180 $^{\circ}$ 1 H gaussian-shaped pulse of C) 20 and D) 30 ms, respectively. In C) phase distorted multiplets are observed due to the excitation of two \mathcal{L} -coupled protons into the same slice. Also note the different SNR observed in C and D in function of the selective 180 $^{\circ}$ 1 H pulse applied.

 $(\Delta\omega)$ but they are not very strongly coupled $(\Delta\omega > \Delta\delta > J)$, couplings within $\Delta\omega$ become active, but the effects of couplings to other spins remain suppressed, retaining much of the resolution advantage. Where spins are fairly strongly coupled $(\Delta\omega > \Delta\delta \approx J)$, weak extra signals appear at intermediate frequencies, and if they are very strongly coupled $(\Delta\omega > J > \Delta\delta)$, it will typically yields distorted signals. The optimum selective 180° pulse and the encoding G_s gradient strength can be calibrated using a *Slice-Selective Single Pulsed Field Gradient Echo* (ss-SPFGE) experiment (Figure 7A). The excitation of two J-coupled protons into the same slice can be observed as phase distorted multiplets (*Anti-Phase* (AP) contributions) in the corresponding 1D ss-SPFGE spectrum (Figure 7C).

1.1.2. Homodecoupling acquisition modes

1.1.2.1. Historical review

Each signal in a 1 H NMR spectrum exhibits a particular multiplet J_{HH} pattern as a result of its through-bond interactions with their neighboring protons. Thus, experimental issues such as signal dispersion, spectral resolution or signal overlap become very relevant to identify and assign each individual signal, in particular when a large number of resonances are present in a narrow range of frequencies. The use of NMR methods affording simplified multiplet structures are of interest because they can facilitate the analysis and the interpretation of the corresponding spectra. The traditional way to achieve such simplification is by frequency-selective continuous-wave irradiation on a single-target signal during the acquisition period. The method has been improved by multiple irradiation of different signals using multiple-frequency homodecoupling, polychromatic pulses of irradiating a group of signals resonating into the same region, among others, being one of the most reported applications the band-selective homodecoupling of the well-defined NH or H_{α} regions in peptides and proteins. All

^[22] W. A. Anderson, R. Freeman, J. Chem. Phys., 1962, 37, 85.

^[23] A. P. D. M. Espindola, R. Crouch, J. R. DeBergh, J. M. Ready, J. B. MacMillan, *J. Am. Chem. Soc.*, 2009, 131, 15994.

^[24] D. Carnevale, T. F. Segawa, G. Bodenhausen, *Chem. Eur. J.*, 2012, *18*, 11573.

^[25] a) C. W. Vander Kooi, E. Kupče, E. R. P. Zuiderweg, M. Pellecchia, J. Biomol. NMR, 1999, 15, 335.
b) A. Hammarström, G. Otting, J. Am. Chem. Soc., 1994, 116, 8847. c) E. Kupče, R. Freeman, J. Magn. Reson. Ser. A, 1993, 102, 364. d) J. P. Jesson, P. Meakin, G. Kneissel, J. Am. Chem. Soc., 1973, 95, 618. E) J. Weigelt, A. Hammarström, W. Bermel, G. Otting, J. Magn. Reson., 1996, 110, 219.

^[26] V. D. M. Koroleva, N. Khaneja, J. Chem. Phys., 2012, 137, 094103.

^[27] a) E. Kupče, H. Matsuo, G. Wagner, "Biological Magnetic Resonance: Modern Techniques in Protein NMR", Springer, (Eds: N. R. Krishna, L. J. Berliner), 1999, 16, 149. b) E. Kupče, G. Wagner, J. Magn. Reson., 1995, 109, 329. c) E. Kupče, G. Wagner, J. Magn. Reson., 1996, 110, 309. d) B. Vögeli, H. Kovacs, K. Pervushin, J. Biomol. NMR, 2005, 31, 1.

these approaches do not provide broadband homodecoupling in the entire spectrum, so only multiplet patterns of some signals are partially simplified according to the irradiated signals, and therefore, success is limited to specific and well-isolated spin systems.

A simple and classical approach to achieve a broadband homodecoupled ¹H spectrum is the 1D projection extracted from the detected dimension of a tilted homonuclear 2D \mathcal{L} resolved experiment. ²⁸ The standard experiment suffers of poor phase-twist lineshapes and alternatives to obtain absorptive homonuclear spectra, such as the incorporation of spatial-selective encoding at expense of important sensitivity losses ^{28k} or using a \mathbb{Z} -filter combined with a post-processing pattern recognition algorithm ^{28l} have been proposed. Another drawback that has been recognized and evaluated in detail is the presence of extra peak artifacts due to strong coupling effects. ^{28j} The use of appropriate data processing in \mathcal{L} resolved experiments has also been an interesting topic to enhance sensitivity. ²⁹ The \mathcal{L} resolved module has been appended as an NMR building block to standard 2D experiments, such as reported for homodecoupled versions of DOSY³⁰ and HMBC experiments, ^{28o} although that the resulting experiments become more time-consuming than the original ones. The \mathcal{L} resolved experiment has also been successfully used in the determination of small chemical shifts differences in complex mixtures, such as metabonomics³¹ or enantiodiferentation²⁸ⁿ studies, among others.

Separation of chemical shifts and J couplings while retaining absorption-mode lineshapes can also be obtained from the diagonal projected spectrum of a modified anti z-COSY experiment. Another group of NMR experiments performs broadband homonuclear decoupling in the indirectly detected dimension of multi-dimensional experiments using time reversal, constant-time evolution, or BIRD editing in the case of heteronuclear experiments.

^[28] a) W. P. Aue, J. Karhan, R. R. Ernst, J. Chem. Phys., 1976, 64, 4226. b) A. Bax, R. Freeman, G. A. Morris, J. Magn. Reson., 1981, 43, 333. c) A. J. Shaka, J. Keeler, R. Freeman, J. Magn. Reson., 1984, 56, 294. d) M. Woodley, R. Freeman, J. Magn. Reson. Ser. A, 1994, 109, 103. e) M. Woodley, R. Freeman, J. Magn. Reson. Ser. A, 1994, 111, 225. f) J. M. Nuzillard, J. Magn. Reson., 1996, 118, 132. g) S. Simova, H. Sengstschmidt, R. Freeman, J. Magn. Reson., 1997, 124, 104. h) V. Mandelshtam, H. Taylor, A. J. Shaka, J. Magn. Reson., 1998, 133, 304. i) P. Mutzenhardt, F. Guenneau, D. Canet, J. Magn. Reson., 1999, 141, 312. j) M. J. Thrippleton, R. A. E. Edden, J. Keeler, J. Magn. Reson., 2005, 174, 97. k) A. J. Pell, J. Keeler, J. Magn. Reson., 2007, 189, 293. l) B. Luy, J. Magn. Reson., 2009, 201, 18. m) U. R. Prabhu, S. R. Chaudhari, N. Suryaprakash, Chem. Phys. Lett., 2010, 500, 334. n) S. R. Chaudhari, N. Suryaprakash, Chem. Phys. Lett., 2013, 555, 286. o) P. Sakhaii, B. Haase, W. Bermel, J. Magn. Reson., 2013, 228, 125.

^[29] P. Sakhaii, W. Bermel, J. Magn. Reson., 2014, 242, 220.

^[30] a) J. C. Cobas, M. Martín-Pastor, J. Magn. Reson., 2004, 171, 20. b) L. H. Lucas, W. H. Otto, C. K. Larive, J. Magn. Reson., 2002, 156, 138.

^[31] C. Ludwig, M. R. Viant, *Phytochem. Anal.*, **2010**, *21*, 22.

^[32] A. J. Pell, R. A. E. Edden, J. Keeler, Magn. Reson. Chem., 2007, 45, 296.

^[33] O. W. Sørensen, C. Griesinger, R. R. Ernst, J. Am. Chem. Soc., 1985, 107, 7778.

Actually, the homonuclear decoupling in most of current pure shift experiments is carried out in the direct dimension (so-called "proton dimension" or "acquisition dimension"). There are two different schemes available to achieve broadband homodecoupling in the acquisition dimension: (i) a pseudo-2D acquisition mode where a 1D homodecoupled *Free Induction Decay* (FID) is reconstructed by concatenating data chunks extracted from individual time domain datasets of a 2D experiment³ and (ii) a real-time acquisition mode that provides directly the homodecoupled 1D FID.^{8,36}

1.1.2.2. Pseudo-2D Zangger-Sterk experiment

The original *Zangger-Sterk* (ZS) experiment, reported in 1997,³ uses a slice-selective 2D pulse timing where a variable delay is incremented stepwise as usual (Figure 8A). The homodecoupling block (see several options in Figure 2) is applied in the middle of this incremented delay to refocus any $J_{\rm HH}$ evolution. A special post-processing is needed, where the first data chunks of each FID are assembling to create a new reconstructed 1D FID that is processed and transformed by ordinary procedures to lead a homodecoupled ¹H NMR spectrum. Later, a more robust ZS pulse scheme version was proposed where the timing of the decoupling element was carefully designed to provide homodecoupling in the middle of each data chunk, whereas PFGs were also applied to afford better spectral quality by suppressing strong signals from passive spins.³⁷

Experimentally, the evolution time (t_1) in the ZS experiment is incremented according to $1/SW_1$, where SW_1 is the defined spectral width in the indirect dimension (typically SW_1 =60-100 Hz), and the first 10-20 ms of each individual FID are selected nad concatenated for a further FID reconstruction. In case of large scalar coupling constants, the increments must be set to smaller values ($SW_1 < J_{HH}$) in order to avoid scalar coupling evolution. The residual effect is a slight decrease in signal intensity either side of the time at which J is refocused so that in each chunk the signal intensity is slightly less at the edges than in the center. Fourier transformation converts this periodic decrease in

^[34] a) M. E. Girvin, J. Magn. Reson. Ser. A, 1994, 108, 99. b) F. J. M. van de Ven, M. E. P. Philippens, J. Magn. Reson., 1992, 97, 637. c) Y. Xia, G. Legge, K. Y. Jun, Y. Qi, H. Lee, X. Gao, Magn. Reson. Chem., 2005, 43, 372. d) M. Rance, G. Wagner, O. W. Sørensen, K. Wüthrich, R. R. Ernst, J. Magn. Reson., 1984, 59, 250. e) A. Bax, R. Freeman, J. Magn. Reson., 1981, 44, 542. f) A. G. Palmer, W. J. Fairbrother, J. Cavanagh, P. E. Wright, M. Rance, J. Biomol. NMR, 1992, 2, 103. g) A. Bax, A. F. Mehlkopf, J. Smidt, J. Magn. Reson., 1979, 35, 167. h) B. T. Farmer, L. R. J. Brown, J. Magn. Reson., 1987, 71, 365. i) J. A. Aguilar, A. A. Colbourne, J. Cassani, M. Nilsson, G. A. Morris, Angew. Chem. Int. Ed., 2012, 51, 6460.

^[35] A. Bax, J. Magn. Reson., 1983, 53, 517.

^[36] N. H. Meyer, K. Zangger, Angew. Chem. Int. Ed., 2013, 52, 7143.

^[37] J. A. Aguilar, S. Faulkner, M. Nilsson, G. A. Morris, Angew. Chem. Int. Ed., 2010, 49, 3901.

intensity into small artifacts, typically in the form of weak sidebands at multiples of SW_1 , around each decoupled signal. The intensity of the sidebands is proportional to the square of J/SW_1 , and it decays rapidly either side of the decoupled signal. In typical SW_1 condition used in these experiments the sidebands are of comparable intensity to that of the ¹³C satellites. On the other hand, the resolution of the signals is directly related with the number of increments in the indirect dimension. Normally 16-32 increments are enough to obtain a high-quality 1D homodecoupled spectrum with optimum resolution and narrow line widths. Only as a reference, typical standard parameters to afford a nice 1D homodecoupled spectrum in ~5-10 minutes for a sample concentration about 10 mM would involve Gaussian or rSNOB shaped 180° ¹H pulses with a duration of 40-60 ms and an encoding G_s gradient around 0.5-1 G/cm. Under these general conditions, the pseudo-2D ZS method would afford only ~1-5% of the sensitivity of a conventional ¹H spectrum. SNR could be improved by using shorter and less selective pulses and/or less intense encoding gradients but always with an increased probability of accidental excitation of two coupled protons within the same z-slice. The original ZS experiment was based on slice-selection³ and a BIRD-based ZS experiment has also been reported, ¹⁰ but in both cases the sensitivity is still far from that obtained in conventional ¹H NMR spectra.

In a recent improvement, referred to as *Pure Shift Yielded by Chirp Excitation* (PSYCHE) experiment,³⁸ a pair of low flip angle swept-frequency pulses applied during a weak PFG are used as a selective inversion element (Figure 2H). By adjusting the pulse flip angle of the adiabatic pulse, it is possible to balance optimum sensitivity and full broadband homodecoupling for all signals in a given sample. PSYCHE can offer sensitivity improvements of almost one order of magnitude over conventional ZS methods performed by slice-selection or BIRD pulses.

The pseudo-2D ZS experiment has been recently applied to measure homonuclear³⁹ and heteronuclear coupling constants, ^{12c,40} and successfully implemented into a number of 2D experiments, as reported for pure shift DOSY, ^{37,41} TOCSY, ⁴² NOESY, ³⁴ⁱ HSQC^{6,11,12a}

^[38] M. Foroozandeh, R. W. Adams, N. J. Meharry, D. Jeannerat, M. Nilsson, G. A. Morris, *Angew. Chem. Int. Ed.*, **2014**, *53*, 6990.

^[39] S. R. Chaudhari, N. Suryaprakash, ChemPhysChem, 2015, 16, 1079.

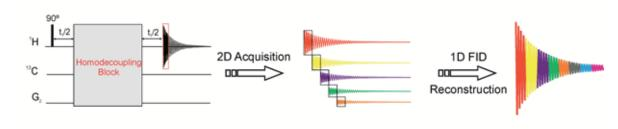
^[40] a) S. R. Chaudhari, N. Suryaprakash, *RSC Adv.*, **2014**, *4*, 15018. b) I. Timári, T. Z. Illyés, R. W. Adams, M. Nilsson, L. Szilágyi, G. A. Morris, K. E. Kövér, *Chem. Eur. J.*, **2015**, *21*, 3472.

^[41] a) M. Nilsson, G. A Morris, *Chem. Commun.*, **2007**, 933. b) S. Islam, J. A. Aguilar, M. W. Powner, M. Nilsson, G. A. Morris, J. D. Sutherland, *Chem. Eur. J.*, **2013**, *19*, 4586.

^[42] a) G. A. Morris, J. A. Aguilar, R. Evans, S. Haiber, M. Nilsson, J. Am. Chem. Soc., 2010, 132, 12770. b) J. J. Koivisto, Chem. Commun., 2013, 49, 96. C) M. Foroozandeh, R. W. Adams, M. Nilsson, G. A. Morris, J. Am. Chem. Soc., 2014, 136, 11867.

and HSQMBC.^{40b} The main drawback of these resulting pseudo-3D experiments is that their overall acquisition times can become extremely long for routine use.

A) Pseudo-2D ZS Experiment



B) Real-time ZS Experiment

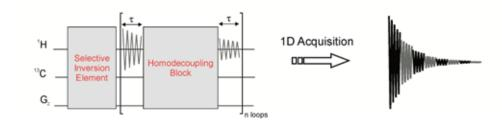


Figure 8: General schemes leading to 1D broadband homodecoupled ¹H NMR spectra: A) The original ZS method is based on a 2D acquisition mode followed by an FID reconstruction from the initial data chunks of each increment; B) The real-time ZS experiment incorporates periodically the homodecoupling block in the middle of the FID acquisition. The homodecoupling block in both approaches can be any option described in Figure 2.

1.1.2.3. Real-time ZS experiments

Real-time broadband homodecoupling was initially proposed using the BIRD element as homodecoupling block during data acquisition, and shortly after, a slice selective version was also reported using the general scheme of Figure 8B. This new acquisition technique, referred to as real-time ZS or *HOmodecoupled BroadBand* (HOBB), directly generates a single 1D FID that after standard processing can lead to a broadband homodecoupled 1D H NMR spectrum. This method offers instant and speed-up data acquisition and an improved SNR per time unit compared to the original ZS experiment, although the attainable sensitivity is still far from a regular H spectrum because of the involved ¹³C editing or slice selection procedures.

In the real-time ZS method, instead of recording each fraction of the FID in a serie of individual experiments, the FID is collected directly in a single scan. The acquisition is interrupted after every τ period to perform either slice-selective or BIRD-based

homodecoupling, as shown in Figure 9A. Note, that the first fraction of acquisition is only half as long as the subsequent ones. Thereby, full scalar decoupling is achieved in the middle of each fraction of the FID. These acquisition segments are assembled consecutively in a conventional FID which can be treated like a regular 1D NMR experiment. The τ period is defined as AQ/2n where AQ is the acquisition time and n the number of loops. As long as $\tau \ll 1/J_{HH}$, homonuclear J modulations occurring during these acquisition segments can be disregarded with no compromise in the final spectral resolution, leading to the potential collapse of all $J_{\rm HH}$ splittings. As in the pseudo-2D acquisition mode, deviations from this condition lead to incomplete homodecoupling and the appearance of distinct decoupling sidebands flanking each purely shifted resonance at spacing multiples of 2n/AQ. Moreover, while the acquisition is interrupted for decoupling, the magnetization is relaxing, and therefore, it is critical to keep the interruptions as short as possible, especially for larger molecules that have shorter \mathcal{T}_2 relaxation times. As longer time interruptions, there are more differences in intensity between previous and next acquired FID. Fourier transform converts this periodic FID discontinuity in sidebands at multiples of 2n/AQ, around each decoupled signal. The intensity of these sidebands is greater the larger is the FID discontinuity. On the other hand, it is also important to keep the interruptions as short as possible because the signals are slightly broadened due to the extra \mathcal{T}_2 relaxation during this refocusing time. If a BIRD-based homodecoupling block is used, the FID is interrupted about 6-8 ms (to $^{1}J_{CH}$ between 120-160 Hz). In the case of use a selective 180° pulse, a compromise duration of 5-10 ms balances between an optimum slice selection and an effective homodecoupling of nearby signals, while minimizes the T_2 relaxation effects.

In practice, real-time ZS acquisition reduces the overall experimental time and improving SNR per time unit but at some cost in spectral quality and the achievement of wider line widths. As an example, the HOBB spectrum of cyclosporine, quickly acquired in a single scan, shows full homodecoupling for most of the signals (except in some aliphatic CH₂ resonances) thanks to the well dispersed spin systems (Figure 9C). Importantly, the SNR of the HOBB experiment also suffers of the unavoidable losses due to slice selection (~8% of the maximum theoretical signal).

The real-time ZS acquisition mode becomes an attractive NMR building block for the design of pure shift methods and, as a major advantage, it can be incorporated as a detection scheme in standard multidimensional experiments without increase their original dimensionalities and continuing to use the same data-processing protocols. This represents a boost in SNR per time unit when compared to the pseudo-2D ZS experiment,

as reported recently for HOBB-DOSY,⁴³ HOBB-TOCSY,³⁶ HOBB-ROESY,⁴⁴ and HOBB-HSQC^{9,12b,45} experiments. From a strategic point of view, it is advisable to optimize first a 1D HOBB experiment in order to determine the best homodecoupling conditions for the sample under study. The signal simplification observed in the resulting 2D HOBB spectra will be the same obtained in a 1D HOBB spectrum recorded under the same conditions.

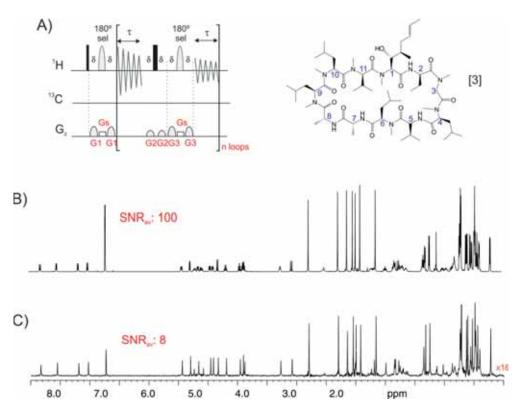


Figure 9: A) General pulse scheme of the real-time 1D HOBB experiment; B) 600 MHz conventional 1 H spectrum of cyclosporine [3]; C) 1D HOBB spectrum acquired with a RE-BURP pulse of 5 ms for both excitation and decoupling and G_s =1.1 G/cm. For an objective comparison of real sensitivities, the experimental averaged SNR is indicated for each 1D dataset. For a real comparison, both spectra have been recorded and processed in the same way: with the same receiver gain, using a single scan, processed with a Fourier transformation without any additional window function and plotted with the same absolute vertical scaling factor.

^[43] S. Glanzer, K. Zangger, Chem. Eur. J., 2014, 20, 11171.

^[44] V. M. R. Kakita, J. Bharatam, *Magn. Reson. Chem.*, **2014**, *52*, 389.

^[45] N. H. Meyer, K. Zangger, Chem. Commun., 2014, 50, 1488.

1.1.3. Homodecoupled experiments and applications

Recently, all of the aforementioned ZS methodologies, using BIRD or slice-selective homodecoupling and pseudo-2D or real-time acquisition modes, have been implemented in different 1D and 2D NMR experiments (Table 1). It is important to note that a requirement for a success implementation of any ZS module is to have IP proton-proton magnetization because experiments involving AP signals, like those found in conventional COSY or HMBC, cancel out under homodecoupling conditions.

Pure shift NMR spectra have a wide range of potential uses, as demonstrated for the analysis of complex mixtures,³⁷ to carry out structural elucidation studies,^{9,11,12b,34i,36,42a,42b,44,45} to analyze diffusion data⁴³ and to measure homonuclear³⁹ and heteronuclear coupling constants.^{6,11,12c,40} A more exhaustive description of the different applications can be found in a recent review work publish by us.¹ As a complement to this introduction, two excellent and very comprehensive revision works about broadband homodecoupling methods, including detailed description of all indirect methods, have been also reported recently.⁴⁶

Table 1: Summary of reported broadband homodecoupled 1D and 2D ¹H NMR experiments.

		Hom	nodecoupling	Acquisitio	on mode	
N	MR Experiment	BIRD	Slice selection	Pseudo-2D	Real-time	References
		✓		✓		[10][12c]
	¹ H NMR		✓	✓		[3][37][38][40a][47][48]
1D		✓			✓	[8][12d]
			✓		✓	[36]
	Quick-Serf		✓		✓	[49][50]
	T0.00V		✓	✓		[42]
	TOCSY		✓		✓	[36]
	DOSY		✓	✓		[37][41]
			✓		✓	[43]
2.5	NOESY		✓	✓		[34i]
2D	ROESY		✓		√	[44]
			✓		✓	[45]
	HSQC/HSQCed	✓		✓		[6][7][11][12a]
		✓			✓	[9]
	HSQMBC		✓	✓		[40b]

^[46] a) N. H. Meyer, K. Zangger, ChemPhysChem, 2014, 15, 49. b) R. W. Adams, eMagRes, 2014, 3, 295.

^[47] P. Sakhaii, B. Haase, W. Bermel, R. Kerssebaum, G. E. Wagner, K. Zangger, J. Magn. Reson., 2013, 233, 92.

^[48] N. Lokesh, N. Suryaprakash, Chem. Commun., 2014, 50, 8550.

^[49] N. Gubensäk, W. M. F. Fabian, K. Zangger, *Chem. Commun.*, **2014**, *50*, 12254.

^[50] N. Lokesh, S. R. Chaudhari, N. Suryaprakash, *Chem. Commun.*, **2014**, *50*, 15597.

1.2. 2D HSQC and HSQMBC NMR experiments⁵¹

Proton-detected heteronuclear 2D NMR experiments, essentially based on two different pulse schemes referred to as *Heteronuclear Single Quantum Correlation* (HSQC)⁵² and *Heteronuclear Multiple Quantum Correlation* (HMQC),⁵³ have been key NMR tools during many years for chemists and biochemists to provide valuable structural information on ¹H-¹³C (and ¹H-¹⁵N) chemical bonds. These experiments provide information about structure, conformation and dynamics of rigid and flexible molecules in solution, as well as they can serve for many other interests such as structural validation methods, determine intermolecular interactions or to measure *Residual Dipolar Couplings* (RDCs) in molecules dissolved in weakly aligned media. Nowadays, these experiments are usually performed in a complete automation mode in both data acquisition and processing steps, practically without any need for direct user intervention. The resulting 2D maps are very simple to analyze and to interpret, even for non-experienced NMR users, typically displaying well dispersed cross-peaks that correlate ¹H (direct F2 dimension) and ¹³C (indirect F1 dimension) chemical shifts between directly attached ¹H-¹³C groups, through the ¹J_{CH} transfer mechanism.

The HMQC scheme is simpler in terms of the number of pulses, but its major complication relies on that proton magnetization is located in the transverse plane during the entire pulse sequence. Additionally, proton-proton coupling constants ($J_{\rm HH}$) also evolve during the variable t_1 period and, as a result, cross peaks present strongly distorted twist-phased patterns along the detected F2 dimension and a characteristic skew shape along the indirect F1 dimension of the 2D map. On the other hand, the HSQC experiment uses *Insensitive Nuclei Enhanced by Polarization Transfer* (INEPT) blocks for heteronuclear magnetization transfer, and the evolution during the t_1 period is not affected by $J_{\rm HH}$. However, the influence of $J_{\rm HH}$ coupling evolution during the INEPT period on the phase and amplitude signal modulation must be considered when a detailed analysis is required.

To better understand the improved HSQC-related experiments described in the "Results and Discussion" section, this introduction aims to explain the fundamental key points of HSQC-type experiments. Special focus will made on the effects of the intensity and phase signal modulation dependence with respect to J_{CH} and J_{HH} . A recommendable

^[51] Part of this introduction has been adapted from: L. Castañar, T. Parella, Annu. Rep. NMR Spectrosc., 2015, 84, 163.

^[52] G. Bodenhausen, D. J. Ruben, Chem. Phys. Lett., 1980, 69, 185.

^[53] A. Bax, R. Griffey, B. Hawkins, *J. Mag. Reson.*, **1983**, *55*, 301.

Introduction: HSQC and HSQMBC

work describing the different features, options and practical details of both HMQC and HSQC experiments is available as a complementary reading to this introduction.⁵⁴

1.2.1. The HSQC experiment

Since its introduction, the HSQC experiment has been modified in so many different ways in order to improve important experimental aspects (such as sensitivity, resolution, efficiency, robustness and performance) and to provide additional and complementary information from a single NMR experiment. All these modifications have been done changing and/or introducing some elements or building blocks in the pulse scheme, therefore a detailed study of the basic HSQC pulse sequence is advisable for a better understanding and further improvements.

1.2.1.1. Basic HSQC pulse scheme

Figure 10C shows the five basic independent steps that can be identified in a standard 2D gradient-selected HSQC pulse scheme:

- 1- The pre-scan period is usually defined by a long recycle delay (some seconds of duration, accordingly to the existing $\mathcal{T}_1(^1H)$ relaxation times) to allow the recovery of the 1H magnetization to a pre-equilibrium state just before to start the sequence.
- 2- After the initial ¹H excitation, heteronuclear transfer takes place using an INEPT block optimized to single ¹ J_{CH} value, accordingly to $\Delta=1/(2^1J_{CH})$.
- 3- Anti-Phase (AP) 13 C Single Quantum Coherences (SQCs) evolve during a variable t_1 period under the effect of 13 C chemical shift whereas the evolution of 13 C_H is refocused by the central 180° 1 H pulse.
- 4- During the refocused INEPT element, 13 C magnetization is reconverted to AP 1 H magnetization followed by the subsequent $^{1}J_{CH}$ evolution to generate *In-Phase* (IP) magnetization prior to acquisition.
- 5- The sequence finishes with a ¹H detection period under optional broadband heteronuclear decoupling.

^[54] P. K. Mandal, A. Majumdar, Conc. Magn. Reson., 2004, 20A, 1.

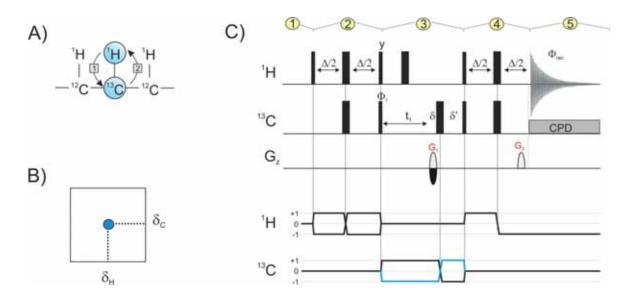


Figure 10: Schematic representation of the A) molecular transfer mechanism; B) cross-peak pattern and C) pulse sequence of a standard 2D 1 H- 13 C HSQC experiment. Thin and thick vertical rectangles represent 90° and 180° hard pulses, respectively. The delay Δ should be set to $1/(2^{1}J_{CH})$ and δ represents the duration of the PFG and its recovery delay. Coherence selection is performed by the gradient pair $G_1:G_2$ (±80:20.1) using the echo-antiecho protocol. A basic two-step phase cycling is executed with Φ_1 = x,-x and Φ_{rec} = x,-x. Below, the corresponding coherence transfer pathway diagram is shown: blue line stands for N-type magnetization (echo dataset), while black line stands for P-type magnetization (anti-echo dataset).

Historically, a major development in HSQC pulse sequence was the incorporation of PFGs for *Coherence Transfer Pathway* (CTP) selection. PFGs allow a clear distinction between $^{1}\text{H}-^{12}\text{C}$ vs $^{1}\text{H}-^{13}\text{C}$ magnetization, which results in the collection of high-quality HSQC spectra under standard routine conditions. One of the most widely protocols used to achieve coherence selection using PGFs is the *Echo/Anti-echo* (E/A) method. For a successful implementation of such methodology, two different PFGs must be properly inserted into the HSQC pulse sequence (Figure 10C): the encoding G_1 gradient will select CTPs in which only G_2 gradient will select CTPs in which only G_3 gradient will select CTPs in which only G_4 magnetization is in the transverse plane during the detection G_4 period.

An important aspect when applying PFGs during t_1 is that the signal obtained is not sine/cosine amplitude-modulated but phase modulated, which means that is modulated according to the rotation sense of the magnetization (S^+ , echo; or S, anti-echo). This results in P-type data selection (anti/echo), in which the sense of the frequency modulation is the same in t_1 and t_2 , and in N-type data selection (echo), in which the sense is the opposite:

^[55] a) T. Parella, Magn. Reson. Chem., 1998, 36, 467. b) W. Willker, D. Leibfritz, R. Kerssebaum, W. Bermel, Magn. Reson. Chem, 1993, 31, 287.

^[56] J. Keeler, "Understanding NMR spectroscopy", John Wiley and Sons, Ltd, England, 2007.

Introduction: HSQC and HSQMBC

$$S(t_1, t_2)_{anti-echo} = \gamma. e^{i\Omega_S t_1}. e^{i\Omega_S t_2}$$
 Eq. 1.8

$$S(t_1, t_2)_{echo} = \gamma. e^{-i\Omega_S t_1}. e^{i\Omega_S t_2}$$
 Eq. 1.9

That signal phase encoding makes the gradient only able to select one of the two desired CTPs in each scan. Therefore, the spectrum will present cross peaks with undesirable phase-twisted lineshapes. To solve that problem the acquisition of the E/A pathways has to be done in alternate acquisitions and then combined in a proper way during the processing step to provide amplitude-modulated signals, so that phase-sensitive spectra can be obtained.

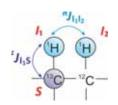
For data coherence selection, the gradient strengths have to be adjusted to:

$$\frac{G_1}{G_2} = \frac{\gamma_I}{\gamma_S}$$
 Eq. 1.10

where γ_1 and γ_S are the gyromagnetic ratio of sensitive (I) and insensitive (S) nuclei, respectively. In the case of ${}^1\text{H-}{}^{13}\text{C}$ correlation experiments such ratio is $\gamma_H/\gamma_C \approx 4$. N-type coherence (blue line in Figure 10C) is selected using $G_1:G_2=4$ (typical experimental ratio of 80:20.1 in percentage), while P-type coherence (black line in Figure 10C) is selected by $G_1:G_2=-4$ (typical experimental ratio of -80:20.1 in percentage).

In terms of sensitivity, the use of PFGs during t_1 produces a SNR decrease by a factor of $\sqrt{2}$ with respect to the original experiment because only one CTP can be selected. Nonetheless, the main advantages are that higher quality spectra are obtained, strong solvent signals (typically water) are efficiently suppressed, t_1 noise is better cleaned, and a considerable decrease in the overall acquisition time is achieved if the use of an extended phase cycle is avoided.

The signal intensity and phase dependences generated during the INEPT periods can be easily analyzed by the PO formalism.⁵ To carry out this analysis, a weakly coupled I_1I_2S spin system has been defined with a heteronuclear coupling constant (${}^1J_{1S}$) and a homonuclear coupling constant (${}^nJ_{1112}$).



At the beginning of the sequence (step 1 in Figure 10C), the initial magnetization (+ I_{1z}) is rotated to the *y*-axis (- I_{1y}). During the Δ delay (step 2 in Figure 10C), the magnetization evolves simultaneously under the effects of chemical shift (Ω) and coupling constants (J). In weakly coupled spin systems, these effects commute and they can be analyzed in

cascade⁵⁷. In the following analysis, each effect is separately analyzed for a better compression.

• Effect of chemical shift (Ω_l) evolution during the INEPT block

The magnetization evolves during the first $\Delta/2$ delay and then, the $180^{\circ}(l_x)$ inverts the l_1 magnetization along the x-axis:

$$-I_{1y} \xrightarrow{\Omega_{I}\Delta/2} -I_{1y}\cos\left(\Omega_{I_{1}}\Delta/2\right) + I_{1x}\sin\left(\Omega_{I_{1}}\Delta/2\right) \xrightarrow{180^{o}(I_{x})} +I_{1y}\cos\left(\Omega_{I_{1}}\Delta/2\right) + I_{1x}\sin\left(\Omega_{I_{1}}\Delta/2\right)$$
 Eq. 1.11

During the second $\Delta/2$ delay, all components evolve again under the chemical shift effect:

After applying trigonometric identities:

$$+I_{1y}\left[\cos^2\left(\Omega_{I_1}\Delta/2\right)+\sin^2\left(\Omega_{I_1}\Delta/2\right)\right] \xrightarrow{\cos^2\theta+\sin^2\theta=1} +I_{1y}$$
 Eq. 1.13

It can be stated that, during the INEPT block, the magnetization does not evolve under the effect of the /chemical shift and therefore it is refocused to its original position.

• Effect of heteronuclear coupling constant (¹J_{I1S}) evolution during the INEPT block

The magnetization evolves during the first $\Delta/2$ delay under the effect of $^1J_{ls}$, the $180^{\circ}(I_x)$ pulse inverts the I_1 magnetization along the x-axis and the $180^{\circ}(S_x)$ pulse inverts the α/β -labels of the doublet /component:

Eq. 1.14

^[57] G. Bodenhausen, R. Freeman, J. Magn. Reson., 1979, 36, 221.

During the second $\Delta/2$ delay, both components evolve again under the $^{1}J_{\rm IS}$ effect:

$$\begin{split} Eq. \, 1.14 & \xrightarrow{\pi \, J_{IS} \, \Delta/2} & + I_{1y} \cos \left(\pi J_{I_1S} \Delta/2\right) \cos \left(\pi J_{I_1S} \Delta/2\right) \\ & - 2 I_{1x} S_z \cos \left(\pi J_{I_1S} \Delta/2\right) \sin \left(\pi J_{I_1S} \Delta/2\right) \\ & - 2 I_{1x} S_z \sin \left(\pi J_{I_1S} \Delta/2\right) \cos \left(\pi J_{I_1S} \Delta/2\right) \\ & - I_{1y} \sin \left(\pi J_{I_1S} \Delta/2\right) \sin \left(\pi J_{I_1S} \Delta/2\right) \end{split}$$
 Eq. 1.15

Regrouping the terms and applying basic trigonometric identities:

$$+ I_{1y}[\cos^{2}(\pi J_{I_{1}S}\Delta/2) - \sin^{2}(\pi J_{I_{1}S}\Delta/2)] \xrightarrow{\cos^{2}\theta - \sin^{2}\theta = \cos 2\theta} I_{1y}\cos(\pi J_{I_{1}S}\Delta)$$

$$-2I_{1x}S_{z}[2\cos(\pi J_{I_{1}S}\Delta/2)\sin(\pi J_{I_{1}S}\Delta/2)] \xrightarrow{2\cos\theta\sin\theta = \sin 2\theta} I_{1y}\cos(\pi J_{I_{1}S}\Delta)$$

$$-2I_{1x}S_{z}\sin(\pi J_{I_{1}S}\Delta)$$
Eq. 1.16

Now, if the effect of homonuclear J_{I1I2} coupling is not considered, a $90^{\circ}(I_{\gamma})$ pulse generates ZZ-magnetization in the form of $2I_{1z}S_z$ and a $90^{\circ}(S_x)$ pulse returns the magnetization to the XY-plane but now converted into AP magnetization of the nucleus S:

$$Eq. 1.16 \xrightarrow{90^{\circ}(I_{y})} + I_{1y} \cos(\pi J_{I_{1}S}\Delta) + 2I_{1z}S_{z} \sin(\pi J_{I_{1}S}\Delta) \xrightarrow{90^{\circ}(S_{x})} I_{1y} \cos(\pi J_{I_{1}S}\Delta) - 2I_{1z}S_{y} \sin(\pi J_{I_{1}S}\Delta)$$

$$Eq. 1.17$$

In summary, during the INEPT block the initial IP $-l_{1y}$ magnetization has been transferred to the S nucleus in the form of AP $2l_{1z}S_y$ magnetization. This coherent heteronuclear magnetization transfer process is the key in most modern multidimensional NMR experiments.

• Effect of homonuclear coupling constant $(J_{11/2})$ evolution during INEPT block

In conventional HSQC experiments, the effects of the homonuclear $J_{17/2}$ evolution during the INEPT blocks are usually neglected because the contribution of the resulting components is considered low. However, a detailed analysis, as described from Eq. 1.11-1.17, leads to the following four terms at the end of the first INEPT period:

$$\begin{split} I_{1z} & \xrightarrow{INEPT} + I_{1y} \cos \left(\pi J_{I_1I_2}\Delta\right) \cos \left(\pi J_{I_1S}\Delta\right) - 2I_{1z}S_y \cos \left(\pi J_{I_1I_2}\Delta\right) \sin \left(\pi J_{I_1S}\Delta\right) \\ & + 2I_{1z}I_{2x} \sin \left(\pi J_{I_1I_2}\Delta\right) \cos \left(\pi J_{I_1S}\Delta\right) + 4I_{1z}I_{2x}S_y \sin \left(\pi J_{I_1I_2}\Delta\right) \sin \left(\pi J_{I_1S}\Delta\right) \end{split}$$
 Eq. 1.18

Thus, the initial I_{1z} magnetization has been converted to four different terms: i) an IP term (I_{1y}), ii) an AP heteronuclear SQC term ($2I_{1z}S_y$), iii) an AP homonuclear SQC term ($2I_{1z}I_{2x}$), and iv) an heteronuclear *Multiple Quantum Coherence* (MQC) term ($4I_{1z}I_{2x}S_y$). Only the second term will be selected by the encoding PGF (G_1 in Figure 10C), which evolves during the I_1 period (step 3 in Figure 10C) according to the heteronuclear chemical shift (Ω_S). By applying an $180^{\circ}(I)$ pulse at the middle of the I_1 period, the evolution of the heteronuclear coupling constant is refocused. Hence at the end of this increment I_1 delay, two different components remain:

$$\xrightarrow{t_1} \begin{array}{c} +2I_{1z}S_y\cos(\Omega_S t_1)\cos(\pi J_{I_1I_2}\Delta)\sin(\pi J_{I_1S}\Delta) \\ -2I_{1z}S_x\sin(\Omega_S t_1)\cos(\pi J_{I_1I_2}\Delta)\sin(\pi J_{I_1S}\Delta) \end{array}$$

Eq. 1.19A

In terms of shift operators⁵⁸ the Eq. 19A can be described as:

$$+ \frac{1}{i} I_{1z} (S^{+} + S^{-}) \cos(\Omega_{S} t_{1}) \cos(\pi J_{I_{1}I_{2}} \Delta) \sin(\pi J_{I_{1}S} \Delta)$$

$$-I_{1z} (S^{+} + S^{-}) \sin(\Omega_{S} t_{1}) \cos(\pi J_{I_{1}I_{2}} \Delta) \sin(\pi J_{I_{1}S} \Delta)$$

Eq. 1.19B

As it is described in Eq.1.10, G_1 and G_2 gradients select the E/A pathways in alternate acquisitions to obtain the N-type (S^{+} , echo) and P-type (S, antiecho).

Then, two simultaneous $90^{\circ}(I_x)$ and $90^{\circ}(S_x)$ pulses are applied:

$$Eq. 1.19A \xrightarrow{90^{\circ} (I_x)} -2I_{1y}S_z \cos(\Omega_S t_1) \cos(\pi J_{I_1I_2}\Delta) \sin(\pi J_{I_1S}\Delta) +2I_{1y}S_x \sin(\Omega_S t_1) \cos(\pi J_{I_1I_2}\Delta) \sin(\pi J_{I_1S}\Delta)$$

Eq. 1.20

Finally, these two components evolve again under chemical shift, homonuclear and heteronuclear coupling constant effects during the Δ delay of the refocused 13 C-to- 1 H

$$I^{+} = I_{x} + iI_{y}$$
 $I_{x} = \frac{1}{2}(I^{+} + I^{-})$
 $I^{-} = I_{x} - iI_{y}$ $I_{y} = \frac{1}{2i}(I^{+} + I^{-})$

^[58] To describe the effects of PFGs, it is convenient to convert the Cartesian operators I_x and I_y in terms of raising and lowering operators I_y and I_z :

Introduction: HSQC and HSQMBC

INEPT block (step 4 in Figure 10C). A decoding PGF (G_2 in Figure 10C) is applied prior to acquisition, which only will select those CTPs involving SQCs of the /spin. The observable magnetization for the heteronuclear three spin system can be described as a mixture of IP and AP components as follows:

$$\begin{split} & + I_{1x} \cos^2(\pi J_{I_1 I_2} \Delta) \sin^2(\pi J_{I_1 S} \Delta) & \text{Term I} \\ & - 2 I_{1y} S_z \cos^2(\pi J_{I_1 I_2} \Delta) \sin(\pi J_{I_1 S} \Delta) \cos(\pi J_{I_1 S} \Delta) & \text{Term II} \\ & + 2 I_{1y} I_{2z} \cos(\pi J_{I_1 I_2} \Delta) \sin(\pi J_{I_1 I_2} \Delta) \sin^2(\pi J_{I_1 S} \Delta) & \text{Term III} \\ & + 4 I_{1y} I_{2z} S_z \cos(\pi J_{I_1 I_2} \Delta) \sin(\pi J_{I_1 I_2} \Delta) \cos(\pi J_{I_1 S} \Delta) & \text{Term IV} \end{split}$$

Eq. 1.21

The IP term I is the more relevant in HSQC spectra, showing an amplitude signal dependence to a $\cos^2(\pi J_{I_1I_2}\Delta)\sin^2(\pi J_{I_1S}\Delta)$ function.

2D HSQC cross-peaks can show strongly distorted twist-phased patterns along the detected F2 dimension due to these unwanted AP components (terms II, III and IV). These terms arise from two main factors:

- The mismatch between the experimental value of Δ delay (ideally optimized to single J value, accordingly to $\Delta=1/(2^1J_{CH})$ and the magnitude of the different $^1J_{CH}$, because Δ may not simultaneously satisfy the heteronuclear coupling arising for different spins of the molecule. This affects all terms having AP heteronuclear components (term II and IV).
- The evolution under the homonuclear coupling constants during the INEPT and refocused INEPT periods. This affects terms having AP homonuclear components (term III and IV).

In practice, the magnitudes of $^1J_{CH}$ (120–250 Hz) are generally more than one order of magnitude larger than J_{HH} (0–15 Hz) therefore, the deleterious effects of J_{HH} on the detected signal have usually been neglected in HSQC experiments. Table 2 shows the theoretical contribution of each term of Eq. 1.21 to the final detected signal in a conventional HSQC experiment assuming J_{H1H2} = 10 Hz and 30 Hz.

Towns	Contribution (%)		
Term –	<i>J</i> _{HH} =10Hz	<i>J</i> _{HH} =30Hz	
1	85.1	70.1	
II	4.8	3.9	
III	9.6	24.5	
IV	0.5	1.4	

Table 2: Effect of $J_{\rm HH}$ on the different magnetization components to the detected signal in a conventional HSQC experiment ($^1J_{\rm CH1}$ =145 Hz; Δ =3.6 ms).

Phase distortions in 2D cross peaks are a huge source of error when a precise and accurate measurement of homo- and heteronuclear coupling constants or volume integrations are carried out. On the other hand, the complex signal intensity dependence also hinders any attempt for the quantitative analysis of HSQC datasets. Therefore, to solve or minimize these problems the design of more robust and improved J_{HH} and J_{CH} -compensated HSQC sequences are strongly required.

Applying broadband heteronuclear decoupling during the acquisition in HSQC experiments presents several advantages: (i) substantial spectral simplification due to the heteronuclear J splitting is removed, (ii) improved SNR due to the collapse of the multiplets to singlets, and (iii) the phase distortion problems due to AP contributions of J_{CH} are removed. As it was mentioned before, a mixture of IP and AP components are available just prior to the acquisition (see Eq.1.21). Under heterodecoupling conditions, terms II and IV in Eq. 1.21 are converted to non-observable MQCs. Therefore, only two terms will contribute to the final signal detected:

$$+ I_{1x} \cos^2(\pi J_{I_1 I_2} \Delta) \sin^2(\pi J_{I_1 S} \Delta)$$
 Term I
$$+ 2I_{1y} I_{2z} \cos(\pi J_{I_1 I_2} \Delta) \sin(\pi J_{I_1 I_2} \Delta) \sin^2(\pi J_{I_1 S} \Delta)$$
 Term III

Eq. 1.22

1.2.1.2. HSQC with PEP: improved sensitivity

The *Preservation of Equivalent Pathways* (PEP) methodology⁵⁹ is based on the implementation of a second refocused INEPT (90° shifted in relation to the first refocused

^[59] L. E. Kay, P. Keifer, T. Saarinen, *J. Am. Chem. Soc.*, **1992**, *114*, 10663.

INEPT) into the regular HSQC pulse sequence (Figure 11), which allows to obtain a maximum sensitivity enhancement by a factor of $\sqrt{2}$ for IS spin systems.

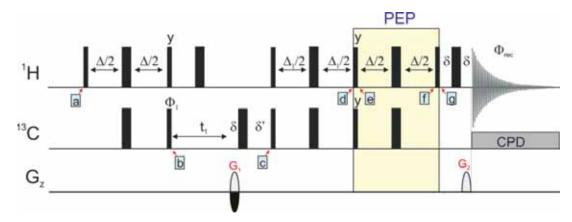


Figure 11: $^{1}\text{H}-^{13}\text{C}$ HSQC-PEP pulse sequence using the E/A method. $\Delta=1/(2^{1}J_{\text{CH}})$, $\Delta_{1}=\Delta$ for CH multiplicities, $\Delta_{1}=1/(4^{1}J_{\text{CH}})$ for all multiplicities. A basic two-step phase cycling is executed with $\Phi_{1}=x$,-x and $\Phi_{\text{rec}}=x$,-x. Coherence selection is performed by the gradient pair $G_{1}:G_{2}$ ($\pm 80:20.1$) using the echo-antiecho protocol.

For a simple *IS* spin system, the most important magnetization components at different points of the HSQC-PEP sequence are:

Point a	Point b	Point c		
$+I_z$	$+ I_y \cos(\pi J_{IS}\Delta)$	$-2I_zS_y\cos(\Omega_St_1)\sin(\pi J_{IS}\Delta)$		
	$-2I_zS_v\sin(\pi J_{IS}\Delta)$	$+2I_zS_x\sin(\Omega_St_1)\sin(\pi J_{IS}\Delta)$		

Eq. 1.23

In the original HSQC experiment, the conventional refocused INEPT converts the AP term $2I_zS_y$ into detectable IP proton magnetization (I_x) while the AP $2I_zS_x$ term is converted into non-observable $2I_yS_x$ MQCs (point d). At this point, a second refocusing INEPT is added in the HSQC-PEP version to recover this MQC. The strategy is based on keeping momentarily the observable magnetization I_x along to the I_z -axis I_z , whereas the I_z -axis (I_z), whereas the I_z -axis converted into AP I_z -axis (I_z), whereas the

$$\xrightarrow{r \, INEPT} \begin{array}{c} +I_x \cos(\Omega_S t_1) \sin(\pi J_{IS} \Delta) \sin(\pi J_{IS} \Delta_1) & \xrightarrow{90^{\circ} \, (I_y)} & +I_z \cos(\Omega_S t_1) \sin(\pi J_{IS} \Delta) \sin(\pi J_{IS} \Delta_1) \\ +2I_y S_x \sin(\Omega_S t_1) \sin(\pi J_{IS} \Delta) & & +2I_y S_z \sin(\Omega_S t_1) \sin(\pi J_{IS} \Delta) \end{array}$$

$$\begin{array}{c} \text{Point d} & \text{Point e} \end{array}$$

Eq. 1.24

After the second refocused INEPT (point f), the $2I_yS_z$ term evolves to IP magnetization in the form of I_x , while the I_z term is still kept along the *z*-axis. Finally, a 90° I_x converts the I_z term to I_y magnetization whereas the other I_x term is not affected (point g):

$$\xrightarrow{\Delta/2 - 180^{\circ}(I_{x}), 180^{\circ}(S_{x}) - \Delta/2} + I_{z} \cos(\Omega_{S}t_{1}) \sin(\pi J_{IS}\Delta) \sin(\pi J_{IS}\Delta_{1})$$

$$+ I_{x} \sin(\Omega_{S}t_{1}) \sin^{2}(\pi J_{IS}\Delta)$$

Because two orthogonal magnetization terms with sine and cosine modulation are retained in each acquisition, the detected signal is sine/cosine phase-modulated and therefore, a sensitivity enhancement of $\sqrt{2}$ is obtained when compared with the conventional HSQC pulse sequence. Very importantly, such gain is retained even by the use the E/A method because the experiment is fully compatible with the phase-modulated nature of the signals. Nevertheless, it is not possible to completely refocus both magnetization terms for all multiplicities⁶⁰ so that the Δ_1 delay must be adjusted accordingly to the maximum sensitivity enhancement that can be reached for a given spin system. When only /S pairs are to be observed, the INEPT delays should be optimized to $\Delta = \Delta_1 = 1/(2J_{\text{IS}})$, whereas for the detection of all multiplicities (/S, I_2S and I_3S) the Δ_1 period should be reduced to an average $1/(4J_{\text{IS}})$ value.

1.2.1.3. Measurement of heteronuclear ${}^{1}J_{CH}/{}^{1}T_{CH}$ coupling constants

Heteronuclear one-bond (${}^{1}J_{CH}$) and long-range coupling constants (${}^{n}J_{CH}$; n>1) are important parameters in the structural, stereochemical, and conformational analysis of small- medium-sized organic compounds, natural products and biomolecules. ${}^{1}J_{CH}$ are related to the S-character of the CH bond and, for instance, can be key tools for the rapid characterization of anomeric centers in carbohydrates or to identify acetylenic functional groups, among others. Two-bond coupling constants (${}^{2}J_{CH}$) can be experimentally

^[60] J. Schleucher, M. Schwendinger, M. Satller, P. Schmidt, O. Schedletzky, S. J. Glaser, O. W. Sorensen, C. Griesinger, J. Biomol. NMR, 1994, 4, 301.

^[61] R. H. Contreras, J. E. Peralta, Prog. Nucl. Magn. Reson. Spectrosc., 2000, 37, 321.

^[62] a) I. Tvaroska, F. R. Taravel, Carbohydr. Res., 1991, 221, 83. b) S. Uhrinova, D. Uhrin, T. Liptaj, J. Bella, J. Hirsch, Magn. Reson. Chem., 1991, 29, 912. c) I. Tvaroska, F. R. Taravel, J. Biomol. NMR, 1992, 2, 421. d) N. C. Maiti, Y. P. Zhu, I. Carmichael, V. E. Anderson, J. Org. Chem., 2006, 71, 2878.

correlated with substitution patterns and bond orientations in ${}^{1}\text{H-C-}{}^{13}\text{C-X}$ spin systems. On the other hand, three-bond coupling constants (${}^{3}\mathcal{J}_{\text{CH}}$) can be correlated with dihedral angles in ${}^{1}\text{H-C-C-}{}^{13}\text{C}$ spin systems following classical Karplus-type relationships. 63

In recent years, it has appeared an enormous interest for the measurement of *Residual Dipolar Coupling* (RDC) constants, especially one-bond proton—carbon RDC constants ($^1D_{CH}$) in small molecules dissolved in weakly aligned anisotropic media. 64 RDCs are anisotropic NMR parameters, which become observable if the compound in question is (marginally) oriented with respect to the magnetic field. If the degree of order is very small, the dipolar coupling interaction D is scaled down by the same factor affording a residual dipolar coupling value. In these cases RDCs are obtained from the difference in multiplet splitting between anisotropic (T = J + D) and isotropic samples (J). As they are calculated from the difference of two coupling constants it is of prime importance to measure J and T with high accuracy and precision. Due to their global orientation information content, RDCs have shown significant impact on the structure determination of large label biomolecular and natural abundance organic compounds. 64

The HSQC experiment has been largely used for the sensitive measurement of ${}^{1}\mathcal{J}_{CH}$ / ${}^{1}\mathcal{T}_{CH}$ coupling constants in solution and anisotropic media, respectively. ${}^{1}\mathcal{J}_{CH}$ values are large in magnitude (in the range of 120–250 Hz) and positive in sign, and they can be quickly measured for the large doublet observed in F1- or F2-heterocoupled HSQC spectra. In the case of ${}^{n}\mathcal{J}_{CH}$, their values are in the same range as \mathcal{J}_{HH} , typically between 0 and 15 Hz, and they are more complicated to measure. Nowadays, both ${}^{1}\mathcal{J}_{CH}$ and ${}^{n}\mathcal{J}_{CH}$ coupling constants can be efficiently measured by modern NMR methods based on HSQC-and HMBC/HSQMBC-related methods.

The nature of a cross-peak coupling pattern obtained from a particular NMR experiment is an important factor that must be taken into account when measuring quantitatively ${}^{1}J_{CH}$ or ${}^{n}J_{CH}$. Different methodologies to extract coupling constants values according to their coupling pattern can be devised, as illustrated in Figure 12.

^[63] R. Aydin, H. Günther, *Magn. Reson. Chem.*, **1990**, *28*, 448.

^[64] a) S. Uhrinova, D. Uhrin, T. Liptaj, J. Bella, J. Hirsch, Magn. Reson. Chem., 1991, 29, 912. b) C. M. Thiele, Concepts Magn. Reson. Part A, 2007, 30, 65. c) C. M. Thiele, Eur. J. Org. Chem., 2008, 34, 5673. d) G. Kummerlowe, B. Luy, Trends Anal. Chem., 2009, 28, 483. e) G. Kummerlowe, B. Luy, Annu. Rep. NMR Spectrosc., 2009, 68, 193. f) R. R. Gil, Angew. Chem. Int. Ed., 2011, 50, 7222.

^[65] a) N. Tjandra, A. Bax, Science, 1997, 278, 1111. b) M. Blackledge, Prog. Nucl. Magn. Reson. Spectrosc., 2005, 46, 23.
c) J. R. Tolman, K. Ruan, Chem. Rev., 2006, 106, 1720. d) A. Annila, P. Permi, Concepts Magn. Reson., 2004, 23A, 22.
e) M. Ottiger, F. Delaglio, A. Bax, J. Magn. Reson., 1998, 131, 373. f) M. H. Lerche, A. Meissner, F. M. Poulsen, O. W. Sorensen, J. Magn. Reson., 1999, 140, 259. g) L. S. Yao, J. F. Ying, A. Bax, J. Biomol. NMR, 2009, 43, 161.

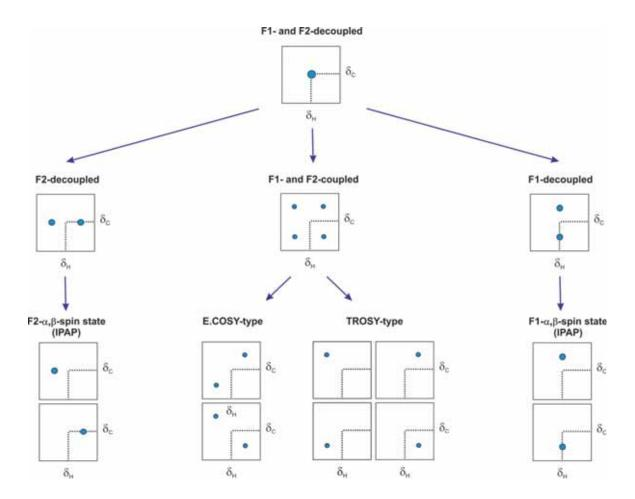


Figure 12: Coupling patterns obtained for a CH cross-peak in different 2D HSQC-type spectra.

HSQC-based pulse schemes have been generally chosen for measuring ${}^{1}J_{CH}/{}^{1}T_{CH}$ but the accuracy and the simplicity on these experimental determinations are subjects of discussion. Some topics of recent interest have been:

- The design of general and robust NMR methods that works efficiently for all multiplicities.
- ii. The discussion about whether the ${}^{1}J_{CH}/{}^{1}T_{CH}$ splitting should be measured from the direct F2 (${}^{1}H$) or the indirect F1 (${}^{13}C$) dimension of a coupled 2D HSQC spectrum.
- iii. The optimum measurement when large variations of $^1J_{CH}/^1T_{CH}$ values are present.
- iv. The accurate measurement of ${}^{1}J_{CH}/{}^{1}T_{CH}$ for individual protons in diastereotopic CH₂ or NH₂ groups.
- v. The simultaneous determination of additional coupling constants from the analysis of the same cross-peak, being the maximum interest the sign-sensitive determination of geminal ${}^2J_{HH}/{}^2T_{HH}$ values.
- vi. The detection and recognition of the presence of undesired strong coupling effects and evaluation of their influence on the accuracy of the measurement.

CLIP-HSQC: Measurement of ¹J_{CH} along the detected F2 dimension

The easier method to measure ${}^1J_{\text{CH}}/{}^1T_{\text{CH}}$ is from the detected dimension of a conventional HSQC experiment recorded without heteronuclear decoupling during proton acquisition, referred to as F2-coupled HSQC experiment (Figure 13A). The main advantages of such an approach are (i) its easy and direct measurement due to the presence of large doublets (Figure 13C), (ii) the high levels of digital resolution readily available in the proton dimension, and (iii) different peaks belonging to diastereotopic CH₂ groups can be individually analyzed. The main drawback is that signals exhibit the typical $J_{\text{HH}}/T_{\text{HH}}$ multiplet pattern structure along F2 dimension, which can hamper the accurate ${}^1J_{\text{CH}}/{}^1T_{\text{CH}}$ measurement. In addition, broad signals and/or the large contributions of RDCs can generate poorly defined multiplets that make even more difficult accurate measurements.

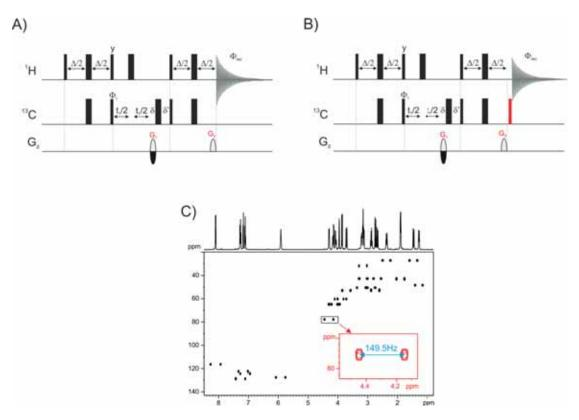


Figure 13: A) F2-coupled HSQC and B) CLIP-HSQC pulse schemes for the measurement of ${}^1J_{\text{CH}}$ along the direct F2 dimension. The interpulse delay Δ is set to $1/(2^1J_{\text{CH}})$ and a basic two-step phase cycling is executed with Φ_1 = x,-x and Φ_{rec} = x,-x. Gradients for coherence selection using the E/A protocol are represented by G_1 and G_2 (G_1 : G_2 =±80:20.1) and δ stands for the duration and the gradient and its recovery delay. The final 90° (13 C) stands for the so-called CLIP pulse to remove heteronuclear AP contributions. C) F2-coupled CLIP-HSQC spectrum of strychnine [2] recorded in a 500 MHz spectrometer. The magnitude of $^{1}J_{\text{CH}}$ can be easily measured from the large clean IP doublet observed along the detected dimension, as shown in the inset.

The effects on the phase and the intensity observed in different HSQC cross-peaks as a function of the magnitudes of J_{HH_1} $^1J_{CH}$, and the delay Δ optimization for several

F2-heterocoupled HSQC schemes can be monitored from 1D spectral simulations (Figure 14A). Thus, the phase anomalies observed in conventional F2-heterocoupled HSQC cross-peaks (Figure 14A) result from the mismatch between the optimized Δ delay and the active ${}^{1}J_{CH}$ value (terms II and IV derived in Eq. 1.21), and from the evolution of J_{HH} during the INEPT periods (term III and IV in Eq. 1.21). Such distortions limit any attempt to realize an accurate analysis in terms of signal quantification via peak integration or direct measurement of ${}^{1}J_{CH}$ and J_{HH} magnitudes.

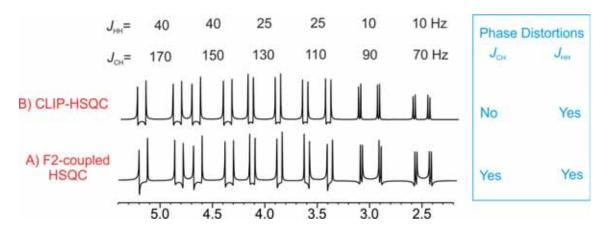


Figure 14: Simulated 1D spectra showing the phase peak distortion effects in 140-Hz optimized A) F2-heterocoupled HSQC and B) CLIP-HSQC spectra. Six protons belonging to three different diastereotopic CH₂ groups have been simulated with a wide range of J_{HH} and $^1J_{CH}$ values, as shown in the upper part.

A simple solution to partially solve these phase distortions was proposed with the *CLean In-Phase* HSQC (CLIP-HSQC) experiment⁶⁶ which applies a 90° ¹³C pulse (from the *x*-axis) just prior the acquisition (Figure 13B). In this way, the AP contributions due to ${}^{1}\mathcal{L}_{H}$ are converted to MQCs (terms IIa and IVa) and, apparently, clean IP patterns should be obtained in the absence of any \mathcal{L}_{HH} coupling (term IIIa).

$$\begin{split} Eq. \, 1.21 \\ & \qquad \qquad \downarrow \quad 90^{\circ} \, (C_x) \\ & \qquad \qquad + \, H_{1x} \cos^2 \! \left(\pi J_{H_1 H_2} \Delta \right) \sin^2 \! \left(\pi J_{H_1 C} \Delta \right) & \qquad \text{Term Ia} \\ & \qquad \qquad + \, 2 H_{1y} C_y \cos^2 \! \left(\pi J_{H_1 H_2} \Delta \right) \sin \! \left(\pi J_{H_1 C} \Delta \right) \cos \! \left(\pi J_{H_1 C} \Delta \right) & \qquad \text{Term IIa} \\ & \qquad \qquad \qquad - \, 2 H_{1y} H_{2z} \cos \! \left(\pi J_{H_1 H_2} \Delta \right) \sin \! \left(\pi J_{H_1 H_2} \Delta \right) \sin^2 \! \left(\pi J_{H_1 C} \Delta \right) & \qquad \text{Term IIIa} \\ & \qquad \qquad - \, 4 H_{1y} H_{2z} C_y \cos \! \left(\pi J_{H_1 H_2} \Delta \right) \sin \! \left(\pi J_{H_1 H_2} \Delta \right) \cos \! \left(\pi J_{H_1 C} \Delta \right) & \qquad \text{Term IVa} \end{split}$$

Eq. 1.26

^[66] A. Enthart, J. C. Freudenberger, J. Furrer, H. Kessler, B. Luy, J. Magn. Reson., 2008, 192, 314.

However, in the presence of J_{HH} , a mixture of observable IP (term Ia) and AP components (term IIIa) are still active, as shown in the simulated spectrum of Figure 14B. In practice, due to the large difference of magnitudes between $^1J_{CH}$ and J_{HH} , these unwanted contributions are small and they have been traditionally omitted in cross-peak analysis in CLIP-HSQC or F2-heterodecoupled HSQC experiments. A simple calculation shows that these effects may become important. For instance, the relative percentage of the term IIIa with respect to Term Ia in a 140-Hz optimized CLIP-HSQC experiment is of 5.6% and 17% for J_{HH} values of 5 and 15 Hz, respectively. Such percentages can be more pronounced when measuring RDCs in anisotropic media, where higher J_{HH} values are usually involved.

The CLIP-HSQC experiment (Figure 13B) proves to be an efficient tool to determine the ${}^{1}J_{CH}/{}^{1}T_{CH}$ value from the resulting clean in-phase doublets. However, strong J_{HH} coupling effects can generate a high degree of asymmetry between the high- and low-field multiplet lines in F2-coupled HSQC spectra, which can preclude reliable determination of ${}^{1}J_{CH}/{}^{1}T_{CH}$ coupling constants values. This drawback has already been described, particularly for CH spin systems in carbohydrates or on the typical strong geminal interaction found in diastereotopic CH_2 spin systems, and some practical solutions have been proposed.

• BIRD-HSQC: Measurement of ¹J_{CH} along the indirect F1 dimension

The measurement of ${}^{1}J_{\text{CH}}/{}^{1}T_{\text{CH}}$ exclusively along the indirect F1 dimension of a HSQC spectrum is recommended to avoid the interferences of $J_{\text{HH}}/T_{\text{HH}}$ splittings, but a major inconvenient arises for the need of a large number of t_{1} increments, and therefore longer acquisition times. The successful use of *Non-Uniform Sample* (NUS) techniques, ${}^{68}J_{\text{Scaling}}$ factors or spectral folding/aliasing can speed up data acquisition and/or increase the digital resolution in the F1 dimension. Several F1-coupled HSQC pulse schemes have been compared and evaluated by Thiele and Bermel. 69 The most simple approach results from the removing of the central 180° H pulse placed in the middle of the t_{1} evolution period in the conventional HSQC experiment, referred to as F1-coupled HSQC experiment

^[67] a) C. M. Thiele, J.Org. Chem., 2004, 69, 7403. b) B. W. Yu, H. van Ingen, S. Vivekanandan, C. Rademacher, S. E. Norris, D. I. Freedberg, J. Magn. Reson., 2012, 215, 10. c) B. W. Yu, H. van Ingen, D. I. Freedberg, J. Magn. Reson., 2013, 228, 159. d) P. Tzvetkova, S. Simova, B. Luy, J. Magn. Reson., 2007, 186, 193. e) K. Fehér, S. Berger, K. E. Kövér, J. Magn. Reson., 2003, 163, 340.

^[68] a) K. Kazimierczuk, V. Y. Orekhov, *Angew. Chem. Int. Ed.*, **2011**, *50*, 5556. b) K. Kazimierczuk, W. Kozminski, I. Zhukov, *J. Magn. Reson.*, **2006**, *179*, 323.

^[69] C. M. Thiele, W. Bermel, J. Magn. Reson., 2012, 216, 134.

(Figure 15A). A more convenient method incorporates a G-BIRD^x module (Figure 15B) to allow the simultaneous evolution of both ${}^1J_{\text{CH}}/{}^1T_{\text{CH}}$ (with optional k scaling factor) and ${}^{13}\text{C}$ chemical shift evolution while contributions from ${}^{n}J_{\text{CH}}/{}^{n}T_{\text{CH}}$ are efficiently refocused. ^{69e} The better line shapes along the indirect dimension allow the determination of ${}^{1}J_{\text{CH}}/{}^{1}T_{\text{CH}}$ by simply measuring the frequency difference between the peak maxima of singlets instead of the centers of complex multiplets.

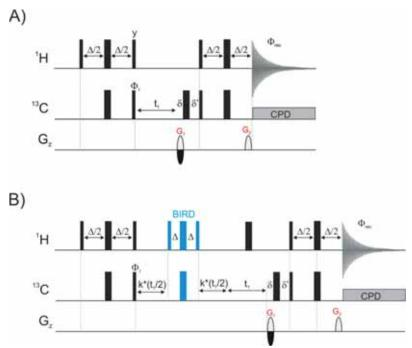


Figure 15: Several pulse schemes to achieve F1-heterocoupled HSQC spectra: A) F1-coupled HSQC, and B) F1-coupled BIRD-HSQC. The interpulse delay in INEPT and BIRD elements are optimized according to Δ =1/(2 $^{1}J_{\text{CH}}$). A minimum two-step phase cycling is executed with Φ_{1} =x,-x and Φ_{rec} = x,-x, all other unlabeled pulses are from the x-axis. Gradients G_{1} and G_{2} are used for coherence selection using E/A (G_{1} : G_{2} =±80:20.1).

The accurate measurement of the two ${}^1J_{\text{CH}}/{}^1T_{\text{CH}}$ values and particularly the geminal ${}^2J_{\text{HH}}/{}^2T_{\text{HH}}$ coupling in diastereotopic C_{HAHB} groups has always been a challenging task, particularly for F1-coupled HSQC experiments. Several methods have been proposed for measuring them either from the F1 or from the F2 dimension, but they all present some drawbacks that have prevented their general use. For instance, the passive ${}^1J_{\text{CHB}}/{}^1T_{\text{CHB}}$ value can be separately measured into the active H_A cross-peak, and vice versa, along the F1 dimension of a J-resolved HMQC experiment. To In addition, the large doublet is further split by the ${}^2J_{\text{HAHB}}/{}^2T_{\text{HAHB}}$ coupling yielding a doublet of doublets. The disadvantage is that additional experiments can be required to measure ${}^1J_{\text{CH}}/{}^1T_{\text{CH}}$ for CH or CH $_3$ spin systems, and significant distortions on the cross-peaks (banana shape peaks) are frequently observed in the spectra of complex small molecules. Another important group of NMR experiments are those based on spin-state selection specifically designed for methylene

^[70] K. E. Kövér, K. Fehér, J. Magn. Reson., 2004, 168, 307.

groups that yield simplified coupling patterns, and where the sign and the magnitude of the geminal $^2J_{HH}/^2T_{HH}$ can sometimes be additionally extracted.⁷¹

1.2.2. The HSQMBC experiment

The Heteronuclear Multiple Bond Correlation (HMBC)⁷² and the Heteronuclear Single Quantum Multiple-Bond Correlation (HSQMBC) experiment⁷³ are the long-range optimized versions of the HMQC and HSQC experiment, respectively. They provide heteronuclear correlations between protons and both protonated and non-protonated carbon atoms separated by more than one bond, (usually two- and three-bond correlations). Long-range proton-carbon correlations routinely extracted from HMBC and HSQMBC spectra are key elements in the structural characterization of small and medium-sized molecules in solution.⁷⁴ The HMBC experiment usually gives better sensitivity ratios but, in many cases, the equivalent HSQMBC is the preferred technique because it generally affords a better performance in terms of simplicity, peak phase behavior and pulse sequence analysis.

Additionally, the measurement of $^{n}J_{CH}$ (n>1) has been another hot topic of interest in small molecule NMR.⁷⁵ Typically, the $^{n}J_{CH}$ values cover a range from 0 to 15 Hz and this makes that HMBC and HSQMBC experiments present some additional problems compared to their analogs HMQC and HSQC experiments, respectively:

i. HMBC/HSQMBC experiments are usually optimized to 5-8 Hz, which means that the inter-pulse delay lasts about 50-70 ms, whereas in HSQC/HMQC pulse sequences such delay is about 3.5 ms (usually optimized to $^1\mathcal{L}_{CH}$ =140 Hz). For that reason, the pulse sequences can become too long and relaxation losses are more severe, especially for molecules with short \mathcal{T}_2 relaxation times. To reduce the duration of the

^[71] a) M. Ottiger, F. Delaglio, J. L. Marquardt, N. Tjandra, A. Bax, J. Magn. Reson., 1998, 124, 365. b) P. Nolis, T. Parella, Curr. Anal. Chem., 2007, 3, 47. c) T. N. Pham, T. Liptaj, K. Bromek, D. Uhrin, J. Magn. Reson., 2002, 157, 200. d) T. Carlomagno, W. Peti, C. Griesinger, J. Biomol. NMR, 2000, 17, 99. e) P. Permi, J. Biomol. NMR, 2002, 22, 27. f) E. Miclet, D. C. Williams Jr., G. M. Clore, D. L. Bryce, J. Boisbouvier, A. Bax, J. Am. Chem. Soc., 2004, 126, 10560. g) G. Guichard, A. Violette, G. Chassaing, E. Miclet, Magn. Reson. Chem., 2008, 46, 918. h) T. Parella, M. Gairí, J. Am. Chem. Soc., 2004, 126, 9821. i) P. Permi, J. Magn. Reson., 2001, 153, 267. j) E. Miclet, E. O'Neil-Cabello, E. P. Nikonowicz, D. Live, A. Bax, J. Am. Chem. Soc., 2003, 125, 15740. k) P. Nolis, J. F. Espinosa, T. Parella, J. Magn. Reson., 2006, 180, 39.

^[72] A. Bax, M. Summers. J. Am. Chem. Soc., 1986, 108, 2093.

^[73] a) R. Marek, L. Kralik, V. Sklenar. *Tetrahedron Lett.*, **1997**, *38*, 665. b) R. T. Williamson, B. L. Márquez, W.H. Gerwick, K. E. Kover, *Magn. Reson. Chem.*, **2000**, *38*, 265.

^[74] R. C. Breton, W. F. Reynolds, *Nat. Prod. Rep.*, **2013**, *30*, 501.

^[75] a) B. L. Márquez, W. H. Gerwick, R. T. Williamson, *Magn. Reson. Chem.*, **2001**, *39*, 499. b) T. Parella, J. F. Espinosa, *Prog. Nucl. Magn. Reson. Spectrosc.*, **2013**, *73*, 17.

sequence as much as possible, these experiments are usually recorded under non-refocusing conditions and the resulting cross-peaks present AP multiplet pattern with respect to the active $^{n}J_{CH}$.

ii. Since J_{HH} and $^{n}J_{CH}$ values have similar sizes, simultaneous evolutions of J_{HH} and $^{n}J_{CH}$ during the inter-pulse delays generate mixtures of IP and AP magnetization components. This results in highly phase-distorted and complex cross-peaks and can produce important reduction of signal intensities due to signal cancellation, which can lead to difficult data analysis.

1.2.2.1. Basic HSQMBC pulse scheme

Similarly to HSQC, the HSQMBC experiment is based on the heteronuclear polarization INEPT transfer through $^{n}J_{CH}$, via the selection of SQCs during the t_1 period. The transfer mechanism allows to obtain long-range heteronuclear correlations between protons and both protonated and non-protonated carbon atoms (Figure 16). Experimentally, the only requirement is the re-optimization of the inter-pulse Δ delay to a small coupling value, about typically 5–8 Hz (Figure 16C). Under these conditions, the undesired effects of J_{HH} evolution during the long INEPT periods become very important because the magnitudes of J_{HH} and $^{n}J_{CH}$ coupling values are similar in size. The HSQMBC experiment has been traditionally used in a non-refocused mode 73b to minimize losses by T_2 relaxation.

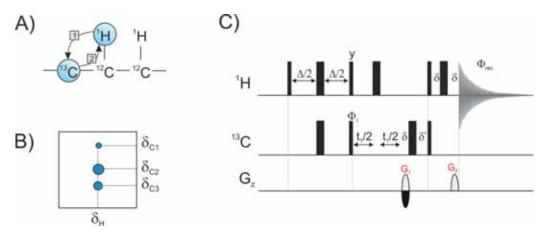


Figure 16: Schematic representation of the A) transfer mechanism; B) cross-peak pattern and C) pulse sequence of the standard non-refocused HSQMBC experiment. Thin and thick vertical rectangles represent 90° and 180° hard pulses, respectively. The delay Δ should be set to $1/(2^{n}J_{CH})$ and δ represents the duration of the PFG and its recovery delay. Coherence selection is performed by the gradient pair G_{1}/G_{2} using the E/A protocol (G_{1} : G_{2} =±80:20.1). A basic two-step phase cycling is executed with Φ_{1} = x,-x and Φ_{rec} = x,-x.

Introduction: HSQC and HSQMBC

HSQMBC has a great advantage with respect to the HMBC experiment because J_{HH} evolution is not present during the t_1 period. In addition, data can be presented in a phase sensitive mode with pure absorption lineshapes which means that is perfectly suitable for easy measurement of $^nJ_{CH}$.

The PO analysis of the HSQMBC pulse sequence is exactly like HSQC (see section 1.2.1.1.), the only change is that the interpulse Δ delay of the INEPT block is adjusted to $^{n}J_{CH}$ instead of $^{1}J_{CH}$ and the refocused INEPT period is not applied. So that, if a weakly coupled $H_{1}H_{2}C$ spin system is considered, the observable magnetization just before acquisition can be described as:

$$-2H_{1y}C_z\cos(\pi J_{H_1H_2}\Delta)\sin(\pi^n J_{H_1C}\Delta)$$
 Eq. 1.27

In the case of a refocused HSQMBC, the detected signal is described as shown in Eq. 1.21. As a result, the cross peaks of the 2D $^{1}\text{H-}^{13}\text{C}$ HSQMBC spectrum appear phase distorted because of the AP character with respect to $^{n}J_{\text{CH}}$ (term II and IV) and J_{HH} (term III and IV) modulations during the long INEPT period. Table 3 shows the contribution of each term to the final detected signal in a refocused HSQMBC experiment:

Table 3: Contribution of each magnetization to the final detected signal in a conventional HSQMBC experiment ($^{n}J_{CH1}$ = 6 Hz, J_{H1H2} = 10 Hz, Δ = 62.5 ms)

Term	Contribution (%)
I	20.7
II	8.6
Ш	50.0
IV	20.7

In addition, cross-peak intensities in HSQMBC strongly depend on the mismatch between Δ optimization and the corresponding $^nJ_{CH}$ values and also on the potential losses by T_2 relaxation. The hard analysis of these complex multiplets has prevented its general use as a routine task.

1.2.2.2. Improvements in HSQMBC experiments

Due to the above mentioned problems associated to the simultaneous evolution of J_{HH} and $^{n}J_{CH}$ coupling constants during the INEPT blocks, several improvements have been proposed, specially focused on the easy measurement of $^{n}J_{CH}$, without need of sophisticated and time-consuming post-processing tasks. Some of these new HSQMBC experiments are described below.

Implementing BIRD block: BIRD-HSQMBC

The BIRD^{4b} element is generally used for two main purposes: (i) to selectively observe protons bound to 13 C and suppress those bound to 12 C (see section 1.1.1.1.), and (ii) to differentiate direct from long-range heteronuclear correlations thanks to the large difference in their values. As an application of the BIRD^y module, Figure 17B shows the pulse scheme for the HSQMBC-BIRD experiment. It is a non-refocused HSQMBC experiment where the BIRD block is introduce in the middle of the INEPT element to minimize direct $^1J_{CH}$ responses. In addition, J_{HH} are partially refocused (except for $^2J_{HH}$) reducing phase distortions and additional J_{HH} signal modulation in the resulting crosspeaks.

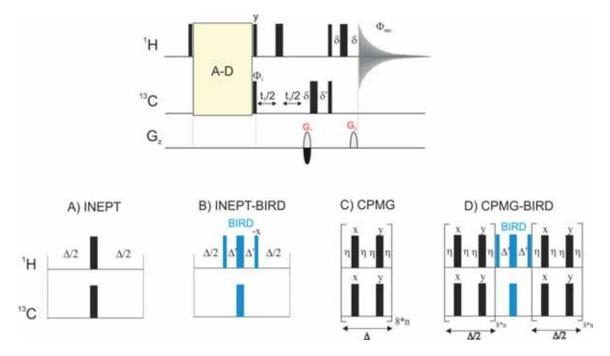


Figure 17: Several 2D non-refocused HSQMBC pulse schemes to obtain heteronuclear long-range correlation spectra (Δ =1/[2ⁿ/_{CH}]). The initial transfer step is: A) a basic INEPT, B) an INEPT-BIRD block (Δ' =1/[2¹/_{CH}]); C) a CPMG XY-16 super cycle consisting of simultaneous ¹H and ¹³C pulses applied at intervals 2 η ; D) a CPMG-BIRD element combining the features described in B and C.

Implementing CPMG pulse train: CPMG-HSQMBC

It has been also reported that by applying a *Carr-Purcell-Maiboom-Gill* (CPMG) pulse train during the INEPT period⁷⁶ (Figure 17C), the $J_{\rm HH}$ evolution can be minimized if the interpulse delay between the π pulses is shortening than $1/2\sqrt{J^2+\Delta\nu^2}$. In case of weak coupling the condition can be approximated as $1/2\Delta\nu_{max}$, where $\Delta\nu_{max}$ is the larger chemical shift difference between the weakly coupled proton partners.

Thus, with the use of the CPMG element the effect of undesired homonuclear J_{HH} modulation from HSQMBC-like sequences could be minimized. However, it has been accepted that J_{HH} coupling constants cannot be completely removed for all spin systems using CPMG due to the need to use a very short delays between pulses ($2\eta < 100~\mu s$). Importantly, the use of very short inter-pulse delays can put in serious troubles the limits of the probehead due to sample heating effects. In addition, it is import to remark that homonuclear TOCSY transfer can be also effective during the CPMG period.

In general, the proposed CPMG-HSQMBC experiment performs better than the original HSQMBC sequence and it has been demonstrated that an efficient measurement of ${}^{n}J_{CH}$ can be carried out. Williamson and co-workers published the BIRD-CPMG-HSQMBC experiment 77 where the concepts of BIRD and CPMG were implemented into the same pulse sequence (Figure 17D) obtaining spectra with minimum distortions.

■ Implementing frequency-selective 180° ¹H pulses: selHSQMBC

Despite the fact that BIRD-HSQMBC and CPMG-HSQMBC experiments have proved efficient for the measurement of $^{n}J_{CH}$ in both protonated and non-protonated carbon atoms, the modulation of the intensity by the homonuclear J_{HH} couplings still remain as the most important drawback to overcome. A very simple solution to avoid such J_{HH} interferences in HSQMBC pulse schemes was proposed by our research group. The central 180° H pulse into the INEPT periods can be replaced by a frequency-selective 180° H pulse (Figure 18A) to prevent the undesired J_{HH} coupling evolution, whereas selective heteronuclear polarization transfer for the selected proton is still achieved. The proposed selective experiment has been implementing in the refocused HSQMBC version

^[76] K. E. Kövér, G. Batta, K. Fehér, *J. Magn. Reson.*, 2006, 181, 89.

^[77] L. Valdemar Jr, V. Gil, M. G. Constantino, C. F. Tormena, R. T. Williamson, B. Marquez, *Magn. Reson. Chem.*, 2006, 44, 95.

^[78] S. Gil, J. F. Espinosa, T. Parella, *J. Magn. Reson.*, **2011**, *213*, 145.

to obtain cross peaks displaying IP coupling pattern with respect to ${}^{n}J_{CH}$. Although that idea can be implemented in the original non-refocused HSQMBC experiment where the resulting cross peaks would present AP coupling pattern with respect to the active ${}^{n}J_{CH}$, accidental line cancelation and/or complex analysis of AP multiplets could still remain, meaning that tedious and time-consuming fitting procedures would be required.

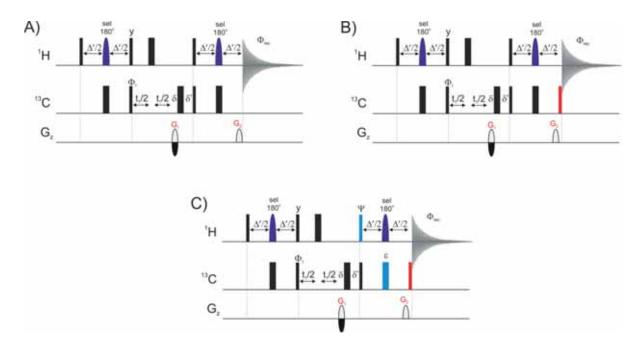


Figure 18: Several 1 H-selective 2D HSQMBC schemes designed to measure long-range proton—carbon coupling constants: A) selHSQMBC; B) CLIP-selHSQMBC; C) CLIP-HSQMBC IPAP. Frequency-selective 180° 1 H pulses represented as shaped pulses are applied in the middle of the INEPT blocks (Δ =1/[2 $^{\rm n}$ / $_{\rm CH}$]= Δ' +p180 where p180 is the duration of the selective 180° 1 H pulse that must be set accordingly to the required selectivity in each case). 1 H data are acquired without 13 C decoupling. In C) the IPAP methodology is applied: two independent IP and AP data are separately collected as a function of the pulses marked with ϵ : IP (Ψ =y and ϵ =on) and AP (Ψ =x and ϵ =off). α / β data are obtained after time-domain addition/subtraction data (AP±IP). A minimum two-step phase cycling is executed with Φ_1 = x,-x and Φ_{rec} = x,-x. All other unlabeled pulses are from the x-axis. Gradients G_1 and G_2 are used for coherence selection using E/A (G_1 : G_2 =±80:20.1).

As it has been shown before, in conventional HSQMBC experiment the observable magnetization just before acquisition can be described as a mixture of IP and AP components (Eq. 1.21). In selHSQMBC experiments the evolution under the $J_{\rm HH}$ is prevented, such that the final magnetization can be described as:

$$+ H_{1x} \sin^2(\pi^n J_{H_1C}\Delta)$$
 IP Term $- 2H_{1y}C_z \sin(\pi^n J_{H_1C}\Delta)\cos(\pi^n J_{H_1C}\Delta)$ AP Term

Eq. 1.28

Introduction: HSQC and HSQMBC

As a result, selHSQMBC cross-peaks show a small AP contribution which distorts the signal phases along the detected F2 dimension. The application of the CLIP technique has been proposed to solve that problem.⁷⁹ The CLIP-HSQMBC experiment yields undistorted IP ¹H multiplets with pure absorptive line shapes along the detected dimension from which the easy, direct, and accurate measurement of ⁿJ_{CH} can be performed. As discussed before for other CLIP experiments, the key point of this sequence is the 90° 13°C pulse applied just prior to acquisition (Figure 18B), which efficiently converts the existing dispersive AP contribution to non-observable MQCs. The resulting cross-peaks show an additional splitting compared to the conventional ¹H multiplet arising from the active proton-carbon coupling because proton acquisition is performed without heteronuclear decoupling (Figure 19A). The magnitude of ⁿJ_{CH} can be extracted directly by analyzing peak frequency separation as usually made for conventional ¹H multiplets. The phase properties of the multiplet and therefore the accurate extraction of ⁿ/_{CH} are independent of experiment optimization, with a small uncertainty of 0.1-0.2 Hz, but important errors of 20-30% should be easily introduced when omitting the CLIP pulse (Figure 19B). In practice, a perfect match between ⁿJ_{CH} and the experiment optimization is not critical, cross-peaks show a clear dependence with the $\sin^2(\pi^n J_{H_1} c\Delta)$ function, and $^n J_{CH}$ values in the range 3-10 Hz can be measured in a 6-8 Hz optimized selHSQMBC experiment (Figure 19B).

For more complex multiplets, the separation of the outer peaks of the multiplet can be compared to that in the 1 H spectrum to extract indirectly the additional splitting. Alternatively, a simple fitting procedure taking the internal satellite 1 J_{CH} component as decoupled reference multiplet can be applied. On the other hand, a double-selective 1D version of a refocused HSQMBC experiment has been also proposed for the fast and accurate measurement of specific n J_{CH} values from pure IP 1D multiplets. 80

^[79] J. Saurí, T. Parella, J. F. Espinosa, Org. Biomol. Chem., 2011, 11, 4473.

^[80] J. F. Espinosa, P. Vidal, T. Parella, S. Gil, *Magn. Reson. Chem.*, 2011, 49, 502.

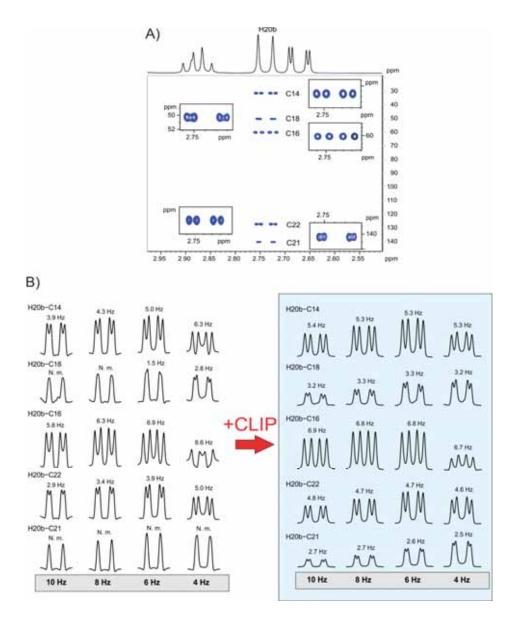


Figure 19: A) 2D CLIP-selHSQMBC spectrum of strychnine [2] after pulsing on H20b with a 20 ms Gaussian-shaped 180° ¹H pulse. The inter-pulse delay Δ was optimized to 62.5 ms (corresponding to $^{\circ}J_{CH} = 8$ Hz). B) Direct extraction of $^{\circ}J_{CH}$ can be made from pure in-phase cross-peaks, independent of experiment optimization (from 4 to 10 Hz).

A powerful alternative for the simple and direct determination of $^{n}J_{CH}$ in broad, unresolved, or highly complex selHSQMBC multiplets is based on the incorporation of the IPAP principle that relies on the separate acquisition of complementary IP and AP datasets⁸¹ (left part of Figure 20). The IP data are generated applying the initial hard 90° ^{1}H pulse of the refocused INEPT (mark in blue) with from *y*-axis (Ψ =y) and the hard 180° ^{13}C pulse (ε =on), whereas the AP data (with a $\sin(\pi^{n}J_{H_{1}C}\Delta)$ signal intensity dependence) are obtained using the same scheme with Ψ =x and omitting the last 180° and 90° ^{13}C pulses to avoid $^{n}J_{CH}$ refocusing (ε =off). Time-domain data combination (IP±AP) affords two

^[81] S. Gil, J.F. Espinosa, T. Parella, *J. Magn. Reson.*, **2011**, *213*, 145.

separate pure-phase α - and β -selHSQMBC subspectra where the $^nJ_{\text{CH}}$ value can be extracted by direct analysis of the relative frequency displacement between these α/β cross-peaks along the highly resolved F2 dimension (right part of Figure 20). In this manner, accurate $^nJ_{\text{CH}}$ values can be easily extracted, irrespective of the multiplet complexity and avoiding the typical overestimation associated to the direct analysis of AP signals or the lack of multiplet definition in IP signals. The success of the IPAP technique relies on the complementarity between the IP and AP data, and the percentage of undesired cross-talk generated during IP \pm AP data combination will be proportional to a $\sin^2(\pi^nJ_{H_1C}\Delta)$ - $\sin(\pi^nJ_{H_1C}\Delta)$ factor. The use of individualized scaling factor (AP $\pm k^*$ IP) factors can compensate unbalanced IPAP cross-peaks. As a bonus, the IPAP methodology offers additional controls to confirm the accuracy of the measurement or the presence of cross-talking. Three different multiplets (IP, AP, and α/β) are available for independent measurements and proper data comparison and validation.

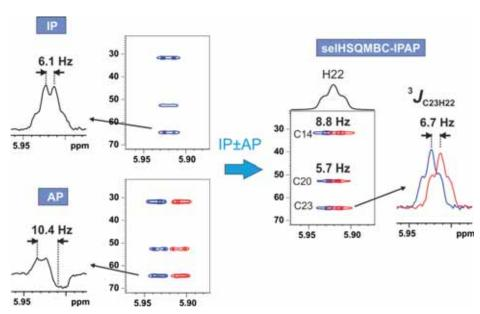


Figure 20: selHSQMBC-IPAP experiments after selective excitation of the olefinic H22 proton in strychnine [2]. The acquired A) IP and B) AP datasets are added/subtracted to provide C) separate α/β subspectra. The relative displacement between α/β cross-peaks along the F2 dimension provides a direct measurement of $^{n}J_{CH}$ without any posterior analysis.

The main limitation of these experiments relies on the selective concept because not all the protons can be simultaneously excited/observed or decoupled/unmodulated at the same time and several experiments may be needed to measure all the targeted couplings. However, multiple protons can be simultaneously studied in a single experiment using region-selective or multiple frequency-selective pulses, provided that all excited protons are not mutually \mathcal{L} -coupled.

As it was mention before, in the case of $^{n}J_{CH}/^{n}T_{CH}$ the values are in the same range as J_{HH}/T_{HH} (ca. 0-15 Hz) and they are more complicated to measure. Most of these available long-range methods rely on the basic HMQC and HSQMBC pulse schemes, or on related hybrid HSQC-TOCSY experiments⁸² with a limited application to protonated carbons. Figure 21 shows different topologies defining the transfer mechanism followed in HSQC/HSQMBC-based experiments designed to measure J_{CH} . In the last few years, several modified selHSQMBC methods (c.a. selHSQMBC-TOCSY⁸³ and selHSQMBC-COSY⁸⁴) have been developed for the measurement of the sing and the magnitude of $^{n}J_{CH}$.

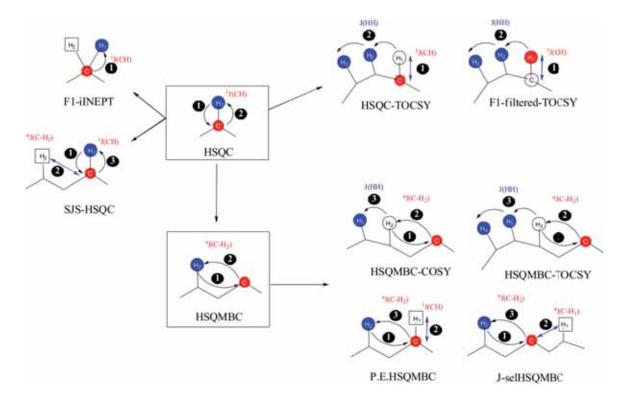


Figure 21: Schematic representation of several spin systems that can be studied by HSQC and HSQMBC type experiments

^[82] W. Kozminski, J. Magn. Reson., 1999, 137, 408.

^[83] J. Saurí, J. F. Espinosa, T. Parella, Angew. Chem. Int. Ed., 2012, 51, 3919.

^[84] J. Saurí, T. Parella, Magn. Reson. Chem., 2012, 50, 717.

2. OBJECTIVES

The general and specific aims of this doctoral thesis are briefly described below:

- Learn the main theoretical, technical and practical aspects of the NMR spectroscopy and acquire experience working on different spectrometers, in the implementation and set-up of NMR experiments and in pulse programming skills. All these knowledge are essential to be able to carry out the rest of the proposed objectives.
- Know, evaluate and compare the existing NMR methods related with the field we
 wanted to study, in order to better understand the advantages/drawbacks of each
 methodology.
- Design of new NMR methods to overcome the different drawbacks/limitations observed in the existing ones and its application to solve real chemical problems. As a starting point, a main objective was especially focused on the development of improved HSQC and HSQMBC experiments to measure coupling constants, with special interest in the determination of small coupling values, their positive/negative sign, and the implementation of fast and accurate methods to extract J values from the direct analysis of multiplets.
- Explore the possibilities of modern NMR methodologies, with special interest in broadband homodecoupled techniques. Analysis of pros and cons, and evaluation of their potential to solve real chemical problems, such as the eternal problem of NMR signal overlap.
- Special interest in optimizing NMR experiments that offer the following basic features:
 - Easy implementation with emphasis to achieve the maximum level of automation.
 - Simple in terms of data acquisition and without extensive and sophisticated set-up and post-processing tasks.
 - General applicability covering a wide range of sample and NMR experimental conditions.
 - Optimal spectral quality in terms of resolution and sensitivity.

3. RESULTS AND DISCUSSION

This section is centered on the experimental results obtained during this doctoral thesis in relation to the development and application of modern pure shift NMR methodologies and improved HSQC and HSQMBC experiments. The results have been published in different scientific journals as ten original research papers. Below, a brief description of each publication is presented:

- In Publication 1 an improved sensitivity-improved slice-selective NMR method based on a multiple-slice excitation concept is proposed. The success of the method is demonstrated by enhancing SNR by more than one order of magnitude in ZS experiments.
- In **Publication 2** a new, fast and full-sensitive pure shift NMR technique, referred to as *HOmodecoupled Band-Selective* (HOBS), is presented. HOBS experiments yields broadband homodecoupled spectra in particular areas of the ¹H spectrum where do not appear mutually \mathcal{F} coupled protons. Implementation on 2D experiments is also illustrated with practical examples.
- Practical applications of the HOBS methodology have been published to differentiate signals with small chemical shift differences, such as shown in the analysis of individual signal intensity decays for measuring \mathcal{T}_1 and \mathcal{T}_2 relaxation times in overlapped regions (Publication 3), in enantiodifferentiation studies by using chiral solvating agents (Publication 4) and in the measurement of long-range heteronuclear coupling constants or the design of pure shift selHSQMBC experiments (Publication 6).
- Introduction to the concept of ultra-high-resolution NMR spectroscopy. It is shown that pure shift HSQC experiments incorporating broadband homonuclear decoupling along the acquisition F2 dimension combined with other resolution-enhanced NMR techniques, such as spectral aliasing or NUS along the indirect F1 dimension improve key NMR features, such as spectral resolution and digital resolution, using standard spectrometer configurations. These new highly-resolved experiments have been applied to determine very small chemical shift differences simultaneously for ¹³C and ¹H in enantiodifferentiation studies (Publication 5) and to analyze highly complex mixtures of very similar stereoisomers exhibiting near-identical ¹H and ¹³C NMR spectra. (Publication 7).

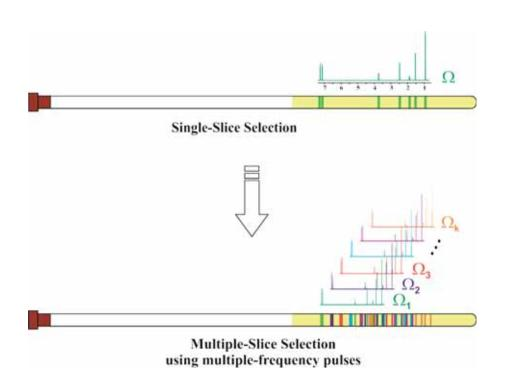
- In **Publication 8**, a new *Pure In-Phase* (PIP) heteronuclear correlation NMR experiment (referred to as PIP-HSQC and PIP-HSQMBC) is proposed as a method to avoid complex data analysis. In these new experiments, all the undesired AP contributions present in conventional HSQC and HSQMBC experiments are efficiently suppressed, obtaining spectra where all the cross-peaks display perfect IP multiple patterns which are suitable for an accurate extraction of scalar *J* couplings and RDCs.
- In **publication 9**, an improved HSQC experiment (referred to as perfect-HSQC) is proposed for the efficient suppression of phase and amplitude J_{HH} modulations. The features of the obtained spectrum allow carrying out an accurate measurement of homo- and heteronuclear scalar and dipolar coupling constants. In addition, guidelines are provided for the future use of HSQC datasets as a quantitative NMR tools by peak volume integration.
- In Publication 10, a compilation and discussion of the different improvements reported for HSQC and HSQMBC experiments in the last years is presented. Some of the new experiments exposed along this doctoral thesis are also included and exemplified with practical examples.

Since every published paper has gone through a review process by chemists and NMR experts, not much attention is devoted to the discussion of the results beyond what is discussed into each original publication. Nevertheless, a little introduction is presented for each one of the published papers.

PUBLICATION 1

Simultaneous multi-slice excitation in spatially encoded NMR experiments

Laura Castañar, Pau Nolis, Albert Virgili and Teodor Parella. *Chem. Eur. J.,* **2013**, *19*, 15472-15475.



Introduction

The most serious drawback of spatially encoded NMR experiments is their reduced SNR because the observed signal only arises from a discrete slice of the sample. Therefore, novel approaches are required to improve the inherent low SNR of slice-selective NMR experiments and make them of practical and general use with moderately concentrated samples.

In the last few years, several approaches have been reported to enhance SNR per time unit in slice-selective experiments:

- i. Sequential slice excitation with the aim of reducing the long recycle delay and shortening the overall acquisition time in 1D and 2D experiments or performing continuous data acquisition, as described in fast monitoring reaction studies. This strategy uses a fast pulsing approach with around 100 ms of recycle delay, and after each scan, the offset of the selective shaped pulse is changed to access fresh equilibrium magnetization from adjacent frequency/spatial regions. Sakhaii *et al.* reported how an optimized division of the NMR tube in eight slices by changing the offset accordingly affords an experiment increment by a $\sqrt{8}$ factor in the original ZS experiment. Similarly, spatially selective HMQC spectra have been rapidly recorded within 45-90 s dividing the NMR tube of protein samples in four *z*-slices.
- ii. It has been reported that the use of the so-called through-polarization sharing can afford an average enhancement by a factor of two. ⁴⁸ This approach is based on the original *Acceleration by Sharing Adjacent Polarization* (ASAP) technique that uses a short recycle delay consisting of a 40 ms isotropic DIPSI-2 pulse train flanked by two gradients. ⁸⁷ The method presents some limitations because sensitivity enhancement is not uniform for all signals and strongly dependent of the different relaxation properties of the excited protons while other spins remain unperturbed, preventing any attempt of quantification.

In this article a novel strategy to enhance the experimental sensitivity in spatially encoded NMR experiments applying a multiple-frequency modulated pulse to simultaneously excite different slices in a single NMR experiment is proposed. The

^[85] a) M. Vega-Vazquez, J. C. Cobas, M. Martin-Pastor, *Magn. Reson. Chem.*, 2010, 48, 749. b) B. Sathyamoorthy, D. M. Parish, G. T. Montelione, R. Xiao, T. Szyperski, *Chemphyschem*, 2014, 15, 1872.

^[86] G. E. Wagner, P. Sakhaii, W. Bermel, K. Zangger, *Chem. Commun.*, 2013, 49, 3155.

^[87] R. Freeman, E. Kupče, Magn. Reson. Chem., 2007, 45, 2.

increased sensitivity observed in the 1 H spectrum is proportional to number of offsets applied. The proposal is based on the careful setting of multiple offsets to avoid the excitation of mutually \mathcal{F} coupled protons within the same slice which would result in distorted multiplets due to J_{HH} evolution. As a proof of the method, we have applied it on a sample of the anti-inflammatory drug ibuprofen, that contains a relative simple 1 H spectrum, and on a sample of cyclosporine, which presents a more complex 1 H spectrum. In both cases, the sensitivity of slice-selective experiments has been substantially improved compared with the conventional experiments.

One of the advantages of this proposal is the easy implementation of multi-frequency pulses without the need to modify existing pulse sequences, having a considerable impact on the success of a wide variety of NMR applications. As predicted theoretically, the SNR in pure shift ¹H NMR spectra of the cyclopeptide cyclosporine recorded with the pseudo-2D ZS and real-time techniques is enhanced by an average experimental factor of ~7 when an 8-site multiple-frequency 180° pulse is applied instead of a conventional single-frequency pulse.



DOI: 10.1002/chem.201303272

Simultaneous Multi-Slice Excitation in Spatially Encoded NMR Experiments

Laura Castañar, Pau Nolis, Albert Virgili, and Teodor Parella*[a]

Recently, there has been a growing interest in spatially localized NMR spectroscopic techniques based on the incorporation of the traditional slice selection concept implemented in magnetic resonance imaging (MRI) applications. Several high-resolution NMR methods applying spatial frequency encoded excitation along an NMR tube have been suggested as means of obtaining specific information from a particular slice. For instance, selective spin-lattice T₁ relaxation times[1] and all proton-proton coupling constants for a selected proton resonance from a slice-selective J-resolved (G-SERF) experiment have been measured,[2] broadband homodecoupled 1H spectra with the Zangger-Sterk (ZS) method have been obtained,[3-5] slice-selective diffusion experiments have been carried out[6] and diagonal-suppressed 2D experiments are also possible. [7] Sequential multi-slice selection has been exploited for cases in which nuclear spins in different parts of the NMR tube are exclusively excited during subsequent transients by changing the offset frequency while the previously used spins have time to relax towards equilibrium before being excited again, resulting in significantly shorter overall acquisition times. Examples have been utilized to accelerate data acquisition in multidimensional NMR experiments,[8] to improve the signal-tonoise ratio (SNR) per time unit in the ZS method[9] or to study the kinetics of a reaction on the ms time scale.[10] The use of multiple-frequency pulses[11] has been recently suggested as a method of effective broadband 13C homodecoupling in slice-selected HSQC experiments for highly-enriched 13C samples.[12]

Experimentally, spatial frequency encoding is achieved easily by simultaneous application of a frequency-selective 90° or 180° ¹H pulse and a spatial-encoding gradient, G_{ν} . The range of sampled frequencies (SW_G) is defined by the strength of G_{ν} according to $SW_G = \gamma L G_S$, in which γ is the gyromagnetic ratio of the spatially encoded nucleus and L is the active volume coil length. On the other hand, the carrier frequency (Ω) and the selective pulse bandwidth $(\Delta\omega)$ determine the z-position of each nuclear spin $(z = \Omega/(\gamma G_{\nu}))$ and the slice thickness $(\Delta z = \Delta\omega/(\gamma G_{\nu}))$, respectively. Thus,

the overall SNR of a slice-selective experiment will depend both on the strength of the encoding gradient and on the selectivity of the pulse. For instance, a typical 20 ms Gaussianshaped 180° pulse (bandwidth of 60.7 Hz) applied simultaneous with a gradient of 0.743 G cm-1 (this is 1.39% of the maximum gradient strength of 53.5 G cm-1 delivered by our gradient unit) splits the sample height (L=1.8 cm) into around 94 slices along the z axis, defining a slice thickness of about 0.019 cm and covering a SWG of 5694 Hz (9.47 ppm in a 600 MHz spectrometer). Thus, under these general conditions, the single-slice selection procedure would afford only about 1% of the sensitivity of a conventional 'H spectrum. This low SNR could be improved by using shorter and less selective pulses and/or less intense encoding gradients but always with an increase in the probability of accidental excitation of two coupled spins within the same slice.

As mentioned, the most serious drawback of spatially encoded NMR experiments is their reduced sensitivity because the observed signal only arises from a discrete slice of the sample. Therefore, novel approaches are required to improve the low SNR and to make these types of experiments practical for use with moderately concentrated samples. Herein, we exploit the sensitivity benefits of applying a multiple-frequency modulated pulse to simultaneously excite different slices in a single NMR experiment. Our proposal is based on the careful setting of multiple offsets to avoid the excitation of mutually J-coupled protons within the same slice (Figure 1) which would result in distorted multiplets due to J_{H-H} evolution.

We have used two basic experiments to evaluate the effectiveness of multiple-frequency pulses in slice-selective experiments. The 1D z-profile image of the sample can be obtained with the conventional echo gradient pulse sequence including an initial selective 180° pulse and a simultaneous encoding gradient to visualize the frequency excitation achieved in the z direction (Figure 2A). The experimental effects on the NMR spectrum can be quickly monitored by recording spatially encoded single pulsed-field gradient echo (se-SPFGE) experiments (Figure 2B). This sequence consists of a selective gradient echo in which a slice-selection gradient (G_s) is switched on in conjunction with the central refocusing 180° 1H pulse. When Gs is not applied, this is the conventional SPFGE pulse sequence used for frequency-selective excitation, in which the G1 gradients act as defocusing/refocusing coherence elements.

Figures 2 C-H show 1D z-profile images of a D₂O sample as a function of the number of offsets defined by the shape

 [[]a] L. Castañar, Dr. P. Nolis, Prof. A. Virgili, Dr. T. Parella Servei Ressonància Magnètica Nuclear and Departament de Química Universitat Autònoma de Barcelona 08193 Bellaterra, Barcelona (Spain)
 E-mail: teodor.parella@uab.cat

Supporting information for this article is available on the WWW under http://dx.doi.org/10.1002/chem.201303272.

COMMUNICATION

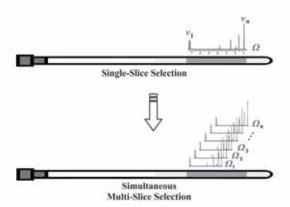


Figure 1. Schematic representation of a conventional single-slice pulse sequence compared to simultaneous multi-slice selection by a multiple-frequency pulse modulated according to different offset frequencies ($\Omega_1 \dots \Omega_k$). A methodology is described that avoids the simultaneous excitation of mutually J-coupled spins within the same z slice.

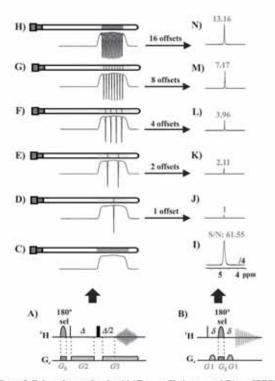


Figure 2. Pulse schemes for the A) 1D z-profile image and B) se-SPFGE experiments. C-H) Schematic z-profile of a 99.96% D_2O sample (obtained with the pulse sequence shown in A) with a multiple-frequency pulse with 0 ($G_s = off$), 1, 2, 4, 8 and 16 different offsets, respectively; J-N) se-SPFGE spectra (obtained with the pulse sequence shown in B) with a multiple-frequency pulse with 1, 2, 4, 8 and 16 different offsets and with the experimental signal-to-noise ratio related to the conventional ¹H NMR spectra (I). In all experiments, a 20 ms Gaussian-shaped 180° ¹H pulse was simultaneous applied with an encoding gradient $G_s = 0.865 \, \mathrm{G\,cm^{-1}}$.

of the selective pulse, in which the exact z-position of each selected slice along the NMR tube is evident. The relative SNR of the corresponding se-SPFGE spectra follow a clear dependence on the number of offsets applied (Figure 21-N). As expected, whereas a 1.6% of the maximum attainable sensitivity is reached in the single-slice experiment, a substantial signal increase by a factor of 13 is achieved with a 16-site multiple-frequency pulse generated with a linear increment of 300 Hz. The small deviation with respect to the theoretical gain can be related to the imperfect top hat profile of the Gaussian-shaped selective pulse and the decreased sensitivity obtained at both edges of the coil due to the non-uniformity of the gradients. The use of a reduced and centered volume for which uniformity is better and/or the use of other pulse shapes offering a better inversion profile at the expense of longer durations is advisable in some

The situation becomes more complex in real samples because multiple signals with different frequencies are present and, in addition, each of them is individually localized at different z positions as a function of the applied offset. The probability that two J-coupled protons are excited within the same slice is increased and, therefore, a procedure for the calculation of a set of offsets to avoid this must be designed. Let us assume we have a conventional 1H NMR spectrum containing n different signals with frequencies v_1 , $\nu_2...$ ν_n , being ν_1 and ν_n the lowest (upfield) and the highest (downfield) frequencies, respectively. The complete spectral width to be excited will be defined by $SW_G = \nu_n - \nu_1$ and the center position by $\Omega = (\nu_1 + \nu_n)/2$. As an initial recommendation, we propose the use of a spectral width amplification factor k (kSW; in which k>1) to increase the offset range that will not cause the signals from the edges of the spectrum to appear beyond the coil position. In this case, the required encoding gradient will be redefined by G_s = $kSW_G/(\gamma L)$. In a second step, a complete set of offset values is calculated to excite different parts of the sample with the restriction that two or more mutually J-coupled protons are not perturbed within the same slice, especially those which are strongly coupled. The interval of possible offsets to be used will be a range between two values, Ω_1 and Ω_k , representing offsets for which the ν_1 and ν_n frequencies appear at the top and bottom of the active volume coil, respectively [Eq. (1) and (2)].

$$Ω1 = (L \gamma Gs)/2 + ν1$$
(1)

$$\Omega_k = -(L \gamma G_s)/2 + \nu_n \qquad (2)$$

For each selected offset $(\Omega_p; 1 , the z position of each individual resonance <math>(z(i,\Omega_p))$ may be theoretically known from the relationship given in Equation (3):

$$z(i,\Omega_p) = (\Omega_p - \nu_i)/(\gamma G_s)$$
 (3)

Therefore, taking the frequencies of each resonance extracted from the ¹H spectrum as input values, a complete

Chem. Eur. J. 2013, 19, 15472-15475

© 2013 Wiley-VCH Verlag GmbH & Co. KGaA, Weinheim

www.chemeurj.org

---- 15473

T. Parella et al.

A EUROPEAN JOURNAL

position-dependent calculation can be created for a set of offset values which must be incremented in a stepwise fashion as a function of the resulting slice thickness $(\Delta \Omega > \Delta z)$.

Successful application of the multi-slice selection concept to an unknown sample containing many different resonances will depend of the complexity of its 1H spectrum. The se-SPFGE pulse sequence is an effective and rapid tool to check the viability of the multi-slice selection process as a function of the spectral width to be excited, the number of resonances contained into it and also the probability of two coupled protons in close proximity. Experimentally, the unwanted excitation of different J-coupled protons within the same slice would be quickly observed by the anti-phase contributions in the corresponding J multiplet structure. As a proof of the method, we have applied it to a sample of ibuprofen which has a relatively simple 1H spectrum (Figure 3 A). The single-slice experiment recorded with a normalization factor of k=1 (Figure 3C) suffers from the poor gradient homogeneity at the ends of the coil. This is evidenced by the decreased SNR observed for the outer signals with respect to the central ones. More uniform response can be obtained with a factor of k=2 because data is collected in the central part of the coil but with some sensitivity penalty due to the thinner slice thickness (Figure 3D). Very interestingly, an average SNR improvement factor of 13.5 is obtained when applying a 15-site multiple-frequency pulse versus its conventional single-slice counterpart (Figure 3E). In other words, increases of up to 22% of the maximum attainable signal are fully recovered taking individual SPFGE signals as a reference (see Figure 3B) and without observing phase distortions due to J_{H-H} evolution.

An additional signal enhancement at the risk of non-uniform excitation can be achieved by moving the spectrum partially out of the limits of the active coil. This increases the potential number of offsets to be used although some signals do not contribute equally to the data collected. For a more complex spectrum, such as those of the alkaloid strychnine, the use of a 11-site excitation affords an averaged SNR enhancement of 9.2% with respect to the $^1\mathrm{H}$ spectrum if the selection is restricted to the $\pm L/2$ area, whereas a further improvement up to 12.8% is achieved with a 16-site multiple-frequency pulse when unrestricted offsets are allowed in the calculation (see Supporting information). The latter approach could be useful in situations for which quantitative analysis is not necessary.

The advantage of the easy implementation of multi-frequency pulses without the need to modify existing pulse sequences can have a considerable impact on the success of a wide variety of NMR applications. As an example, Figure 4 shows how the SNR in a broadband homodecoupled 'H NMR spectrum of the cyclopeptide cyclosporine recorded with the pure-shift pseudo-2D ZS technique^[3,15] is enhanced by an average experimental factor of 6.7 when an 8-site multiple-frequency 180° pulse is applied instead of a conventional single-frequency pulse (Figure 4B vs. 4C). Similar sensitivity gains can also be achieved with the recently proposed instant pure-shift ZS technique (see the

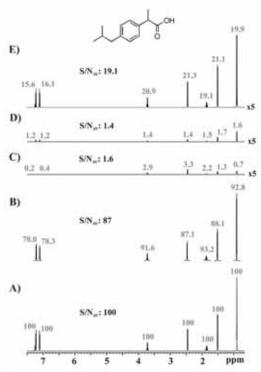


Figure 3. A) Conventional ^1H NMR spectra of ibuprofen in CDCl₃. The experimental signal-to-noise ratio in the ^1H NMR spectra has been normalized for each individual signal. B) Signals arising of individual SPFGE experiments ($G_s = 0$) to account for T_2 relaxation losses during the echo; C and D) single-slice se-SPFGE spectra with a normalized scaling k factor of 1 and 2, respectively; E) Multi-slice se-SPFGE spectrum with 15 different offsets to avoid the simultaneous excitation of different coupled protons into the same slice. A single scan and a 20 ms Gaussian-shaped pulse were used in all experiments. Spectrum C was recorded with an amplification k factor of 1 (SW $_G = 3793$ Hz), a square-shaped encoding gradient (G_s) of 0.495 Gcm $^{-1}$. Spectra D and E were recorded with an amplification k factor of 2 (SW $_G = 7586$ Hz), a square-shaped encoding gradient of 0.99 Gcm $^{-1}$.

Supporting Information), [3] and probably such enhancements could offer important SNR benefits in more time-consuming multidimensional slice-selective NMR experiments, [13-45]

In conclusion, an improved data collection technique with simultaneous multi-slice data acquisition has been presented. The sensitivity of slice-selective NMR experiments can be substantially improved by simultaneously applying a multiple-frequency pulse and spatial encoding gradient. The experimental procedure to fulfill the sampled frequency requirement is simple and the results can be immediately adapted to a wide range of applications. Further investigations are in progress to develop novel applications and other new and/or complementary strategies to further improve the sensitivity and the performance of spatially encoded NMR experiments.

Spatially Encoded NMR Experiments

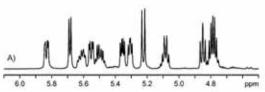


Figure 4. Sensitivity-enhanced broadband-homodecoupled ¹H NMR spectra of cyclosporine with the pure-shift pseudo-2D technique.[0,19] Expanded H, region from the A) conventional; B and C) single-slice and 8-site multi-slice pure-shift 'H spectra, respectively. The 8 offsets were limited to the sample coil and the experimental sensitivity enhancement was around 6.7%. All experimental details remain the same for spectra B and C; an amplification k factor of 2 (SW $_0\!=\!9140\,\rm Hz),$ a square-shaped encoding gradient of 1.13 Gcm $^{-1}$ and a 80 ms Rsnob 180° $^{1}\rm H$ pulse to achieve a perfect homodecoupling for the strong coupled AB proton spin system resonating at 5.50 and 5.61 ppm. 4 transients were collected for each one of the 32 t_1 increments in an experimental time of ≈ 4 min. More details can be found in the supporting information.

Experimental Section

All NMR Experiments were performed in a 600 MHz BRUKER Avance-III spectrometer equipped with a TXI probe and a gradient unit delivering 53.5 Gcm-1. The samples used were 99.96% D2O, 100 mm of ibuprofen in CDCl3, and 25 mm cyclosporine in [D6]benzene. Additional details about experimental NMR conditions and offsets calculation can be found in the Supporting Information.

COMMUNICATION

Acknowledgements

Financial support for this research provided by MICINN (project CTQ2012-32436) and Bruker Española S.A. is gratefully acknowledged. We thank to the Servei de Ressonância Magnètica Nuclear, Universitat Autònoma de Barcelona, for allocating instrument time to this project. The authors also thank Prof. K. Zangger for providing experimental details and the pulse program code for the original instant experiment.

Keywords: multiple-frequency pulses · multi-slice selection · NMR spectroscopy · pure-shift NMR · spatial encoding

- [1] N. M. Loening, M. J. Thrippleton, J. Keeler, R. G. Griffin, J. Magn. Reson. 2003, 164, 321-328.
- N. Giraud, L. Béguin, J. Courtieu, D. Merlet, Angew. Chem. 2010, 122, 3559-3562; Angew. Chem. Int. Ed. 2010, 49, 3481-3484.
- [3] K. Zangger, H. Sterk, J. Magn. Reson. 1997, 124, 486-489.
- [4] N. Giraud, M. Joos, J. Courtieu, D. Merlet, Magn. Reson. Chem. 2009, 47, 300-306.
- [5] N.H. Meyer, K. Zangger, Angew. Chem. 2013, 125, 7283-7286; Angew. Chem. Int. Ed. 2013, 52, 7143-7146.
- [6] a) B. Antalek, Concepts Magn. Reson. 2002, 14, 225-258; b) K. D. Park, Y. J. Lee, Magn. Reson. Chem. 2006, 44, 887-891.
- [7] S. Glanzer, E. Schrank, K. Zangger, J. Magn. Reson. 2013, 232, 1-6.
- [8] M. Vega-Vázquez, J. C. Cobas, M. Martin-Pastor, Magn. Reson. Chem. 2010, 48, 749-752.
- [9] P. Sakhaii, B. Haase, W. Bermel, R. Kerssebaum, G. E. Wagner, K. Zangger, J. Magn. Reson. 2013, 233, 92-95.
- [10] G. E. Wagner, P. Sakhaii, W. Bermel, K. Zangger, Chem. Commun. 2013, 49, 3155-3157.
- [11] S. L. Patt, J. Magn. Reson. 1992, 96, 94-102.
- [12] M. Foroozandeh, P. Giraudeau, D. Jeannerat, ChemPhysChem 2011, 12, 2409-2411.
- [13] a) G. A. Morris, J. A. Aguilar, R. Evans, S. Haiber, M. Nilsson, J. Am. Chem. Soc. 2010, 132, 12770-12772; b) J. J. Koivisto, Chem. Commun. 2013, 49, 96-98.
- [14] J. A. Aguilar, A. A. Colbourne, J. Cassani, M. Nilsson, G. A. Morris, Angew. Chem. 2012, 124, 6566-6569; Angew. Chem. Int. Ed. 2012, 51, 6460-6463.
- [15] a) M. Nilsson, G. A. Morris, Chem. Commun. 2007, 933-935; b) J. A. Aguilar, S. Faulkner, M. Nilsson, G. A. Morris, Angew. Chem. 2010, 122, 3993-3995; Angew. Chem. Int. Ed. 2010, 49, 3901-

Received: August 20, 2013 Published online: October 7, 2013

15475



Supporting Information

© Copyright Wiley-VCH Verlag GmbH & Co. KGaA, 69451 Weinheim, 2013

Simultaneous Multi-Slice Excitation in Spatially Encoded NMR Experiments

Laura Castañar, Pau Nolis, Albert Virgili, and Teodor Parella*[a]

chem_201303272_sm_miscellaneous_information.pdf

Contents

- Experimental Section.
- Fig. S1: Schematic illustration of the single-offset slice selection.
- Fig. S2: Schematic illustration of the multiple-offset slice selection.
- Fig. S3: Multiple-frequency spatially encoded SPFGE spectra of ibuprofen.
- Fig. S4: Calculated z-position in ibuprofen for 15 different offsets.
- Fig. S5: Multiple-frequency spatially encoded SPFGE spectra of strychnine.
- Fig. S6: Multiple-frequency spatially encoded SPFGE spectra of cyclosporine.
- Fig. S7: Effect of multiple-offset in the broadband-homodecoupled pseudo-2D Zangger-Sterk NMR experiment of cyclosporine.
- Fig. S8: Effect of multiple-offset in the instant broadband-homodecoupled NMR experiment of cyclosporine.
- Short description of Java script for multi offset calculation
- Four examples of offset calculation and screen captures of the input/output files

Experimental Section

All the NMR experiments were carried out on a 14.1T (600MHz) Bruker AVANCE III spectrometer equipped with a 5mm TXI probe and with a z field gradient unit of maximum strength of 53.5 G cm⁻¹. The probe temperature was set to 298 K. The four samples used in this work were 99.96% D₂O, 0.1M ibuprofen (in CDCl₃), 0.1M strychnine (in CDCl₃) and 25mM cyclosporine (in Benzene-d6).

1D image experiments (Figures 2C-2H)

Imaging profiles of the 99.96% D_2O sample in Fig. 2C-H were obtained with the pulse sequence of Fig. 2A. All the experiments were recorded using a single scan (without dummy scans), and the inter-pulse Δ delay and the acquisition time (3K data points) were both set to 10 ms. Square-shape gradients of 5.35 G cm⁻¹ were used and applied during 10 ms (G2) and 15 ms (G3). In Fig. 2C, the selective 180° pulse and the encoding gradient (G_8) were not applied. In Fig. 2D-2H, a 20 ms Gaussian-shaped 180° pulse (bandwidth of 60.74 Hz) was applied simultaneous with a square-shaped encoding gradient (G_8) of 0.865 G/cm. The number to offsets used in each experiment and its values are: D) 1 offset (5 ppm); E) 2 offsets (7 and 3 ppm); F) 4 offsets (8, 6, 4 and 2 ppm); G) 8 offsets (1.5, 2.5, 3.5, 4.5, 5.5, 6.5, 7.5 and 8.5 ppm) and H) 16 offsets (1.25, 1.75, 2.25, 2.75, 3.25, 3.75, 4.25, 4.75, 5.25, 5.75, 6.25, 6.75, 7.25, 7.75, 8.25 and 8.75 ppm). Data were processed using a Gaussian window function (LB=-20 and GB=0.5) and zero filling to 32K prior to Fourier Transformation.

Conventional and se-SPFGE ¹H NMR experiments recorded on 99.96% D₂O sample (Figures 2I-2N)

Conventional ¹H NMR spectrum (Fig. 2I) was recorded using 1 scan (without dummy scans) and an acquisition time of about 3 s (32K data points). Fig. 2J-2N show several se-SPFGE spectra obtained with the pulse sequence of Fig. 2B using 1 scan (without dummy scans), an acquisition time of 2.73 s (32K data points), a gradient (G1) with a duration of 1 ms and a strength of 8.03 G cm⁻¹ with a smoothed squared shape (SMSQ10.100 in BRUKER nomenclature), a 20 ms Gaussian-shaped 180° pulse (bandwidth of 60.74 Hz) and an square-shaped encoding gradient (G_S) of 0.865 G cm⁻¹. The number of offsets used in each experiment (and values in ppm) were set to: J) 1 offset (5 ppm); K) 2 offsets (7 and 3 ppm); L) 4 offsets (8, 6, 4 and 2 ppm); M) 8 offsets (1.5, 2.5, 3.5, 4.5, 5.5, 6.5, 7.5 and 8.5 ppm) and N) 16 offsets (1.25, 1.75, 2.25, 2.75, 3.25, 3.75, 4.25, 4.75, 5.25, 5.75, 6.25, 6.75, 7.25, 7.75, 8.25 and 8.75 ppm). Data were processed using a conventional Fourier Transformation.

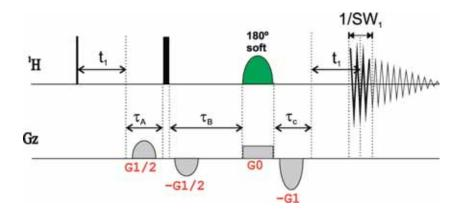
se-SPFGE ¹H NMR experiments recorded on ibuprofen (Figure 3)

Conventional ¹H NMR spectrum of ibuprofen (Fig. 3A) was recorded using 1 scan (without dummy scans) and an acquisition time of 3 s (32K data point). The experimental signal-to-noise ratio in the ¹H NMR spectra was normalized to 100 for each individual signal. In order to take in account T2

relaxation signal lost, several ¹H-frequency-selective SPFGE spectra of ibuprofen (Fig. 3B) were acquired with the pulse sequence of Fig. 2B but without applying the encoding gradient in order to know signal losses associated to the T2 relaxation. All experiments were recorded using 1 scan (without dummy scans), an acquisition time of 3s, a 1ms shaped SMSQ10.100 gradient (G1) of 8.03 G cm⁻¹ and a 20 ms Gaussian-shaped 180° pulse (bandwidth of 60.74 Hz). se-SPFGE spectra (Fig. 3C-E) were recorded using 1 scan (without dummy scans), an acquisition time of 3s, a 1ms shaped SMSQ10.100 gradient (G1) of 8.03 G cm⁻¹ and a 20 ms Gaussian-shaped 180° pulse (bandwidth of 60.74 Hz). Experiment 3C was recorded using an amplification k factor of 1 (SW_G=3793 Hz), a square-share encoding gradient (G_S) of 0.495 G cm⁻¹ and a single-frequency selective pulse (2454 Hz). Experiment 3D and 3E were recorded using a amplification k factor of 2 (SW_G=7586 Hz), a square-shaped encoding gradient of 0.99 G/cm and a selective pulse with 1 (2454 Hz) and 15 offsets, respectively, automatically calculated using the java script *calcoff* (4259, 4035, 3534, 3236, 3042, 2784, 2557, 2291, 2063, 1832, 1561, 1378, 1086, 901 and 638 Hz) respectively. Data were processed using a conventional Fourier Transformation.

Pure-shift 1D experiment (Figure 4)

Pure shift spectra of Fig. 4B and 4C were acquired with the original pseudo-2D ZS pulse sequence described in ref 15b.



The pulse program named push1dzs obtained from Manchester NMR methodology group website (http://nmr.chemistry.manchester.ac.uk) was used for data acquisition. The experiments were recorded using an amplification k factor of 2 (SW_G=7586 Hz), a square-shaped encoding gradient of 0.99 G cm⁻¹ and a 20 ms Gaussian-shaped 180° pulse (bandwidth of 60.74 Hz); 8 transients were collected for each one of the 32 t_1 increments of 0.68 s each were acquired with $1/SW_1 = 10$ ms and a relaxation delay of 1 s, in total time of 8 min. Coherence transfer selection gradient pulses were smoothed squared shaped (SMSQ10.100) with a duration of 1 ms and amplitude G1= 13.4 G cm⁻¹ (25%); the delays τ_a , τ_b and τ_c are automatically calculated so that $\tau_a + \tau_c = \tau_b$; $\tau_a = \tau_c$; $\tau_a = 1/4*SW_1$. The pulse offset (o1) and the spectral width (SW₂) were set to 2454.5 Hz and 10.0 ppm, respectively. Spectrum of Fig. 4C used exactly the same set up as described in Fig 4B but using a 8 multi-frequency shaped pulse irradiating simultaneously at frequencies: 3534, 3236, 3042, 2784, 2557, 2291, 2063 and 1832 Hz (automatically calculated using the home made calcoff java script). The power level of the shaped pulse was decreased 18 dB compared to those of Fig. 4B. Data was processed automatically with the AU program named pshift provided at Manchester NMR methodology group website http://nmr.chemistry.manchester.ac.uk. This AU program converts the raw data to a new experiment that contains the pure shift FID, which is Fourier transformed with a 0.3 line broadening.

Automatic calculation of offsets: calcoff

A calculation script written in java language is available from the authors on request. Basically, the script searches a set of offsets that avoid accidental overlap of mutually coupled protons into the same z-slice. The program needs some input parameters: coil length, probe gradient strength, bandwidth and shape of the selective pulse, a frequency list from a .txt file, the amplification k factor and how many offsets wants to calculate. After some calculation iterations, the script returns a list of calculated offsets with a z-position matrix for all available frequencies. Some examples are provided at the end of this supplementary information.

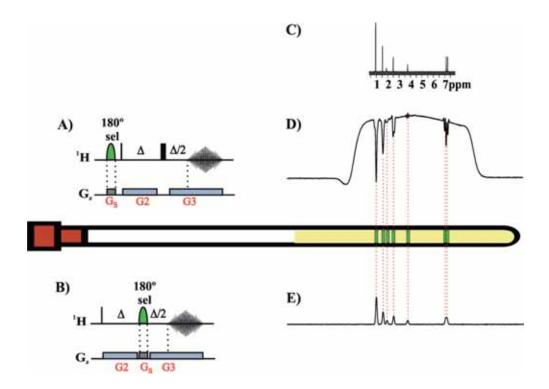


Figure S1: Schematic illustration of the single-offset slice selection. A,B) Pulse schemes used to obtain 1D z-profile images. C) Conventional ¹H NMR spectra of ibuprofen. D) 1D z-profile image experiment obtained with the pulse sequence A. E) 1D z-profile image experiment obtained with the pulse sequence B. A selective 20 ms Gaussian-shaped 180° pulse was applied simultaneous with a square-shaped encoding gradient (G_S) of 0.742 G cm⁻¹ to obtain an image profile using a single offset (2454 Hz). All other experimental parameters as described in Fig. 2.

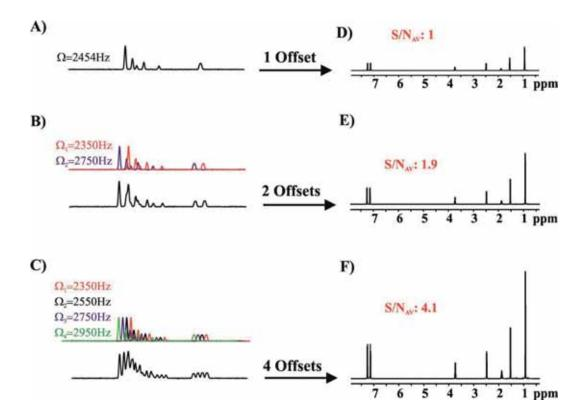


Figure S2: Schematic illustration of the multiple-offset slice selection. A-C) 1D z-profile image experiments of ibuprofen obtained with the pulse sequence of Fig. S1B. D-F) Slice selective SPFGE spectra obtained with the pulse sequence of Fig. 2B. In all experiments a 20 ms Gaussian-shaped 180° selective pulse was applied simultaneous with a square-shape encoding gradient (G_S) of 0.742 G cm⁻¹. A-C) The experiments were recorded using 1 scan (without dummy scans), Δ =10ms, an acquisition time of 10 ms, and a selective pulse with 1, 2 and 4 offsets respectively. Square-shaped gradients of 5.35G/cm were used and applied during 10ms (G2) and 15 ms (G3). D-F) All spectra were recorded using 1 scan (without dummy scans), an acquisition time of 3s, a 1ms shaped SMSQ10.100 gradient (G1) of 8.03 G cm⁻¹ and a selective pulse with 1, 2 and 4 offsets respectively. In each spectrum, the averaged signal-to-noise ratio (S/N_{AV}) is reported for comparison.

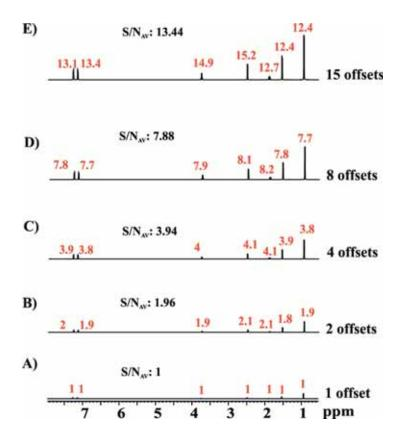


Figure S3: Multiple-frequency se-SPFGE spectra of ibuprofen. All experiments were recorded with the pulse sequence of Fig. 2B using 1 scan, an acquisition time of 3 s, a 1 ms SMSQ10.100 shape refocused gradient (G1) of 8.03 G cm⁻¹, an amplification k factor of 2 (SW_G=7586 Hz), a square-shaped encoding gradient of 0.99 G cm⁻¹ and a 20 ms Gaussian-shaped 180° pulse (bandwidth of 60.74 Hz). The number to offsets used in each experiment (and its values in Hz) are: A) 1 offset (2454 Hz); B) 2 offsets (2557 and 2291 Hz); C) 4 offsets (2784, 2557, 2291 and 2063 Hz); D) 8 offsets (3534, 3236, 3042, 2784, 2557, 2291, 2063, 1832 Hz) and E) 15 offsets (4259, 4035, 3534, 3236, 3042, 2784, 2557, 2291, 2063, 1832, 1561, 1378, 1086, 901 and 638 Hz ppm). In each spectrum, the averaged signal-to-noise ratio (S/N_{AV}) is reported for comparison.

Constant Parameters	Gyromagnetic Ratio of ¹ H ($\square_{\square\square}$	4257,8 Hz/G
Probe parameters	Length of the active volume coil (L)	1.8 cm
	Maximum gradient strength (G _z)	53,5 G/cm
180° selective pulse parameter	Shape	Gaussian
	Duration (p12)	20 ms
	Bandwidth half height ($\Delta\omega_{1/2}$)	60,74 Hz
	Bandwidth in the base ($\Delta\omega$)	183 Hz
Parameters calculated	Spectral width (SW _G)	3793Hz
	Amplification factor (k)	2
	Spectral width and amplification factor (SW_G*k)	7586 Hz
	Center of the spectrum (o1)	2454 Hz
	Spatial-encoding gradient (G _S)	0,99 G/cm
	Offset limits	558-4351 Hz

	Signal position [cm]						
Offsets[Hz]	z (H ₁₂)	z (H ₃)	z (H ₁₁)	z (H ₁₀)	z (H ₂)	z (H ₆)	z (H ₅)
638	0,019	-0,066	-0,116	-0,201	-0,380	-0,864	-0,881
901	0,081	-0,004	-0,053	-0,139	-0,318	-0,801	-0,819
1086	0,125	0,040	-0,009	-0,095	-0,274	-0,757	-0,775
1378	0,195	0,109	0,060	-0,026	-0,205	-0,688	-0,705
1561	0,238	0,153	0,103	0,018	-0,161	-0,645	-0,662
1832	0,302	0,217	0,168	0,082	-0,097	-0,580	-0,598
2063	0,357	0,272	0,222	0,137	-0,042	-0,526	-0,543
2291	0,411	0,326	0,276	0,191	0,012	-0,471	-0,489
2557	0,474	0,389	0,340	0,254	0,075	-0,408	-0,426
2784	0,528	0,443	0,393	0,308	0,129	-0,354	-0,372
3042	0,589	0,504	0,455	0,369	0,190	-0,293	-0,311
3236	0,635	0,550	0,501	0,415	0,236	-0,247	-0,265
3534	0,706	0,621	0,571	0,486	0,307	-0,177	-0,194
4035	0,825	0,740	0,690	0,605	0,426	-0,058	-0,075
4259	0,878	0,793	0,743	0,658	0,479	-0,005	-0,022

Figure S4: Calculated z-positions of all signals in ibuprofen as a function of spatial encoded NMR parameters.

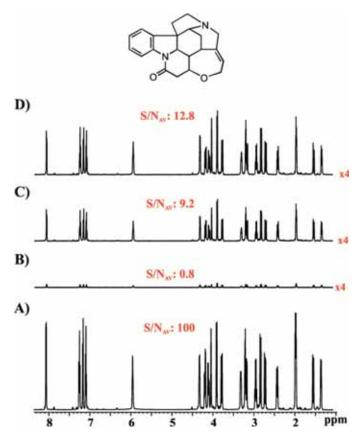


Figure S5: A) ¹H NMR spectrum of strychnine in CDCl₃; B) Single-slice se-SPFGE spectrum after using a selective gaussian-shaped pulse of 30ms and an encoding gradient strength of G_s =1.068 G/cm; C) Multiple-slice se-SPFGE experiment acquired as B) but using a 11-site multiple-frequency pulse and using the restricted condition that only offsets that contain all signals into the volume coil are used; D) The same as C) but using a 16-site multiple-frequency pulse that include offsets that include some protons out of the limits of the coil. The averaged signal-to-noise ratio percentage (S/N_{av}) is shown in each spectrum. As a reference, the S/N_{av} values of individual SPFGE experiments (Gs=0) is about 81% of the levels achieved in the conventional ¹H spectrum (data not shown). Spectra B-D were collected with the pulse sequence of Fig. 2B using 1 scan (without dummy scans), an acquisition time of 3 s, a 1 ms SMSQ10.100 gradient (G1) of 8.03 G cm⁻¹, an amplification k factor of 2 (SW_G=8188 Hz), a squareshaped encoding gradient (G_S) of 1.068 G cm⁻¹ and a 30 ms Gaussian-shaped 180° pulse (bandwidth of 40.49 Hz). B and C was recorded using a selective pulse with 1 (2801 Hz) and 11 offsets (4760, 4360, 3960, 3560, 3160, 2760, 2360, 1960, 1560, 1160 and 760 Hz) respectively. In the later experiment, the offsets used were restricted so that all the signals were excited inside the active coil region. In the spectrum D, an additional signal enhancement was obtained using a selective pulse with 16 offsets (5960, 5560, 5160, 4760, 4360, 3960, 3560, 3160, 2760, 2360, 1960, 1560, 1160, 760, 360 and -160 Hz) where a non-uniform excitation was obtained because for higher and lower offsets a small portion of the signals from the edges of the spectrum appear beyond of the limits of the active coil (as can be seen in the z-position matrix). Data were processed using a conventional Fourier Transformation.

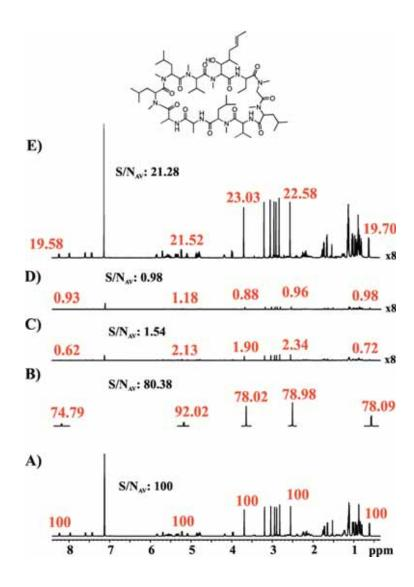


Figure S6: Multiple-frequency se-SPFGE spectra of cyclosporine. It was recorded using 1 scan (without dummy scans) and an acquisition time of 3s. The experimental signal-to-noise ratio in the ¹H NMR spectrum (A) was normalized to 100 for each individual signal. B) Signal arising of conventional SPFGE (G_s=0) to take into account for T₂ relaxation signal lost during the selective echo. C,D) single-slice se-SPFGE spectra using normalized scaling k factor of 1 and 2 respectively; E) Multi-frequency se-SPFGE were collected with the pulse sequence of Fig. 2B using 1 scan (without dummy scans), an acquisition time of 3s, a 1 ms SMSQ10.100 shape refocused gradient (G1) of 8.03 Gcm⁻¹, an amplification k factor of 2 (SW_G=9168 Hz), a square-shaped encoding gradient (G_S) of 1.196 G cm⁻¹ and a 20 ms Gaussian-shaped 180° pulse with 22 offsets (4861, 4661, 4441, 4241, 4041, 3841, 3621, 3421, 3221, 3021, 2801, 2601, 2401, 2201, 1981, 1781, 1581, 1381, 1161, 961, 761 and 551Hz). In each spectrum, the averaged signal-to-noise ratio (S/N_{AV}) is reported for comparison.

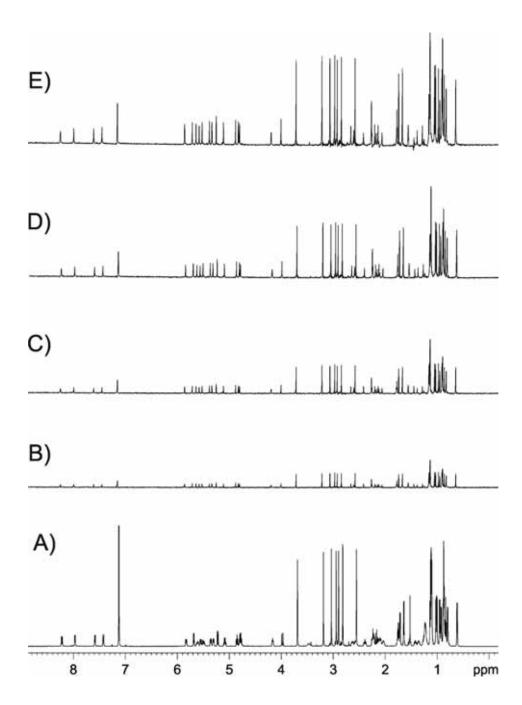


Figure S7: A) ¹H NMR spectrum of 25 mM cyclosporine in d-benzene (600 MHz). B) Single-slice (offset set to 2507 Hz) and C-E) multi-slice broadband homonuclear ZS spectra recorded with 2, 4 and 8 offsets, respectively, using the pseudo-2D pulse sequence described previously in the experimental section. ^{15b} The 8 offsets used in spectrum E were set to 3200, 3000, 2800, 2600, 2400, 2200, 2000 and 1800 Hz, and the average sensitivity gain with respect to spectrum B is 6.7. All other experimental details as described in Fig. 4 which shows an expanded area covering signals resonating between 4.5 and 6ppm.

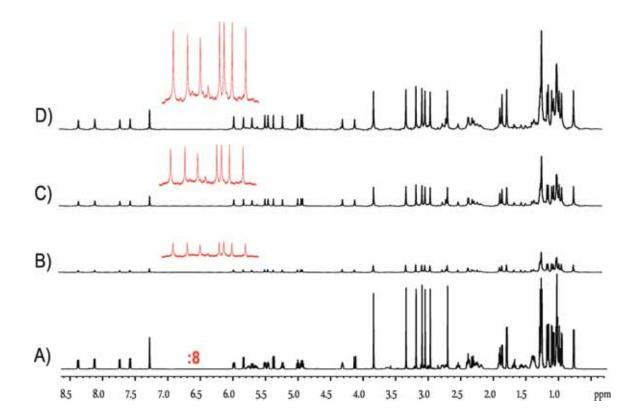


Figure S8: Effect of the use of multiple-frequency pulses into the Instant broadband-homodecoupled ¹H NMR spectra of a sample 25mM cyclosporine in benzene-d6 acquired with the sequence reported in ref. 5. 8 scans were collected for each 1D dataset using a 10 ms Gaussian shaped selective 180 ¹H pulse and an encoding gradient of 1.06 G cm⁻¹. 30 loops were used, with a recycle delay of 1 second. This selective pulse was frequency modulated with B) single (2700Hz), C) two (2800 and 2400Hz) and D) four (3200, 2800, 2400 and 2000Hz) different offsets. The experimental sensitivity gains are proportional to the number of applied offsets.

Publication 1

Short description of Java script for multi offset calculation

The script asks some parameters about user and also about frequencies and couplings of a given molecule or spin system. The user may introduce a shaped-pulse band width, a security amplification k

factor (read the article for more information) and how many offsets want to search for. Then the script

searches for a solution. If any solution is found after 50000 iterations then it decrease the number of

offsets by one, and start the calculation again.

Experimental considerations:

The script asks you which protons are coupled. If you don't know you can perform the calculation just

by inserting the restriction that frequencies don't match each other (like if everything was coupled), but

this is a very restrictive way of working that usually give you few offsets compared to what you can

really use. Our experience says us that it is better to work the other way around. So, start like if the

system is not coupled, and if some distortions in a pair of signal are seen in the spectrum, just introduce

that coupled pair in the calculation as a restriction.

To execute the java script download the given multi_offset.jar file and save it in C:\ directory (or

whatever), then open the Windows command Prompt and once being situated in the C:\

Type: C:\java –jar multi_offset.jar

And the java script will launch.

Examples

In order to show how the java script works we present 4 examples concerning ibuprofen sample in

different situations.

In the first example, we don't consider any coupling and we observe 16 offsets are found in just a single

iteration.

In example the restriction of the strong aromatic coupling2 is introduced. The script takes longer time to

find the solution of 16 offsets. In that case 642 iterations were needed.

In a third example, we introduce the whole coupling network. It is seen that there is no possible solution

that avoids completely any random overlapping using 16 offsets, and the solution given is 10 offsets

after 45185 iterations.

Then a fourth example analogous to third but reducing pulse band width half shows that 14 offset can be

used. Notice, that one have to take into account that the slice thickness now is reduced half and is

important to realize that third example setup will give higher SNR although less offsets are found.

74

Java script multi offset calculation example 1:

Sample: ibuprofen

Coupling spin system taken into account: NO

Band Width = 60 HzSecurity facotr K = 2

16 offsets as insert (16 obtained)

SCREEN CAPTURES OF THE INPUT FILE

```
//USER INSERT PARAMETERS//
Insert coil length in cm?: 1.8
Insert gradient strength in G/cm?: 53.5
Insert pulse band width in Hz?: 60
How many peaks to introduce?: 7
Insert peaks in ascending order:
Insert peak in Hz: 542
Insert peak in Hz: 903
Insert peak in Hz: 1110
Insert peak in Hz: 1471
Insert peak in Hz: 2228
Insert peak in Hz: 4264
Insert peak in Hz: 4336
Does frequence 542 couple to 903 (y/n): n
Does frequence 542 couple to 1110 (y/n): n
Does frequence 542 couple to 1471 (y/n): n
Does frequence 542 couple to 2228 (y/n): n
Does frequence 542 couple to 4264 (y/n): n
Does frequence 542 couple to 4336 (y/n): n
Does frequence 903 couple to 1110 (y/n): n
Does frequence 903 couple to 1471 (y/n): n
Does frequence 903 couple to 2228 (y/n): n
Does frequence 903 couple to 4264 (y/n): n
Does frequence 903 couple to 4336 (y/n): n
Does frequence 1110 couple to 1471 (y/n): n
Does frequence 1110 couple to 2228 (y/n): n
Does frequence 1110 couple to 4264 (y/n): n
Does frequence 1110 couple to 4336 (y/n): n
Does frequence 1471 couple to 2228 (y/n): n
Does frequence 1471 couple to 4264 (y/n): n
Does frequence 1471 couple to 4336 (y/n): n
Does frequence 2228 couple to 4264 (y/n): n
Does frequence 2228 couple to 4336 (y/n): n
Does frequence 4264 couple to 4336 (y/n): n
Insert k factor for not being out of tube pulsing: 2
How many offset do you want to generate? 16
```

SCREEN CAPTURES OF THE OUPUT RESULT

```
//CHECK IF YOUR INSERT VALUES ARE CORRECT//
Coupling matrix is:
      542 Hz 903 Hz 1110 Hz 1471 Hz 2228 Hz 4264 Hz 4336 Hz
542 Hz | 1 0 0 0 0 0
                     0
                                   0
                                         0
               1
                            0
903 Hz | 0
1110 Hz | 0
              0
                     1
                            0
                                   0
                                         0
1471 Hz | 0
               0
                     0
                            1
                                   0
                                         0
               0
                                   1
2228 Hz | 0
                     0
                            0
                                         0
4264 Hz | 0
               0
                     0
                            0
                                   0
                                          1
                                 0 1
            0
                     0 0
4336 Hz | 0
                                              1|
0 = not coupled protons
1 = coupled protons and diagonal
Spectral width is (higher freq - lower freq) = 3794.0 Hz
Spectral width with security factor (2) is: 7588.0 Hz
Pulse Bandwith was set to 60
Coil length was set to 1.8 cm
Probe gradient strength was set to 53.5 G/cm
//CALCULATION RETURN//
______
Solution found after 1 iterations
Offset set to be used for multifrequence shaped pulse is: 16
855 Hz
1003 Hz
1418 Hz
1802 Hz
1889 Hz
2052 Hz
2192 Hz
2573 Hz
2699 Hz
3113 Hz
3428 Hz
3664 Hz
3824 Hz
4028 Hz
4117 Hz
4266 Hz
Set G0 to 1,85%
```

Z-position matrix (cm) 542 Hz 903 Hz 1110 Hz 1471 Hz 2228 Hz 4264 Hz 4336 Hz 855 Hz | 0,074 -0,011 -0,060 -0,146 -0,326 -0,809 -0,826 | 1003 Hz |0,109 0,024 -0,025 -0,111 -0,291 -0,774 -0,791| 1418 Hz | 0,208 0,122 0,073 -0,013 -0,192 -0,675 -0,692 | 1802 Hz |0,299 0,213 0,164 0,079 -0,101 -0,584 -0,601| 1889 Hz |0,320 0,234 0,185 0,099 -0,080 -0,563 -0,580| 2052 Hz |0,358 0,273 0,223 0,138 -0,042 -0,525 -0,542| 2192 Hz |0,391 0,306 0,257 0,171 -0,009 -0,492 -0,509| 2573 Hz | 0,482 0,396 0,347 0,261 0,082 -0,401 -0,418 | 2699 Hz | 0,512 0,426 0,377 0,291 0,112 -0,371 -0,388 | 3113 Hz | 0,610 0,524 0,475 0,390 0,210 -0,273 -0,290 | 3428 Hz |0,685 0,599 0,550 0,464 0,285 -0,198 -0,215| 3664 Hz |0,741 0,655 0,606 0,520 0,341 -0,142 -0,159| 3824 Hz |0,779 0,693 0,644 0,558 0,379 -0,104 -0,121| 4028 Hz |0,827 0,741 0,692 0,607 0,427 -0,056 -0,073| 4117 Hz | 0,848 0,762 0,713 0,628 0,448 -0,035 -0,052 | 4266 Hz | 0,883 0,798 0,749 0,663 0,483 0,000 -0,017 |

rows = generated offset frequencies for shaped pulse columns = input frequencies from user

NMR tube is divided into 126 slices

Slice thickness is: 0,014 cm

Experimental sensitivity respect to 1H spectrum should be around 12,7 which is given by the ratio: number of offsets/number of slices

Java script multi offset calculation example 2:

Sample: ibuprofen
Coupling spin system taken into account: Only aromatic strong coupling
Band Width = 60~Hz
Security facotr K=2
16 offsets as insert (16 obtained)

SCREEN CAPTURES OF THE INPUT FILE

```
//USER INSERT PARAMETERS//
Insert coil length in cm?: 1.8
Insert gradient strength in G/cm?: 53.5
Insert pulse band width in Hz?: 60
How many peaks to introduce?: 7
Insert peaks in ascending order:
Insert peak in Hz: 542
Insert peak in Hz: 903
Insert peak in Hz: 1110
Insert peak in Hz: 1471
Insert peak in Hz: 2228
Insert peak in Hz: 4264
Insert peak in Hz: 4336
Does frequence 542 couple to 903 (y/n): n
Does frequence 542 couple to 1110 (y/n): n
Does frequence 542 couple to 1471 (y/n): n
Does frequence 542 couple to 2228 (y/n): n
Does frequence 542 couple to 4264 (y/n): n
Does frequence 542 couple to 4336 (y/n): n
Does frequence 903 couple to 1110 (y/n): n
Does frequence 903 couple to 1471 (y/n): n
Does frequence 903 couple to 2228 (y/n): n
Does frequence 903 couple to 4264 (y/n): n
Does frequence 903 couple to 4336 (y/n): n
Does frequence 1110 couple to 1471 (y/n): n
Does frequence 1110 couple to 2228 (y/n): n
Does frequence 1110 couple to 4264 (y/n): n
Does frequence 1110 couple to 4336 (y/n): n
Does frequence 1471 couple to 2228 (y/n): n
Does frequence 1471 couple to 4264 (y/n): n
Does frequence 1471 couple to 4336 (y/n): n
Does frequence 2228 couple to 4264 (y/n): n
Does frequence 2228 couple to 4336 (y/n): n
Does frequence 4264 couple to 4336 (y/n): y
Insert k factor for not being out of tube pulsing: 2
How many offset do you want to generate? 16
```

SCREEN CAPTURES OF THE OUPUT RESULT

```
//CHECK IF YOUR INSERT VALUES ARE CORRECT//
Coupling matrix is:
      542 Hz 903 Hz 1110 Hz 1471 Hz 2228 Hz 4264 Hz 4336 Hz
542 Hz | 1 0 0 0 0 0
903 Hz | 0
                 1
                         0
                                0
                                        0
                                                0
1110 Hz | 0
                 0
                        1
                                0
                                        0
                                               0
1471 Hz | 0
2228 Hz | 0
4264 Hz | 0
                 0
                         0
                                1
                                        0
                                               0
                 0
                        0
                                0
                                        1
                                               0
                                    0
                                              1
                 0
                        0
                                0
4336 Hz |
          0
                 0
                         0
                                0
0 = not coupled protons
1 = coupled protons and diagonal
Spectral width is (higher freq - lower freq) = 3794.0 Hz
Spectral width with security factor (2) is: 7588.0 Hz
Pulse Bandwith was set to 60
Coil length was set to 1.8 cm
Probe gradient strength was set to 53.5 G/cm
//CALCULATION RETURN//
Solution found after 643 iterations
Offset set to be used for multifrequence shaped pulse is: 16
602 Hz
929 Hz
1123 Hz
1329 Hz
1465 Hz
1639 Hz
1917 Hz
2141 Hz
2848 Hz
3012 Hz
3371 Hz
3528 Hz
3677 Hz
3895 Hz
4114 Hz
4299 Hz
Set G0 to 1,85%
```

```
Z-position matrix (cm)
_____
      542 Hz 903 Hz 1110 Hz 1471 Hz 2228 Hz 4264 Hz 4336 Hz
602 Hz |0,014 -0,071 -0,121 -0,206 -0,386 -0,869 -0,886|
929 Hz |0,092 0,006 -0,043 -0,129 -0,308 -0,791 -0,808|
1123 Hz |0,138 0,052 0,003 -0,083 -0,262 -0,745 -0,762|
1329 Hz |0,187 0,101 0,052 -0,034 -0,213 -0,696 -0,713|
1465 Hz |0,219 0,133 0,084 -0,001 -0,181 -0,664 -0,681|
1639 Hz | 0,260 0,175 0,125 0,040 -0,140 -0,623 -0,640 |
1917 Hz |0,326 0,241 0,191 0,106 -0,074 -0,557 -0,574|
2141 Hz |0,379 0,294 0,245 0,159 -0,021 -0,504 -0,521|
2848 Hz | 0,547 0,461 0,412 0,327 0,147 -0,336 -0,353 |
3012 Hz |0,586 0,500 0,451 0,366 0,186 -0,297 -0,314|
3371 Hz |0,671 0,585 0,536 0,451 0,271
                                           -0,212 -0,229|
3528 Hz |0,708 0,623 0,574 0,488 0,308
3677 Hz |0,744 0,658 0,609 0,523 0,344
3895 Hz |0,795 0,710 0,661 0,575 0,395
                                           -0,175 -0,192|
                                           -0,139 -0,156|
                                           -0,088 -0,105|
4114 Hz |0,847 0,762 0,713 0,627 0,447 -0,036 -0,053|
4299 Hz |0,891 0,806 0,756 0,671 0,491 0,008 -0,009|
rows = generated offset frequencies for shaped pulse
columns = input frequencies from user
-----
NMR tube is divided into 126 slices
Slice thickness is: 0,014 cm
Experimental sensitivity respect to 1H spectrum should be around 12,7
which is given by the ratio: number of offsets/number of slices
```

Java script multi offset calculation example 3:

Sample: ibuprofen
Coupling spin system taken into account: all
Band Width = 60 Hz
Security facotr K = 2
16 offsets as insert (10 obtained)

SCREEN CAPTURES OF THE INPUT FILE

```
//USER INSERT PARAMETERS//
Insert coil length in cm?: 1.8
Insert gradient strength in G/cm?: 53.5
Insert pulse band width in Hz?: 60
How many peaks to introduce?: 7
Insert peaks in ascending order:
Insert peak in Hz: 542
Insert peak in Hz: 903
Insert peak in Hz: 1110
Insert peak in Hz: 1471
Insert peak in Hz: 2228
Insert peak in Hz: 4264
Insert peak in Hz: 4336
Does frequence 542 couple to 903 (y/n): n
Does frequence 542 couple to 1110 (v/n): v
Does frequence 542 couple to 1471 (y/n): n
Does frequence 542 couple to 2228 (y/n): n
Does frequence 542 couple to 4264 (y/n): n
Does frequence 542 couple to 4336 (y/n): n
Does frequence 903 couple to 1110 (y/n): n
Does frequence 903 couple to 1471 (y/n): n
Does frequence 903 couple to 2228 (y/n): y
Does frequence 903 couple to 4264 (y/n): n
Does frequence 903 couple to 4336 (y/n): n
Does frequence 1110 couple to 1471 (y/n): y
Does frequence 1110 couple to 2228 (y/n): n
Does frequence 1110 couple to 4264 (y/n): n
Does frequence 1110 couple to 4336 (y/n): n
Does frequence 1471 couple to 2228 (y/n): n
Does frequence 1471 couple to 4264 (y/n): n
Does frequence 1471 couple to 4336 (y/n): n
Does frequence 2228 couple to 4264 (y/n): n
Does frequence 2228 couple to 4336 (y/n): n
Does frequence 4264 couple to 4336 (y/n): y
Insert k factor for not being out of tube pulsing: 2
How many offset do you want to generate? 16
```

SCREEN CAPTURES OF THE OUPUT RESULT

```
//CHECK IF YOUR INSERT VALUES ARE CORRECT//
Coupling matrix is:
      542 Hz 903 Hz 1110 Hz 1471 Hz 2228 Hz 4264 Hz 4336 Hz
542 Hz | 1 0 1 0 0 0 0 |
903 Hz | 0
               1
                      0
                             0
                                    1
                                           0
1110 Hz | 1
               0
                                   0
                      1
                             1
                                           0
               0
                             1
1471 Hz | 0
                                    0
                                           0
                      1
                                                  0 [
                                           0
                      0
                             0
2228 Hz | 0
               1
                                    1
                                                 0 [
                      0
                            0
4264 Hz | 0
               0
                                   0
                                           1
                                                 1|
4336 Hz | 0
              0
                      0
                            0
                                   0
                                          1
                                                 1|
0 = not coupled protons
1 = coupled protons and diagonal
Spectral width is (higher freq - lower freq) = 3794.0 Hz
Spectral width with security factor (2) is: 7588.0 Hz
Pulse Bandwith was set to 60
Coil length was set to 1.8 cm
Probe gradient strength was set to 53.5 G/cm
//CALCULATION RETURN//
Solution found after 45185 iterations
Offset set to be used for multifrequence shaped pulse is: 10
975 Hz
1172 Hz
1458 Hz
1458 Hz
1959 Hz
2153 Hz
2419 Hz
2616 Hz
2894 Hz
3843 Hz
Set G0 to 1,85%
```

Z-position matrix (cm) 542 Hz 903 Hz 1110 Hz 1471 Hz 2228 Hz 4264 Hz 4336 Hz 975 Hz |0,103 0,017 -0,032 -0,118 -0,297 -0,780 -0,797| 1172 Hz |0,149 0,064 0,015 -0,071 -0,251 -0,733 -0,751| 1458 Hz |0,217 0,132 0,083 -0,003 -0,183 -0,666 -0,683| 1959 Hz |0,336 0,251 0,201 0,116 -0,064 -0,547 -0,564| 2153 Hz |0,382 0,297 0,247 0,162 -0,018 -0,501 -0,518| 2419 Hz | 0,445 0,360 0,311 0,225 0,045 -0,438 -0,455 | 2616 Hz | 0,492 0,406 0,357 0,272 0,092 -0,391 -0,408 | 2894 Hz |0,558 0,472 0,423 0,338 0,158 -0,325 -0,342| 3843 Hz |0,783 0,697 0,648 0,563 0,383 -0,100 -0,117| 4322 Hz |0,897 0,811 0,762 0,676 0,497 0,014 -0,003| rows = generated offset frequencies for shaped pulse columns = input frequencies from user NMR tube is divided into 126 slices Slice thickness is: 0,014 cm Experimental sensitivity respect to 1H spectrum should be around 7,9 which is given by the ratio: number of offsets/number of slices

Java script multi offset calculation example 4:

Sample: ibuprofen
Coupling spin system taken into account: all
Band Width = 30 Hz
Security facotr K = 2
16 offsets as insert (14 obtained)

SCREEN CAPTURES OF THE INPUT FILE

```
//USER INSERT PARAMETERS//
Insert coil length in cm?: 1.8
Insert gradient strength in G/cm?: 53.5
Insert pulse band width in Hz?: 30
How many peaks to introduce?: 7
Insert peaks in ascending order:
Insert peak in Hz: 542
Insert peak in Hz: 903
Insert peak in Hz: 1110
Insert peak in Hz: 1471
Insert peak in Hz: 2228
Insert peak in Hz: 4264
Insert peak in Hz: 4336
Does frequence 542 couple to 903 (y/n): n
Does frequence 542 couple to 1110 (y/n): y
Does frequence 542 couple to 1471 (y/n): n
Does frequence 542 couple to 2228 (y/n): n
Does frequence 542 couple to 4264 (y/n): n
Does frequence 542 couple to 4336 (y/n): n
Does frequence 903 couple to 1110 (y/n): n
Does frequence 903 couple to 1471 (y/n): n
Does frequence 903 couple to 2228 (y/n): y
Does frequence 903 couple to 4264 (y/n): n
Does frequence 903 couple to 4336 (y/n): n
Does frequence 1110 couple to 1471 (y/n): y
Does frequence 1110 couple to 2228 (y/n): n
Does frequence 1110 couple to 4264 (y/n): n
Does frequence 1110 couple to 4336 (y/n): n
Does frequence 1471 couple to 2228 (y/n): n
Does frequence 1471 couple to 4264 (y/n): n
Does frequence 1471 couple to 4336 (y/n): n
Does frequence 2228 couple to 4264 (y/n): n
Does frequence 2228 couple to 4336 (y/n): n
Does frequence 4264 couple to 4336 (y/n): y
Insert k factor for not being out of tube pulsing: 2
How many offset do you want to generate? 16
```

SCREEN CAPTURES OF THE OUPUT RESULT

```
//CHECK IF YOUR INSERT VALUES ARE CORRECT//
Coupling matrix is:
     542 Hz 903 Hz 1110 Hz 1471 Hz 2228 Hz 4264 Hz 4336 Hz
542 Hz | 1 0 1 0 0 0
903 Hz | 0
               1
                     0
                            0
                                   1
                                          0
1110 Hz | 1
              0
                     1
                            1
                                   0
                                          0
                                                 0 [
                                   0
1471 Hz | 0
              0
                     1
                            1
                                          0
                                                 0 [
                   0
2228 Hz | 0
               1
                            0
                                   1
                                          0
             0
4264 Hz | 0
                     0
                            0
                                   0
                                          1
                                                 1|
4336 Hz | 0
              0
                     0
                            0
                                   0
                                          1
                                                1|
0 = not coupled protons
1 = coupled protons and diagonal
Spectral width is (higher freq - lower freq) = 3794.0 Hz
Spectral width with security factor (2) is: 7588.0 Hz
Pulse Bandwith was set to 30
Coil length was set to 1.8 cm
Probe gradient strength was set to 53.5 G/cm
//CALCULATION RETURN//
_____
Solution found after 8057 iterations
Offset set to be used for multifrequence shaped pulse is: 14
584 Hz
795 Hz
828 Hz
998 Hz
1524 Hz
1795 Hz
2009 Hz
2207 Hz
2490 Hz
3000 Hz
3627 Hz
3766 Hz
4022 Hz
4249 Hz
```

Z-position matrix (cm)

rows = generated offset frequencies for shaped pulse columns = input frequencies from user

NMR tube is divided into 253 slices

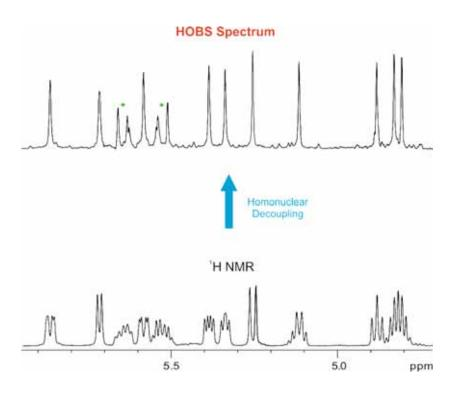
Slice thickness is: 0,007 cm

Experimental sensitivity respect to 1H spectrum should be around 5,5 which is given by the ratio: number of offsets/number of slices

PUBLICATION 2

Full sensitivity and enhanced resolution in homodecoupled band-selective NMR experiments

Laura Castañar, Pau Nolis, Albert Virgili and Teodor Parella. *Chem. Eur. J.,* **2013**, *19*, 17283-17286.



Introduction

Chemical shifts and coupling constants are fundamental parameters in the analysis and interpretation of NMR spectra. Multiplicity information can be extracted from the analysis of the fine multiplet structure and it can be related to structural parameters such as dihedral angles or the number of neighboring nuclei. The signal resolution in ¹H NMR spectra is rather poor, owing to the narrow proton chemical shift range and to the signal splitting by homonuclear coupling. As it has been show in Introduction, over recent years a high interest has emerged to develop broadband homodecoupled ¹H NMR techniques that offer increased resolution by simplifying the typical J_{HH} multiplet pattern to singlet lines, and therefore reducing signal overlapping. Most of the pure shift NMR experiments recently published are based on the Zangger-Sterk (ZS) method³, which uses the spatial encoding concept along the z-dimension to obtain ¹H fully homodecoupled spectra. The main drawback of ZS methods is their very low sensitivities because signal only comes from selected z-slices. Thus the main challenge in this field is to design experiments which improve sensitivity.

In this publication a simple modification of the slice-selective 1D HOBB experiment³⁶ allows the collection of broadband homodecoupled spectra of specific regions of the ¹H spectrum without sacrificing sensitivity. As a major feature, this *Homodecoupled Band-Selective* (HOBS) NMR method does not use the spatial encoding gradient G_s applied simultaneously with the selective pulses, and therefore, pure shift 1D spectra can be quickly recorded without the sensitivity losses characteristic of the slice selection process. The main limitation of this frequency-selective experiment is that only a particular part of the ¹H spectrum is monitored in a single-NMR spectrum. However, HOBS promises to have a potential use in spectra presenting a set of equivalent spin systems in well-separated and defined regions, such as the typical NH or H_{α} protons in peptides and proteins or those found in nucleic acids.

COMMUNICATION

DOI: 10.1002/chem.201303235

Full Sensitivity and Enhanced Resolution in Homodecoupled Band-Selective NMR Experiments

Laura Castañar, [a, b] Pau Nolis, [a] Albert Virgili, [b] and Teodor Parella*[a]

Chemical shifts and coupling constants (J) are fundamentals in the analysis and interpretation of NMR spectra. Multiplicity information and J values can be extracted from the analysis of the fine multiplet structure, and they can be related to structural parameters, such as the number of neighbouring spins, the trace of trough-bond connectivities or dihedral angle constraints. Over recent years, a significant interest has emerged to develop homodecoupled ¹H NMR spectroscopy techniques that offer increased resolution by simplifying the homonuclear splitting pattern, and therefore reducing signal overlapping.

The simplest approach for homodecoupling is the use of semiselective shaped pulse decoupling during signal detection, where the receiver and the decoupling are alternatively activated.[1] If the semiselective pulse is applied in a region A of the spectrum, the multiplet structure of J coupled signals resonating in a different region B appear simplified while they are detected. However, this is not a broadband method because protons from a third region C would not be decoupled, and therefore the corresponding coupling splittings will remain in the partially decoupled spectrum. Although the use of sophisticated multiple-region decoupling using different and simultaneous decoupling waveforms could be applied, it is difficult to achieve a perfect decoupling for all resonances and, moreover, without the interference of undesired decoupling sidebands.[2] Alternatively, the internal projection in the chemical shift dimension of J-resolved experiments[3] or the diagonal signals in anti-z-COSY experiments[4] have been also proposed to obtain broadband homodecoupled NMR spectra. They require the collection of more time consuming 2D/3D data and post-processing tasks can be further required. Some years ago, the so-called Zangger-Sterk (ZS) method based on the implementation of the spatially encoded concept along the z-dimension was also proposed.[5] The ZS method has been further refined and several applications have been reported to obtain high-resolved pure-shift multidimensional NMR spectra. [6-8] The main drawbacks of ZS methods are their low sensitivities because signal only comes from selected z slices and, on the other hand, the need for an FID reconstruction method by means of a time-consuming 2D/3D mode acquisition. Very recently, a new NMR detection scheme has been proposed for the instant and speed-up acquisition of ZS-decoupled spectra in a one-shot single-scan experiment. [9] The instant technique greatly improves the sensitivity per time unit ratio although the attainable sensitivity is still far from a regular ¹H spectrum. Analogous ZS methods incorporating isotopic ¹³C editing by using BIRD elements have been also reported to efficiently minimise the effects of strong coupling, but an important penalty in sensitivity remains due to the low natural abundance of ¹³C (1.1%). [10]

Based on the instant ZS experiment, a novel NMR spectroscopy method for the fast acquisition of full-sensitive, homodecoupled band-selective (HOBS) NMR spectra is proposed here. It is noteworthy that the spatial encoding gradients applied simultaneously with the selective pulses in the original instant scheme are here omitted, avoiding sensitivity losses due to spatial slice selection. In addition, the HOBS method incorporates a number of advantages, such as: 1) an effective homodecoupling NMR block consisting of a pair of hard/selective 180° pulses flanked by pulsed field gradients (Figure 1), 2) an excellent spectral quality related to the use of selective gradient echoes, 3) real-time data collection without need of additional reconstruction methods that also allows conventional FID data processing, and 4) an easy implementation in multidimensional experiments. In our hands, the best results in terms of selectivity and optimum

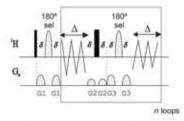


Figure 1. Schematic representation of the 1D homodecoupling band-selective (HOBS) experiment. Homodecoupling during detection is achieved by applying a pair of hard/semiselective $180^{\rm h}$ H pulses (represented as solid and shaded shapes) at the middle of $2\Delta = AQ/n$ periods, in which AQ is the acquisition time and n the number of concatenated loops; δ is the duration of gradients and the recovery delay.

Wiley Online Library

— 17283

 [[]a] L. Castañar, Dr. P. Nolis, Dr. T. Parella Servei Ressonância Magnètica Nuclear Universitat Autônoma de Barcelona 08193 Bellaterra, Barcelona (Spain) E-mail: teodor.parella@uab.cat

[[]b] L. Castañar, Prof. A. Virgili Departament de Química, Universitat Autònoma de Barcelona 08193 Bellaterra, Barcelona (Spain)

Supporting information for this article is available on the WWW under http://dx.doi.org/10.1002/chem.201303235.

CHEMISTRY

A EUROPEAN JOURNAL



relaxation are obtained using 180° REBURP semiselective pulses of 5–10 ms for both region-selective excitation and decoupling as a function of the selected region, and applied at intervals of $2\Delta = 10{\text -}15 \text{ ms.}^{[11]}$

Peptides and proteins are good targets for evaluating the efficiency of band-selective NMR spectroscopy experiments because a set of equivalent spins (amide NH, Ha or aliphatic side-chain protons) appear in well-separated regions. We chose the cyclic peptide cyclosporine (1) to verify the selectivity and sensitivity aspects of the proposed HOBS experiment. Figure 2B and C compare the individual single-scan 1D HOBS spectra obtained after selection of the H, and NH region, respectively, with the 1H spectrum acquired with the regular 90° pulse-acquisition method (Figure 2 A). Clearly, all Ha or NH signals are fully homodecoupled, independent of their coupling pattern and also independent of the rest of the spectrum. It is very important to highlight that clean spectra are achieved, with minimum set-up and, in contrast to slice-selective ZS experiments, the same sensitivity levels as the conventional 1H spectrum are retained.



Figure 2. A) Regular pulse-acquisition, and B), C) HOBS 1 H NMR spectra of cyclosporine (I) after selection of H_n and NH regions, respectively. All spectra were recorded with the same receiver gain, with a single scan and processed with a Fourier transformation without any additional window function. All spectra are plotted with the same absolute vertical scaling factor for a comparison of their real sensitivity. HOBS spectra were recorded by applying 5 ms 180° REBURP pulses (about 1200 Hz of bandwith) for both excitation and decoupling in the region of interest. The 8 K data points were acquired using an acquisition time (AQ) of 576 ms (40 loops (n) were used with $\Delta = 7.2$ ms) and a recycle delay of 1 s. Gradients G1:G2:G3 with a duration of 500 µs were set to 23, 41 and 63% of the maximum attainable strength (53.5 Gcm $^{-1}$). The asterisks marked in (B) stand for unavoidable non-decoupled effects of an AB two-spin system.

The Ha region (Figure 2B) additionally contains an AB two-spin system corresponding to the side-chain olefinic system of the residue 1, which can be used to evaluate the effects of mutual coupling in HOBS experiments as a function of the pulse selectivity. Sensitivity and selectivity always present opposite and conflicting points in all homodecoupling experiments. It can be shown that these protons are not fully decoupled and display their mutual coupling, because both experience the effects of the semiselective REBURP pulse. This unwanted J effect is not exclusive for the HOBS method, it is also present in the original instant and pseudo-2D ZS experiments recorded with the same selectivity conditions. Even the use of more selective pulses in the instant experiment (for instance, a Gaussian-shaped 180° pulse of 10 ms with an effective bandwidth of 121 Hz) does not provide complete decoupling for this spin system. Whereas the pseudo-2D ZS method can efficiently collapse these multiplets using a high-selective 60 ms Rsnob-shaped 180° pulse (effective bandwidth of 39 Hz), but at the expense of a dramatic sensitivity penalty, the instant and HOBS experiments completely fail under these conditions by severe relaxation due to the long pulse duration.

When trying to incorporate the pseudo-2D ZS method into multidimensional experiments, the overall acquisition time becomes extremely long because of the need for a 3D acquisition mode and for its reduced sensitivity. An important feature of the proposed HOBS detection scheme is its easy implementation as a powerful and general building block in existing multidimensional NMR spectroscopy experiments, with the same selectivity conditions as reproduced with the 1D version and retaining the maximum sensitivity levels of the original experiments. As an example, Figure 3 compares the conventional TOCSY versus the HOBS-TOCSY spectra of 1 acquired with the same experimental conditions and time. The 1D row analysis reveals a much better resolution in the direct dimension without affecting sensitivity, spectral quality and performance. Note that strong coupling effects remain exactly as observed in the 1D version. Other attempts to obtain pure-shift TOCSY spectra require a more extensive experimental time. [5,7]

Similarly, the non-refocused version of a F2-coupled

¹H-¹⁵C HOBS-HSQC spectrum shows collapsed signals with improved resolution and even better sensitivity, making it highly suitable for the reliable measurement of one-bond proton-carbon coupling constants from simplified singlet lines, and demonstrating its potential for measuring accurate residual dipolar couplings (RDCs) in anisotropic media under high-sensitivity conditions (Figure 4).

^[12] The HOBS scheme is also fully compatible with simultaneous broadband heteronuclear decoupling during acquisition. Details of the pulse timing on the simultaneous homo- and heteronuclear decoupling and its implementation into the conventional HSQC spectrum are available in the Supporting Information.

In summary, a new band-selective detection scheme has been proposed to collect homodecoupled NMR spectra of specific regions without sacrificing sensitivity. The imple-

17284 ----

www.chemeurj.org

© 2013 Wiley-VCH Verlag GmbH & Co. KGaA, Weinbeim

Chem. Eur. J. 2013, 19, 17283-17286

COMMUNICATION

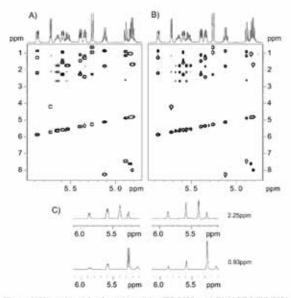


Figure 3, H_a -region selective: A) regular TOCSY, and B) HOBS-TOCSY spectra of 1 (mixing time of 60 ms); C) 1D slices taken at two different frequencies to compare the relative sensitivity and resolution levels. Four scans were collected for each 128 t_1 increments of 2 K complex points, giving an experimental time of 13 min for each 2D spectrum. Homodecoupling was achieved using 20 loops and Δ =4.3 ms (AQ=170 ms) whereas all other experimental parameters were as described in the legend of Figure 2.

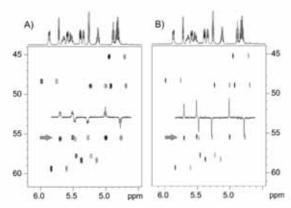


Figure 4. A) Regular, and B) HOBS spectra of the non-refocused F2 coupled $^{1}\text{H-}^{12}\text{C}$ HSQC experiment of **I**. The interpulse delays were optimised to 145 Hz. Two scans were collected for each one of the 64 t_1 increments of 2 K complex data points. Homodecoupling was achieved using n=50, $\Delta=5.7$ ms. AQ=570 ms. sw=1800 Hz and a REBURP 180° pulse of 5 ms. The experimental time for each 2D spectrum was of 5 min.

mentation of the HOBS approach becomes easy and reliable for a large number of multidimensional applications and guarantees rapid data acquisition even for samples at low concentrations. In particular, it can become very attractive for biomolecular NMR spectroscopy applications, particularly if combined with the gains in sensitivity and resolution offered by cryogenic probes and high magnetic fields. For instance, it could be used to remove contributions to line broadening due to residual HH dipolar couplings when working with partially oriented proteins in anisotropic media^[13] or to improve the sensitivity and resolution of band-selective ¹³C-detected NMR experiments with active *J*(CC) coupling constants, such as those applied on ¹³C-labeled proteins ^[14] HOBS methodology is also fully compatible with other homodecoupling methods applied in the indirect dimension of multidimensional NMR experiments^[15] and many aspects are currently being explored to demonstrate the power of these pure-shift NMR solutions.

Experimental Section

All NMR spectroscopy experiments were performed in a 600 MHz Bruker Avance-III spectrometer equipped with a TXI probe and a gradient unit delivering 53.5 Gcm⁻¹. The sample used was 25 ms cyclosporine in [D₆]benzene. More experimental details and pulse sequence diagram of 2D HOBS versions of the refocused HSQC-CLIP and fully homo- and heteronuclear decoupled HSQC experiments can be found in the Supporting Information.

Acknowledgements

Financial support for this research provided by MICINN (project CTO2012-32436) and Bruker Española S.A. are gratefully acknowledged. We also thank to the Servei de Ressonância Magnètica Nuclear, Universitat Autònoma de Barcelona, for allocating instrument time to this project. The authors also thank Prof. K. Zangger for providing experimental details and the pulse program code of the original instant experiment.

Keywords: band selective • homodecoupling • NMR spectroscopy • sensitivity enhancement • structure elucidation

- a) J. P. Jesson, P. Meakin, G. Kneissel, J. Am. Chem. Soc. 1973, 95, 618–620;
 b) A. Hammarström, G. Otting, J. Am. Chem. Soc. 1994, 116, 8847–8848;
 c) J. Weigelt, A. Hammarström, W. Bermel, G. Otting, J. Magn. Reson. Ser. B 1996, 110, 219–224.
- a) E. Kupče, G. Wagner, J. Magn. Reson. Ser. B 1995, 109, 329-333;
 b) E. Kupče, G. Wagner, J. Magn. Reson. Ser. B 1996, 110, 309-312;
 c) E. Kupče, H. Matsuo, G. Wagner, in Biological Magnetic Resonance Modern Techniques in Protein NMR, Vol. 16 (Eds.: N. R. Krishna, L. J. Berliner), Springer, Heidelberg, 1999, 16, pp. 149-193;
 d) B. Vögeli, H. Kovacs, K. Pervushin, J. Biomol. NMR 2005, 31, 1-0
- [3] a) A. J. Pell, J. Keeler, J. Magn. Reson. 2007, 189, 293-299; b) B.
 Luy, J. Magn. Reson. 2009, 201, 18-24; c) P. Sakhaii, B. Haase, W.
 Bermel, J. Magn. Reson. 2013, 228, 125-129.
- [4] A. J. Pell, R. A. Edden, J. Keeler, Magn. Reson. Chem. 2007, 45, 296-316.
- [5] K. Zangger, H. Sterk, J. Magn. Reson. 1997, 124, 486–489.
- [6] a) M. Nilsson, G.A. Morris, Chem. Commun. 2007, 933-935;
 b) J.A. Aguilar, S. Faulkner, M. Nilsson, G.A. Morris, Angew. Chem. 2010, 122, 3993-3995; Angew. Chem. Int. Ed. 2010, 49, 3901-3903.

www.chemeurj.org

17285

CHEMISTRY

T. Parella et al.

A EUROPEAN JOURNAL

- [7] a) G. A. Morris, J. A. Aguilar, R. Evans, S. Haiber, M. Nilsson, J. Am. Chem. Soc. 2010, 132, 12770–12772; b) J. J. Koivisto, Chem. Commun. 2013, 49, 96–98.
- [8] J. A. Aguilar, A. A. Colbourne, J. Cassani, M. Nilsson, G. A. Morris, Angew. Chem. 2012, 124, 6566-6569; Angew. Chem. Int. Ed. 2012, 51, 6460-6463.
- [9] N. H. Meyer, K. Zangger, Angew. Chem. 2013, 125, 7283-7286; Angew. Chem. Int. Ed. 2013, 52, 7143-7146.
- [10] a) A. Lupulescu, G. L. Olson, L. Frydman, J. Magn. Reson. 2012, 218, 141–146; b) J. A. Aguilar, M. Nilsson, G. A. Morris, Angew. Chem. 2011, 123, 9890–9891; Angew. Chem. Int. Ed. 2011, 50, 9716– 9717.c) P. Sakhaii, B. Haase, W. Bermel, J. Magn. Reson. 2009, 199, 192–198.
- [11] H. Geen, R. Freeman, J. Magn. Reson. 1991, 93, 93-141.

- [12] A. Enthart, J. C. Freudenberger, J. Furrer, H. Kessler, B. Luy, J. Magn. Reson. 2008, 192, 314–322.
- [13] C. W. Vander Kooi, E. Kupče, R. P. Zuiderweg, M. Pellecchia, J. Biomol. NMR 1999, 15, 335–338.
- [14] a) I. Bertini, I. C. Felli, R. Kümmerle, D. Moskau, R. Pierattelli, J. Am. Chem. Soc. 2004, 126, 464-465; b) W. Bermel, I. Bertini, L. Duma, I. C. Felli, L. Emsley, R. Pieratelli, P. R. Vasos, Angew. Chem. 2005, 117, 3149-3152; Angew. Chem. Int. Ed. 2005, 44, 3089-3092.
- [15] V. V. Krishnamurthy, J. Magn. Reson. A 1996, 113, 46–52; b) V. V. Krishnamurthy, Magn. Reson. Chem. 1997, 35, 9–12.

Received: August 16, 2013 Published online: November 11, 2013



Supporting Information

© Copyright Wiley-VCH Verlag GmbH & Co. KGaA, 69451 Weinheim, 2013

Full Sensitivity and Enhanced Resolution in Homodecoupled Band-Selective NMR Experiments

Laura Castañar, [a, b] Pau Nolis, [a] Albert Virgili, [b] and Teodor Parella*[a]

chem_201303235_sm_miscellaneous_information.pdf

Experimental Section

All experiments were acquired on a Bruker AVANCE spectrometer (Bruker BioSpin, Rheinstetten, Germany) operating at 600.13 MHz proton frequency, equipped with a 5 mm triple resonance inverse probe and a z-axis pulsed field gradient accessory (maximum strength of 53.5 G/cm). The spectra were collected on a 25 mM sample of the cyclic peptide cyclosporine dissolved in benzene-d6 at a temperature T = 298 K, and processed with the software TOPSPIN 2.1.

The non-selective ¹H 180 pulses were of 8.0 μs duration. For all 1D and 2D HOBS experiments, a 180° band-selective REBURP shaped pulse of 5.0 ms was used for both excitation and homodecoupling. It was generated using the *stdisp* pulse shaping program available in Topspin NMR software. The setting of this pulse was initially tested and optimized using a single-scan SPFGE experiment (as Fig.1 with a conventional detection period), as shown in Fig. S1B. The strengths of the G1, G2 and G3 gradients were set to 12.3, 21.9 and 33.7 G/cm, respectively, with durations of 500 μs followed by a recovery delay of 20 μs.

1D HOBS spectra of Fig. 2B and 2C were recorded using a single scan and 1 s of recycle delay. The spectral width was 7200 Hz, and 8K complex points were recorded during an acquisition time of 576 ms. 40 loops (n) were concatenated with Δ =AQ/2n=7.2ms. The 1D time-domain data were directly transformed without any sensitivity or resolution enhancement.

The regular 2D TOCSY spectrum (Fig. 3A) was acquired using the *dipsi2ph* pulse program, using a z-filtered DIPSI-2 spinlock of ca. 8 kHz effective field strength was used with a mixing time of 60ms. The HOBS-TOCSY spectrum (Fig. 3B) was acquired using the pulse sequence displayed in Fig. S4A, with the same parameters described for the regular TOCSY and 1D HOBS experiments. Two scans of 2048 complex points were collected over an observed spectral width of 6000 Hz for each of the 128 t_1 values. Experimental parameters: AQ=170ms, n=20, Δ =4.3ms, and recycle delay of 1s. Data were transformed with a shifted sine window function along both the F1 and F2 dimensions and with a zero-filling to 1K in F1. The total experimental time was about 13 minutes for each 2D spectrum.

The non-refocused version of the 2D ¹H-¹³C HSQC spectrum (Fig. 4A) was optimized to 1/(2*J_{CH})=145Hz. Two scans of 1024 complex points were collected over an observed spectral width of 1800 Hz for each of the 128 t₁ values. Data were transformed with a shifted sine window function along both the F1 and F2 dimensions and with a zero-filling to 1K in F1. The corresponding HOBS-HSQC spectrum (Fig. 4B) was acquired using the pulse sequence displayed in Fig. S4B, with the same parameters described for the regular HSQC and 1D HOBS experiments. The 90° and 180° band-selective pulses were EBURP-2 of 3.5 ms and REBURP of 5.0 ms, respectively. The total experimental time was about 5 minutes for each 2D spectrum. The above conditions were also applied for the HOBS-HSQC-CLIP (see the pulse scheme in Fig. S4C and the corresponding spectrum in Fig. S5B) and fully-decoupled HOBS-HSQC experiments (see the pulse scheme in Fig. S6B and the corresponding spectrum in Fig. S7B). To achieve heteronuclear decoupling during the HOBS detection scheme, the pulse timing described in Fig. S7A was applied.

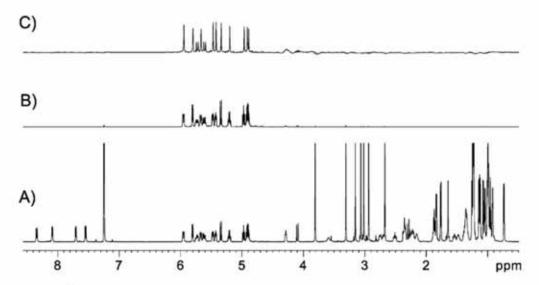


Figure S1: (A) ¹H spectrum of cyclosporine; B) Band-selective spectrum acquired with the single-pulsed-field gradient echo (SPFGE) sequence using a semiselective RE-BURP-shaped 180° ¹H pulse of 5 ms; and C) 1D HOBS spectra acquired with the pulse sequence of Fig. 1 using a 5ms REBURP-shaped pulse.

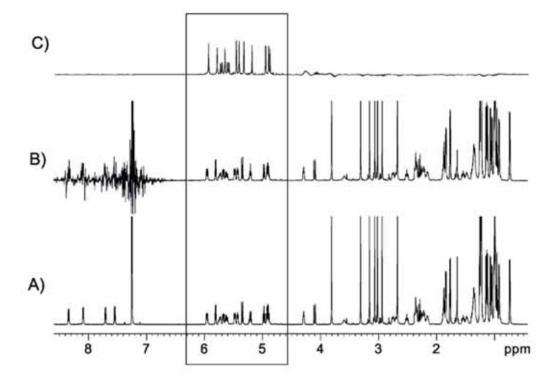


Figure S2: Comparison between the A) standard ^{1}H spectrum; B) ^{1}H spectrum (acquired with 4 scans) after SESAM decoupling of the NH region during acquisition using a *mlevsp180* pulse train with a 5 ms REBURP shaped pulse as inversion element (pulse program called zghc.3); C) Clean 1D HOBS spectra acquired with the pulse sequence of Fig. 1 using a 5ms REBURP-shaped ^{1}H pulses. See Fig. S3 for a better visualization of the expanded ^{1}H region.

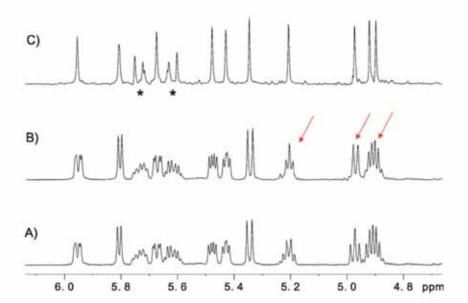
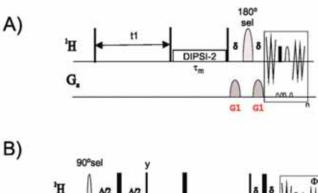
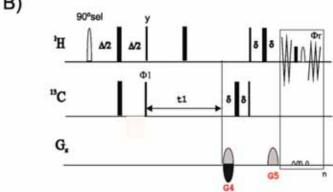


Figure S3: Expanded H_{α} region corresponding to the spectra of Fig. S2. The selective decoupling of the NH region in B only simplifies the H_{α} protons with a resolved J(NH- H_{α}) coupling (see arrows). Note that other couplings between H_{α} and other side-chain H_{β} protons are not affected. In C) all couplings are collapsed except the active J(HH) of the olefinic AB spin system (marked with asterisks).





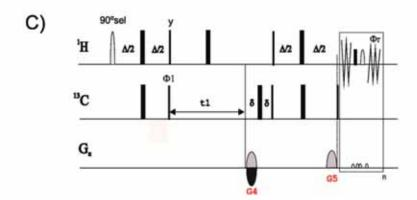


Figure S4: Basic illustration of the incorporation of the HOBS technique in conventional 2D homo- and heteronuclear NMR experiments. General pulse schemes for the A) HOBS-TOCSY, B) non-refocused HOBS-HSQC, and C) refocused HOBS-HSQC-CLIP experiments. Basically, all these experiments have been easily adapted from conventional sequences by substituting an appropriate hard 90° pulse by a selective 90° or a 90°-δ-180sel- δ SPFGE block, and changing the conventional detectino period by the HOBS scheme, as reported in Fig.1 of the manuscript. The parameters working in the 1D HOBS sequence can be directly implemented in these 2D versions without any additional calibration. All pulse powers and durations, delays, gradient strengths and phase cycles are exactly the same as set in the conventional 2D experiments. The hard and semi-selective 180 pulses in the HOBS scheme are applied from the x axis, without any further phase cycling.

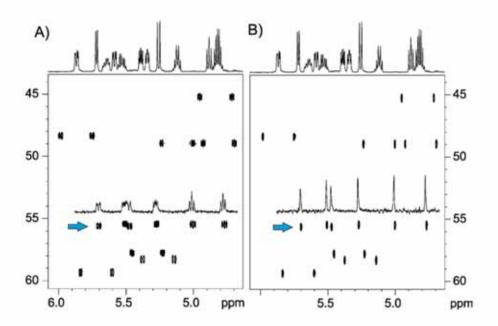
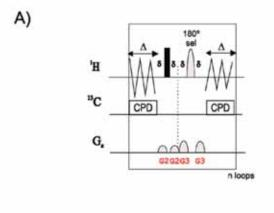


Figure S5: A) Conventional and B) HOBS versions of the F2-coupled HSQC-CLIP spectra of cyclosporine obtained using the non-refocused version of Fig. S4B with the same experimental conditions as described in Fig. 4. More details can be found in the experimental section.



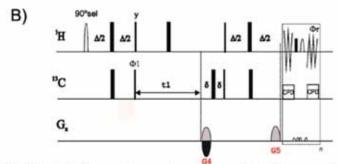


Figure S6: A) 1D HOBS detection scheme to perform simultaneous broadband homo- and heteronuclear decoupling. Heteronuclear Decoupling (CPD) is only applied during data writing and it is switch off during the application of the gradient-based inversion elements; B) Pulse scheme of the fully homo- and heteronuclear decoupled HOBS-HSQC experiment.

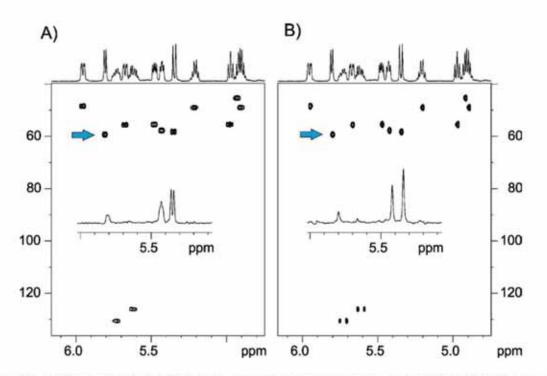
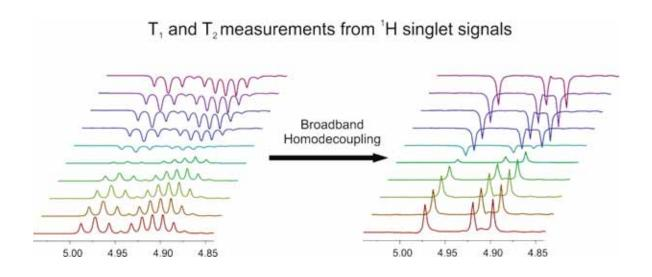


Figure S7: A) Conventional and B) fully homo- and heteronuclear decoupled HOBS-HSQC spectra of cyclosporine obtained using the non-refocused version of Fig. S6B with the same experimental conditions as described in Fig. 4. Note the J(HH) doublet splitting of the two olefinic AB protons. More details can be found in the experimental section.

PUBLICATION 3

Measurement of T_1/T_2 relaxation times in overlapped regions from homodecoupled ¹H singlet signals

Laura Castañar, Pau Nolis, Albert Virgili and Teodor Parella. *J. Magn. Reson.*, **2014**, *244*, 30-35.



Introduction

The measurement of relaxation rates by NMR spectroscopy provides important insights into the dynamics of molecules in solution. Longitudinal spin-lattice T_1 relaxation times are usually determined from *Inversion Recovery* (IR) experiment⁸⁸ whereas transverse spin–spin T_2 relaxation times are measured from *Carr–Purcell–Meiboom–Gill* (CPMG) sequences.⁸⁹ One drawback of CPMG pulse trains is the presence of multiplet distortions due to J_{HH} evolution that can affect the accuracy of the measurement. An improved perfect CPMG sequence that achieves *Periodic Refocusing Of J Evolution by Coherence Transfer* (referred to as PROJECT) has been proposed recently to minimize the effects of *J* evolution during the echo periods, obtaining pure in-phase signals.⁹⁰

On other hand, T_1 and T_2 values are usually extracted from the analysis of mono-exponential signal decays monitored in a series of 1D spectra. However, signal overlap hampers a simple data analysis due to the superposition of several individual decays. In these cases, the use of more sophisticated methods, such as deconvolution, line fitting techniques or the analysis of multiple-exponential decay can be required to obtain correct values for each individual signal.

In this article, the implementation of the HOBS technique (see **Publication 2**) in standard IR and PROJECT experiments is proposed to solve overlapping problems. The new homodecoupled 1D HOBS-IR and HOBS-PROJECT experiments allows the accurate measure of T_1 and T_2 relaxation times from the resulting singlet lines using conventional mono-exponential curve-fitting methods. These experiments have been tested on crowded areas of cyclosporine and progesterone samples. The experimental T_1 and T_2 data obtained from HOBS versions agree with data extracted from conventional IR and PROJECT experiments.

^[88] a) P. B. Kingsley, *Concepts Magn. Reson.*, **1999**, *11*, 29. b) P. B. Kingsley, *Concepts Magn. Reson.*, **1999**, *11*, 243. [89] a) H. Y. Carr, E. M. Purcell, *Phys. Rev.*, **1954**, *274*, 630. b) S. Meiboom, D. Gill, *Rev. Sci. Instrum.*, **1958**, *29*, 688.

Journal of Magnetic Resonance 244 (2014) 30-35



Contents lists available at ScienceDirect

Journal of Magnetic Resonance

journal homepage: www.elsevier.com/locate/jmr



Measurement of T_1/T_2 relaxation times in overlapped regions from homodecoupled 1H singlet signals



Laura Castañar, Pau Nolis, Albert Virgili, Teodor Parella

Servei de Ressonância Magnètica Nuclear und Departament de Química, Universitat Autônoma de Barcelona, E-08193 Bellaterra, Catalonia, Spain

ARTICLE INFO

Article history: Received 26 February 2014 Revised 2 April 2014 Available online 24 April 2014

Keywords: Pure-shift NMR Relaxation times T₁ T₂ Inversion-Recovery CPMG PROJECT HOBS

ABSTRACT

The implementation of the HOmodecoupled Band-Selective (HOBS) technique in the conventional Inversion-Recovery and CPMG-based PROJECT experiments is described. The achievement of fully homodecoupled signals allows the distinction of overlapped $^1\mathrm{H}$ resonances with small chemical shift differences. It is shown that the corresponding T_1 and T_2 relaxation times can be individually measured from the resulting singlet lines using conventional exponential curve-fitting methods.

© 2014 Elsevier Inc. All rights reserved.

1. Introduction

The measurement of relaxation rates by Nuclear Magnetic Resonance (NMR) spectroscopy can provide important insights into the dynamics of molecules in solution [1]. Longitudinal spin-lattice T1 relaxation times are usually determined from the Inversion-Recovery (IR) experiments [2,3] whereas transverse spin-spin T2 relaxation times are measured from Carr-Purcell-Meiboom-Gill (CPMG) sequences [4,5]. Recently, an improved compensated CPMG sequence that achieves Periodic Refocusing Of J Evolution by Coherence Transfer (PROJECT) has been proposed to minimize the effects of J evolution during the echo periods, allowing a more accurate extraction of T2 values by fitting the experimental data to a clean exponential decay of pure-phase, non-J-modulated signals [6,7]. A common feature of all these experiments is that measurements are based on exponential signal decays that can be described by first-order differential equations. In spectral regions with well resolved peaks the corresponding time constants are easily determined from nonlinear least-squares fits of each decaying signal to a separate mono-exponential function. However, simple data analysis are hampered in spectral regions with significant peak overlap, where the observed signal decays may be the result of superposition of several individual

Corresponding author.
 E-mail address: teodor.parella@uab.cat (T. Parella).

http://dx.doi.org/10.1016/j.jmr.2014.04.003 1090-7807/0 2014 Elsevier Inc. All rights reserved. decays which are difficult to distinguish and require the use of sophisticated fitting methods [8–10]. Several NMR approaches have been proposed to avoid signal overlapping in relaxation experiments, such as the initial use of selective coherence by TOC-SY transfer from an isolated signal [11], although the improved signal dispersion achieved in 2D/3D NMR experiments has become the common technique to study the conformational and dynamics aspects of biomolecules in solution [12].

On the other hand, a number of broadband homodecoupled NMR methods have been reported to obtain simplified ¹H singlet signals without the typical fine J(HH) multiplet structure [13-24], and recently an excellent overview of the homodecoupling techniques and applications has been reviewed [18]. The most recent applications, that have been encompassed under the term "pure-shift NMR", are based on the original Zangger-Sterk (ZS) experiment [14]. Basically exists two different acquisition protocols: (i) a time-consuming pseudo-2D acquisition mode based on adding the first part of different interferograms [14,15], and (ii) a real-time one-shot mode that reduce the experimental time and do not need for sophisticated processing tools [17]. Most of them use spatial encoded techniques, and therefore pronounced sensitivity losses due to slice selection are unavoidable that requires long acquisition times. Other homodecoupling methods using the BIRD module [19] do not suffer of sensitivity penalties but their applications are limited to heteronuclear correlation experiments [24]. Alternatively, a novel HOmodecoupled Band-Selective (HOBS) approach [25,26], closely related to the instant ZS experiment [17] has been proposed. The HOBS technique is not a broadband homodecoupling method that covers all the spectral width, rather it is a frequency-selective inverse homodecoupled method. However, it has been shown to be a sensitive and valuable practical tool when focusing specifically on a narrow part of the whole spectrum and applications have been provided for enantiodifferentiation studies [27], discrimination of diastereoisomers [28] or the measurement of heteronuclear coupling constants [29]. The main drawback is that it is a frequency-selective experiment and only a particular part of the 1H spectrum can be monitored in a single experiment. As a major advantage, the HOBS method omits the spatial encoding gradient applied simultaneously with the selective pulses in the original instant scheme, avoiding any sensitivity loss and allowing its performance with reasonable experimental times. This communication reports the straightforward implementation of the HOBS technique in standard IR and PROJECT experiments (Fig. 1) with the aim to resolve overlapped ¹H resonances with small chemical shift differences. Thus, T_1 and T_2 relaxation times can be accurately measured from the resulting singlet lines using conventional exponential curve-fitting methods, without need for additional data analysis based on deconvolution or line fitting techniques [30,31].

2. Results and discussion

The major novelty with respect to the original experiments is the incorporation of the homodecoupled element during the detection period that consists of a pair of hard/selective 180° ¹H pulses (represented as solid and shaded shapes) at the middle of 2.4 * AQ/n periods, where AQ is the acquisition time and n the number of concatenated loops [25,26]. In addition, a ¹H-selective gradient echo has been inserted prior to acquisition to select the area of interest, where the involved selective 180° ¹H pulse is the same as used for homodecoupling. For a perfect broadband homodecoupling, these experiments should be applied to particular areas of the ¹H spectrum where appear overlapped protons that are not mutually J coupled.

HOBS experiments can use the same automated data acquisition, processing and fitting analysis subroutines as the original experiments. A series of 1D 1H spectra are sequentially recorded as a function of the recovery delay (t) or the total echo time (te = 4mt') in IR (Fig. 1A) and PROJECT (Fig. 1B) experiments, respectively. Fig. 2 compares the experimental results obtained for the IR and HOBS-IR experiments applied to the Ha proton region in the peptide cyclosporine. Good agreement is observed between the T1 measured for all isolated signals with both methods demonstrating that the incorporation of homodecoupling does not distort the measurement (Table 1). The excellence of the method is illustrated by distinguishing the individual decays of the overlapped H₇ and H₈ resonances at 4.78-4.80 ppm. Clearly, the successful analysis of the two resolved singlets (separated by 13 Hz) allows an accurate determination of each distinct T1 value without resorting to more complex data analysis. The same strategy can be applied for T2 measurements. The simplicity and the accuracy of the measurements is demonstrated when comparing the equivalent CPMG, PROJECT and HOBS-PROJECT spectra, all of which acquired with a total echo time of 156 ms (Fig. 3B-D). Whereas the standard CPMG spectrum shows strong multiplet distortions due to the unavoidable Jint evolution, perfect in-phase multiplets are obtained from both PROJECT spectra.

Clearly, the in-phase properties are fully retained in the HOBS-PROJECT spectra (Fig. 3D), where improved sensitivity and resolution are obtained due to the efficient multiplet collapsing. The method works equally well for mutually J-coupled protons that experience the effect of the selective 180° pulse, and therefore they are not fully homodecoupled. T₂ measurements on the partially decoupled olefinic H1_E and H1_S protons (asterisks in Fig. 3D) can be also monitored efficiently from the simplified doublet patterns.

The HOBS methods can be very useful to simplify highly congested areas, such as those found in the aliphatic region of the steroid progesterone (Fig. 4). Three resonances with complex multiplet patterns appear completely overlapped at 2.0 ppm. The simplified HOBS spectrum shows clean singlets for each of these signals, with small chemical differences of 14–18 Hz. Note the equivalence between IR and HOBS-IR data by observing the same exact null point for the strong methyl signal (see experimental details and experimental T_1/T_2 values in the supporting information).

Experimentally, the HOBS technique requires a very simple and fast implementation. Only two parameters need to be defined in a

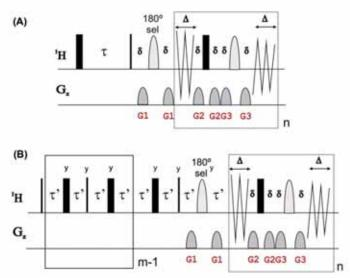


Fig. 1. NMR pulse schemes of the HOBS-IR and HOBS-PROJECT experiments used to measure T1 and T2 relaxation times, respectively, in overlapped proton signals.



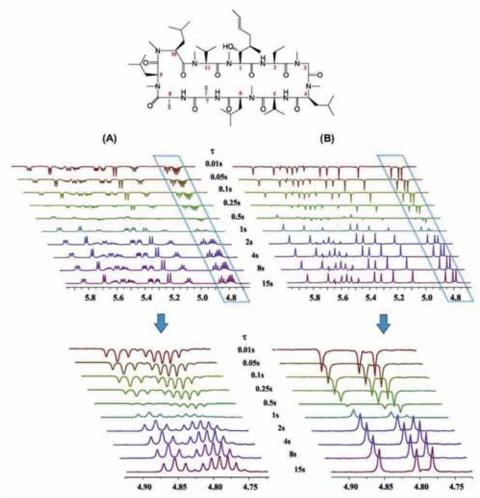


Fig. 2. 600 MHz 1 H NMR spectra obtained from the (A) conventional IR and (B) HOBS-IR experiments to determine T_1 values for all H_{∞} protons on 25 mM cyclosporine in benzene- d_0 . At the bottom, the clean differentiation between the overlapped H7 and H8 protons is shown. All spectra were collected under the same experimental conditions and plotted at the same absolute vertical scale. Homodecoupling was achieved using the detection scheme described in Fig. 1A with a 5 ms REBURP 180° pulse, A = 8.9 ms, AQ = 569 ms and B = 32.

Table 1 Experimental T_1 and T_2 values obtained from IR, HOBS-IR, PROJECT and HOBS-PROJECT experiments for H_3 and olefinic protons in cyclosporine, calculated using a simple mono-exponential decay.

32

Proton	ă (ppm)	T ₁ measurement (s)		T ₂ measurement (s)	
		IR	HOBS-IR	PROJECT	HOBS-PROJECT
Н9	5.83	0.41 ± 0.01	0.43 ± 0.01	0.37 ± 0.01	0.36 ± 0.01
HI	5.69	0.60 ± 0.01	0.60 ± 0.01	0.29 ± 0.02	0.33 ± 0.01
H4	5.55	0.89 ± 0.01	0.88 ± 0.01	0.32 ± 0.01	0.34 ± 0.01
H6	5.36	0.55 ± 0.01	0.57 ± 0.01	0.33 ± 0.01	0.33 ± 0.01
H10	5.31	0.41 ± 0.01	0.42 ± 0.01	0.27 ± 0.01	0.30 ± 0.02
H11	5.23	0.81 ± 0.02	0.85 ± 0.01	0.41 ± 0.03	0.35 ± 0.04
H2	5.09	0.94 ± 0.01	0.92 ± 0.01	0.35 ± 0.02	0.32 ± 0.01
H5	4.85	0.88 ± 0.02	0.88 ± 0.01	0.41 ± 0.01	0.38 ± 0.02
H8	4.80		0.98 ± 0.02		0.47 ± 0.01
H7	4.78	1.14 ± 0.01	1.22 ± 0.01	0.48 ± 0.01	0.50 ± 0.01
HIE	5.61	1.41 ± 0.01	1.39 ± 0.02	0.57 ± 0.01	0.56 ± 0.01
HIL	5.50	1.27 ± 0.01	1.29 ± 0.01	0.56 ± 0.01	0.55 ± 0.02

single-scan 1D acquisition mode; the offset and the selectivity of the 180° 1H pulse as a function of the crowded area to be analyzed. It is also worth to mention that maximum sensitivity is retained, although multiple experiments would be required to monitor different overlapped areas. This fact no means a severe impediment to the method as proton relaxation times do not consume large amounts of spectrometer time. Alternatively, broadband homodecoupled for all signals present in the 1H spectrum should be feasible using the instant ZS experiment [17], simply applying a gradient during the selective 180° pulses in schemes of Fig. 1, but high levels of sensitivity would be lost due to spatial encoding selection. Moreover, we can anticipate that the HOBS technique could be successfully implemented to improve the analysis in other related relaxation methods [32-34], including the measurement of selective T_1 relaxation times (T_{1sel}) [35,36] or spin-lattice relaxation times in the rotating frame (T_{1rho}) [11]. Other potential applications should be the study of reaction kinetics in complex areas or the determination of individual diffusion coefficients in

L. Castañar et al./Journal of Magnetic Resonance 244 (2014) 30-35

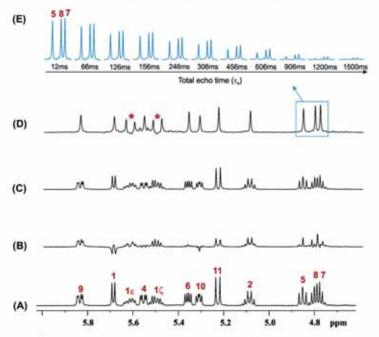


Fig. 3. Comparison of 1D (A) conventional ¹H, (B) CPMG, (C) PROJECT, and (D) HOBS-PROJECT spectra of cyclosporine acquired with a total echo time of τ_e = 156 ms (m = 26 and τ' = 1.5 ms). All spectra were collected under the same experimental conditions as described in Fig. 2 and are plotted at the same absolute vertical scale. (E) Signal T_2 decays for the H5, H8 and H7 protons in the HOBS-PROJECT experiment.

multi-component systems as similarly reported for analogous pure-shift DOSY experiments [15,16].

3. Conclusions

In summary, homodecoupling can improve the appearance of crowded areas of the ^1H spectrum by collapsing multiplet structure to singlet lines. The implementation of the HOBS technique in standard IR and PROJECT experiments can enhance the simplicity and accuracy by which T_1 and T_2 relaxation times are measured from overlapped resonances, while the sensitivity of the original experiments are retained. It has been shown that in absence of signal overlapping, individual mono-exponential decays from simplified singlet signals can be easily monitored using standard fitting procedures.

4. Methods and materials

All NMR experiments were collected at 298 K on a Bruker AVANCE spectrometer (Bruker BioSpin, Rheinstetten, Germany) operating at 600.13 MHz proton frequency, equipped with a 5 mm triple resonance inverse probe and a z-axis pulsed field gradient accessory (maximum strength of 53.5 G/cm) acquired and processed using the software TOPSPIN 3.1 (Bruker BioSpin, Rheinstetten, Germany).

The two samples used in this work were 25 mM cyclosporine (in benzene-d6) and 100 mM progesterone (in DMSO-d6). Hard 90° ¹H pulses of duration 7.8 μs (for cyclosporine) and 8.3 μs (for progesterone) were used in each sample. A 180° band-selective REBURP shaped pulse of 5.0 ms (for cyclosporine) and 20 ms (for progesterone) was used for both excitation and homodecoupling in HOBS experiments. The strengths of the G1, G2 and G3 gradients were set to 9.1, 21.9 and 33.7 G/cm, respectively, with durations of 500 μs followed by a recovery delay of 20 μs (δ = 520 μs). The ^{1}H

spectral width was set to 7200 Hz and 8 K complex points were recorded during an acquisition time of 569 ms. 32 (for cyclosporine) and 23 (for progesterone) loops (n) were concatenated with Δ periods of 8.9 and 12.37 ms, respectively ($\Delta = AQ/2n$). The first and the last chunks are half size (AQ/2n) relative to the rest of chunks (AQ/n).

10 experiments with different values of recovery delay $\tau(0.01, 0.05, 0.1, 0.25, 0.5, 1, 2, 4, 8)$ and $15 \, \text{s}$ were acquired for each IR and HOBS-IR experiment, using 8 scans and $15 \, \text{s}$ of recycle delay, 12 experiments with different number of echoes (m-1=1,5,10,20,25,40,50,75,100,150,200) and 250) and a relaxation delay τ' of 1.5 ms were acquired for each PROJECT and HOBS-PROJECT experiments, using a single scan and $10 \, \text{s}$ of recycle delay, 10 time-domain data were transformed without any sensitivity or resolution enhancement, and the same phase and baseline corrections were applied for all resulting 1D spectra.

The standard IR and CPMG experiments were recorded using the tlir and cpmg1d pulse programs that are available in the Bruker library. Pulse programs codes for Bruker spectrometers are available in our blog (http://sermn.uab.cat).

The calculation of longitudinal T_1 relaxation times was carried out with the subroutine t1guide included into the TOPSPIN3.1 software package. A set of 1D spectra recorded with different recovery delays τ were stored in a 2D data set and T_1 values were extracted by fitting the data to the equation:

$$\frac{A}{A_0} = 1 - 2e^{\left(-\frac{1}{T_1}\right)}$$
(1)

where A is the integrated area of the peak in the spectrum and A_0 is the area when $\tau \to \infty$.

The transversal T_2 relaxation times values were extracted from fitting the integrated area of a given signal as a function of total echo time τ_e assuming single exponential decay process. This natural exponential function can be rewritten in natural logarithmic

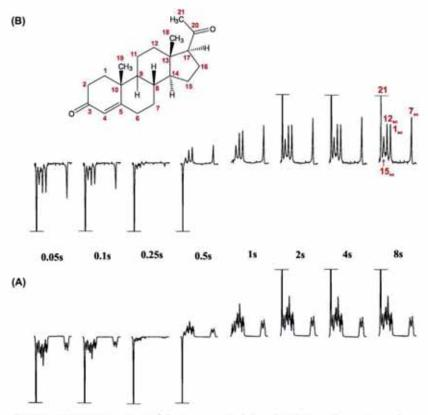


Fig. 4. Experimental decays in (A) IR and (B) HOBS-IR experiments of all protons resonating in the region 1.8-2.1 ppm in progesterone. All spectra are plotted in the same absolute vertical scale. Homodeocupling was achieved using the detection scheme described in Fig. 1A with a 20 ms REBURP 180° pulse, 4 = 12.37 ms, AQ = 569 ms and n = 23.

form where A and τ_e present a linear dependence and T_2 can be extracted from the slope:

$$A = A_0 \cdot e^{\left(-\frac{2\pi}{T_2}\right)} \ln A = \ln A_0 - \frac{1}{T_2} \tau_e \tag{2}$$

where τ_e is calculated as $\tau_e = 4m\tau'$.

Acknowledgments

Financial support for this research provided by the spanish MINECO (project CTQ2012-32436) is gratefully acknowledged. We also thank the Servei de Ressonància Magnètica Nuclear, Universitat Autònoma de Barcelona, for allocating instrument time to this project.

Appendix A. Supplementary material

Supplementary data associated with this article can be found, in the online version, at http://dx.doi.org/10.1016/j.jmr.2014.04.003.

References

- [1] V.J. Bakhmutov, Practical NMR Relaxation for Chemists, John Wiley & Sons. Chichester, 2005.
- Chichester, 2005.
 [2] P.B. Kingsley, Signal intensities and T₁ calculations in multiple-echo sequences with imperfect pulses. Conc. Magn. Reson. 11 (1999) 29–49.
 [3] P.B. Kingsley, Methods of measuring spin-lattice (T₁) relaxation times: an annotated hibliography, Conc. Magn. Reson. 11 (1999) 243–276.
 [4] H.Y. Carr, E.M. Purcell, Effects of diffusion and free precession in nuclear magnetic resonance experiments, Phys. Rev. 94 (1954) 630–638.

- [5] S. Meiboom, D. Gill, Modified spin-echo method for measuring nuclear
- relaxation times. Rev. Sci. Instrum. 29 (1958) 688-691.
 [6] J.A. Aguilar, M. Nilsson, G. Bodenhausen, G.A. Morris, Spin-echo NMR spectra without J modulation, Chem. Commun. 48 (2012) 811-813.
- [7] T.F. Segawa, G. Bodenhausen, Determination of transverse relaxation rates in systems with scalar-coupled spins: the role of antiphase coherences, J. Magn.
- Reson. 237 (2013) 139-146.
 [8] AA. Istratov, O.F. Vyvenk, Exponential analysis in physical phenomena, Rev. Sci. Instrum. 70 (1999) 1233-1257.
 [9] K. Holmström, J. Petersson, A review of the parameter estimation problem of fitting positive exponential sums to empirical data, Appl. Math. Comput. 126 (2002) 31-61.

- fitting positive exponential sums to empirical data, Appl. Math. Comput. 126 (2002) 31-61.

 [10] G.L. Bretthorst. W.C. Hutton, J.R. Garbow, J.J.H. Ackerman, Exponential parameter estimation (in NMR) using Bayesian probability theory, Conc. Magn. Reson. Part A 27 (2005) 55-63.

 [11] B. Boulat, R. Romat, I. Burghardt, G. Bodenhausen, Measurement of relaxation rates in crowded NMR spectra by selective coherence trainsfer, J. Am. Chem. Soc. 114 (1982) 5412-5414.

 [12] L.E. Kay, D.A. Torchia, A. Bax, Backbone dynamics of proteins as studied by ¹⁵N inverse detected heteronuclear NMR spectroscopy: application to staphylococcal nuclease, Biochemistry 2B (1989) 8972-8979.

 [13] S. Simowa, H. Sengstschmid, R. Freeman, Proton chemical-shift spectra, J. Magn. Reson. 124 (1997) 104-121.
- Reson, 124 (1997) 104-121.
 [14] K. Zangger, H. Sterk, Homonuclear broadband-decoupled NMR spectra, J.
- Magn. Reson. 124 (1997) 486-489.
 [15] J.A. Aguilar, S. Faulkner, M. Nilsson, G.A. Morris, Pure shift ¹H NMR: a resolution of the resolution problem?, Angew Chem. Int. Ed. 49 (2010) 3901-
- M. Nilsson, G.A. Morris, Pure shift proton DOSY: diffusion-ordered ¹H spectra without multiplet structure, Chem. Commun. 9 (2007) 933–935.
 N.H. Meyer, K. Zangger, Simplifying proton NMR spectra by instant homoeniclear broadband decoupling, Angew. Chem. Int. Ed. 52 (2013) 7143–7146.
- [18] N.H. Meyer, K. Zangger, Boosting the resolution of ¹H NMR spectra by homonuclear broadband decoupling, ChemPhysChem 15 (2014) 49–55.
 [19] J.E. Garbow, D.P. Weitekamp, A. Pines, Bilinear rotation decoupling of homonuclear scalar interactions, Chem. Phys. Lett. 93 (1982) 504–509.

- P. Sakhaii, B. Haase, W. Bermel, Experimental access to HSQC spectra decoupled in all frequency dimensions, J. Magn. Reson. 199 (2009) 192–198,
 A. Lupulescu, G.L. Olsen, L. Frydman, Toward single-shot pure-shift solution ¹H NMR by trains of BIRD-based homonuclear decoupling, J. Magn. Reson. 218
- (2012) 141–146.
 P. Sakhati, B. Haase, W. Bermel, R. Kerssebaum, G.E. Wagner, K. Zangger, Broadhand homodecoupled NMR spectroscopy with enhanced sensitivity, J.
- Broadhand homodecoupled NMR spectroscopy with enhanced sensitivity, J. Magn. Reson. 233 (2013) 92–95.
 [23] T. Reinsperger, B. Luy, Homonuclear BIRD-decoupled spectra for measuring one-bond couplings with highest resolution: CLIP/CLAP-RESET and constant-time-CLIP/CLAP-RESET, J. Magn. Reson. 239 (2014) 110–120.
- time-CLIP/CLAIN-RESET, J. Magn. Reson. 239 (2014) 110–120.
 I. Timári, L. Kaltschnee, A. Koliner, R.W. Adams, M. Nilsson, C.M. Thiele, G.A. Morris, K.E. Kövér, Accurate determination of one-bond heteronaclear coupling constants with "pure shift" broadband proton-decoupled CLIP/CLAP-HSQC experiments, J. Magn. Reson. 239 (2014) 130–138.
 L. Castañar, P. Nolis, A. Virgili, T. Parella, Full sensitivity and enhanced resolution in homodeciupled band-selective NMR experiments, Chem. Eur. J. 19 (2013) 17283–17286.
 L. Vine, J. Porbe, A. Bas. Meanwarder despending for a contraction.
- [26] J. Ying, J. Roche, A. Bax, Homonuclear decoupling for enhancing resolution and sensitivity in NOE and RDC measurements of peptides and proteins, J. Magn. Reson, 241 (2014) 97–102.
- [27] L. Casañar, M. Férez-Trujillo, P. Noiis, E. Monteagudo, A. Virgili, T. Parella, Enantiodifferentiation through frequency-selective pure-shift ¹H nuclear magnetic resonance spectroscopy, Chemi³hysChemi 15 (2014) 8534-857.
 [28] R.W. Adams, L. Byrne, P. Kirsly, M. Foroozandeh, L. Paudel, M. Nilsson, J. Clayden, G.A. Morris, Diastereomeric ratio determination by high sensitivity

- hand-selective pure shift NMR spectroscopy, Cliem. Commun. 50 (2014)
- [29] L. Castafiar, J. Saurf, P. Nolis, A. Virgili, T. Parella, Implementing homo- and heterodecoupling in region-selective HSQMBC experiments, J. Magn. Reson. 238 (2014) 63-69,

- [30] G.A. Morris, H. Barjar, T.J. Horne, Reference deconvolution methods, Prog. NMR Spectrosc. 31 (1997) 197-257.
 [31] M. Geppi, C. Forte, The SPORT-NMR software: a tool for determining relaxation times in unresolved NMR spectra, J. Magn. Reson. 137 (1999) 177-185.
 [32] N.M. Loening, M.J. Thrippleton, J. Keeler, R.G. Griffin, Single-scan longitudinal relaxation measurements in high-resolution NMR spectroscopy, J. Magn. Reson. 164 (2003) 231-239. Reson, 164 (2003) 321-328,
- [33] R. Bhattacharyy, A. Kumar, A fast method for the measurement of long spin-lattice relaxation times by single scan inversion recovery experiment, Chem. Phys. Lett. 383 (2004) 99–103.
 [34] P.E.S. Smith, K.J. Donovan, O. Szekely, M. Baias, L. Frydman, Ultrafast NMR T1
- relaxation measurements: probing molecular properties in real time.
 ChemPhysChem 13 (2013) 3138–3145.

 [35] F.W. Dahlquist, K.J. Longmur, R.B. Du Vernet, Direct observation of chemical exchange by a selective pulse NMR technique, J. Magn. Reson. 17 (1975) 406–
- [36] D.A. Leigh, A. Murphy, J.P. Smart, M.S. Deleuze, F. Zerbetto, Controlling the frequency of macrocyclic ring rotation in benzylic amide [2]catenanes, J. Am. Chem. Soc. 120 (1998) 6458-6467.

Supporting Information

Measurement of T1/T2 relaxation times in overlapped regions from homodecoupled ¹H singlet signals

Laura Castañar, Pau Nolis, Albert Virgili and Teodor Parella*

Contents

Figure S1: Stacked plot showing to the PROJECT and HOBS-PROJECT spectra of the H_{α} region in cyclosporine.

Figure S2: Experimental mono-exponential T_2 signal decays for some overlapped H_{α} protons of cyclosporine in PROJECT and HOBS-PROJECT experiments.

Figure S3: 1D ¹H HOBS spectrum after selective excitation and homodecoupling of two different aliphatic regions in cyclosporine.

Figure S4: IR and HOBS-IR experiments of the selected aliphatic areas described in Fig. S3.

Figure S5: 1D ¹H HOBS spectrum after selective excitation and homodecoupling at 2.0 ppm in progesterone.

Figure S6: Stacked plot corresponding to the PROJECT and HOBS-PROJECT spectra of the selected area displayed in Fig. S5.

Table S1: Experimental T_1 values obtained from IR and HOBS-IR experiments for the proton signals displayed in the aliphatic areas of cyclosporine represented in Fig. S4.

Table S2: Experimental T_1 and T_2 values obtained from IR, HOBS-IR, PROJECT and HOBS-PROJECT experiments for the five different proton signals resonating at the region 1.8-2.1 ppm in progesterone.

Pulse program codes for the HOBS-IR and HOBS-PROJECT experiments

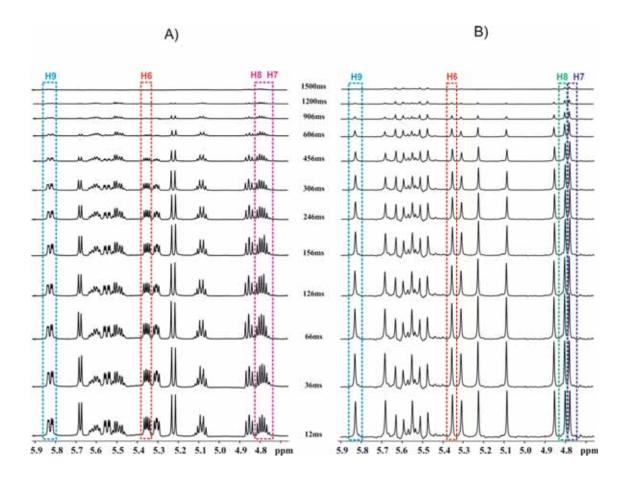


Figure S1: Stacked plot of the A) PROJECT and B) HOBS-PROJECT spectra corresponding to the H_{α} region of cyclosporine (see Fig. 1B of the manuscript), using the conditions described in the experimental section. The Fig. 3E in the manuscript shows an expanded area of the spectra B covering signals resonating between 4.76 and 4.90 ppm.

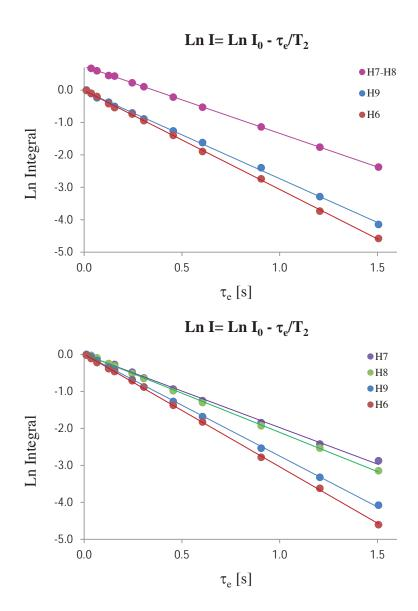


Figure S2: Comparison of the experimental mono-exponential T_2 signal decays for the isolated H6 and H9 protons and also for the overlapped H7 and H8 protons of cyclosporine in (top) PROJECT vs (bottom) HOBS-PROJECT experiments. See experimental values in Table 1.

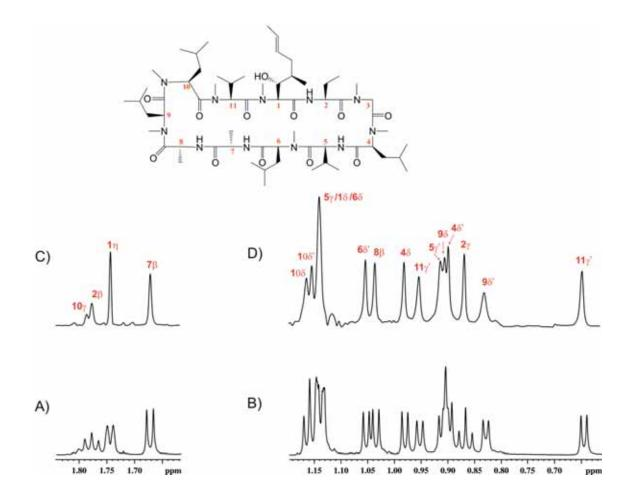


Figure S3: 600MHz 1D 1 H A-B) conventional and C-D) HOBS spectrum of cyclosporine after selective excitation and homodecoupling of two different aliphatic regions (Reburp 180° 1 H pulse of 20 ms in C and 10 ms in D, Δ =8.1 ms, AQ=569 ms and n=35 as a homodecoupling conditions). These same conditions have been used in the HOBS-IR experiment shown in Fig. S4. Both spectra are plotted in the same absolute vertical scale to compare absolute sensitivities after signal collapsing.

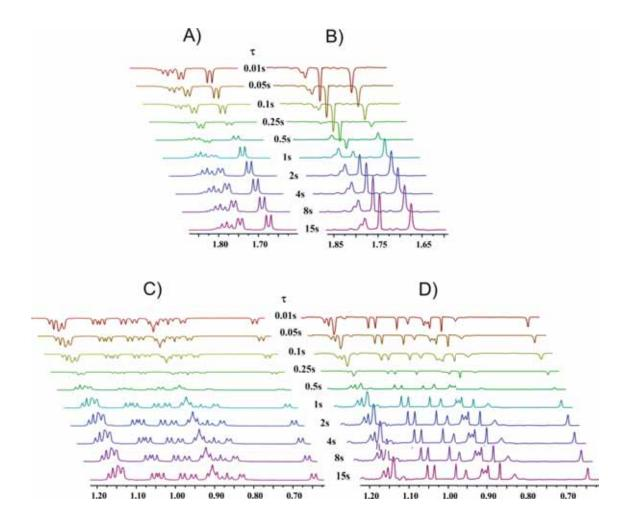


Figure S4: IR and HOBS-IR experiments of the selected aliphatic areas described in Fig. S3. The homodecoupling conditions in B and D were the same as described in Fig. S3 and the experimental T_1 values are shown in Table S1.

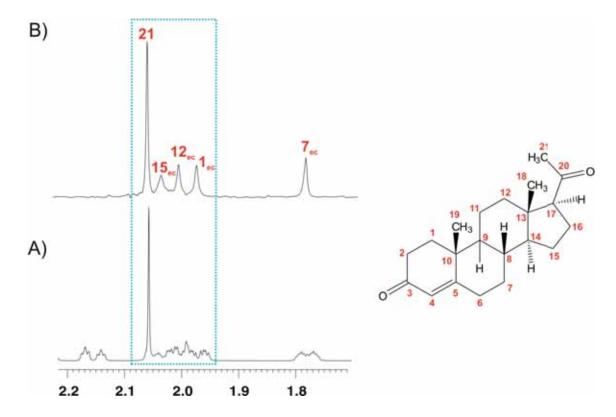


Figure S5: 600MHz 1D 1 H A) conventional and B) HOBS spectrum after selective excitation and homodecoupling at 2.0 ppm in progesterone (Reburp 180 $^{\circ}$ 1 H pulse of 20ms, Δ =12.37 ms, AQ=569 ms and n=23 as a homodecoupling conditions). These same conditions have been used in the HOBS-IR experiment shown in Fig. 4 of the manuscript and in the HOBS-PROJECT shown in the next Fig. S6. A single scan was collected and both spectra are plotted in the same absolute vertical scale to compare absolute sensitivities after signal collapsing.

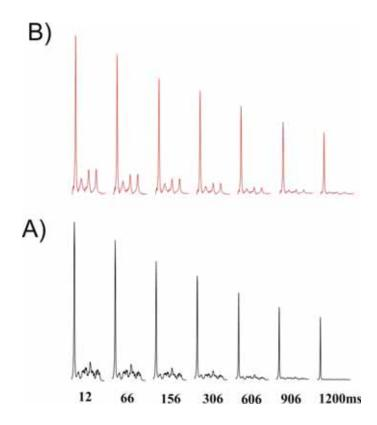


Figure S6: Stacked plot of the 600 MHz 1D spectra of progesterone acquired with the A) PROJECT and B) HOBS-PROJECT experiments using the conditions described in experimental section and Fig. S5. The individual T_2 values can be found in Table S2.

		T ₁ measurement [s]		
Proton	δ [ppm]	IR	HOBS-IR	
Η10γ	1.79	0.52 + 0.01	0.58 ± 0.01	
Н2β	1.78	0.53 ± 0.01	0.51 ± 0.01	
H1η	1.74	1.00 ± 0.02	1.02 ± 0.02	
Η7β	1.67	0.52 ± 0.01	0.50 ± 0.02	
Η10δ	1.16		0.41 ± 0.02	
H10δ'	1.15		0.44 ± 0.01	
Η5γ		0.48 ± 0.01		
Η1δ	1.14		0.52 ± 0.01	
Н6δ				
Η6δ'	1.06	0.49 ± 0.01	0.48 ± 0.01	
Н8β	1.03	0.49 ± 0.01	0.50 ± 0.01	
Η4δ	0.98	0.52 ± 0.01	0.53 ± 0.01	
Η11γ	0.95	0.38 ± 0.01	0.40 ± 0.02	
Η5γ'	0.91		0.50 ± 0.02	
Н98	0.90	0.48 ± 0.01	$0.48 \pm 0,02$	
Η4δ'	0.89		$0.48 \pm 0,02$	
Η2γ	0.86	0.65 ± 0.01	0.62 ± 0.03	
Н98	0.83	0.52 ± 0.01	0.52 ± 0.01	
Η11γ'	0.65	0.58 ± 0.01	0.59 ± 0.01	

The error is given by the error of the exponential fit.

Table S1: Experimental T_1 values obtained from IR and HOBS-IR experiments for the proton signals displayed in the aliphatic areas of cyclosporine represented in Fig. S4.

		T ₁ measurement [s]		T ₂ measurement [s]	
H signal	δ [ppm]	IR	HOBS-IR	PROJECT	HOBS-PROJECT
H ₂₁	2.07	1.38 ± 0.02	1.36 ± 0.02	1.35 ± 0.01	1.36 ± 0.01
$H15_{eq}$	2.05		0.55 ± 0.01		0.56 ± 0.01
$H12_{eq}$	2.02	0.46 ± 0.01	0.46 ± 0.01	0.50 ± 0.01	0.51 ± 0.01
$H1_{eq}$	1.99		0.41 ± 0.01		0.44 ± 0.01
H7 _{eq}	1.80	0.40 ± 0.01	0.42 ± 0.01	0.51 ± 0.01	0.50 ± 0.01

The error is given by the error of the exponential fit

Table S2: Experimental T_1 and T_2 values obtained from IR, HOBS-IR, PROJECT and HOBS-PROJECT experiments for the five different proton signals resonating at the region 1.8-2.1 ppm in progesterone.

Pulse Program Code for Bruker: HOBS-IR

```
;HOmodecoupled Band-Selective Inversion Recovery NMR experiment (HOBS-IR)
;T1 measurement using inversion recovery
;1D Experiment
;Avance III version (17/07/2013)
;Topspin3.1
#include <Avance.incl>
#include < Grad.incl>
#include < Delay.incl>
#include <De.incl>
dwellmode explicit
"p2=p1*2"
"d2=aq/I0"
"d3=d2/2"
"I1=I0-1"
"acqt0=-p1*2/3.1416"
1 ze
2 d1 pl1:f1
 50u UNBLKGRAD
 p2 ph1
 d7 pl1:f1
 p1 ph2
 d16 pl0:f1
 p16:gp1
 (p12:sp2 ph3)
 p16:gp1
 d16
                                      ;starts HOBS
 ACQ_START(ph30,ph31)
 0.05u setrtp1|0
 0.1u setrtp1|5
 d3:r
 0.1u setrtp1^5
 0.05u setrtp1^0
 p16:qp2
 d16 pl1:f1
 p2 ph4
 p16:gp2
 d16
 p16:gp3
 d16 pl0:f1
 (p12:sp2 ph3)
 p16:gp3
 d16
```

```
3 0.05u setrtp1 | 0
 0.1u setrtp1|5
 d2:r
 0.1u setrtp1<sup>5</sup>
 0.05u setrtp1^0
 p16:gp2
 d16 pl1:f1
 p2 ph4
 p16:gp2
 d16
 p16:qp3
 d16 pl0:f1
 (p12:sp2 ph3)
 p16:gp3
 d16
lo to 3 times I1
 0.05u setrtp1|0
 0.1u setrtp1 | 5
 d3
 5m
 0.1u setrtp1^5
 0.05u setrtp1^0
rcyc=2
wr #0
exit
ph1=0
ph2=0
ph3=0
ph30=0
ph31=0
;pl1 : f1 channel - power level for pulse (default)
;p1 : f1 channel - 90 degree high power pulse
;p2: f1 channel - 180 degree high power pulse
;p12 : f1 channel - 180 degree band-selective pulse [ms]
;p16: homospoil/gradient pulse [500 us]
;sp2: f1 channel - shaped pulse power level for band-selective excitation
;spnam2: shaped pulse for selective excitation [REBURP]
;d1:relaxation delay; 1-5 * T1
;d7 : delay for inversion recovery
;NS: 1 * n, total number of scans: NS * TD0
;I1: number of concatenated loops
;use gradient files:
;gpnam1: SMSQ10.100
;gpnam2: SMSQ10.100
;gpnam3: SMSQ10.100
```

Pulse Program Code for Bruker: HOBS-PROJECT

```
;use gradient files:
;gpnam1: SMSQ10.100
;HOmodecoupled Band-Selective Periodic Refocusing of J Evolution
; by Coherence Transfer NMR experiment (HOBS-PROJECT)
;T2 measurement
;1D Experiment
;Avance III version (13/07/2013)
;Topspin3.1
#include <Avance.incl>
#include < Grad.incl>
#include < Delay.incl>
#include <De.incl>
"p2=p1*2"
"d12=20u"
"DELTA1=d20-p1*2/3.1416"
"DELTA2=d20-p16-d16-de"
"DELTA3=d20-p16-d16"
"acqt0=0"
dwellmode explicit
"d2=aq/I0"
"d3=d2/2"
"|1=|0-1"
1 ze
2 30m
 d1
 50u UNBLKGRAD
 d12 pl1:f1
 p1 ph1
 DELTA1
 p2 ph2
 d20
3 d20
 p2 ph2
 d20
 p1 ph2
 d20
 p2 ph2
 d20
 lo to 3 times 14
 DELTA3 pl0:f1
 p16:gp1
 d16
 p12:sp2:f1 ph2
 p16:gp1
```

;starts HOBS

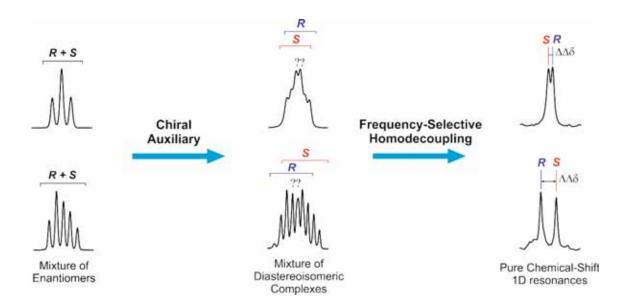
```
d16
 DELTA2
ACQ_START(ph30,ph31)
 0.05u setrtp1|0
 0.1u setrtp1 | 5
 d3:r
 0.1u setrtp1^5
 0.05u setrtp1^0
 p16:gp2
 d16 pl1:f1
 p2 ph4
 p16:gp2
 d16
 p16:gp3
 d16 pl0:f1
 (p12:sp2 ph3)
 p16:gp3
 d16
4 0.05u setrtp1|0
 0.1u setrtp1|5
 d2:r
 0.1u setrtp1^5
 0.05u setrtp1^0
 p16:gp2
 d16 pl1:f1
 p2 ph4
 p16:gp2
 d16
 p16:gp3
 d16 pl0:f1
 (p12:sp2 ph3)
 p16:gp3
 d16
lo to 4 times I1
 0.05u setrtp1|0
 0.1u setrtp1 | 5
 d3
 5m
 0.1u setrtp1^5
 0.05u setrtp1^0
rcyc=2
wr #0
exit
```

```
ph1=0
ph2=1
ph4=0
ph3=0
ph30=0
ph31=0
;pl1 : f1 channel - power level for pulse (default)
;p1 : f1 channel - 90 degree high power pulse
;p2 : f1 channel - 180 degree high power pulse
;p12 : f1 channel - 180 degree band-selective pulse [ms]
;sp2: f1 channel - shaped pulse power level for band-selective excitation
;spnam2: shaped pulse for selective excitation [REBURP]
;d1: relaxation delay; 1-5 * T1
;d12: delay for power switching
                                           [20 usec]
;p16: homospoil/gradient pulse
                                           [500 us]
;d20: fixed echo time to allow elimination of J-mod. effects
;l1: number of concatenated loops for homodecoupling
;I4: loop for T2 filter
                                    [4 - 20]
;NS: 1 * n, total number of scans: NS * TD0
:DS: 0
;use gradient files:
;gpnam1: SMSQ10.100
;gpnam2: SMSQ10.100
;gpnam3: SMSQ10.100
```

PUBLICATION 4

Enantiodifferentiation through frequency-selective pure shift ¹H nuclear magnetic resonance spectroscopy

Laura Castañar, Miriam Pérez-Trujillo, Pau Nolis, Eva Monteagudo, Albert Virgili and Teodor Parella. *ChemPhysChem,* **2014**, *15*, 854-857.



Introduction

NMR spectroscopy has proved to be a valuable technique to determine enantiomeric purity using a great variety of auxiliary chiral sources, as for example *Chiral Solvating Agents* (CSAs). ⁹¹ In the case of using CSAs, the initial indistinguishable mixture of enantiomers is converted into a chemical-shift δ -resolved mixture of complementary diastereomeric complexes. As soon as there is enough chemical shift difference to achieve resolution between the signals of analogous nuclei in these diastereomeric complexes, the measure of enantiomeric purity can be carried out by direct signal integration. However, J_{HH} broaden ¹H NMR resonances and accurate enantiomeric excess quantification is often hampered because of partial signal overlapping.

The features of pure shift experiments provide a great tool to avoid these overlapping problems. In this article, the HOBS methodology (see **Publication 2**) is proposed for the fast and efficient determination of very small chemical-shift differences between overlapped resonances. It is demonstrated that the frequency-selective homodecoupled method is a robust and sensitive analytical NMR spectroscopy tool for the fast and simple enantiodifferentiation and determination of the enantiomeric excess of organic molecules using CSAs. Its major advantage lies in the single-scan and 1D real-time acquisition modes, as the resulting simplified singlet signals facilitate a better analysis. Additionally, it has been shown that homodecoupled signals can also be retrieved for resonances obscured by other more intense signals or in overcrowded regions by using a preparatory TOCSY editing.

[91] a) S. R. Chaudhari, S. N, Suryaprakash, *J. Indian Inst. Sci.*, **2014**, *94*, 485. b) W. H. Pirkle, D. J. Hoover, *NMR Chiral Solvating Agents*, **2007**, vol. 13 of Topics in Stereochemistry, Wiley, Hoboken.





DOI: 10.1002/cphc.201301130

Enantiodifferentiation through Frequency-Selective Pure-Shift ¹H Nuclear Magnetic Resonance Spectroscopy

Laura Castañar, Míriam Pérez-Trujillo, Pau Nolis, Eva Monteagudo, Albert Virgili, and Teodor Parella*[a]

A frequency-selective 1D ¹H nuclear magnetic resonance (NMR) experiment for the fast and sensitive determination of chemical-shift differences between overlapped resonances is proposed. The resulting fully homodecoupled ¹H NMR resonances appear as resolved 1D singlets without their typical J(HH) coupling constant multiplet structures. The high signal dispersion that is achieved is then exploited in enantiodiscrimination studies by using chiral solvating agents.

Nuclear magnetic resonance (NMR) spectroscopy in the presence of chiral auxiliaries is a particularly well-adapted technique for determining the enantiomeric purity and, in some cases, the absolute configuration of chiral molecules.[1] Different approaches are available to accomplish enantiodifferentiation, including chemical derivatization,[2] chiral solvating agents (CSAs),[1] and the use of chiral liquid crystals.[4] In the case of CSAs, the NMR method simply requires the use of a suitable chiral derivative that converts the initial indistinguishable mixture of enantiomers into a chemical-shift (à)-resolved mixture of complementary diastereomeric complexes. As soon as there is a large enough & nonequivalence to achieve resolution between the signals $(\Delta\Delta\delta)$ of analogous nuclei in these diastereomeric complexes, integration can enable the direct measurement of enantiomeric purity. However, homonuclear scalar couplings (J(HH)) broaden 'H NMR resonances, and accurate enantiomeric excess (ee) quantification by optimum signal discrimination is often hampered because of partial signal overlapping and low chemical-shift dispersion ($\Delta\Delta\delta \ll \Delta\omega$, where $\Delta \omega$ is the overall width of the multiplet). The use of selective homonuclear decoupling to simplify the multiplet structure is insufficient to completely resolve overlapping. (5) However, the analysis of better-resolved fully decoupled singlet resonances in heteronuclear-decoupled ¹³C NMR spectra is an alternative, which avoids signal overlapping, but its low sensitivity remains a limiting factor for practical use. [6] Recently, several NMR methods have been proposed to obtain pure chemical-shift 1H NMR spectra.[7-11] Based on a recent instant broadband ho-

version that does not suffer sensitivity loss but maintains the benefits of obtaining simplified singlet resonances has been reported.[11] We evaluate here the potential of this strategy for the fast and efficient enantiodifferentiation of organic molecules using CSAs.

The proposed NMR experiment (Figure 1) can be understood as a homodecoupled version of the regular 1D single pulsedfield-gradient echo (SPFGE) scheme, in which a frequency-se-

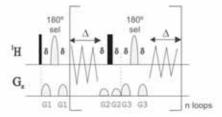


Figure 1. Pulse sequence for obtaining fully homodecoupled singlet resonances in a selected narrow part of the ¹H NMR spectrum. Broadband homodecoupling during detection was achieved by applying a pair of hard/selective 180° pulses (represented as solid and shaded shapes) at the middle of $2\Delta = AQ/n$ periods. Gradients G1, G2, and G3 flanking the refocusing pulses are individually optimized to provide a clean spectrum. à represents the duration of a pulsed field gradient and its recovery delay.

lective 180° pulse is applied to 'H NMR resonances of interest; the novelty lies in the incorporation of a broadband homodecoupling element into the acquisition period.[11] The resulting 1D 1H NMR spectrum only shows the selected resonances as collapsed singlet lines, without their typical J(HH) multiplet structure, and from which accurate chemical-shift values can be determined, even for overlapped resonances. As the sensitivity is fully retained, data acquisition can be performed quickly with the same spectrometer time required for a conventional H NMR spectrum. Experimentally, only a single selective 180 pulse needs to be setup, as a function of its excitation offset and the required selectivity for both excitation/homodecoupling purposes. We found that Gaussian-shaped pulses with a duration of around 10-20 ms provide good results, in terms of resolution, without a considerable decrease in the signal-tonoise ratio (SNR), owing to transverse relaxation during acquisition. Average line widths at half height of the singlets ($v_{1/2}$) of about 3.5-4.0 Hz are achieved by using homodecoupling settings of $\Delta = 15-25$ ms, n = 11-20, and AQ = 600 ms (where AQis the acquisition time and n the number of concatenated loops), whereas $v_{1/2} = 2.3-2.7$ Hz values are generally found in

modecoupled experiment,[10] an analogous region-selective

[[]a] L. Castañar, Dr. M. Pérez-Trujillo, Dr. P. Nolis, Dr. E. Monteagudo, Prof. A. Virgili, Dr. T. Parella Servei de Ressonància Magnètica Nuclear and Departament de Química Universitat Autónoma de Barcelona, 08193 Bellaterra (Spain) Tel: (+34) 935812291 E-mail: teodor.parella@uah.cat

Supporting Information for this article is available on the WWW under http://dx.doi.org/10.1002/cphc.201301130.

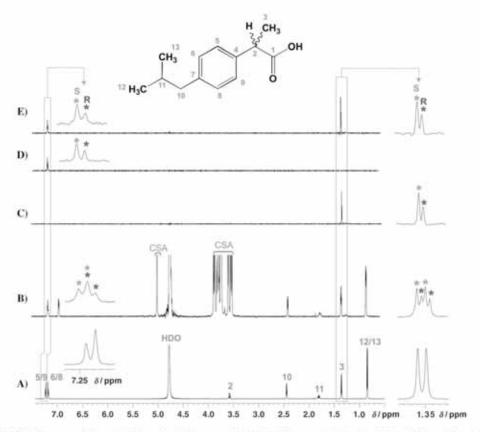


Figure 2. 600 MHz 1 H NMR spectra of 2.8 mm (*R*,5)-ibuprofen (35:65 proportion) in D₂O: A) before and B) after the addition of 3.6 equivalents of [I-CD as the CSA. Selective pure-shift 1 H NMR spectra acquired according to Figure 1 after selection of the C) H3, D) H5, and E) both H3 and H5 protons with a Gaussian-shaped 180° pulse of 20 ms (Δ = 25.8 ms, AQ = 568 ms, and n = 11). For comparison, all spectra were acquired and processed under the same conditions (a single scan for each individual 1D spectrum has been recorded with the same receiver gain) and plotted in the same vertical scale to visualize real absolute sensitivities.

the regular ¹H NMR spectrum (see Figure S1 in the Supporting Information).

As a proof of principle, the practicality of the method is demonstrated in the study of an (R,S) mixture of ibuprofen in the presence of β -cyclodextrin (β -CD) as the CSA (Figure 2). Whereas the conventional "H NMR spectrum shows poor signal separation between equivalent diastereomeric protons (Figure 2B), the clean homodecoupled 1D spectra simplifies the appearance of complex peaks and shows separated singlet resonances, which facilitates a better analysis and quantification (Figure 2C, D). It is worth noting that the sensitivity for each individual selective homodecoupled 1D spectrum is keep at a similar level to the conventional "H NMR spectrum, and, therefore, each one of these spectra can be obtained by using a single scan within few seconds and without any extra data processing requirement.

Figure 3 shows another example of the fast and sensitive discrimination of several ¹H NMR resonances belonging to a racemic mixture of (R,S)-1-aminoindan in the presence of Pirkle alcohol as the CSA. ^{3cl} A straightforward comparison between the conventional (Figure 3B) and the fully homodecou-

pled multiplets (Figure 3 C) shows that a simpler and more reliable determination of the chemical-shift differences and R/S molar ratios is possible, considering the highly dispersed singlets that are independent of the original multiplet complexity. In terms of quantification, it is important to note that deviations of the homodecoupling conditions ($\Delta \ll 1/J_{\rm HH}$)⁽¹⁰⁾ can lead to sidebands flanking each pure-shifted resonance at a spacing of 2n/AQ (see Tables S1 and S2 in the Supporting Information).

Although one limitation of the method could be its frequency-selective nature, it is not restricted to a single resonance for each individual experiment, because multiple signals can be simultaneously monitored by using band-selective^[11] or multiple-frequency pulses,^[12] as long as the excited protons are not mutually *J*-coupled (Figure 2 E). The proposed method surpasses some other NMR approaches to discriminate enantiomers because it avoids time-consuming 2D acquisitions and/or measurements made from the unresolved indirect dimension.^[13] However, homodecoupled ¹H NMR signals for all available resonances in the spectrum can be obtained by using other broadband pure chemical-shift NMR methods^[7,11-13] although they can suffer significant decreases in sensitivity. The

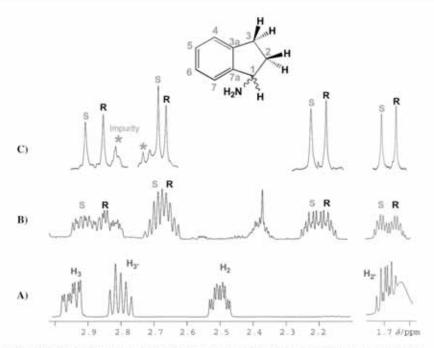


Figure 3. 600 MHz ¹H NMR spectra of 50 mm (R,5)-1-aminoindan (1:1 proportion) in CDCl₃: A) before and B) after the addition of 4.5 equivalents of (R)-(-)-1-(9-anthryl)-2,2,2-trifluoroethanol (Pirkle alcohol) as the CSA. C) Expanded multiplets extracted from individual selective 1D homodecoupled experiments acquired according to Figure 1 by using a Gaussian-shaped 180° pulse of 20 ms (Δ = 18.93 ms, AQ = 2.27 s, and n = 60). For comparison, all spectra were acquired and processed under the same conditions (a single scan for each individual 1D spectrum has been recorded with the same receiver gain) and plotted in the same vertical scale to visualize real absolute sensitivities.

projection along the detected dimension of a J-resolved experiment requires a 2D-acquisition mode, and, therefore, the SNR reduction is proportional to the number of acquired increments.[7] Otherwise, the original Zangger-Sterk (ZS) method shows better line widths, but it requires a pseudo-2D data-collection process and presents severe sensitivity losses, owing to spatial frequency encoding.[8] Recently, single-shot ZS methods have been proposed for the fast acquisition of broadband homodecoupled 1D ¹H NMR spectra, but they also experience considerable sensitivity losses because of 13C editing[9] or spatial selection. 101 The use of multiple slice selection through sequential or simultaneous slice excitation[14] can improve the relative SNR, but the sensitivity levels are still far from those obtained in the conventional 1H NMR spectra. In terms of SNR per time unit, a single selective method is more than one order of magnitude more sensitive than the aforementioned pure-shift methods, which ensures that, for small molecules, recording series of individual selective 1D experiments can be faster and more effective than running a broadband experiment. As an example, the experimental SNR of each selective experiment is about 20 times higher than the real-time instant ZS experiment.[10] A comparison on the relative SNR for several pureshifts methods can be found in Figure S2 (see the Supporting Information).

Interestingly, the proposed homodecoupled 1D method can be extended for the rapid visualization of singlet signals for

those resonances that appear in highly overcrowded areas and that, in many cases, cannot be directly observed. This is the case for the H2 proton of ibuprofen, which resonates just below the large signals belonging to the CSA in the conventional 1H NMR spectrum (Figure 4B). This hidden signal can quickly become observable by using a sensitive total correlation spectroscopy (TOCSY) transfer from another isolated proton resonance (Figure 4C).[15] Thus, a homodecoupled version of the selective TOCSY experiment can be designed by incorporating the detection period, described in Figure 1, into the conventional experiment (see Figure S3 in the Supporting Information). The two simplified singlets, corresponding to the H2 proton in R and S derivatives, can rapidly be distinguished, resolved, and quantified ($\Delta\Delta\delta = 10.44$ Hz) with enhanced sensitivity and without CSA signal interference (Figure 4C,D).

In summary, we have demonstrated that the homodecoupled SPFGE method is a robust and sensitive analytical NMR spectroscopy tool for the fast and simple discrimination of chemical-shift differences in overlapped signals and for the determination of the ee in the presence of CSAs. Its major advantage lies in the single-scan and 1D acquisition modes, as the resulting simplified singlet signals facilitate a better analysis. It has been shown that homodecoupled signals can also be retrieved for resonances obscured by other more intense signals or in overcrowded regions by using a preparatory TOCSY editing. Much work is in progress to use these powerful pure-shift methodologies for solving other common problems caused by NMR signal overlapping.

Experimental Section

All NMR experiments were performed by using a 600 MHz BRUKER Avance-III spectrometer equipped with a TXI probe. Complete experimental details, a comparison of the experimental sensitivity of several pure-shift NMR experiments, a description of the homodecoupled selective TOCSY pulse scheme, and a table showing the measured $\Delta\Delta\delta$ and R/S molar ratio values measured by signal integration and line fitting can be found in the Supporting Information.

CHEMPHYSCHEM COMMUNICATIONS

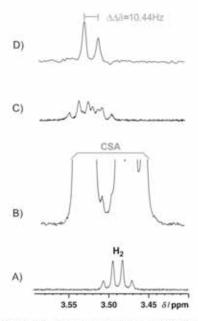


Figure 4. A, B) Expanded region corresponding to the 'H NMR spectra of Figure 2A and 2B, respectively. C) Conventional and D) homodecoupled 1D TOCSY spectra showing the H2 proton after initial selective excitation of the H3 proton followed by a 60 ms TOCSY transfer. Gaussian-shaped 180° pulses of 20 ms were used for both excitation (on H3 protons at δ = 1.35 ppm) and homodecoupling (on H2 protons). Spectra B-D) were acquired (four scans each one, with the same receiver gain), processed and plotted under the same conditions (see the Supporting Information) to visualize real absolute

Acknowledgements

Financial support for this research provided by MINECO (project CTQ2012-32436) is gratefully acknowledged. We also thank the Servei de Ressonància Magnètica Nuclear, Universitat Autònoma de Barcelona, for allocating instrument time to this project.

shift Keywords: chemical homodecoupling enantioselectivity · nmr spectroscopy · single pulsed-fieldgradient echo

- [1] a) T. J. Wenzel, Discrimination of Chiral Compounds Using NMR Spectroscopy; Wiley-VCH, Weinheim, 2007; b) T. J. Wenzel, C. D. Chischolm, Prog. Nucl. Magn. Reson. Spectrosc. 2011, 59, 1-63.
- [2] J. M. Seco, E. Quiñoá, R. Riguera, Chem. Rev. 2004, 104, 17-117,

- [3] a) W. H. Pirkle, D. J. Hoover, NMR Chiral Solvating Agents, Vol. 13 of Topics in Stereochemistry (Eds.: N. L. Allinger, E. L. Eliel, S. H. Wilen), Wiley, Hoboken, 2007; b) M. Pomares, F. Sánchez-Ferrando, A. Virgili, A. Alvarez-Larena, J. F. Piniella, J. Org. Chem. 2002, 67, 753-758; c) C. Estivill, M. Pomares, M. Kotev, P. Ivanov, A. Virgili, Tetrahedron: Asymmetry 2005, 16, 2993-2997; d) C. J. Núñez-Agüero, C. M. Escobar-Llanos, D. Díaz, C. Jaime, R. Garduño-Juárez, Tetrahedron 2006, 62, 4162-4172.
- [4] a) M. Sarfati, P. Lesot, D. Merlet, J. Courtieu, Chem. Commun. 2000, 2069-2081; b) J. Farion, D. Merlet, J. Maan. Reson. 2011, 210, 24-30; c) K. Kobzar, H. Kessler, B. Luy, Angew. Chem. 2005, 117, 3205-3207; Angew. Chem. Int. Ed. 2005, 44, 3145-3147.
- [5] a) J. P. Jesson, P. Meakin, G. J. Kneissel, J. Am. Chem. Soc. 1973, 95, 618-620; b) A. P. D. M. Espindola, R. Crouch, J. R. Debergh, J. M. Ready, J. B. MacMillan, J. Am. Chem. Soc. 2009, 131, 15994-15995
- [6] a) V. Marathias, P. A. Tate, N. Papaioannou, W. Massefski, Chirolity 2010. 22, 838-843; b) M. Pérez-Trujillo, E. Monteagudo, T. Parella, Anal. Chem. 2013, 85, 10887-10894; c) T. J. Wenzel, J. D. Wilcox, Chirality 2003, 15, 256-270; d) A. Meddour, P. Berdague, A. Hedli, J. Courtieu, P. Lesot, J. Am. Chem. Soc. 1997, 119, 4502-4508; e) M. Rivard, F. Gullien, J. C. Flaud, C. Aroulanda, P. Lesot, Tetrahedron: Asymmetry 2003, 14, 1141-1152; f) M. Sugiura, A. Kimura, H. Fujiwara, Magn. Reson. Chem. 2006, 44 121-126
- [7] a) A. J. Pell, J. Keeler, J. Magn. Reson. 2007, 189, 293-299; b) B. Luy, J. Magn. Reson. 2009, 201, 18-24; c) S. R. Chaudhari, N. Suryaprakash, Chem. Phys. Lett. 2013, 555, 286-290; d) M. Pérez-Trujillo, J. C. Lindon, T. Parella, J. K. Nicholson, H. C. Keun, T. J. Athersuck, Anal. Chem. 2012, 84, 2868 - 2874.
- [8] a) K. Zangger, H. Sterk, J. Magn. Reson. 1997, 124, 486-489; b) J. A. Aguilar, S. Faulkner, M. Nilsson, G. A. Morris, Angew. Chem. 2010, 122, 3993 - 3995; Angew. Chem. Int. Ed. 2010, 49, 3901 - 3903; c) G. A. Morris, J. A. Aguilar, R. Evans, S. Haiber, M. Nilsson, J. Am. Chem. Soc. 2010, 132, 12770-12772; d) J. A. Aguilar, A. A. Calbourne, J. Cassani, M. Nilsson, G. A. Morris, Angew. Chem. 2012, 124, 6566-6569; Angew. Chem. Int. Ed. 2012, 51, 6460-6463.
- [9] a) A. Lupulescu, G. L. Olson, L. Frydman, J. Magn. Reson. 2012, 218, 141-146; b) J. A. Aguilar, M. Nilsson, G. A. Morris, Angew. Chem. 2011, 123, 9890-9891; Angew. Chem. Int. Ed. 2011, 50, 9716-9717.
- [10] N. H. Meyer, K. Zangger, Angew. Chem. 2013, 125, 7283-7286; Angew. Chem. Int. Ed. 2013, 52, 7143-7146.
- [11] L. Castañar, P. Nolis, A. Virgili, T. Parella, Chem. Eur. J. 2013, 19, 17283-17286
- [12] S. L. Patt, J. Magn. Reson. 1992, 96, 94-102.
- [13] a) N. Giraud, M. Joos, J. Courtieu, D. Merlet, Magn. Reson. Chem. 2009, 47, 300-306; b) N. Nath, D. Kumari, N. Suryaprakash, Chem. Phys. Lett. 2011, 508, 149-154; c) R. P. Uday, N. Suryaprakash, J. Phys. Chem. A 2010, 114, 5551-5557.
- [14] a) P. Sakhaii, B. Haase, W. Bermel, J. Magn. Reson. 2013, 228, 125-129; b) L. Castañar, P. Nolis, A. Virgili, T. Parella, Chem. Eur. J. 2013, 19, 15472-15475
- [15] F. Fernández-Trillo, E. Fernandez-Megia, R. Riguera, J. Org. Chem. 2010, 75. 3878 - 3881.

Received: November 28, 2013 Revised: January 2, 2014 Published online on February 20, 2014

CHEMPHYSCHEM

Supporting Information

© Copyright Wiley-VCH Verlag GmbH & Co. KGaA, 69451 Weinheim, 2014

Enantiodifferentiation through Frequency-Selective Pure-Shift ¹H Nuclear Magnetic Resonance Spectroscopy

Laura Castañar, Míriam Pérez-Trujillo, Pau Nolis, Eva Monteagudo, Albert Virgili, and Teodor Parella*^[a]

cphc_201301130_sm_miscellaneous_information.pdf

Supporting Information

Experimental Section

All experiments were carried out at T=298 K on a Bruker AVANCE spectrometer (Bruker BioSpin, Rheinstetten, Germany) operating at 600.13 MHz proton frequency, equipped with a 5 mm triple resonance inverse probe and a z-axis pulsed field gradient accessory (maximum strength of 53.5 G/cm). Data were collected and processed using the software TOPSPIN 3.1 (Bruker BioSpin, Rheinstetten, Germany).

1D homodecoupled SPFGE spectra of Fig. 2B-E were recorded using a single scan, the same receiver gain and 1 s of recycle delay. The spectral width was 7200 Hz, and 8K complex points were recorded during an acquisition time of 567.98 ms. 11 loops (n) were concatenated with Δ =AQ/2n=25.81 ms and the selective 180° ¹H pulse had a Gaussian shape and a duration of 20 ms. A Gaussian-window function (LB=-3, GB=0.5) was applied before Fourier transformation. All 1D spectra of Fig. 3 were recorded using a single scan, the same receiver gain and 1 s of recycle delay for comparison purposes. The spectral width was 7200 Hz, and 32K complex points were recorded during an acquisition time of 2,273 s. In homodecoupled experiments, 60 loops (n) were concatenated with Δ =AQ/2n=18,93 ms and the selective 180° ¹H pulse had a Gaussian shape and a duration of 20 ms. The 1D time-domain data was directly transformed without any sensitivity or resolution enhancement.

Although the homodecoupled SPFGE experiment (Fig. 1) has been executed in a single-scan to demonstrate the power of the method, a minimum four-step cycle is recommended in which the initial selective 180° pulse and the receiver are cycled using an EXORCYCLE scheme: $\Phi(180^{\circ})=x,y,-x,-y$ and $\Phi(\text{receiver})=x,-x$. The strengths of the G1, G2 and G3 gradients were set to 40.7, 21.9 and 33.7 G/cm, respectively, with durations of 500 μ s followed by a recovery delay of 20 μ s.

The samples used were the same used and described in a prior article published by us (Pérez-Trujillo et al. Analytical Chemistry 2013, 85, 10887-10894, reference 6b of the main manuscript). In the case of ibuprofen samples the preparation was as follows. 600 μ L of a 2.2 mM solution of racemic ibuprofen was prepared mixing 100 μ l of a 13.2 mM stock solution of (RS)-ibuprofen and 500 μ L of D₂O, for the sample without CSA, and with 500 μ L of a 12.1 mM β -CD solution in D₂O, for the sample with CSA. After that, both solutions were spiked with 70 μ L of a 8.0 mM S-ibuprofen solution, resulting in a 2.8 mM solution of (R,S)-ibuprofen (35:65) in D₂O and in a second solution analogous to the former but containing 3.6 equivalents of β -CD. In the case of the racemic 1-aminoindan samples, (RS)-1-aminoindan was dissolved in CDCl₃ (50 mM) and after that 4.5 equivalents of R-(-)-1-(9-anthryl)-2,2,2-trifluoroethanol (Pirkle alcohol, PA) were added to the sample.

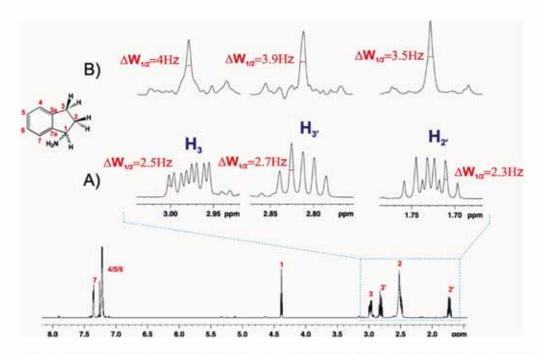


Figure S1: Experimental linewidths measured a 50mM (*RS*)-aminoindan sample dissolved in CDCl₃: A) conventional ^{1}H and B) homodecoupled ^{1}H SPFGE spectra after individual selection of each proton. All data were processed without any window function. The homodecoupling conditions in B) were: a 20 ms Gaussian shaped 180° ^{1}H pulse, Δ =19 ms, n=15 and AQ=568 ms.

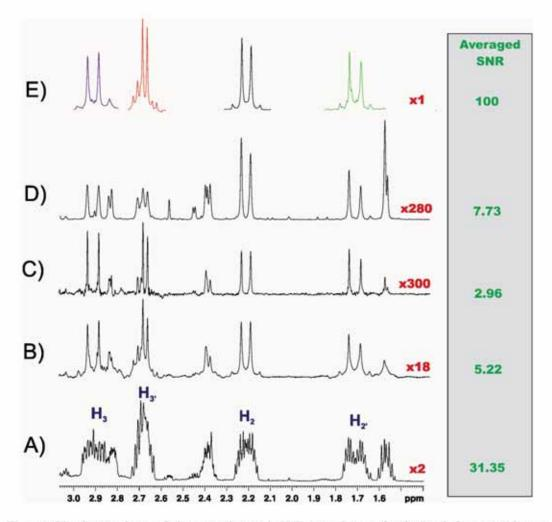


Figure S2. Comparison of the experimental SNR per time unit obtained for several pure chemical-shift NMR experiments using a sample of 50mM (RS)-1-aminoindan with 4.5 equivalents of (R)-(-)-1-(9-anthryl)-2,2,2-trifluoroethanol (Pirkle alcohol) in CDCl3. A) Conventional ¹H spectrum; B) real-time instant 1D ZS spectrum (ref. 7); C) pseudo-2D ZS spectrum (ref. 12); D) Internal projection extracted along the detected dimension of a conventional 2D J-resolved after a tilting process; and E) selective homodecoupled 1D SPFGE spectra (using the scheme of Fig. 1, this work) after individual selection of each selected resonance. For an accurate SNR per time unit comparison, each experiment was recorded in equivalent conditions, using a 1.5s of recycle delay, the same receiver gain value and a total spectrometer time about 5 min. All spectra has been plotted using the selective SPFGE as a normalized intensity reference (see scaling factor) and with the averaged experimental SNR (green value) calculated from the selected four resonances in each experiment. The nonselective 90° ¹H pulse was of 7.3 µs. A) Conventional ¹H NMR spectrum was recorded using 76 scans. The spectral width was 7200 Hz, and 32K complex points were recorded during an acquisition time of 2.27s. Experiments B) and E) were recorded using 123 scans, spectral width of 7200 Hz, 8K complex points were collected during an acquisition time of 567.98 ms and 15 loops (n) were concatenated with Δ=AO/2n=18.93 ms. The strengths of the G1, G2 and G3 gradients (smoothed squared shaped; SMSQ10.100 in Bruker format) were set to 40.7 (76%), 21.9 (41%) and 33.7 G/cm (63%), respectively, with durations of 500 µs followed by a

recovery delay of 20 μs. A 180° frequency-selective Gaussian-shaped ¹H pulse of 20 ms was used for both excitation and homodecoupling in spectra B, C and E. B) and C) experiments used a square-shaped encoding gradient of 0.2 G cm⁻¹ (0.4%) for spatial frequency encoding. C) The pseudo-2D ZS spectrum was recorded using 4 transients for each one of the 32 t₁ increments and gradient pulses were smoothed squared shaped with a duration of 1 ms and amplitude G1= 26.8 G cm⁻¹ (50%). All 1D time-domain data were directly transformed without any sensitivity or resolution enhancement. D) In the J-resolved spectrum 4 transients were collected for each one of the 32 t₁ increments. The spectral width was 7200 Hz, and 8K complex points were recorded during an acquisition time of 568 ms. Data were processed using a non-shifted sine-bell window function followed by a tilting process.

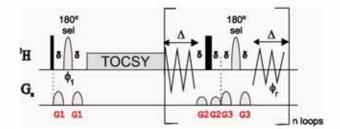


Figure S3: Pulse scheme for the selective and homodecoupled 1D TOCSY experiment. A minimum four-step phase cycle is used: ϕ_1 =x,y,-x,-y and ϕ_r =x,-x. In contrast to the original homodecoupled SPFGE scheme (Fig. 1 of the manuscript), the features of the two selective 180° pulses are here different: the first selective 180° pulse is applied to an isolated resonance whereas the selective 180° pulse applied during the detection period is applied to a relayed resonance. Therefore, the selectivity and the offset of these pulses must be determined in each case according to the required selectivity.

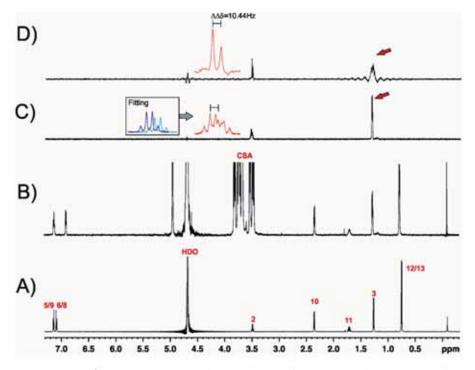


Figure S4: 600MHz ¹H NMR spectra of (*R,S*)-ibruprofen (35:65) in D₂O: A) before and B) after the addition of 3.6 equivalents of β-CD; C) conventional selective 1D TOCSY spectrum after initial selection of the H3 proton; D) broadband homodecoupled selective 1D TOCSY spectrum acquired using the pulse sequence of Fig. S3. Spectra C and D were recorded under the same experimental conditions: the H3 proton was selective excited by a 20ms Gaussian-shaped 180° ¹H pulse, and the H2 proton was fully homodecoupled during the acquisition period (Gaussian shaped pulse of 20 ms, Δ=14.2 ms, n=20 and AQ=568 ms) in D). Four scans were collected for each experiment using a recycle delay of 1s, a TOCSY mixing time (MLEV-17) of 60 ms and the same receiver gain value. Data were Fourier transformed without any window function.

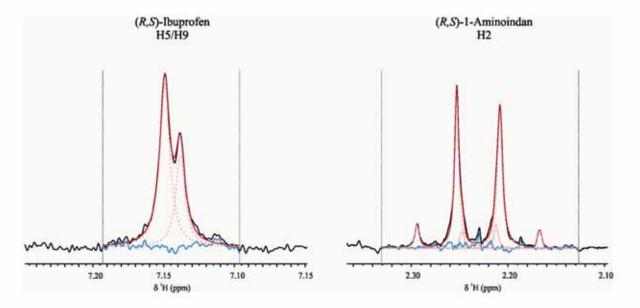


Figure S5: Examples of line fitting achieved for the singlets obtained from the HOBS spectra after selection the H5/H9 protons of (*R*,*S*)-ibuprofen (35:65) and H2' in (*RS*)-1-aminoindan samples. The experimental results are listed in Table S1.

Table S1: $\Delta\Delta\delta$ and S/R molar ratio values for the samples studied in this work.

Sample	Experiment	Nucleus	eus Enantiodifferentiation			R/S molar ratio			
Theoretical S/R ratio (S:R)			ΔΔδ (Hz)	W ^a (Hz)	E,	Measurement by integration	Error ^b (%)	Measurement by line fitting ^c	Error ^b (%)
(RS)-Ibuprofen 1,85 (65:35)	lusus	Н3	3.84	9.79	0.4	1.691 ^d	8.6	1.648	11.3
	1H-NMR	H5/9	7.32	10.79	0.7	1.780 ^d	3.8	1.747	5.9
	¹ H _{sel} -HOBS	H3	3.78	2.06	1.8	1.869	1.1	1.806	2.8
		H5/9	6.48	2.06°	3.1	1.859	0.5	1.875	1.0
	¹ H-NMR	H2'	33,43	32.91	1	0.953	4.7	ıt.	27.3
		H2	h	40.11		0.804	19.6	a.	
		H3'	14.13	35.32	0.4	1	100		
(RS)-1-Aminoindan 1 (50:50)		Н3	32.83	30.23	1.1	1.098	9.8	18	
	1	H2'	33.34	3.58	9.3	1.014 k	1.4	1.041 ^k	4.1
		H2	26.83	3.11	8.6	0.994*	0.6	1.019 ^k	1.9
	¹ H _{sel} -HOBS	H3'	13.53	3.64	9.0	1	47	1	
		НЗ	32.73	4.01	3.4	1	-	0.987 ^k	1.3

^{*}The enantiodifferentiation quotient, E, for an enantiodifferentiated signal is defined as $\Delta\Delta\delta/W$; where $\Delta\Delta\delta$ is the chemical shift non-equivalence of that signal in presence of the CSA and W is de overall width of the same signal (singlet or multiplet) before adding the CSA. For more details see Pérez-Trujillo et al. Anal. Chem. 85 (2013) 10887-10894.

^b Error calculated as the absolute value of (measured value - theoretical value)*100/theoretical value.

^c Line fitting (deconvolution) done based on a Lorentzian/Gaussian function using MestreNova software (Mestrelab Research S. L., Santiago de Compostela, Spain).

d Measurement done by integrating the end peaks of the partially enantioresolved multiplet.

^e This value was not possible to be measured, due to the proximity of H5/9 signal to H6/8 peak. An estimated value (the same than that obtained for H3 signal) was used for the determination of E.

f Measurement done by integrating each half of the partially enantioresolved multiplet from the central point.

⁸ Not possible due to complex multiplicity.

h Not possible to measure due to severe overlap.

¹ Measurement done by superposing and shifting the ¹H NMR spectrum without CSA.

Overlapped with an impurity.

^{*} Sidebands have been included in determination of R/S molar ratio

Table S2: Comparison of R/S molar ratios obtained from the HOBS and the pseudo-2D ZS methods for the (RS)-1-aminoindan sample.

Sample	Experiment	Nucleus	R/S molar ratio ^a				
Theoretical S/R ratio (S:R)			Measurement by integration	Error* (%)	Measurement by line fitting ^b	Error ^a (%)	
	¹ H _{sel} -HOBS	H2'	1.014 °	1.4	1.041 ^c	4.1	
		H2	0.994 °	0.6	1.019°	1.9	
		H3'	d	1.5	d	-	
(RS)-1-Aminoindan		нз	d		0.987 ^c	1.3	
(50:50)	pseudo-2D ZS	H2'	1,001	0,1	1,014	1,4	
(30.30)		H2	1,007	0,7	1,026	2,6	
		H3'	d		d		
	experiment	Н3	0,993	0,7	0,991	1,1	

Values extracted from spectra of Fig. S2C and S2E

^a Error calculated as the absolute value of (measured value - theoretical value)*100/theoretical value.

^b Line fitting (deconvolution) done based on a Lorentzian/Gaussian function using MestreNova software (Mestrelab Research S. L., Santiago de Compostela, Spain).

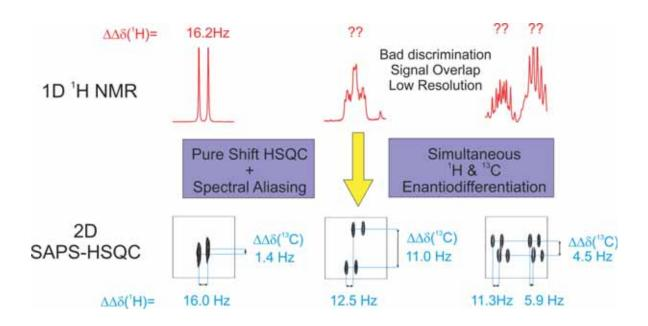
^c Sidebands have been included in determination of R/S molar ratio.

d Overlapped with an impurity.

PUBLICATION 5

Simultaneous ¹H and ¹³C NMR enantiodifferentiation from highly-resolved pure shift HSQC spectra

Miriam Pérez-Trujillo, Laura Castañar, Eva Monteagudo, Lars T. Khun, Pau Nolis, Albert Virgili, Robert Thomas Williamson and Teodor Parella. *Chem. Commun.,* **2014**, *50*, 10214-10217.



Introduction

In the previous work (**Publication 4**), the practical usefulness of 1D HOBS pure shift ¹H NMR experiments in enantiodifferentiation studies to distinct signals separated by more than 2 Hz in a 600 MHz spectrometer has been reported. On the other hand, recently, the conventional fully decoupled 1D ¹³C{¹H} spectrum, one of the oldest pure shift NMR experiments, has successfully been applied in enantiodifferentiation studies. ⁹²

In this publication a new pure shift NMR approach is report to carry out enantiodifferentiation studies using CSAs. The proposed experiment is a highly-resolved 2D HSQC where the complementary features of the pure shift and spectral aliasing⁹³ approaches are combined in a single NMR experiment. As it is shown along this thesis work, the pure shift methodology highly improves signal resolution along the ¹H dimension simplifying the typical J_{HH} multiplicity pattern of ¹H signals to singlets. Spectral aliasing methodology is a very straightforward method that allows the increase of digital resolution along the indirect dimension within the same total experimental time. This method does not required any change in the pulse sequence and experimentally is easily implementable reducing the 13C spectral width in HSQC experiments (for instance, from the typical 160 ppm to 5 ppm). In that manner, it is possible improve digital resolution and signal dispersion by one or two orders of magnitude along the ¹³C dimension compared to classical acquisition when SNR is not a limiting factor. The experimental consequence to apply spectral aliasing is the temporary loss of the real chemical shift value along the indirect dimension. The new position of each aliased 13 C peak is exactly a multiple of the spectral width (SW_C) and its real position (δ_r) can be determined from the relationship:

$$\delta_r = \delta_{obs} + (K.SW_C)$$

where δ_{obs} is the experimental $\delta(^{13}\text{C})$ measured in the aliased spectra using a given ^{13}C offset Ω_c and K is the aliasing factor which can be determined, for instance, from a reference non-aliased HSQC spectrum using a moderate number of t_1 increments. Several automated strategies have been proposed to determine the correct ^{13}C δ_r values and to reconstruct the entire spectrum. 93

^[92] M. Pérez-Trujillo, E. Monteagudo, T. Parella, Anal. Chem., 2013, 85, 10887.

^[93] a) D. Jeannerat, Magn. Reson. Chem., 2003, 41, 3. b) I. Baskyr, T. Brand, M. Findeisen, S. Berger, Angew. Chem. Int. Ed., 2006, 45, 7821. c) D. Jeannerat, J. Magn. Reson., 2007, 186, 112. d) B. Vitorge, S. Bieri, M. Humam, P. Christen, K. Hostettmann, O. Muñoz, S. Loss, D. Jeannerat, Chem. Commun., 2009, 950. e) G. B. B. Njock, D. E. Pegnyem, T. A. Bartholomeusz, P. Christen, B. Vitorge, J. M. Nuzillard, R. Shivapurkar, M. Foroozandeh, D. Jeannerat, Chimia, 2010, 64, 235. f) M. Foroozandeh, D. Jeannerat, ChemPhysChem, 2010, 11, 2503. g) A. Cotte, M. Foroozandeh, D. Jeannerat, Chimia, 2012, 66, 764.

This new *Spectral Aliasing Pure Shift* HSQC (SAPS-HSQC) method has been successfully applied to enantiodifferentiation studies and it has been proved that it is a fast and very efficient tool for the detection and accurate differentiation and quantification of very small $\Delta\Delta\delta$ values, simultaneously for ¹H and ¹³C. Enantiodifferentiation analysis through the SAPS-HSQC spectrum has been shown to be superior to the conventional 1D ¹H, the conventional ¹³C or even the broadband homodecoupled 1D ¹H ZS spectrum. It is also important to remark that the relative sensitivity of standard HSQC experiment is retained in SAPS-HSQC experiments and even improved due to the collapse of the signals to singlets.

ChemComm



COMMUNICATION

View Article Online



Cite this: Chem. Commun., 2014, 50, 10214

Received 28th May 2014, Accepted 14th July 2014

DOI: 10.1039/c4cc04077e

www.rsc.org/chemcomm

Simultaneous ¹H and ¹³C NMR enantiodifferentiation from highly-resolved pure shift HSQC spectra†

Miriam Pérez-Trujillo, ^a Laura Castañar, ^a Eva Monteagudo, ^a Lars T. Kuhn, ^b Pau Nolis, ^a Albert Virgili, ^a R. Thomas Williamson ^c and Teodor Parella*

NMR enantiodifferentiation studies are greatly improved by the simultaneous determination of ¹H and ¹³C chemical shift differences through the analysis of highly resolved cross-peaks in spectral aliased pure shift (SAPS) HSQC spectra.

The determination of enantiomeric purity can be accomplished by NMR spectroscopy using a great variety of auxiliary chiral sources.1 Of these, chiral solvating agents (CSAs), such as the so-called Pirkle alcohol (PA) or cyclodextrins (CDs), have been widely used. They do not typically introduce significant linebroadening, the sample is easily prepared and the analysis is quickly performed by observing chemical shift differences $(\Delta\Delta\delta)$ between the resulting diasteromeric complexes in conventional ¹H NMR spectra. However, signal enantiodifferentiation using CSAs is not uniform for all protons and in many cases, low $\Delta\Delta\delta$ values and signal overlap caused by complex multiplets lead to the lack of spectral signal dispersion that preclude a straightforward analysis. Alternatively, enantiodifferentiation using 13C NMR spectroscopy can be more advantageous because singlet signals are analyzed, although its routine use is limited by its low sensitivity.2 Another strategy to deconvolute these enantiodifferentiated data is to take advantage of improved signal dispersion offered by multidimensional spectra as shown for instance in the chiral recognition of camphor and α-pinene enantiomers with CDs made through HSQC spectra.3 Recently, pure shift NMR spectroscopy has emerged as a promising tool to simplify the typical J(HH) multiplicity pattern of 1H signals to singlets.4-8 This affords a general improvement on signal dispersion that allows an improved analysis of complex and overcrowded resonances. Recently, this concept has proved its usefulness in the detection of $\Delta\Delta\delta$ values between diastereosiomeric complexes involving CSAs.⁸

In this study we utilized a racemic mixture of compound (1), a precursor for a series of diarylether lactams as cancer chemotherapeutic agents, 9 complexed with R-PA as a CSA. Its 1H NMR spectrum (Fig. 1A) does show some well-differentiated signals (for instance, H12 appears at around 7.10–7.15 ppm as two triplet signals separated by 20.9 Hz or 34.8 ppb), but most of the signals cannot be individually distinguished. For example, H13 is hidden under the stronger H2 signal from R-PA (6.6 ppm), and the splitting in signals resonating in the congested

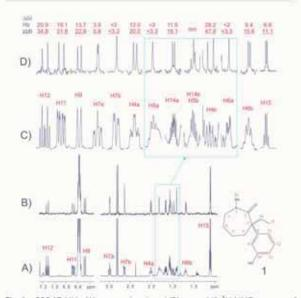


Fig. 1 600.13 MHz (A) conventional and (B) pure shift 3 H NMR spectra of 29 mM racemic compound 1 complexed with 9.6 equiv. of R-PA in CDCl₅. (C and D) Comparison of expanded 3 H multiplets for determining accurate $\Delta\Delta\delta i^4$ H) values (shown in Hz and ppb).

10214 | Chem. Commun., 2014, 50, 10214-10217

This journal is @ The Royal Society of Chemistry 2014

Servei de Ressonància Magnètica Nuclear and Departament de Química, Universitat Autònoma de Barcelona, E-08193 Bellaterra, Barcelona, Spain. E-mail: teodor.parellaijiuab.cat; Tel: +34 935812291

⁸ DFG Research Center Moiecular Physiology of the Brain (CMPB) & European Neuroscience Institute Göttingen (ENI-G), Göttingen, Germany

NMR Structure Elucidation, Process and Analytical Chemistry, Merck & Co. Inc., 126 E. Lincoln Avenue, Rahway, NJ 07065, USA

[†] Electronic supplementary information (ESI) available: Esperimental details and NMR spectra. See DOI: 10.1039/e4ec04077e

View Article Online

ChemComm

Communication

aliphatic area at 1.4-1.8 ppm cannot be clearly observed due to spectral overlap. Other protons present complex multiplet patterns (H4a or H6b) or are poorly resolved (H7a), hindering their direct analysis. On the other hand, up to 9 signals appear split in the conventional 13C spectrum of racemic 1 acquired after 9 hours, with a maximum $\Delta\Delta\delta(^{13}C)$ of 84.1 ppb (Fig. S3, ESI†). As an alternative to the acquisition and analysis of 1D 13C NMR data, pure shift 1D 1H NMR experiments can be employed to simplify the analysis and provide a much more sensitive approach in the determination of small $\Delta\Delta\delta(^{1}H)$ values (Fig. 1B). In this 1D pure shift 1H spectrum acquired in 9 min using the pseudo-2D Zangger-Sterk (ZS) method,4 the separation of each individual signal can be visualized allowing the accurate measurement of ΔΔδ(1H) as small as 2 Hz (3.3 ppb), even for signals that would exhibit very complex multiplets and serious overlapping in a standard 1D 1H NMR (Fig. 1C vs. D).

In this communication, we show how highly resolved 2D HSOC spectra can be an efficient tool for enantiodifferentiation studies and also for the detection and accurate quantification of very small $\Delta\Delta\delta$ values. Traditionally, attempts to obtain highly resolved HSQC spectra over the entire 13C spectral width involved an enormous investment in instrument time. Our method is based on the concerted leveraging of several approaches to improve signal dispersion in 2D HSQC spectra. First, spectral aliasing (SA) is incorporated to improve resolution along the indirect dimension by one or two orders of magnitude without increasing the total experimental time by using a reduced 13C spectral width.10 Secondly, a sensitivity-improved version11 of the pure shift (PS) HSQC experiment (Fig. 2A),6 referred to as psHSQCsi, is applied to enhance the resolution in the alternate 1H dimension. This experiment applies 180°(1H)-BIRD modules for homodecoupling and also heteronuclear decoupling during the t acquisition periods to obtain fully decoupled 1H singlet signals. Diastereotopic protons belonging to methylene AB spin systems appear as doublets because geminal 2f(HH) magnetization is inverted together during the BIRD filter and is therefore not decoupled.5 Finally, resolution can be further improved using non-uniform sampling12 in combination with zero-filling and linear prediction during data processing.

Fig. 2B compares a portion of the SAPS-HSQC vs. SA-HSQC spectra of 1, in order to evaluate multiplet simplification, signal dispersion and relative sensitivity. These data, acquired using a reduced 13C spectral width of 2.5 ppm in a 600 MHz spectrometer with 256 t₁ increments per 2046 points each, provide a digital resolution of around 2-3 Hz pt-1 in both dimensions before data processing. It is shown that improved signal dispersion due to the combined effects of ¹H and ¹³C δ differentiation is further enhanced by the multiplet pattern simplification provided by homo- and heteronuclear decoupling. The pure shift approach can afford a general sensitivity enhancement by 10-40% through the collapse of the multiplet structure. As expected, the proposed psHSQCsi version affords a substantial SNR improvement for CH cross-peaks when compared to the psHSQC (Fig. S4, ESI†). In terms of spectral quality, homodecoupling during acquisition in psHSQC/psHSQCsi experiments generates small sidebands at specific frequencies around the main signal

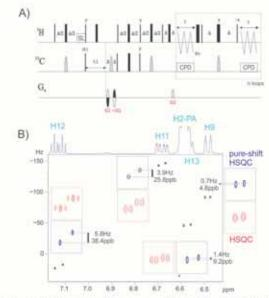


Fig. 2 (A) Pulse scheme of the pure shift sensitivity-improved HSOC experiment ($A = 1/(2 \times {}^{1}J(CH)))$; (B) expanded areas comparing some cross-peaks in SA- (red) and SAPS-HSQC (blue) spectra of the racemic compound $\mathbf{1}$ -R-PA mixture acquired with a reduced 13 C spectral width of 2.5 ppm.

and a minimum broadening of the signal (~ 3 Hz vs. ~ 3.5 Hz) when compared to traditional experiments (Fig. S4, ESI†).⁶ In practice, this does not affect the $\Delta\Delta\delta$ determination, and signal discrimination less than 0.5 Hz (0.8 ppb for ¹H and 3.3 ppb for ¹³C) can typically be achieved (Table 1), even for NMR signals with no apparent splitting in the ¹³C spectrum.

The analyzed sample contains several examples that illustrate the power of the proposed method which, a priori, could detect enantiodifferentiated signals even in the case that $\Delta\Delta\delta(^{1}H)$ or $\Delta\Delta\delta(^{13}C)$ is close to 0, whenever one of the two are sufficiently dispersed. In the example shown, of the 16 available proton signals, 5 are detected as enantiodifferentiated in the 1H spectrum, 10 in the 1D ZS and 15 in the psHSQCsi. In addition, of the 11 signals of protonated carbons, 6 are detected as enantiodifferentiated in the 1D 13C spectrum and 10 in the psHSQCsi (Table 1). A new parameter $\Delta\Delta\delta(CH)^2 = \Delta\Delta\delta(^1H)^2 +$ ΔΔδ(13C)2 is defined to describe mathematically the signal dispersion in HSQC cross-peaks (Fig. S5, ESI†). In general, we can say that both $\Delta\Delta\delta(^{1}H)$ and $\Delta\Delta\delta(^{13}C)$ values can be measured when $\Delta\Delta\delta(CH) > 5$ ppb (Table 1). For instance, the two singlets corresponding to the NMe group in 1 (H16) are well resolved in the regular 1H spectrum (27.0 ppb) whereas the corresponding C16 carbon is not resolved in the 13C spectrum <13.2 ppb). From the HSQC cross-peak an accurate value of $\Delta\Delta\delta(C16)$ = 9.9 ppb can be obtained. Similar analysis can be made for the H9/C9 and H13/C13 pairs where the carbon signals do not appear split in the 1D 13C spectrum but values of 4.6 ppb and 9.2 ppb, respectively, can be extracted from the 2D analysis (Fig. 2B and Fig. S8, ESI†). Another challenging

View Article Online

ChemComm Communication

Table 1 ¹H and ¹³C NMR chemical shift differences (ΔΔδ(¹H) and ΔΔδ(¹⁵C)) of the racemic compound 1 (29 mM) enantiodifferentiated with R-PA (9.6 equiv.) measured at 600 MHz and 298 K

	$\Delta\Delta\delta(^{1}H)$ [i	in ppb]		$\Delta\Delta\delta(^{13}C)$ [i			
Label 1D ¹ H	1D 1H	1D ZS- ¹ H	SAPS-HSQC ^c	1D 13C	SAPS-HSQC ^e	SA-HSQMBC ^{b,c}	ΔΔδ(CH) [in ppb]
2		-		14.5		14.5	30.3 ^b
3		-	-	< 13.2	-	3.3	12.4b
4a/4b	x^{α}/x^{α}	20.0/47.0	20.8/46.1	72.9	73.5		76.4/86.7
5a/5b	$\mathbf{x}^{\mathrm{st}}/\mathbf{x}^{\mathrm{st}}$	<3.3/x"	2.5/21.0	< 13.2	5.3		5.9/21.7
6a/6b	x^{α}/x^{α}	< 3.3/15.6	< 3.3/16.7	< 13.2	< 3.3	-	<4.7/17.0
7a/7b	x^{α}/x^{α}	5.8/<3.3	4.6/1.2	13.9	13.2	-	14.0/13.2
8	1997	-		84.1		84.1	90.9 ^b
9	22.4	22.8	23.3	< 13.2	4.6		23.7
10		-	-	43.7	_	44.4	56.2 ^b
11	30.8	31.8	30.6	27.1	25.8	-	40.0
12	34.4	34.8	34.5	39.0	38.4	-	51.6
13	X ^{ee}	X [#]	32.0	< 13.2	9.2	_	33.3
14a/14b	x^{α}/x^{α}	19.1/x ⁶	18,8/9,8	30.4	29.8	-	35.2/31.3
15	11.5	11.1	12.0	21.2	18.5		22.0
16	27.0	27.1	26.6	< 13.2	9.9	-	28.4

[&]quot;Not determined. b Only relevant data on quaternary carbons are shown. Digital resolution of ±0.5 and ±2.6 ppb for H and DC, respectively.

analysis involves the H7a/H7b protons and their C7 carbon, which present very low resolution. A very small $\Delta\Delta\delta(H7b)$ = 1.2 ppb, which is not distinguishable in the ZS 1H spectrum, can be measured from the highly resolved 2D cross-peak.

The same strategy can be followed to determine $\Delta\Delta\delta$ on quaternary carbons from an aliased non-refocused HSOMBC experiment.13 Unfortunately, broadband homodecoupling in a similar manner as that described for the psHSQC experiment cannot be achieved because the detected signals correspond to 1H-12C magnetization that is homonuclear J coupled to other protons with the same 1H-12C topology. Although at least one pure shift HMBC approach has been reported, this technique requires long acquisition times and a complex processing protocol,7 Fig. S9 (ESI+) shows some HSQMBC cross-peaks for the four quaternary carbons of 1 where a very small value of $\Delta\Delta\delta(C3) = 3.3$ ppb can be measured.

In all these spectra, each aliased 13C peak appears without sign inversion at a position that is exactly a multiple of the spectral width (SW_c) from its real position (δ_t) that can be determined from the relationship $\delta_r = \delta_{obs} + (K \times SW_c)$, where δ_{obs} is the experimental $\delta(^{13}C)$ measured in the aliased spectra using a given 13 C offset Ω_c and K is the fold number which can be determined from reference non-aliased HSQC or HSQMBC spectra using a moderate number of t1 increments (Fig. S10, ESI†). Several automated strategies that have been proposed to determine the correct 13 C δ_r values and to reconstruct the entire spectrum could also be applied here.30 The enantiodifferentiation from highly resolved HSQC spectra allows the unambiguous ¹H and ¹³C chemical shift assignment that is not available from the exclusive use of 1D spectra and, in addition, the pure shift nature of cross-peaks makes the proposed technique highly suitable for the quantitative determination of enantiomeric excess by 2D volume integration, because equivalent signals from both diastereoisomers have practically similar J(CH) coupling and T2 relaxation values.

In summary, the combination of spectral aliasing and pure shift HSQC experiments represents an excellent routine tool for NMR enantiodifferentiation studies, yielding simultaneous 1H and 13 C enantiodifferentiated data ($\Delta\Delta\delta(^{1}H)$ and $\Delta\Delta\delta(^{13}C)$) in short times and with high digital resolution and signal dispersion for both ³H and ¹³C nuclei. Its use increases significantly the probability to detect an enantiodifferentiated nucleus since more signals are observed (1H and 13C nuclei), overlapping problems of common 1D 1H experiments are overcome, and poor enantiodifferentiation in 1D experiments can now be detected, allowing the study of cases abandoned in the past for reasons of poor enantioresolution and/or long experimental times. Alternatively, aliased longrange heteronuclear correlation experiments can be used to measure accurately such $\Delta\Delta\delta$ values for quaternary carbons. The method is compatible with other heteronuclei and with the use of other chiral auxiliaries, and it can be of special interest for chiral metabonomic studies, where chiral molecules in complex mixtures are enantiodifferentiated and small chemical shifts need to be resolved in overcrowded spectra.14

Financial support for this research provided by MINECO (project CTQ2012-32436) is gratefully acknowledged. We also thank the Servei de Ressonància Magnètica Nuclear, Universitat Autònoma de Barcelona, for allocating instrument time to this project.

Notes and references

- (a) T. J. Wenzel, Top. Curr. Chem., 2013, 341, 1-68; (b) G. Uccello-Barretta and F. Balzano, Top. Curr. Chem., 2013, 341, 69-131.
- (a) M. Palomino-Schätzlein, A. Virgili, S. Gil and C. Jaime, J. Org. Chem., 2006, 71, 8114-8120; (b) M. Pérez-Trujillo, E. Monteagudo and T. Parella, Anal. Chem., 2013, 85, 10887–10894.
 (a) H. Dodziuk, A. Ejchart, O. Lukin and M. O. Vysotsky, J. Org.
- Chem., 1999, 64, 1503-1507; (b) H. Dodziuk, W. Koźmiński, O. Lukin and D. Sybilska, J. Mol. Struct., 2000, 523, 205-212.
- (a) K. Zangger and H. Sterk, J. Magn. Reson., 1997, 124, 486–489;
 (b) N. H. Meyer and K. Zangger, Argew. Chem., Int. Ed., 2013, 52, 7143–7146;
 (c) N. H. Meyer and K. Zangger, ChemPhysChem, 2014, 15, 49-55; (d) J. A. Aguilar, S. Faulkner, M. Nilsson and G. A. Morris, Angew. Chem., Int. Ed., 2010, 49, 3901-3903; (e) G. A. Morris, J. A. Aguilar, R. Evans, S. Haiber and M. Nilsson, J. Am. Chem. Soc., 2010, 132, 12770-12772.
- 5 J. R. Garbow, D. P. Weitekamp and A. Pines, Chem. Phys. Lett., 1982, 93, 504-509.

10216 | Chem. Commun., 2014, 50, 10214-10217

This journal is @ The Royal Society of Chemistry 2014

View Article Online

Communication ChemComm

- L. Paudel, R. W. Adams, P. Király, J. A. Aguilar, M. Foroozandeh, M. J. Cliff, M. Nilsson, P. Sándor, J. P. Waltho and G. A. Morris, Angew. Chem., Int. Ed., 2013, 52, 11616–11619.
 P. Sakhaii, B. Haase and W. Bermel, J. Magn. Reson., 2013, 228, 125–129.
 L. Castañar, M. Pérez-Trujillo, P. Nolis, E. Monteagudo, A. Virgili
- and T. Parella, ChemPhysChem, 2014, 15, 854-857. 9 (a) S. J. deSolms, T. M. Ciccarone, S. C. MacTough, A. W. Shaw, C. A. Buser, A. J. Gesofms, T. M. Ciccarone, S. C. MacTough, A. W. Shaw, C. A. Buser,
 M. Ellis-Hutchings, C. Fernandes, K. A. Hamilton, H. E. Huber, N. E. Kohl,
 R. B. Lobell, R. G. Robinson, N. N. Tsou, E. S. Walsh, S. L. Graham,
 L. S. Beese and J. S. Taylor, J. Med. Chem., 2003, 46, 2973–2984; (b) M. Pérez-Trujillo and A. Virgili, Tetrahedron: Asymmetry, 2006, 17, 2842–2846.
 (a) D. Jeannerat, Magn. Reson. Chem., 2003, 41, 3–7; (b) D. Jeannerat,
 Rapid Multidimensional NMR: High Resolution by Spectral Aliasing,
- Encyclopedia of Magnetic Resonance, John Wiley, Chichester, 2011; (c) B. Vitorge, S. Bieri, M. Humam, P. Christen, K. Hostettmann, O. Muñoz, S. Loss and D. Jeannerat, Chem. Commun., 2009, 950–952; (d) M. Foroozandeh, P. Giraudeau and D. Jeannerat, ChemPhysChem, 2011, 12, 2409-2411.
- L. Kay, P. Keifer and T. Saarinen, J. Am. Chem. Soc., 1992, 114, 10663–10665.
- 12 K. Kazimierczuk and V. Y. Orekhov, Angew. Chem., Int. Ed., 2011, 50, 5556-5559.
- R. T. Williamson, B. L. Márquez, W. H. Gerwick and K. E. Kövér, Magn. Reson. Chem., 2000, 38, 265–273.
 M. Pérez-Trujillo, J. C. Lindon, T. Parella, H. C. Keun, J. K. Nicholson
- and T. J. Athersuch, Anal. Chem., 2012, 84, 2868-2874.

Electronic Supplementary Material (ESI) for ChemComm. This journal is © The Royal Society of Chemistry 2014

Supporting Information

Simultaneous ¹H and ¹³C NMR enantiodifferentiation from highly resolved pure shift HSQC spectra

Míriam Pérez-Trujillo, Laura Castañar, Eva Monteagudo, Lars T. Kuhn, Pau Nolis, Albert Virgili, R. Thomas Williamson, and Teodor Parella*

Table of Contents:

Experimental Section

Figure S1: ¹H NMR spectrum of racemic compound **1** without and with *R*-PA.

Figure S2: 1D conventional and pure shift ¹H spectrum of compound **1** and *R*-PA.

Figure S3: Heterodecoupled 13 C NMR spectrum of racemic compound **1** and *R*-PA with expanded multiplets to show individual signal splittings due to the enantiodifferenation.

Figure S4: Experimental line widths and relative sensitivities obtained in conventional HSQC, pure shift HSQC (psHSQC) and pure shift sensitivity-improved HSQC (psHSQCsi) experiments.

Figure S5: Schematic representation of $\Delta\Delta\delta(CH)$.

Figure S6. 2D HSQC and psHSQCsi spectra of racemic compound 1 and R-PA.

Figure S7: Expanded area comparing multiplet patterns in SA-HSQC and SAPS-HSQC.

Figure S8: Comparison between the conventional coupled ¹³C-NMR and SAPS-HSQC experiment in terms of resolution. Evaluation of the effect in ¹³C signals when different window functions are applied in the post-processing.

Figure S9: (top) Aliased 2D HSQMBC spectrum of racemic compound 1 and *R*-PA. (bottom) selected 2D cross-peaks corresponding to quaternary carbons.

Figure S10: Experimental ¹³C chemical shifts in aliased and conventional HSQC spectra.

Table S1: 1 H and 13 C NMR chemical shift differences (($\Delta\Delta\delta(^{1}$ H) and $\Delta\Delta\delta(^{13}$ C) in Hz) of racemic compound **1** (2 mM) enantiodifferentiated with *R*-PA (9.6 equiv.) measured from different NMR experiments at 600MHz.

Experimental Section

NMR experiments were performed on a Bruker Avance 600 spectrometer (Bruker AG, Rheinstetten, Germany) equipped with TXI HCN z-grad probes. The temperature for all measurements was set to 298 K and data were acquired and processed with TOPSPIN 3.1 (Bruker AG, Rheinstetten, Germany).

All spectra were recorded on a 600 μ L fresh solution stock of racemic 3-ethyl-3-(3-hydroxyphenyl)-1-methylazepan-2-one (compound **1**, 29 mM) in CDCl₃, containing 9.6 equiv. (46.2 mg) of *R*-Pirkle alcohol (PA). It is referred to as compound **1** throughout the manuscript and this SI.

Slice selection in the 1D Zangger-Sterk (ZS) experiment (Fig. 1B) was performed using a selective 180 ¹H R-Snob pulse of 60 ms applied simultaneously to a weak rectangular gradient of 2%. Data was acquired in a pseudo 2D mode using 4 scans for each one of the 16 t₁ increments and a recycle delay of 1s. The FID reconstruction was performed with the AU program pshift (available at http://nmr.chemistry-manchester.ac.uk), followed by conventional Fourier transformation. The total experimental time was of 9 minutes.

The 2D ¹H-¹³C pure shift HSQC spectrum (pulse scheme of Fig. 2A) was recorded as described in ref. 6. Pulse phases are x unless indicated otherwise and a basic two-step phase cycling scheme is applied: $\Phi_1=x,-x$, $\Phi_r=x,-x$. ¹³C 180° pulses are applied as CHIRP inversion and refocusing pulses of 500 µs and 2000 µs of duration, respectively. The recycle delay was 3 s and the interpulse delays in the INEPT and BIRD modules were optimized for 140 Hz (Δ =3.57 ms). 2 scans were accumulated for each one of the 256 t_1 increments (512 experiments defined applying 50% non-uniform sparse sampling), the spectral windows in F1 and F2 dimensions were 377 Hz (2.5 ppm) and 4200 Hz, respectively, the number of data points in t_2 was set to 2048 and the acquisition time (AQ) was 0.24 s giving a FID resolution of 1.47 and 4.10 Hz, respectively. The total experimental time was of 30 min. Homodecoupling during acquisition was achieved applying 130 loops (n) with τ =7.7 ms. Broadband heteronuclear decoupling was applied during the τ periods using 1.5 ms chirped pulses combined in a p5m4 supercycle scheme. The ratio between the G1:G2 gradients were 40:20.1, measured as percentage of the absolute gradient strength of 53.5 G/cm. Data were acquired and processed using the echo/anti-echo protocol. Sine bell shaped gradients of 1 ms duration were used, followed by a recovery delay of 20 μ s

 $(\delta=1.02\text{ms})$. Prior to Fourier-transformation of each data, zero filling to 1024 in F1, 8192 points in F2, linear prediction in F1 and a $\pi/2$ -shifted sine squared window function in both dimensions were applied. The final digital resolution was of 0.51 and 0.36 Hz in F2 and F1 dimensions, respectively.

To determine $\Delta\Delta\delta$ on quaternary carbons, a conventional non-refocused gradient-enhanced HSQMBC experiment optimized to 8 Hz was collected with the same acquisition and processing parameters described for the HSQC experiments. 16 scans were acquired per t_1 increment giving a total experimental time of 4 hours. Conventional 2D HSQC experiments were recorded under the same conditions as described previously for the pure shift analogues. HSQC and HSQMBC experiments were also recorded with 13 C spectral windows of 5 ppm (Fig. S6 and S9-10).

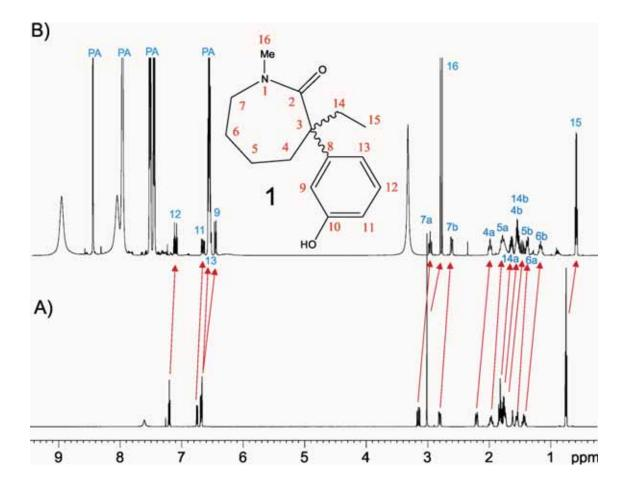


Figure S1: A) ¹H NMR spectrum of racemic compound (1) in CDCl₃; B) Resulting ¹H NMR spectrum after adding 9.6 equivalents of Pirkle Alcohol (*R*-PA).

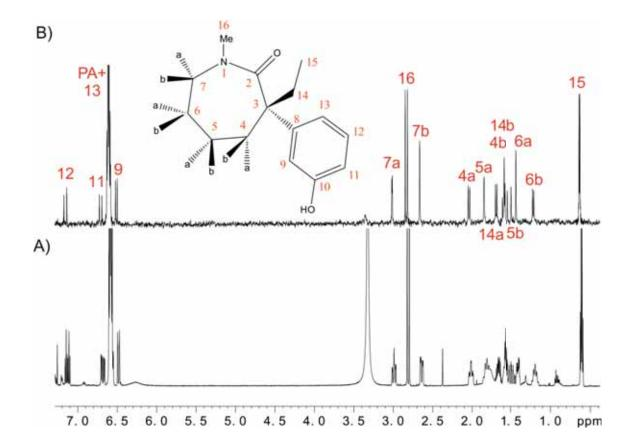


Figure S2: A) 1D conventional and B) pure shift 1 H spectrum of racemic compound 1 and R-PA. The structure of the R-1 enantiomer is shown for stereoassignment purposes. See Fig. 1C and 1D for selected expansions and experimental $\Delta\Delta\delta(^{1}\text{H})$ values.

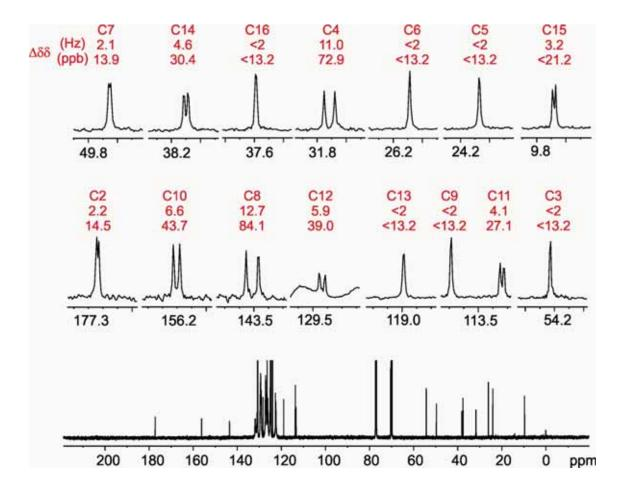


Figure S3: (Bottom) 150.9 MHz Broadband heterodecoupled 13 C NMR spectrum of racemic compound **1** and *R*-PA; (top) expanded multiplets to show individual signal splitting (in Hz and ppb) due to the enantiodifferenation.

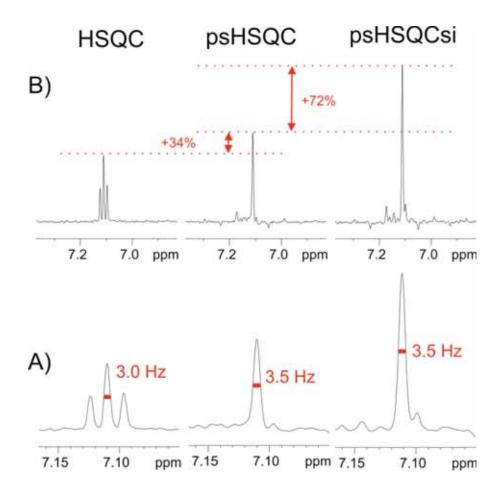


Figure S4: (A) Experimental line widths and B) relative sensitivities obtained in conventional HSQC, pure shift HSQC (psHSQC) and pure shift sensitivity-improved HSQC (psHSQCsi) experiments. 1D traces correspond to the upfield H12/C12 carbon frequency.

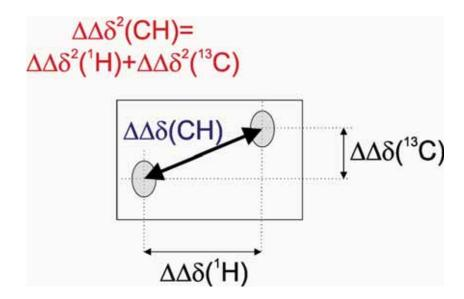


Figure S5: Schematic representation of the new parameter $\Delta\Delta\delta(CH)$ that defines the separation between two cross-peaks from the individual $\Delta\Delta\delta(^1H)$ and $\Delta\Delta\delta(^{13}C)$ separations along each dimension of a 2D map.

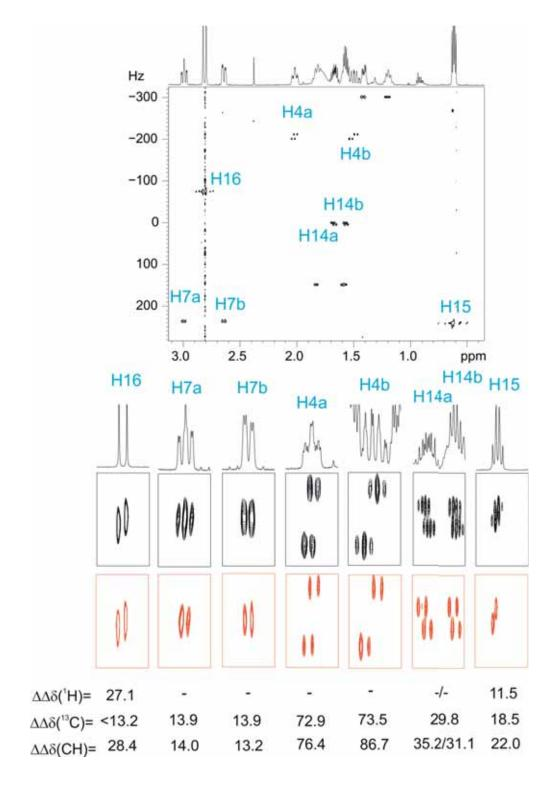


Figure S6: (Top) Expanded area corresponding to the 0.4-3.2 ppm region of the 2D psHSQCsi spectrum of **1** acquired with SW(13 C)=5 ppm; (medium) Expanded crosspeaks show the distinction between enantiomeric signals in 1D 1 H, conventional HSQC and psHSQCsi spectra; (bottom) experimental values extracted from the conventional 1 H spectrum ($\Delta\Delta\delta(^{1}$ H)), 1D 13 C spectrum ($\Delta\Delta\delta(^{13}$ C)) and calculated ($\Delta\Delta\delta(^{13}$ CH)) values calculated from the splitting measured in the 2D spectrum.

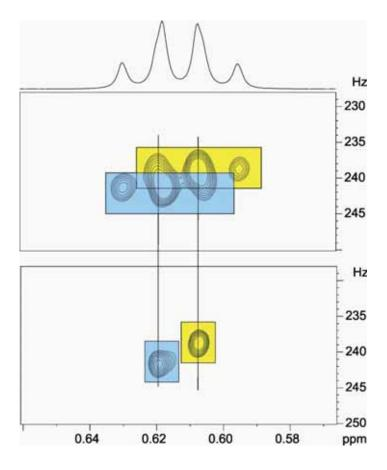


Figure S7: Expanded area corresponding to the C15/H15 cross-peak in (top) SA-HSQC and B) SAPS-HSQC spectra. The H15 signal consists of two overlapped triplets where is difficult to extract the exact ¹H chemical shift in both 1H and conventional HSQC spectra. Note the superior features of the SAPS approach to perform: i) automatic peak picking, ii) accurate and simultaneous determination of ¹H and ¹³C chemical shift differences, and iii) an improved quantification by peak volume integration of each individual singlet signal.

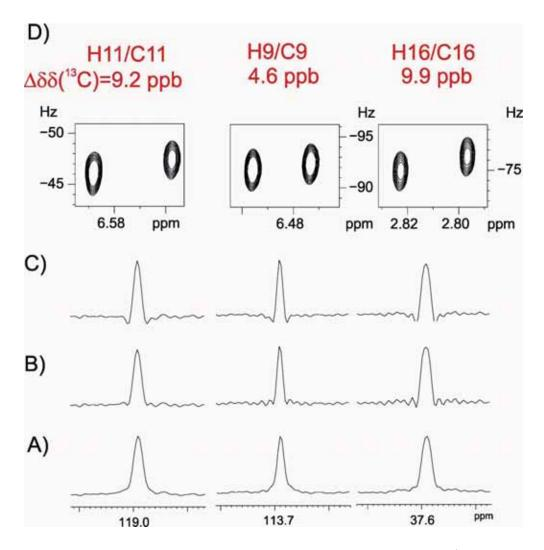


Figure S8: Example showing how the good dispersion along the detected ¹H dimensions allows the differentiation of small chemical shift differences along the indirect ¹³C dimension, even smaller than the line width observed in the conventional ¹³C spectrum. A-C) show some not resolved ¹³C signals obtained in the conventional ¹³C spectrum of 2mM racemic compound 1 complexed with R-PA. Data were acquired with 32K data points and an spectral width of 36057 Hz and further processed with a zero filling up to 64K giving a digital resolution of 0.6 Hz: A) processed with an exponential multiplication with a line broadening of 1 Hz; B) processed without any window function; C) processed with a Gaussian function with LB=-2 Hz and GB=0.5. The line widths at the half of well resolved signals in spectra B was about 1.7 Hz. D) Expansions of the corresponding cross-peaks obtained from the SAPS-HSQC spectra.

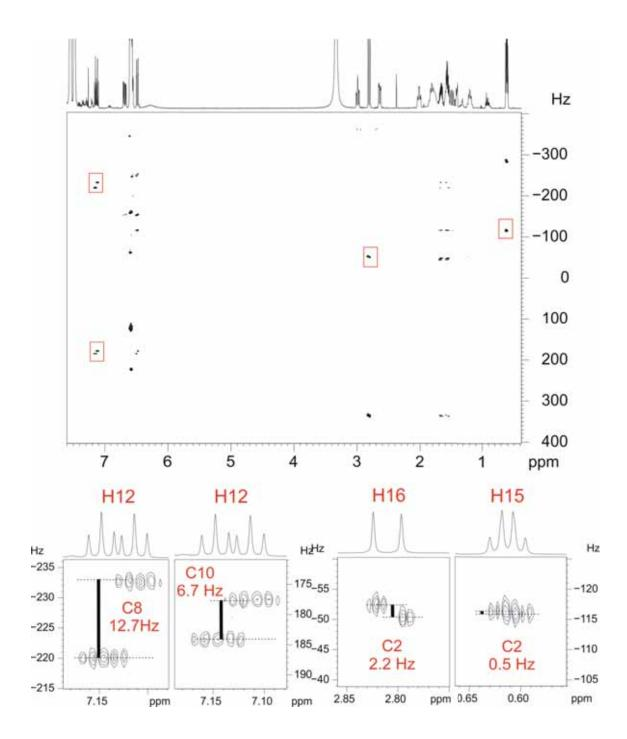


Figure S9: (top) Aliased 2D HSQMBC spectrum of **1**, acquired with a 13 C spectral width of 5.0 ppm. (bottom) Some selected 2D cross-peaks corresponding to quaternary carbons where $\Delta\Delta\delta(^{13}\text{C})$ values ranging from 12.7 to 0.5 Hz (84.1 to 3.3 ppb, respectively) can be extracted from the F1 dimension.

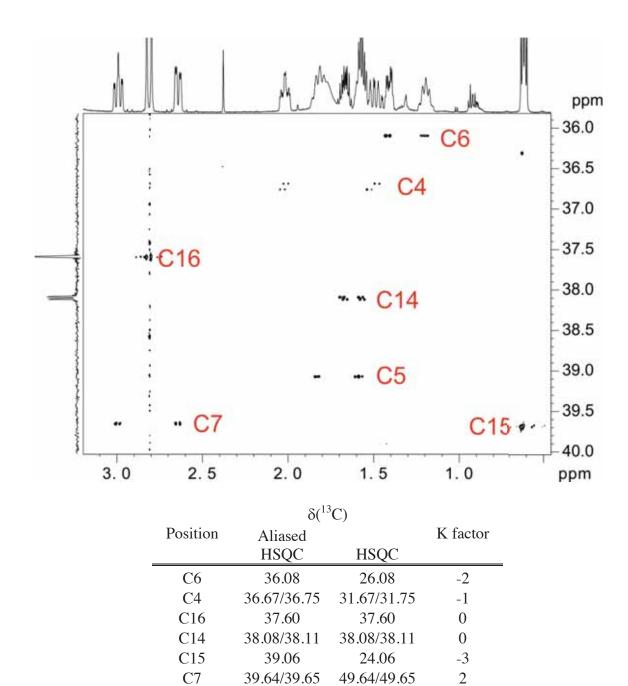


Figure S10: Chemical shifts in aliased and conventional 2D psHSQCsi spectra. Experimental parameters in the indirect dimension: carrier frequency= 38.0 ppm and 13 C spectral width= 5 ppm.

9.67/9.69

-6

39.67/39.69

C15

Table S1: 1 H and 13 C NMR chemical shift differences (($\Delta\Delta\delta(^{1}$ H) and $\Delta\Delta\delta(^{13}$ C) in Hz) of racemic compound 1 (2 mM) enantiodifferentiated with *R*-PA (9.6 equiv.) measured from different NMR experiments at 600MHz.

	4	$\Delta \delta(^{1}\text{H})$ [in	Hz]	Δ	$\Delta\Delta\delta(^{13}\mathrm{C})$ [in Hz]		
Position	1D ¹ H	1D ZS- ¹ H	Pure shift HSQC ^c	1D ¹³ C	Pure shift HSQC ^c	HSQMBC ^b	[in Hz]
2	-	-	-	2.2	-	2.2	16.1
3	-	-	-	<2	-	0.5	7.2
4a/4b	x ^a /x ^a	12.0/28.2	12.5/27.7	11.0	11.1	-	16.7/29.8
5a/5b	x ^a /x ^a	$<2/$ x^a	1.5/12.6	<2	0.8	-	1.7/12.6
6a/6b	x ^a /x ^a	<2/9.4	<2/10.0	<2	< 0.5	-	<1/10.0
7a/7b	x ^a /x ^a	3.5/<2	2.8/0.7	2.1	2.0	-	3.4/2.1
8	-	-	-	12.7	-	12.7	24.3
9	13.5	13.7	14.0	<2	0.7		14.0
10	-	-	-	6.6	-	6.7	21.7
11	18.5	19.1	18.4	4.1	3.9	-	18.8
12	20.7	20.9	20.7	5.9	5.8	-	21.4
13	x ^a	$\mathbf{x}^{\mathbf{a}}$	19.2	<2	1.4	-	19.2
14a/14b	x ^a /x ^a	$11.5/ x^a$	11.3/5.9	4.6	4.5	-	12.1/7.4
15	6.9	6.7	7.2	3.2	2.8	-	7.7
16	16.2	16.3	16.0	<2	1.5	-	16.1

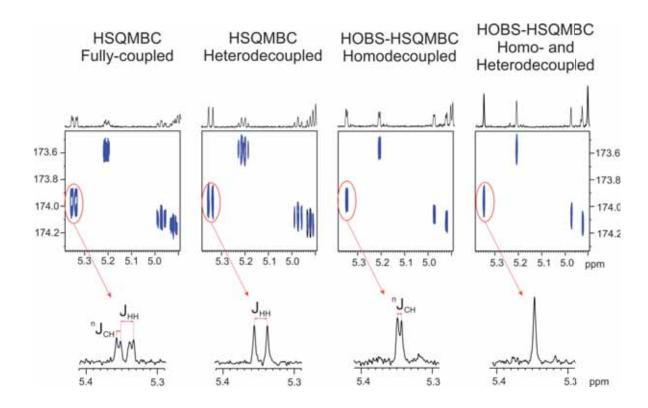
^a Not determined

b Only relevant data on quaternary carbons is shown Digital resolution of ±0.3 and ±0.4 Hz for ¹H and ¹³C respectively.

PUBLICATION 6

Implementing homo- and heterodecoupling in region-selective HSQMBC experiments

Laura Castañar, Josep Saurí, Pau Nolis, Albert Virgili and Teodor Parella. *J. Magn. Reson.*, **2014**, *238*, 63-69.



Introduction

As it was mention in the Introduction (see section 1.2.2) the HSQMBC⁷³ experiment allows obtain correlations between protons and both protonated and non-protonated carbon atoms separated by more than one bond. The main drawback of the conventional HSQMBC experiment is that cross-peaks show important AP contributions due to the J_{HH} evolution during the long INEPT periods (60-70 ms). A series of modified HSQMBC-like experiments have been proposed to obtain IP multiplets which allow measure the $^{n}J_{CH}$ in a more straightforward way (see section 1.2.2.2). It has been show that pure-phase cross-peaks can be obtain from selHSQMBC experiments using region-selective 180^{o} ^{1}H pulses at the middle of the INEPT periods. 80,81 The excellent IP multiplet structure with respect to J_{HH} allows the quantitative and accurate measurement of $^{n}J_{CH}$ from non-distorted pure-phase multiplets along the detected dimension. Importantly, to carry out the measure of the $^{n}J_{CH}$ without additional post-processing fitting or IPAP procedures, high digital resolution levels in the detected dimension is mandatory.

On the other hand, the pure shift methodology greatly improves the spectral resolution in the proton dimension removing the typical J_{HH} multiplet pattern. The incorporation of broadband homodecoupling in experiments detecting AP HH magnetization components, like the regular HSQMBC experiments, fails because multiplet structures should be partially or fully cancelled. However, the excellent IP nature demonstrated for the selHSQMBC experiment allows that homonuclear and/or heteronuclear decoupling can be implemented along the detected dimension using the HOBS technique (see **Publication 2**), obtaining simplified cross-peaks without their characteristic multiplet J_{HH} patterns.

In this article a new method to obtain ¹H-homodecoupled long-range ¹H-¹³C correlations from a selected area of a 2D spectrum has been developed. The new HOBS-HSQMBC experiment shows higher resolution and sensitivity than the original selHSQMBC version and represents a completely new way to measure ⁿJ_{CH}. In the F2-heterocoupled HOBS-HSQMBC version all cross-peaks appear homodecoupled from other protons resonating outside of the selected area, only displaying an IP doublet corresponding to the active ⁿJ_{CH} splitting. The semi-automated extraction of ⁿJ_{CH} can be made by direct analysis of cross-peaks if the multiplet is resolved enough. In cases of poor resolved multiplets or when the accuracy of the measurements may be doubtful, the application of the IPAP methodology can offer a better solution. The HOBS-HSQMBC method is fully compatible with simultaneous heteronuclear decoupling, leading to complete pure shift NMR spectra with enhanced resolution and maximum sensitivity.

Journal of Magnetic Resonance 238 (2014) 63-69



Contents lists available at ScienceDirect

Journal of Magnetic Resonance

journal homepage: www.elsevier.com/locate/jmr



Implementing homo- and heterodecoupling in region-selective HSQMBC experiments



Laura Castañar, Josep Saurí, Pau Nolis, Albert Virgili, Teodor Parella

Servei de Ressonância Magnètica Nuclear and Departament de Química, Universitat Autónoma de Barcelona, E-08193 Bellaterra (Catalonia), Spain

ARTICLE INFO

Article history: Received 21 September 2013 Revised 27 October 2013 Available online 15 November 2013

Keywords: Pure-shift Band-selective HSOMBC Proton-carbon coupling constants Homonuclear decoupling Sensitivity improvement

ABSTRACT

An NMR method to enhance the sensitivity and resolution in band-selective long-range heteronuclear correlation spectra is proposed. The excellent in-phase nature of the selHSQMBC experiment allows that homonuclear and/or heteronuclear decoupling can be achieved in the detected dimension of a 2D multiple-bond correlation map, obtaining simplified cross-peaks without their characteristic fine J multiplet structure. The experimental result is a resolution improvement while the highest sensitivity is also achieved. Specifically, it is shown that the ¹H-homodecoupled band-selective (HOBS) HSQMBC experiment represents a new way to measure heteronuclear coupling constants from the simplified in-phase doublets generated along the detected dimension.

© 2013 Elsevier Inc. All rights reserved.

1. Introduction

Long-range heteronuclear correlation experiments are key NMR tools for the structural characterization of small molecules and natural products in solution. The widely used HMBC/HSQMBC pulse schemes have been modified in several ways in order to improve their success application on a wide range of issues [1-2]. For instance, band-selective excitation in the indirect carbon dimension allows use very reduced spectral widths, and therefore the resolution/dispersion between 13C signals can be strongly increased [3-7]. On the other hand, different attempts have been made to remove the undesired effects due to the evolution of J(HH) that generate cross-peaks with complex phase multiplets. This is particularly severe in HMBC experiments because J(HH) evolves during all the evolution periods, yielding an additional characteristic skew of the cross-peaks that can compromise peak analysis. Constant-time versions of the HMBC experiment have been proposed to remove such inconvenience and their combination with band-selective excitation affords better defined spectra [8-9]. It has been shown that pure-phase cross-peaks can be obtained from HSQMBC experiments using region-selective 180° 1H pulses at the middle of the INEPT periods [10-11]. The excellent in-phase (IP) multiplet structure with respect to J(HH) allows the quantitative and accurate measurement of "J(CH) from non-distorted pure-phase multiplets along the detected dimension. Furthermore, the easy implementation of the IPAP methodology

* Corresponding author. E-mail address: teodor.parella@uab.cat (T. Parella).

http://dx.doi.org/10.1016/j.jmr.2013.10.022

1090-7807/\$ - see front matter @ 2013 Elsevier Inc. All rights reserved.

affords a powerful way to extract them, even when J coupling values are smaller than the linewidth, by analyzing the relative displacement between separate α/β multiplet components [10].

On the other hand, the concept of pure-shift NMR has been introduced in multidimensional NMR experiments as a method to simplify the J(HH) multiplet structure of proton resonances [12-21]. Most of these experiments rely in spatial encoding selection and their reliable applicability strongly depends on the experimental sensitivity. For this reason, pure-shift experiments have been mainly reported for homonuclear applications because its implementation into heteronuclear inverse-detected experiments suffers of important sensitivity success. Using a different concept, a tilted pseudo-3D HMBC experiment has been proposed to achieve ¹H-homodecoupling along the detected dimension by incorporating a J-resolved dimension into the HMBC pulse scheme

Recently, a new detection scheme to obtain HOmodecoupled Band-Selection (HOBS) in the detected dimension of multidimensional NMR experiments has been reported [23]. It has been sucimplemented in homonuclear (TOCSY) and heteronuclear (HSQC) experiments involving in-phase HH magnetization. However, the incorporation of this technique in experiments involving anti-phase HH magnetization, like the regular COSY, HMBC or HSQMBC experiments, fail because the evolution of J(HH) generates anti-phase components that would cancel under homodecoupling conditions. Here we show how the HOBS methodology can be implemented in the pure-phase selHSQMBC experiment in order to obtain pure-shift heteronuclear correlation spectra that offer a considerable enhancement in both resolution

and sensitivity. In addition, the method is also fully compatible with band-selective excitation in the indirect dimension and with broadband heteronuclear decoupling during detection to obtain high-resolved pure-shift region-selective HSQMBC spectra. It will be shown that the method is also amenable to measure small heteronuclear coupling constants from the pure-phase doublet crosspeaks originated along the detected dimension and also fully compatible with the IPAP methodology described early [24]. All these features will be illustrated using the cyclic undecapeptide cyclosporine as test sample.

2. Results and discussion

Fig. 1 displays two basic pulse schemes of the selHSQMBC experiment [10] that incorporates band-selective homodecoupling during the acquisition period using the HOBS technique. Fig. 1A is a conventional experiment offering broadband ¹³C excitation in the indirect dimension, whereas Fig. 1B is a ¹³C band-selective version where the original G1-180°(¹³C)-ō period during the t₁ period has been replaced by a G1+0.5-180°(¹³C_{sel})-G1+(-0.5) block. As in the original experiment, the region-selective 180° ¹H pulses applied on non-mutually coupled protons during the long INEPT delays avoid any J(HH) evolution. Just prior to acquisition, signals present pure IP properties with respect to J(HH) coupling constants that are amenable for the application of the HOBS detection

scheme to collapse the multiplet J structure. The HOBS scheme consists of n concatenated loops that includes a pair of hard/region-selective 180° 1H pulses (each one flanked by the G3 and G4 gradients) applied at intervals of 21 period (1 is set to AQ/ 2n) as shown in the box of Fig. 1. The selective 180° pulses applied in the INEPT and during detection have the same shape and duration, minimizing the requirements for additional experimental setup. Thus, all protons selected by the region-selective 180° 1H pulse appear homodecoupled from all other protons that do not experience this pulse, and the result is a band-selective homodecoupled observation of a specific region of the 1H spectrum. The method is also fully compatible with optional broadband heteronuclear 13C decoupling which is applied only during the FID acquisition periods (A), as shown in Fig. 1. We refer to this technique as a BEHOBS (Broadband-hEterodecoupled and HOmodecoupled Band-Selective) and it affords fully homo- and heteronuclear decoupled spectra consisting only of singlet cross-peaks.

Fig. 2A shows the refocused IP version of the conventionally detected selHSQMBC spectrum of cyclosporine after applying a 5 ms REBURP 180° pulse as a band-selective 180° ¹H pulse on its H_α proton region [10–11]. Clearly, all expected long-range correlations are observed showing perfect IP multiplets with respect to both J(HH) and J(CH) coupling constants along the detected dimension. Fig. 2B shows the analog HOBS-HSQMBC spectrum acquired using the scheme of Fig. 1A but without heteronuclear decoupling. We

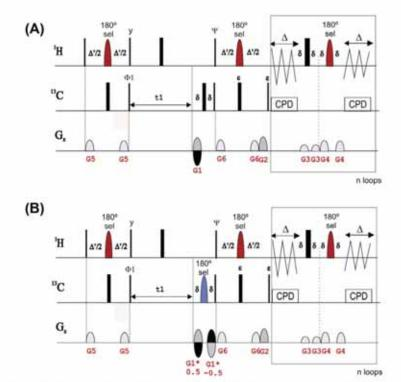


Fig. 1. Experimental pulse schemes for the (Λ) ¹¹C-broadband and (B) ¹²C region-selective HOBS-HSQMBC experiment. Thin and thick bars represent broadband θ 0° and 180° pulses, respectively, whereas shaped pulses are region-selective 180° pulses. The selective 180° ¹⁴ pulse applied at the middle of INEPT periods and during detection have the same shape and duration (p_{180}) and we found that REBURP pulses in the order of 3–10 ms provides the best result as a function of the required selectivity. The INEPT delays are set to $\kappa = 4! + p_{180} + 1/(2 - \frac{9}{3}c_1)$. The basic phase cycling is $\Phi_0 = \kappa_- - \kappa_-$ and $\Phi(\text{receiver}) = \kappa_- - \kappa_-$ all other unlabeled pulses are from the κ -axis. Homonuclear decoupling during the acquisition time (AQ) is performed using a refocusing blocks including a pair of hard/selective 180° ¹⁴H pulses applied at intervals of 2.4 = AQ/n, where n is the number of loops. Optional beteronuclear decoupling (CPD) during data collection can also be applied as shown in the scheme. For the measurement of proton-carbon coupling constants, the IPAP methodology can be applied: two different IP and AP data are recorded without heteronuclear decoupling as a function of the last 90° and 180° ¹³C pulses (IP: $\Psi = \nu$, $\kappa = 0$ ff) and then they are added/subtracted to afford to separate α/β subspectra. More details in the experimental section.

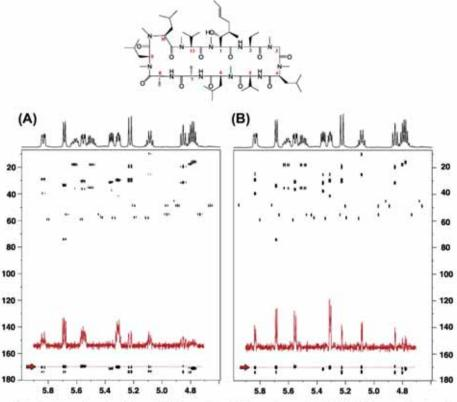


Fig. 2. Practical effects of broadband homodecoupling in the selHSQMBC experiment; (A) Conventional and (B) HORS HSQMBC spectra of cyclosporine acquired under the same experimental time of 20 min. A selected 1D slice is plotted for each spectrum at the same absolute scale to compare the relative sensitivity and resolution achieved in the 2D spectra. The standard 1D spectrum is shown on top of the 2D plot.

can observe how the J(HH) multiplet structures of all H_{α} resonances along the detected dimension are collapsed because of the effective homodecoupling of H_{α} -NH and H_{α} -H $_{\beta}$ coupling constants. A more detailed analysis of a 1D row reveals the enhanced resolution and improved sensitivity achieved with the simple implementation of the HOBS technique.

Fig. 3 shows the improved spectral resolution achieved after combining the band-selective ¹³C excitation of the carbonyl region in conjunction with the HOBS detection scheme, with simultaneous application of homo- and/or heteronuclear decoupling during data acquisition (see pulse scheme of Fig. 1B): non-decoupled (Fig. 3A), with ¹³C-decoupling (BEBS, Fig. 3B), with ¹⁴H-decoupling (HOBS, Fig. 3C) and with simultaneous ¹³C and ¹⁴H-decoupling (BEHOBS, Fig. 3D) HSQMBC spectra. The analysis of 1D row confirms the enhanced resolution and the improved sensitivity by gradual J multiplet simplification, without affecting spectral quality (Fig. 4). The individual analysis of the SNR for each of the observed 19 cross-peaks affords an average enhancement by factors of 1.2 (with heteronuclear decoupling), 1.6 (with homonuclear decoupling) and 2.4 (with both homo- and heteronuclear decoupling) when compared with fully coupled data (normalized average factor of 1).

Of particular interest is the HOBS-HSQMBC spectrum (Fig. 3C) because all cross-peaks are present as pure IP doublets along the F2 dimension. This represents a completely new way to measure coupling constants, because all cross-peaks appear homodecoupled from other protons resonating outside of the selected area, and therefore they only display the active "J_{CH} splitting (Fig. 5). The direct extraction of these couplings can be made by direct analysis of cross-peaks if the multiplet is resolved enough. Because we are dealing with band-selective experiments, the spectral width in the direct dimension can be set to a reduced value and therefore, it is relatively easy to achieve high levels of spectral resolution. It can be shown that direct CH correlations are also observed because any low-pass J filtering method is applied, and therefore the magnitude of one-bond proton-carbon coupling constants, ¹J(CH), can be determined from the well separated singlet satellite lines. Until now, these scalar 1J(CH) and residual dipolar ¹D(CH) coupling constants have been measured from F1- or F2-coupled HSQC experiments [25–29] but the advent of new pure-shift NMR methods will offer a new way to perform this [30–32].

In cases of poor resolved multiplets or when the accuracy of the measurements may be doubtful, the IPAP methodology can offer a better solution. The technique is based in the acquisition of separate IP and AP data as a function of the application of the last 90° and 180° 13 C pulses in schemes of Fig. 1 (labeled with ϵ) followed by time domain IP \pm AP data addition/subtraction. In this way, each individual α and β component of the doublet is obtained in two separate subspectra, rendering the measurement easier by simple determination of their relative mutual shift (Fig. 6). Table 1 shows a perfect agreement between the J(CH) values measured directly from the proposed HOBS and HOBS-IPAP methods with those ex-

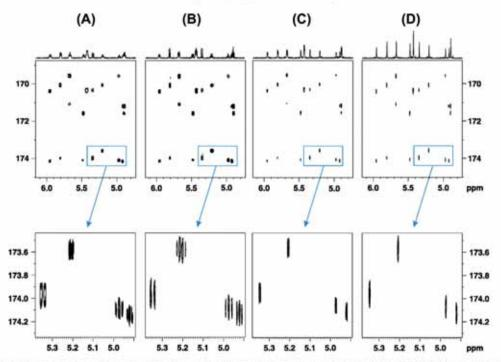


Fig. 3. Resolution enhancement effects after incorporation of homo or/and heteronulear decoupling in region-selected ¹H₂-¹³CO HSQMBC spectra of cyclosporine: (A) conventional; (B) broadband ¹³C-decoupled (BEBS); (C) ¹H-decoupled (HOBS) and (D) ¹H and broadband ¹³C-decoupled (BEHOBS). The internal projection along the detected dimension is shown on top of each 2D plot and all they are plotted with the same absolute scale to compare the relative sensitivity and resolution.

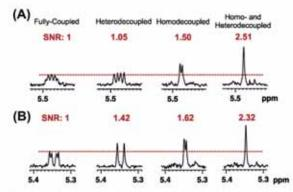


Fig. 4. 1D multiplets corresponding to the (A) C6Hα6 and (B) C11Hα11 cross-peaks obtained from the four different HSQMBC spectra of Fig. 3. The experimental SNR for each signal is shown taking the fully coupled peak (normalized value set to 1) as a reference.

tracted from HSQMBC-TOCSY spectra [33]. The simplicity of the resulting cross-peaks and their IP nature allows an automated peak picking and an easy extraction of "J(CH) values.

3. Conclusions

To conclude, a new method to obtain ¹H-homodecoupled longrange ¹H-¹³C correlations from a selected area of a 2D spectrum has been developed. The method is fully compatible with simultaneous heteronuclear decoupling, leading to pure-shift NMR spectra, with enhanced resolution and maximum sensitivity. HOBS experiments have the restriction that full broadband homodecoupling can only be accomplished in regions containing non-mutually J coupled protons. As shown for cyclosporine, peptides are excellent targets for their success because NH, H_{α} and other aliphatic protons resonate in characteristic regions of the $^{1}\mathrm{H}$ spectrum and there is usually no J interference between them. Alternatives to obtain HOBS spectra for the complete $^{1}\mathrm{H}$ spectral range could be feasible by applying spatial-encoded techniques, as reported for broadband Zangger–Sterk (ZS) techniques [14–17], but this would be related to significant reductions in sensitivity.

In addition, we have focused on the success measurement of long-range heteronuclear coupling constants from the resulting in-phase doublet signals along the high-resolved direct dimension. Implementation of the HOBS and related techniques to other experiments is under development and the application to determine coupling constants from ultra simplified multiplets will be further evaluated.

4. Experimental

NMR experiments were performed on a Bruker Avance 600 spectrometer (Bruker Biospin, Rheinstetten, Germany) equipped with TXI HCN z-grad probes. The temperature for all measurements was set to 298 K. All spectra were recorded on a 25 mM sample of cyclosporine in C₆D₆ and processed with TOPSPIN 2.1 (Bruker Biospin, Rheinstetten, Germany).

The conventional 2D ¹H-¹³C region-selective HSQMBC spectrum of Fig. 2A was recorded using the pulse scheme of Fig. 1A with a normal detection period [10]. The recycle delay was 1 s,



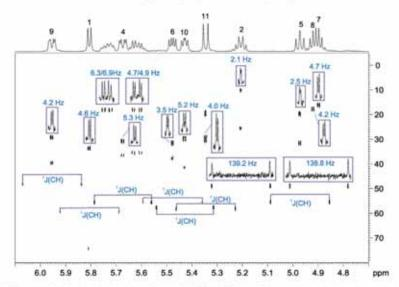


Fig. 5. In-phase HOBS-HSQMBC spectra of cyclosporine showing how the value of J(CH) for all direct and long-range cross-peaks can be extracted directly from the analysis of the clean doublet along the detected dimension (see the extracted value in each individual 1D inset). Note that only the AB spin system (protons resonating at 5.62 and 5.73 ppm) appears as a double of doublets due to their mutual J(HH).

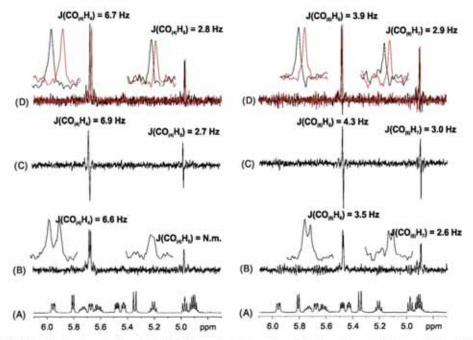


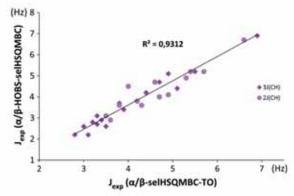
Fig. 6. α/β HOBS-HSQMBC spectra of cyclosporine after applied the IPAP techonology. The separate α and β sub-spectra generated after a combination IP \pm AP are overlayed in black/red colors to distinguish the relative shifts along the detected dimension. (8–D) are 1D slices extracted at two different CO(4) (169.5 ppm) and CO(6) (171.6 ppm) carbonyl frequencies corresponding to the (8) in-phase, (C) anti-phase and (D) α/β multiplets. (For interpretation of the references to color in this figure legend, the reader is referred to the web version of this article.)

the region-selective 180° ^{1}H pulse was a REBURP shape of 5 ms of duration (p_{180}), and the interpulse INEPT delays ($\kappa = A' + p_{180} = 1/(2 * ^{\circ})_{\text{CH}}$) were optimized for 8 Hz. 4 scans were accumulated for each one of the 128 t_1 increments, the spectral windows in F1 and F2 dimensions were 30,180 Hz and 1800 Hz,

respectively, the number of data points in t₂ was set to 4096 and the acquisition time (AQ) was 1.13 s. The total experimental time was of 20 min. The ratio between the G1:G2:G3:G4:G5:G6 gradients were 80:20.1:41:63:11:17, measured as percentage of the absolute gradient strength of 53.5 G/cm. Data were acquired and

67

Table 1
Proton-carbon coupling constant values (in Hz) in cyclosporine measured from the (A) in-phase HOBS-selHSQMBC, (B) IPAP HOBS-selHSQMBC, and (C) IPAP selHSQMBC-TOCSY
[33] experiments. Only the small two- and three-bond proton-carbon coupling constants marked in grey have been represented in the upper graph. The experimental error was of 40.4 Hz.



J(C-H _n)	IP HOBS-selHSQMBC (in Hz)	α/β HOBS-selHSQMBC (in Hz)	α/β selHSQMBC-TOCSY (in Hz
³JC2y~H2	2.1	2.6	3.0
JC7J1-H7	4.7	4.7	4.6
JC1n-H1a(olef)	6.3	6.9	6.9
JC1n-H1b(olef)	4.7	4.9	5.3
JC8ji-H8	4.2	4.5	4.0
JC11y-H11	2.0	2.2	2.8
JC5y-H5	2.5	3.1	3.3
JNMe-H9	4.2	4.4	5.1
JNMe-H10	5.2	5.2	5.5
INMe-H11	4.0	4.2	4.4
INMe-H4	5.3	5.1	4.9
INMe-H6	3.5	3.7	3.8
JC58-H5	4.1	4.1	4.9
INMe-H1	4.6	4.7	4.7
JC8H8	142.5	142.2	
JC9H9	139.3	139.2	139.5
JC2H2	139.2	139.1	138.9
JC7H7	138.8	138.1	+
JC5H5	139.6	139.6	2
IC4H4	135.8	135.6	135.9
JC11H11	140.4	140.4	140.3
JC10H10	135.5	135.6	135.8
јс6н6	141.1	141.0	133.0
JC1H1	139.9	139.8	140.1
ICO4-H4	6.8	6.7	6.6
1CO4-H5		2.8	3.2
CO1-H1	5.0	5.2	5.4
JC01-H2	3.1	3.4	3.9
CO9-H9	3,1	4.0	4.7
CO3-H4		3.1	3.5
CO10-H10	5.8	5.2	5.7
CO10-H11	2.3	2.2	3.1
JC06-H6	3.8	3.8	4.2
JC06-H7	2.5	2.9	3.4
JC07-H7	4.9	4.4	
	3.7	3.6	ov. 3.8
JC011-H11			3.8
JC011-H1	1.9	2.7	
JCO2-H2	3.7	3.6	4.3
JCO5-H5	2.6	2.9	3.6
JCO5-H6	2.1	2.6	3.5
COS-H8	3.1	3.1	3,5
JC08-H9	2.2	3.1	*

processed using the echo/anti-echo protocol. Sine bell shaped gradients of 1 ms duration were used, followed by a recovery delay of 20 μs. Prior to Fourier-transformation of each data, zero filling to 1024 in F1, 8192 points in F2 and a sine squared window function in both dimensions were applied. The analog 2D ¹H-¹³C HOBS-HSQMBC spectrum of Fig. 2B was recorded as described for

Fig. 2A using the detection period represented in Fig. 1A, with 20 loops (n), $\Delta = 28.25$ ms and with the same selective pulse applied in the INEPT period.

All four spectra of Fig. 3 were recorded using the pulse sequence of Fig. 1B using only 64 t_1 increments, 4096 data points in t_2 , a 2.5 ms REBURP pulse as a region-selected ^{13}C pulse applied at

the CO region (172 ppm) to excite the carbonyl carbons and reducing the spectral width in the indirect F1 dimension to 1800 Hz. 2 scans were collected for each t1 increment and the overall experimental time for each 2D spectrum was about 5 min. In (A) a conventional detection period was used, in (B) and (D) broadband heteronuclear decoupling was achieved using a 4 kHz GARP scheme applied on-resonance to the carbonyl region, in (C) and (D) 1H homodecoupling (HOBS) was achieved using the detection period represented in Fig. 1A with 20 loops (n) and $\Delta = 28.25$ ms and with an acquisition time of 1.13 s. The spectrum of Fig. 5 was recorded as Fig. 3C but using 128 t₁ increments (experimental time of 10 min). The IPAP 2D subspectra of Fig. 6 were generated from the corresponding IP and AP-HSQMBC experiments separately acquired in the same conditions as described for Fig. 5, and data were added/subtracted in the time-domain without any scaling factor to provide spin-state selective data.

Acknowledgments

Financial support for this research provided by MINECO (Project CTQ2012-32436) is gratefully acknowledged. We also thank to the Servei de Ressonància Magnètica Nuclear, Universitat Autònoma de Barcelona, for allocating instrument time to this project.

References

- A. Bast, M.F. Summers, J. Am. Chem, Soc. 108 (1986) 2093–2094.
 R.T. Williamson, B.L. Märquez, W.H. Gerwick, K.E. Kövér, Magn. Resnr. Chem. 38 (2000) 265–273.
- [3] R.C. Crouch, T.D. Spitzer, G.E. Martin, Magn. Reson. Chem. 30 (1992) 595–605.
 [4] C. Gaillet, C. Lequart, P. Debeire, J.M. Nuzillard, J. Magn. Reson. 139 (1999) 454–
- [5] S. Yang, J.K., Gard, G. Harrigan, B. Parnas, J. Likos, R. Crouch, Magn. Reson. Chem.
- 41 (2003) 42-48, [6] K. Krishnamurthy, J. Magn. Reson. 153 (2001) 144-150,

- [7] R. Crouch, R.D. Boyer, R. Johnson, K. Krishnamurthy, Magn. Reson. Chem. 42 (2004) 301-307,

- (2004) 301-307,
 T.D.W. Claridge, I. Pérez-Victoria, Org. Biomol. Chem. 1 (2003) 3632-3634,
 J. Furrer, Chem. Comm. 46 (2010) 3366-3398.
 Gil, J.F. Espinosa, T. Parella, J. Magn. Reson. 207 (2010) 312-321,
 J. Sauri, J.F. Espinosa, T. Parella, Org. Biomol. Chem. 11 (2013) 4473-4478,
- A.J. Pell, J. Keeler, J. Magn. Reson. 189 (2007) 293–299.
 B. Luy, J. Magn. Reson. 201 (2009) 18–24.
 K. Zangger, H. Sterk, J. Magn. Reson. 124 (1997) 486–489.

- N.H. Meyer, K. Zangger, Angew. Chem. Intl. Ed. 52 (2013) 7143-7146.
 M. Nilsson, G.A. Morris. Chem. Comm. 9 (2007) 933-935.
- [17] J.A. Aguilar, S. Faulkner, M. Nilsson, G.A. Morris, Angew. Chem. Intl. Ed. 49.
- [18] G.A. Morris, J.A. Aguilar, R. Evans, S. Haiber, M. Nilssun, J. Am, Chem. Soc. 132 (2010) 12770–12772.
 [19] J.A. Aguilar, A.A. Colbourne, J. Cassani, M. Nilsson, G.A. Morris, Angew. Chem.

- Intl. Ed. 51 (2012) 6460–6463.
 [20] A. Lupulescu, G.L. Olson, L. Frydman, J. Magn. Reson. 218 (2012) 141–146.
 [21] J.A. Aguilar, M. Nilsson, G.A. Morris, Angew. Chem. Intl. Ed. 50 (2011) 9715–
- [23] L. Castañar, P. Nolis, A. Virgili, T. Parella, Chem. Eur. J. (2013) in press. http:// dicdoi.org/10.1002/chem.201303235,

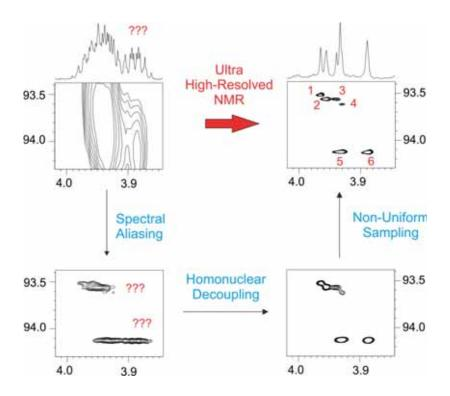
- dx.doi.org/10.1002/cbern.201303235,
 [24] T. Parella, J.F. Espinosa, Prog. Nucl. Magn. Reson. Spectrosc. 73 (2013) 17-55,
 [25] B. Yu, H. van Ingen, S. Vivekanandan, C. Rademacher, S.E. Norris, D.I. Freedberg, J. Magn. Reson. 215 (2012) 10-22.
 [26] B. Yu, H. van Ingen, D.I. Freedberg, J. Magn. Reson. 228 (2013) 159-165,
 [27] J. Farjon, W. Bermel, C. Griesinger, J. Magn. Reson. 180 (2006) 72-82.
 [28] V.M. Marathias, J. Goljer, A.C. Bach H. Magn. Reson. (hem. 43 (2005) 512-519,
 [29] C.M. Thiele, W. Bermel, J. Magn. Reson. 216 (2012) 134-143.
 [30] L. Paudel, R.W. Adams, P. Kiraly, J.A. Aguilar, M. Foroozandeh, M.J. Cliff, M. Nilsson, P. Sandor, J.P. Waltho, G.A. Morris, Angew. Chem. Int. Ed. 52 (2013) 11616-11619. 11616-11619.
- [31] L. Kaltschnee, A. Kolmer, I. Timári, R.W. Adams, M. Nilsson, K.E. Kövér, G.A. Morris, C.M. Thiele, Pure Shift HSQC Measurements with Perfect BIRD Decoupling – A Method to Decouple Disstereotopic Protons, Poster No. 391 Presented at 9th European Magnetic Resonance Conference EUROMAR. 2013.

 [32] I. Timári, L. Kaltschnee, A. Kolmer, R.W. Adams, M. Nilsson, C.M. Thiele, G.A. Morris, K.E. Kövér, J. Magn. Reson., in press. http://dx.doi.org/10.1016/
- [33] J. Sauri, J.F. Espinosa, T. Parella, Angew. Chem. Intl. Ed. 51 (2012) 3919-3922.

PUBLICATION 7

Disentangling complex mixture of compounds with near-identical ¹H and ¹³C NMR spectra using pure shift NMR spectroscopy

Laura Castañar, Raquel Roldán, Pere Clapés, Albert Virgili and Teodor Parella. *Chem. Eur. J.,* **2015**, *21*, 7682-7685.



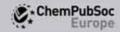
Introduction

As illustrated in **Publication 5**, the incorporation of broadband ¹H homodecoupling in the acquisition F2 dimension is fully compatible with other resolution-enhanced NMR techniques, such as spectral aliasing along the indirect F1 dimension, ⁹³ opening the door to the design of ultra-high-resolved 2D NMR experiments in reasonable acquisition times. As it was previously shown, a common feature of spectral aliasing is its general and very easy implementation, improving the attainable resolution along the F1 dimension up to two orders of magnitude by a simple change of the ¹³C spectral width in HSQC experiments.

In the last years, *Non-Uniform Sampling* (NUS)⁶⁸ has emerged as a very powerful tool to significantly speed up the acquisition of multidimensional NMR experiments due to the fact that only a subset of the usual linearly sampled data in the Nyquist grid is measured. For small molecules, NUS can facilitate significant reductions (~50%) in the time needed to collect 2D HSQC spectra, or otherwise offering gains in spectral resolution along the indirect 13 C dimension by recording less number of t_1 increments. Some of these algorithms are already implemented in modern NMR software packages, and NMR users can use them in a fully transparent and automatic way without any further modification of the standard pulse programs or general setup parameters. The quality of the resulting spectra depends crucially on the sampling schedules and the algorithms for data reconstruction. However, precaution should be taken for the presence of unwanted artifacts that can generate distorted or false cross-peaks.

In the present article, these two enhanced resolution approach (NUS and spectral aliasing) in combination with HOBS methodology (Publication 2) is reported for the development and application of ultra-high-resolved HSQC experiments to analyze highly complex mixtures of similar isomers exhibiting near-identical ^1H and ^{13}C NMR spectra. The whole ensemble of enhancements applied enables the in-situ distinction and assignment of similar organic compounds exhibiting near-identical ^1H and ^{13}C chemical shift and J coupling patterns in the same mixture. Very small $\Delta\delta(^1\text{H})$ and $\Delta\delta(^{13}\text{C})$ have been distinguished and precisely determined, even in the presence of highly overlapped signals or severe chemical shift degeneracy in conventional 1D ^1H and $^{13}\text{C}\{^1\text{H}\}$ NMR spectra. Whereas $\Delta\delta(^1\text{H})$ and $\Delta\delta(^{13}\text{C})$ up to 3 and 17 ppb, respectively, can be established from the singlets obtained in 1D HOBS and ^{13}C NMR spectra, the high signal dispersion achieved in spectral-aliased 2D HOBS-HSQC spectra allows an improved detection level to 1 and 5 ppb, respectively. This strategy combined with the use of HOBS versions into the HSQC-TOCSY and HSQMBC experiments has enabled the unambiguous assignment of ^1H and ^{13}C

chemical shifts for all peaks of different components of a complex mixture of isomers. The proposed strategy will prove to be very useful to facilitate the analysis of highly complex spectra, as found in many daily situations that exhibit high degeneracy of chemical shifts or severe signal overlap, such as the analysis of crude reactions, detection and characterization of intermediates, or reaction monitoring.



DOI: 10.1002/chem.201500521



■ NMR Spectroscopy

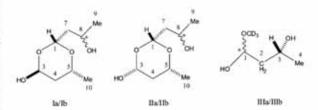
Disentangling Complex Mixtures of Compounds with Near-Identical ¹H and ¹³C NMR Spectra using Pure Shift NMR Spectroscopy

Laura Castañar, [a] Raguel Roldán, [b] Pere Clapés, [b] Albert Virgili, [a] and Teodor Parella*[a]

Abstract: The thorough analysis of highly complex NMR spectra using pure shift NMR experiments is described. The enhanced spectral resolution obtained from modern 2D HOBS experiments incorporating spectral aliasing in the ^{13}C indirect dimension enables the distinction of similar compounds exhibiting near-identical ^{1}H and ^{13}C NMR spectra. It is shown that a complete set of extremely small $\Delta\delta(^{1}\text{H})$ and $\Delta\delta(^{13}\text{C})$ values, even below the natural line width (1 and 5 ppb, respectively), can be simultaneously determined and assigned.

NMR spectroscopy is the most powerful analytical tool to characterize the structure and dynamics of organic molecules in solution. A high spectral resolution is mandatory for identifying individual resonances and to perform accurate measurements of chemical shifts or coupling constants. In past decades, NMR has demonstrated its tremendous capacity to analyze complex mixtures of compounds, where a large number of overlapping signals can be present. However, direct NMR analysis is often limited by the lack of appropriate signal dispersion due to small chemical-shift differences ($\Delta\delta$), the wide $J_{\rm HH}$ coupling patterns that expand the overall multiplet over a range of frequencies, and the natural linewidth $(\Delta v_{1/2})$ of each individual NMR signal. A successful characterization can be further complicated when trying to differentiate structural compounds exhibiting extremely small $\Delta\delta$ values and similar J-coupling patterns between analogous protons, due to the superposition of near-identical NMR spectra. This can be particularly difficult in H NMR spectroscopy, because protons resonate in a relatively narrow range of frequencies (for instance, around 6000 Hz in a 600 MHz spectrometer) whereas each individual multiplet pattern can have a width of some tens of Hz. In contrast, the signal dispersion achieved in standard broadband heteronuclear decoupled ¹³C NMR spectra is an illustrative example demonstrating how a simple and rapid spectral analysis can be performed when simplified singlet signals are available.

It is known that different molecules have different physical properties and therefore they show different NMR spectra. However, under some conditions, NMR spectra of two different molecules can become nearly identical with a high degree of apparent chemical shift degeneracy, even including the possibility that they are indistinguishable.[1] Several approaches have been reported for discerning compounds with very similar NMR spectra.[2,3] In this work we present a simple but very useful experimental NMR strategy that greatly facilitates the analysis of highly congested spectral regions. We will show here how a mixture of compounds with near-identical ¹H and ¹³C NMR spectra can be distinguished using high-resolution NMR methods based on the combination of pure shift NMR^[4-10] and spectral aliasing techniques.^[11-16] The power of the proposed method is illustrated with the analysis of a challenging real sample from our lab, consisting of a mixture of several unknown compounds that were finally determined as three pairs of diastereoisomeric derivatives. These compounds were the result of a nonselective homoaldol addition of acetaldehyde, followed by the ketalization of the aldehyde group of the homoaldol adduct by its hydrate form (Scheme 1 and Scheme S1 in the Supporting Information).[17]



Scheme 1. Structures and numbering of the three pairs of diastereoisomer compounds present in the mixture.

08193 Bellaterra, Barcelona (Spain) E-mail: teodor.parella@uab.cat [b] R. Roldán, Dr. P. Clapés Biotransformation and Bioactive Molecules Group Instituto de Química Avanzada de Cataluña, IQAC-CSIC

Jordi Girona 18-26, 08034 Barcelona (Spain)

[a] L. Castañar, Prof. A. Virgili, Dr. T. Parella
 Servei de RMN and Departament de Química

Universitat Autónoma de Barcelona

Supporting information for this article is available on the WWW under http://dx.doi.org/10.1002/chem.201500521. the homonuclear decoupling band-selective (HOBS) technique [18-21] in order to obtain fully homodecoupled signals for a set of nonmutually *J*-coupled protons resonating in a selected region of the ¹H spectrum. The choice of the HOBS over other existing pure shift techniques has been done for various reasons: i) with the aim to maximize sensitivity and to save spectrometer time; ii) the basic set-up is reduced to a simple cali-

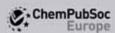
We use a suite of modern pure shift NMR methods based on

Chem. Eur. J. 2015, 21, 7682 - 7685

Wiley Online Library

7682

© 2015 Wiley-VCH Verlag GmbH & Co. KGaA, Weinheim



bration of a selective 180° ¹H pulse according to a selected ¹H NMR region; iii) HOBS allows a facile implementation into 2D experiments, as shown for a family of HOBS versions of standard 2D HSQC, ^[18] HSQC-TOCSY, and HSQMBC, ^[22] experiments for unambiguous assignment purposes. Additionally, it is shown here that using a reduced ¹³C spectral width of a few ppm, optionally combined with nonuniform sampling (NUS), can produce high-resolution 2D HOBS spectra in conventional acquisition times (Figure 1).

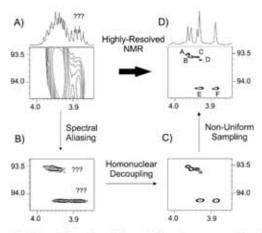


Figure 1, Schematic illustration of the resolution enhancements achieved after combining B) spectral aliasing in the indirect dimension, C) broadband homodecoupling in the detected dimension and D) nonuniform sampling into a single high-resolution HSQC experiment.

At first glance, the conventional analysis of the 1H (Figure 2A) and routine homo- and heteronuclear 2D spectra of the mixture does not provide any evidence of their high complexity, mainly due to the lack of sufficient digital and signal resolution. The presence of multiple components was confirmed from the standard 1D 13 C(1H) spectrum, by virtue of its pure chemical shift nature, where all decoupled signals yield highly disperse singlet lines that usually avoid accidental signal overlap. In our sample, most of the 13 C signals appear split in a range of $\Delta\delta(^{13}\text{C}) = 15$ to 350 ppb (Figure S1 in the Supporting Information), although some peaks did not show observable splitting ($\Delta\delta(^{13}\text{C}) < 15$ ppb) or, in other cases, the presence of multiple peaks in a narrow range of frequencies limited the possibility to differentiate pairs of signals and therefore to determine $\Delta\delta(^{13}\text{C})$.

Four set of signals could be clearly classified and assigned after examination of 1 H, 13 C, and HSQC datasets: A) CH signals resonating at δ 4.65–5.38 (carbons between δ 91–97); B) CH signals resonating at δ 3.75-4.16 (carbons between δ 65–73); C) a large number of highly overlapping diastereotopic CH₂ signals resonating at δ 1.56-1.80 with an additional proton at δ 1.26 (carbons between δ 39–47); D) a large number of CH₃ signals resonating at δ 1.14–1.22 ppm (carbons at δ 21–24). The existence of different CH–CH₂–CH–CH₃ subunits was confirmed by the COSY experiment (data not shown).

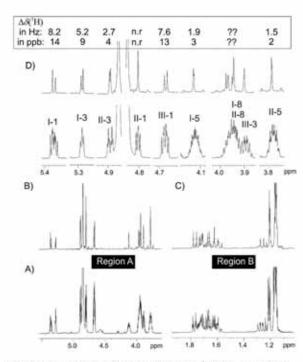


Figure 2. 600 MHz A) conventional and B–C) HOBS ¹H NMR spectra of the mixture; D) expanded ¹H multiplets of region A showing their Δδ(¹H).

To get more insight into the analysis of the 1H spectrum, we collected two separate 1D HOBS spectra with full sensitivity in region A around & 3.5-5.5 (Figure 2B) and region B at & 1.0-1.8 (Figure 2C), respectively, using a 2.5 ms REBURP 1801 H pulse. As a first goal, a quick view of the HOBS spectrum of region A (see Figure 2B and its expanded image in Figure 2D), acquired in just half a minute, shows an excellent simplification of all 1H multiplets to homodecoupled singlet signals with $\Delta v_{1/2}$ about 1.5 Hz (Figure S10 in the Supporting Information). Most of the 'H signals appear doubled and the fast distinction of extremely small Δδ(1H) values, ranging between 2 and 14 ppb, confirmed the presence of very similar species and the strong requirement for a third decimal place in the description of 'H and ¹³C NMR data of very similar compounds.^[2] It can be observed that some signals are not differentiated (see, for instance, II-1 in Figure 2D) and, in other cases, the presence of multiple and complex overlapping resonances (six different signals appear at & 3.86-3.99) prevents the identification of pairs of diastereoisomeric resonances and therefore the determination and assignment of ô('H).

The next step was to perform a complete ¹H/¹³C chemical shift assignment by a spectral-aliased HOBS-HSQC experiment incorporating NUS (a compromise of 50% of sample points was used; see Figure 3). Data were recorded in about 14 min with a reduced spectral width of 5 ppm (754 Hz at 600 MHz) in the ¹³C dimension. The expanded areas comparing standard versus pure shift 2D aliased multiplets exemplifies the significant enhanced signal dispersion achieved in broadband homodecoupled single-component cross-peaks, allowing the differ-

Chem. Eur. J. 2015, 21, 7682 - 7685

www.chemeurj.org

7683

© 2015 Wiley-VCH Verlag GmbH & Co. KGaA, Weinheim



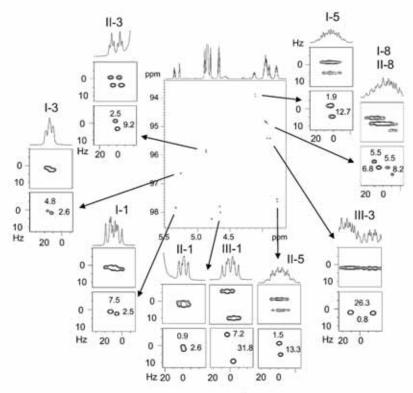


Figure 3. 2D HOBS-HSQC spectrum of region A acquired with SW(13 C) = 5 ppm. Expanded 2D cross-peaks corresponding to the (top) spectral-aliased HSQC and (bottom) spectral-aliased HOBS-HSQC spectra are shown for comparison. Experimental $\Delta\delta$ (14 C) are expressed in Hz.

entiation of signals that were not resolved in conventional 1D 1H, 1D HOBS and 13C spectra. It is very important to note that, in addition to the unambiguous chemical shift assignment for all resonances, determinations of $\Delta\delta(^{1}H)$ and $\Delta\delta(^{13}C)$ to minimum levels of 1 and 5 ppb, respectively, could be done. For instance, protons Ila-1 and Ilb-1 which cannot be distinguished in standard and 1D HOBS 1H spectra, are separated by 0.9 Hz (1 ppb) in the HOBS-HSQC spectrum by the small but sufficient signal dispersion of their directly attached carbon (2.7 Hz or 18 ppb). Moreover, all $\delta(^{1}H)$ and $\delta(^{13}C)$ for the six overlapped I-8, II-8, and III-3 protons could be clearly distinguished and assigned. Finally, as a good example showing the power to analyze high-resolution 2D cross-peaks over conventional 1D 13C data, Δδ(13C) of III-3 was determined to be 5 ppb (0.8 Hz) thanks to its highly dispersed directly attached protons (26.3 Hz or 44 ppb). The excellent signal dispersion achieved between equivalent cross-peaks can allow their quantitative measurements by 2D volume integration. If needed, higher levels of resolution could be achieved using a more drastic reduction of SW(13C) up to 1-2 ppm (Figure S2 in the Supporting Information, SW = spectral width).

As a result of introducing spectral aliasing in HSQC experiments, 13 C chemical shift information is initially lost. Each cross-peak will show an experimental chemical shift value (δ_{ob}) that is exactly a multiple of SW(13 C) from its real position (δ_i)

and it can be determined from relationship $\delta_r = \delta_{obs} \pm$ (K*SW(13C)), where K is the aliasing factor. The true 13C chemical shift values can be deciphered by comparing data from a previously acquired reference 1D 13C or HSQC spectra, or from some reconstruction method. For instance, Figure S3 (in the Supporting Information) shows how K can be easily determined by comparing two different HSQC datasets recorded with F1 spectral widths of 5 and 4.9 ppm.[12]

After the unequivocal assignment of each C/H pair, a complete correlation between all 'H and 13C signals was necessary. Spectral aliasing has been previously reported for traditional HSQC, HSQC-TOCSY, and HMBC experiments,[15] but pure shift experiments retaining the maximum sensitivity are only available for some versions of the HSQC^[18, 19] and HSQMBC^[22] experiments. As another novelty of this work, a HOBS-HSQC-TOCSY experiment is proposed here to assign protons and carbons belonging to the same spin

system, in this case, to correlate each one of the two different I-3 signals with the two different I-5 protons. Thus, to completely assign all spin systems, spectral-aliased HSQC-TOCSY (Figure 4A), HOBS-HSQC-TOCSY (Figure 4B and S4), and HOBS-HSQMBC (Figure 55 in the Supporting Information) experiments were collected with the same spectral resolution conditions as described for the analogous HOBS-HSQC experiment. The HOBS-HSQMBC spectrum was decisive to determine the long-range correlations through the oxygen atoms between protons 1 and 3/5 in diastereoisomers I and II.

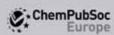
A special mention is required for the analysis of the 20 different resonances of the diastereotopic CH₂ protons appearing in region B at δ 1.6–1.8 region (Figure 2 A, C). The full simplification of this region was more complicated, because these signals cannot be converted to singlets with the HOBS technique, with the remaining active $^2J_{\rm HH}$ observable because the pairs of methylene protons all lie within the same spectral region and hence are not affected by the selective 180° pulse that causes decoupling. Attempts to apply other pure shift methods including BIRD-based HSQC,^[10] or the recently proposed PSYCHE experiment,^[4] also failed (Figure S11 in the Supporting Information). However, the spectral-aliased HSQC-TOCSY experiment (Figure 4 A and S12 in the Supporting Information) was the most useful tool to determine the CH₂ assignments. A complete list of δ (1H), δ (13C), Δ δ (1H), and Δ δ (13C) for all compo-

Chem. Eur. J. 2015, 21, 7682 - 7685

www.chemeurj.org

7684

© 2015 Wiley-VCH Verlag GmbH & Co. KGaA, Weinheim





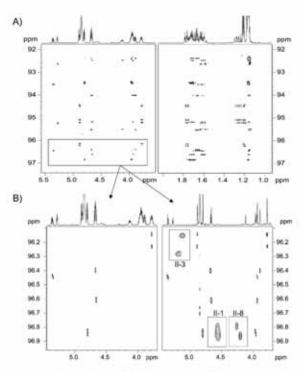


Figure 4. A) Spectral-aliased HSQC-TOCSY spectrum of the mixture acquired with SW("IC) = 5 ppm; B) Expansions to compare the spectral-aliased HOBS-HSQC vs. HOBS-HSQC-TOCSY spectra on region A. In addition to proper assignments, note that relayed cross-peaks can visualize splitting that is not observed with direct correlations.

nents of the mixture are available in Tables S1–S3 in the Supporting Information. Unfortunately, the free rotation of the acyclic subunit makes it virtually impossible to determine the relative configuration of the C8 center in I-II and C1 in III and, therefore, the challenge to completely characterize each individual diastereoisomer remains with us.

In summary, it has been shown that the full sensitivity and the excellent spectral resolution obtained from spectral-aliased 2D HOBS spectra makes it possible to enable the in situ distinction and assignment of similar organic compounds exhibiting near-identical ¹H and ¹³C NMR spectra in the same mixture. Very small $\Delta\delta(^{1}H)$ and $\Delta\delta(^{13}C)$ values can be distinguished and precisely determined, even in the presence of highly overlapping signals or severe chemical shift degeneracy, in conventional 1D ^{1}H and ^{13}C NMR spectra. Whereas $\Delta\delta(^{1}\text{H})$ and $\Delta\delta(^{13}\text{C})$ up to 3 and 17 ppb, respectively, can be established in 1D HOBS and 13C NMR spectra, the excellent signal dispersion achieved in 2D experiments improves the level of detection to 1 and 5 ppb, respectively, as well as to unambiguously assign all peaks for the different components of a mixture. The proposed strategy could be very useful to facilitate the analysis of highly complex spectra, as found in many situations where significant degeneracy of chemical shifts or severe signal overlap is present. There is also potential to use the method with other applications, such as the analysis of crude reactions and detection of intermediates, reaction monitoring, or the analysis of complex mixtures.

Acknowledgements

Financial support for this research, provided by MINECO (projects CTQ2012-32436 and CTQ2012-31605), is gratefully acknowledged. We also thank the Servei de Ressonància Magnètica Nuclear, Universitat Autònoma de Barcelona, for allocating instrument time to this project.

Keywords: homodecoupling • mixture analysis • NMR spectroscopy • pure shift NMR • spectral aliasing

- [1] G. Saielli, A. Bagno, Org. Lett. 2009, 11, 1409-1412.
- [2] J. G. Napolitano, D. C. Lankin, T. N. Graf, J. Brent Friesen, S. N. Chen, J. B. McAlpine, N. H. Oberlies, G. F. Pauli, J. Org. Chem. 2013, 78, 2827 –2839.
- [3] N. Basar, K. Damodaran, H. Liu, G. A. Morris, H. M. Sirat, E. J. Thomas, D. P. Curran, J. Org. Chem. 2014, 79, 7477 – 7490.
- [4] M. Foroozandeh, R. W. Adams, N. J. Meharry, D. Jeannerat, M. Nilsson, G. A. Morris, Angew. Chem. Int. Ed. 2014, 53, 6990–6992; Angew. Chem. 2014, 126, 7110–7112.
- [5] M. Foroozandeh, R. W. Adams, M. Nilsson, G. A. Morris, J. Am. Chem. Soc. 2014, 136, 11867 – 11869.
- [6] J. A. Aguilar, S. Faulkner, M. Nilsson, G. A. Morris, Angew. Chem. Int. Ed. 2010, 49, 3901 – 3903; Angew. Chem. 2010, 122, 3993 – 3995.
- [7] N. H. Meyer, K. Zangger, ChemPhysChem 2014, 15, 49-55.
- [8] K. Zangger, H. Sterk, J. Magn. Reson. 1997, 124, 486-489.
- [9] N. H. Meyer, K. Zangger, Angew. Chem. Int. Ed. 2013, 52, 7143-7146; Angew. Chem. 2013, 125, 7283-7286.
- [10] L. Paudel, R. W. Adams, P. Király, J. A. Aguilar, M. Foroozandeh, M. J. Cliff, M. Nilsson, P. Sándor, J. P. Waltho, G. A. Morris, Angew. Chem. Int. Ed. 2013, 52, 11616–11619; Angew. Chem. 2013, 125, 11830–11833.
- [11] D. Jeannerat, Magn. Reson. Chem. 2003, 41, 3-17.
- [12] I. Baskyr, T. Brand, M. Findeisen, S. Berger, Angew. Chem. Int. Ed. 2006, 45, 7821–7824; Angew. Chem. 2006, 118, 7985–7988.
- [13] D. Jeannerat, J. Magn. Reson. 2007, 186, 112-122.
- [14] G. B. B. Njock, D. E. Pegnyem, T. A. Bartholomeusz, P. Christen, B. Vitorge, J.-M. Nuzillard, R. Shivapurkar, M. Foroozandeh, D. Jeannerat, Chim. Int. J. Chem. 2010, 64, 235–240.
- [15] A. Cotte, M. Foroozandeh, D. Jeannerat, Chim. Int. J. Chem. 2012, 66, 764-769.
- [16] M. Pérez-Trujillo, L. Castañar, E. Monteagudo, L. T. Kuhn, P. Nolis, A. Virgili, R. T. Williamson, T. Parella, Chem. Commun. 2014, 50, 10214–10217.
- [17] M. Vogel, D. Rhum, J. Org. Chem. 1966, 31, 1775-1780.
- [18] L. Castanar, P. Nolis, A. Virgili, T. Parella, Chem. Eur. J. 2013, 19, 17283–17286.
- [19] J. Ying, J. Roche, A. Bax, J. Magn. Reson. 2014, 241, 97-102.
- [20] R. W. Adams, L. Byrne, P. Király, M. Foroozandeh, L. Paudel, M. Nilsson, J. Clayden, G. A. Morris, Chem. Commun. 2014, 50, 2512–2514.
- [21] L. Castañar, M. Pérez-Trujillo, P. Nolis, E. Monteagudo, A. Virgili, T. Parella, ChemPhysChem 2014, 15, 854–857.
- [22] L. Castañar, J. Saurí, P. Nolis, A. Virgili, T. Parella, J. Magn. Reson. 2014, 238, 63-69.

Received: February 8, 2015 Published online on March 27, 2015

7685

www.chemeurj.org



Supporting Information

Disentangling Complex Mixtures of Compounds with Near-Identical ¹H and ¹³C NMR Spectra using Pure Shift NMR Spectroscopy

Laura Castañar, [a] Raquel Roldán, [b] Pere Clapés, [b] Albert Virgili, [a] and Teodor Parella*[a]

chem_201500521_sm_miscellaneous_information.pdf

Table of Contents

- Experimental Section.
- Scheme S1. Formation of Ia/Ib, IIa/IIb and IIIa/IIIb compunds from acetaldehyde.
- Table S1: NMR data of diastereoisomers Ia/Ib.
- Table S2: NMR data of diastereoisomers IIa/IIb.
- Table S3: NMR data of diastereoisomers IIIa/IIIb.
- Figure S1: 1D ¹³C NMR spectrum of the analyzed sample.
- Figure S2: 2D spectral aliased HOBS-HSQC spectrum acquired with SW(¹³C)=1ppm.
- Figure S3: Experimental determination of aliasing factor K.
- Figure S4: Spectral-aliased HOBS-HSQC vs HOBS-HSQC-TOCSY spectra.
- Figure S5: Spectral-aliased HOBS- HSQMBC spectrum.
- Figure S6: NMR pulse sequence diagrams used in this work.
- Figure S7: Selective 1D NOESY spectra after selective excitation on selected protons of isomers Ia/Ib.
- Figure S8: Selective 1D NOESY spectra after selective excitation on selected protons of isomers IIa/IIb.
- Figure S9: Comparison between PSYCHE and HOBS experiments.
- Figure S10: Expanded area between 3.7-5.5 ppm comparing the experimental sensitivity and natural line widths achieved in B) PSYCHE and C) HOBS spectra.
- Figure S11: Expanded area between 1.1-1.8 ppm (diastereotopic CH2 and CH3 spin systems) comparing the experimental sensitivity, multiplet simplification and line widths achieved in B) PSYCHE and C) HOBS spectra.
- Figure S12: Expansion of the spectral aliased HSQC-TOCSY of Figure 4A.
- Figure S13: (top) Conventional and (bottom) broadband homodecoupled HSQC A) III-3 and B) II-3 cross peaks.
- Figure S14: (top) Conventional and (bottom) broadband homodecoupled HSQC A) II-4 (diastereotopic CH₂) and B) I-10 (CH₃) cross peaks.

Experimental Section

Compounds were obtained by stirring an aqueous solution acetaldehyde (20 mL, 5 % v/v) in aqueous buffer trietanolamine (50 mM, pH 8.0) during 48 hours. Then the pH was adjusted to pH 5.6, the aqueous solvent was evaporated under vacuum and then purified by column chromatography on silica. The formation of the compunds Ia/Ib and IIa/IIb (Scheme S1) consists first in the dimerization of acetaldehyde to produce S1 via aldol addition with an ensuing formation of a ketal between the aldehyde group of S1 and the hydrate form of the dimer S2.

Scheme S1. Formation of Ia/Ib, IIa/IIb and IIIa/IIIb compunds from acetaldehyde.

The conformation and relative configurations of isomers Ia/Ib and IIa/IIb (see 3D views in tables S1-S2) have been determined using several NMR evidences:

• Key 1,3-diaxial NOEs were observed between H1 and H5 in derivatives Ia/Ib and between H1 and both H3/H5 in compounds IIa/IIb (see Figures S7 and S8)

- The effect of the hydroxyl group on the C3 position in isomers I and II is clearly observed in $\delta(H5)$ and $\delta(H1)$ values.
- The different axial/equatorial position of the H3 proton is evidenced from their δ values.
- Due to the high level of multiplet overlapping of protons H3 and H5, the accurate measurement of the corresponding J(H3-H4) and J(H5-H4) was not an easy task. However, it is evident from the 1H spectrum large J(H3-H4ax) values for isomers IIa/IIb (H3 is a double-doublet with 2.5 and 9.7 Hz) and small for isomers Ia/Ib (H3 is a double-doublet with 1.3 and 3.5 Hz) which were confirmed by a J-resolved experiments.

All experiments were acquired on a Bruker AVANCE spectrometer (Bruker BioSpin, Rheinstetten, Germany) operating at 600.13 MHz proton frequency, equipped with a 5 mm triple resonance inverse probe and a z-axis pulsed field gradient accessory (maximum strength of 53.5 G/cm). The spectra were collected on sample containing a mixture of unknown compounds dissolved in CD_3OD at a temperature T = 298 K, and processed with the software TOPSPIN 3.1.

The non-selective 1 H 180 pulses were of 8.6 μ s duration. For all 1D and 2D HOBS experiments, a 180° band-selective REBURP shaped pulse of 2.5 ms was used for both excitation and homodecoupling. The strengths of the G1, G2 and G3 gradients were set to 12.3, 21.9 and 33.7 G/cm, respectively, with durations of 500 μ s followed by a recovery delay of 20 μ s.

1D HOBS spectra of Fig. 2B and 2C were recorded using the pulse sequence displayed in Fig. S7A, with four scans and 1 s of recycle delay. The spectral width was 7200 Hz, and 16K complex points were recorded during an acquisition time of 1.13 s. 40 loops (n) were concatenated with τ =AQ/2n=7.2ms. The 1D time-domain data were directly transformed without any sensitivity or resolution enhancement.

The 2D ^{1}H - ^{13}C HOBS-HSQC spectrum (Fig. 4A) was acquired using the pulse sequence displayed in Fig. S6B, optimized to 140 Hz (Δ =1/(2*J_{CH})). Two scans of 2048 complex points were collected over an observed ^{1}H spectral width of 3600 Hz for each of the 256 t₁

values. The acquisition time was of 0.284 ms. Data of Fig. 3 were acquired with SW(13 C)=5ppm (754 Hz) and transformed with a shifted sine window function along both the F1 and F2 dimensions and with a zero-filling to 8K in F2 and 1K in F1. Final resolution was 0.44 and 0.73 Hz/Pt in the F2 and F1 dimensions, respectively. The initial 90° band-selective pulses wasa EBURP-2 shaped pulse of 1.75 ms. For homonuclear decoupling, 130 loops (n) were concatenated with τ =AQ/2n=9 ms. NUS was applied with a sampling density of 50%. The total experimental time was about 13 minutes.

The 2D ¹H-¹³C HOBS-HSQC-TOCSY spectrum was acquired using the pulse sequence displayed in Fig. S6C with a mixing time of 60ms. The number of scans was 8 per t₁ increment and all other acquisition and processing parameters as described for the HSQC experiment. The 2D ¹H-¹³C HOBS-selHQMBC spectrum was acquired using the pulse sequence displayed in Fig. S6D, with 32 scans per t₁ increment and optimized to 1/(2*J_{CH})=8 Hz. All other parameters as described for the HSQC experiment. Standard HSQC, HSQC-TOCSY and selHSQMBC experiments were recorded with the same pulse schemes of Fig. S6 and the same conditions, but including a standard FID period as acquisition.

Table S1: ^{1}H and ^{13}C chemical shift values and $\Delta\delta(^{1}H)$ and $\Delta\delta(^{13}C)$ of the two distinguished diastereoisomers Ia/Ib.

	la		I	b	1D HOBS ^a	1D ¹³ C ^a	HOBS	S-HSQC ^c
	¹ H	¹³ C	¹ H	¹³ C	$\Delta\Delta\delta(^{1}H)$	$\Delta\Delta\delta$ (13 C)	$\Delta\Delta\delta(^{1}H)$	$\Delta\Delta\delta(^{13}C)$
1	5.365	92.802	5.351	92.820	0.014 (8.2)	0.019 (2.2)	0.012 (7.5)	0.016 (2.4)
3	5.278	91.629	5.287	91.611	0.009 (5.2)	0.018 (2.7)	0.008 (4.8)	0.018 (2.7)
4	1.629- 1.582	39.024	1.629- 1.583	38.981	n.d	0.039 (5.9)	n.d	0.043 (6.5)
5	4.126	68.851	4.123	68.937	0.003 (1.9)	0.086 (12.7)	0.003 (1.9)	0.084 (12.7)
7	1.665- 1.638	44.919	1.703- 1.617	44.919	n.d	n.d	n.d	n.d
8	3.944	64.825	3.938	64.879	n.d	n.d	0.009 (5.5)	0.054 (8.1)
9	1.166	23.692	1.166	23.692	n.d	n.d	n.d	n.d
10	1.156	21.862	1.159	21.862	n.d	n.d	n.d	n.d

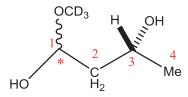
- a) Resolution in HOBS and ¹³C after processing were 0.11 and 0.38 Hz/pt, respectively.
 b) Resolution in the F2 and F1 dimension of the 2D HOBS-HSQC was 0.43 and 0.73 Hz/pt, respectively, after processing.
- c) n.d=not determined; by signal overlap or lack of resolution

Table S2: ^{1}H and ^{13}C chemical shifts (in ppm) and $\Delta\delta(^{1}H)$ and $\Delta\delta(^{13}C)$ (in ppm and Hz) of the two distinguished diastereosiomers IIa/IIb.

	lla		I	Ib	1D HOBS ^a	1D ¹³ C ^a	HOBS-	-HSQC ^c
	¹ H	¹³ C	¹ H	$\Delta\Delta\delta$ (13 C)	$\Delta\Delta\delta(^{1}H)$	$\Delta\Delta\delta$ (13 C)	$\Delta\Delta\delta(^{1}H)$	$\Delta\Delta\delta(^{13}C)$
1	4.805	98.194	4.804	98.215	<0.002 (<2)	0.021 (2.6)	0.001 (0.9)	0.018 (2.7)
3	4.892	95.810	4.888	95.874	0.004 (2.7)	0.062 (9.1)	0.004 (2.5)	0.061 (9.3)
4	1.774- 1.267	41.466	1.774- 1.267	41.466	n.d	n.d	n.d	n.d
5	3.781	72.616	3.783	72.528	0.002 (1.5)	0.092 (13.2)	0.002 (1.6)	0.088 (13.3)
7	1,745- 1.710	44.876	1.736- 1.717	44.829	n.d	n.d	n.d	0.045 (6.8)
8	3.970	64.780	3.961	64.825	n.d	n.d	0.009 (5.4)	0.048 (7.2)
9	1.173	23.776	1.172	23.742	n.d	n.d	n.d	0.038 (5.7)
10	1.209	21.586	1.214	21.572	n.d	0.017(2.7)	0.009 (5.4)	0.014 (2.3)

- a) Resolution in HOBS and ¹³C after processing were 0.11 and 0.38 Hz/pt, respectively.
 b) Resolution in the F2 and F1 dimension of the 2D HOBS-HSQC was 0.43 and 0.73 Hz/pt, respectively, after processing.
- c) n.d=not determined; by signal overlap or lack of resolution

Table S3: ^{1}H and ^{13}C chemical shift values and $\Delta\delta(^{1}H)$ and $\Delta\delta(^{13}C)$ of the two distinguished diastereosiomers IIIa/IIIb.



	IIIa		II	Ib	1D HOBS ^a	1D ¹³ C ^a	HOBS	-HSQC ^c
	¹ H	¹³ C	¹ H	¹³ C	$\Delta\Delta\delta(^{1}H)$	$\Delta\Delta\delta$ (13 C)	$\Delta\Delta\delta(^{1}H)$	$\Delta\Delta\delta$ (13 C)
1	4.680	97.759	4.667	97.974	0.013 (7.59)	0.216 (31.6)	0.012 (7.16)	0.210 (31.75)
2	1.679- 1.663	46.923	1.727- 1.612	46.577	n.d	0.350 (51.6)	n.d	0.343 (51.7)
3	3.894	65.393	3.938	65.385	n.d	n.d	0.044 (26.31)	0.005 (0.81)
4	1.162	23.745	1.166	23.845	n.d	n.d	0.004 (2.4)	0.110 (16.7)

- a) Resolution in HOBS and ¹³C after processing were 0.11 and 0.38 Hz/pt, respectively.
 b) Resolution in the F2 and F1 dimension of the 2D HOBS-HSQC was 0.43 and 0.73 Hz/pt, respectively, after processing.
- c) n.d=not determined; by signal overlap or lack of resolution

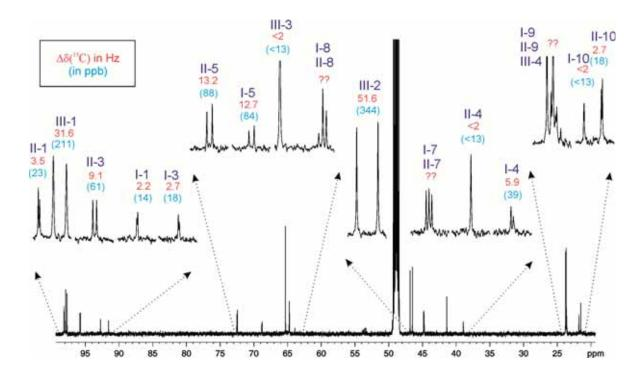


Figure S1: 150.62 MHz 1D ¹³C NMR spectrum of the mixture. Expanded areas shows the chemical shift differences (in Hz and ppb) observed for analog carbons in the mixture of the diastereoisomers Ia/Ib, IIa/IIb and IIIa/IIIb.

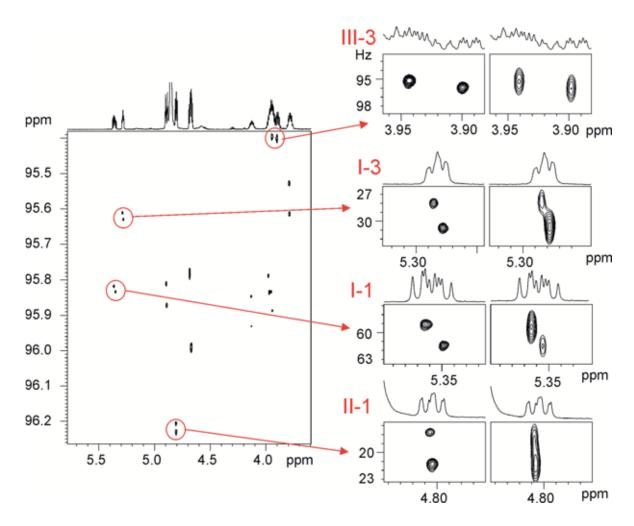


Figure S2: (left) 2D HOBS-HSQC spectrum of the region I acquired with a SW(¹³C)=1 ppm. (right) Comparison of some expanded cross-peaks in HOBS-HSQC spectra acquired with SW(¹³C)=1 and 5 ppm, respectively.

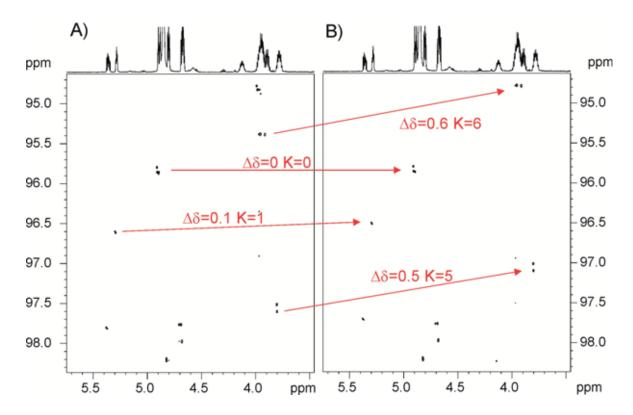


Figure S3: Spectral-aliased HSQC spectra acquired with SW(13 C) of A) 5 ppm and B) 4.9 ppm. The comparison of the observed chemical shift values allows determine the aliasing K factor and the real chemical shift value according to the relationship $\delta(obs)=\delta(real)\pm K*SW(^{13}C)$.

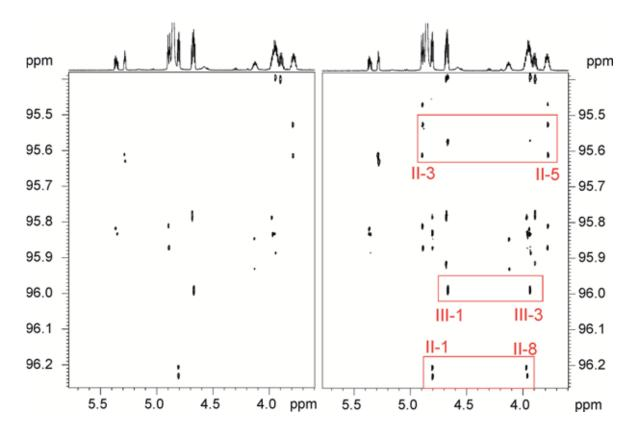


Figure S4: Comparison of spectral-aliased HOBS-HSQC (left) vs HOBS-HSQC-TOCSY (right) spectra of region A acquired with SW(13 C)=1 ppm. Some key correlations are marked for assignment of protons belonging to the same spin system. Experimental parameters as described for spectra in Figure 4.

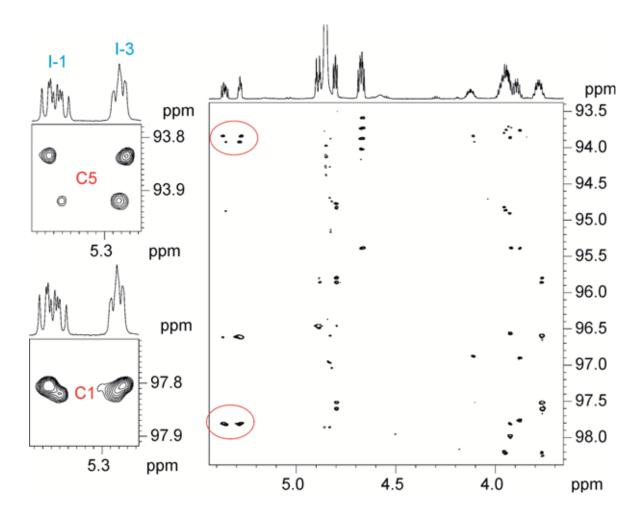


Figure S5: Spectral-aliased 2D ¹H-¹³C HOBS-HSQMBC spectrum acquired with SW(¹³C)=5 ppm. Note the key long-range H3-C1, H1-C5 and H3-C5 correlations in the expansions.

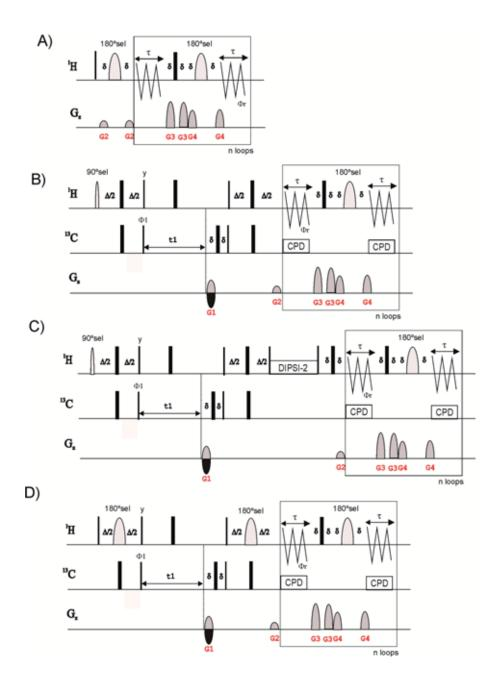


Figure S6: NMR pulse sequences used in this work: A) 1D HOBS; B) 2D 1 H- 13 C HOBS-HSQC; C) 2D 1 H- 13 C HOBS-HSQC-TOCSY; D) 2D 1 H- 13 C HOBS-HSQMBC. Thin and thick bars represent broadband 90° and 180° pulses, respectively, whereas shaped pulses are region-selective 180° pulses. The basic phase cycling is Φ_{1} =x,-x and Φ_{r} =x,-x; all other unlabeled pulses are from the x-axis. Homonuclear decoupling during the acquisition time (AQ) is performed using a refocusing blocks including a pair of hard/selective 180° 1 H pulses applied at intervals of 2τ =AQ/n, where n is the number of loops. Heteronuclear decoupling (CPD) during data collection is applied as shown in the scheme. δ is the duration

of gradients and the recovery delay. The selective 180° ¹H pulse applied at the middle of INEPT periods and during detection have the same shape and duration (p₁₈₀). The INEPT delays are set to $\Delta = 1/2^{*1}J_{\text{CH}}$ in HSQC and HSQC-TOCSY experiment and to $\Delta + \text{p}_{180} = 1/2^{*n}J_{\text{CH}}$ in selHSQMBC experiments. Other details can be found into the experimental section.

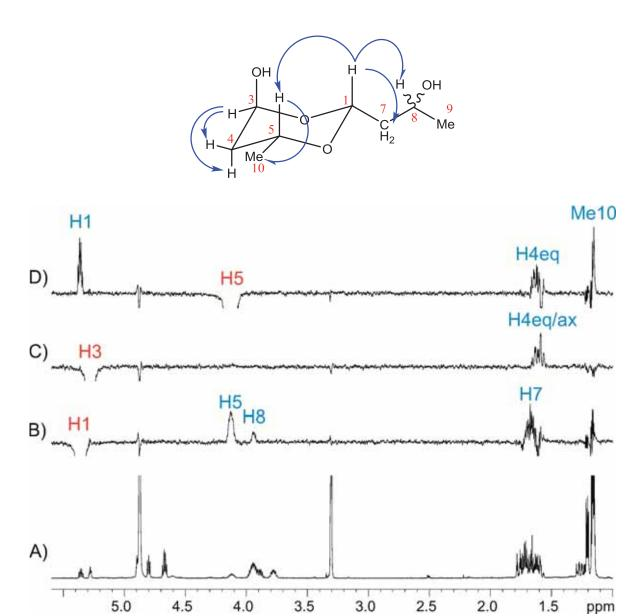


Figure S7: Selective 1D NOESY spectra after selective excitation of some protons belonging to isomers Ia/Ib.

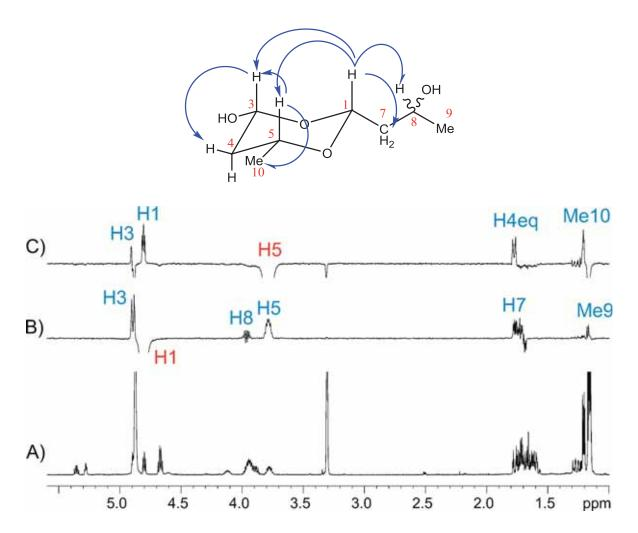


Figure S8: Selective 1D NOESY spectra after selective excitation of some protons belonging to isomers IIa/IIb.

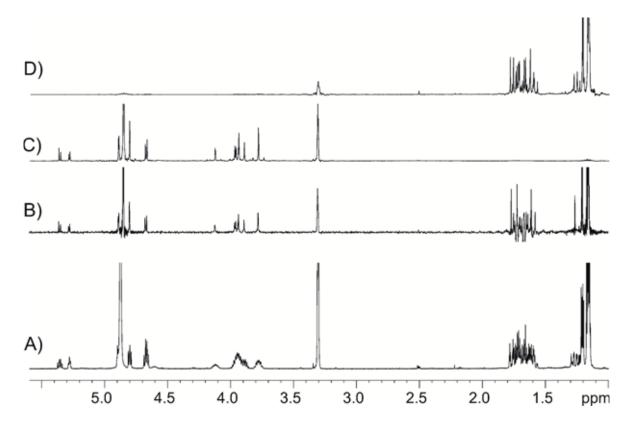


Figure S9: Comparison between the B) PSYCHE (2D acquisition mode using 1 scan per 16 t_1 increments)⁴ and the C-D) individual 1D HOBS experiments (4 scans each one as shown in Figure 2). All spectra were processed without any window function before Fourier transformation. See expanded areas in Figures S10 and S11 for more details.

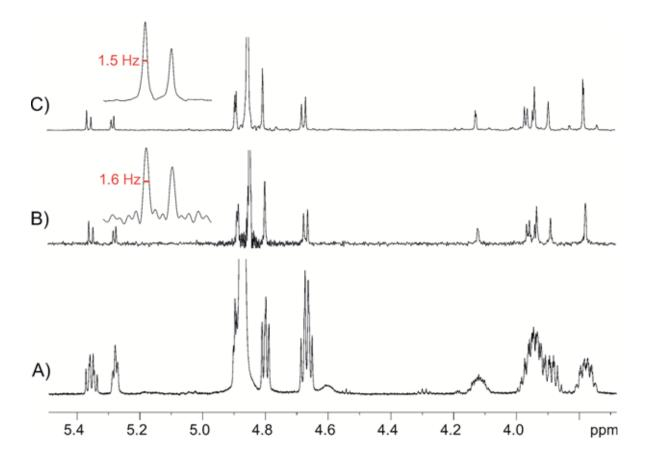


Figure S10: Expanded area between 3.7-5.5 ppm comparing the experimental sensitivity and natural line widths achieved in B) PSYCHE and C) HOBS spectra of Figure S9. Whereas similar spectral quality and experimental line widths (about 1.5-1.6 Hz) were obtained in both experiments, the 1D HOBS spectrum shows an enhanced sensitivity by two orders of magnitude.

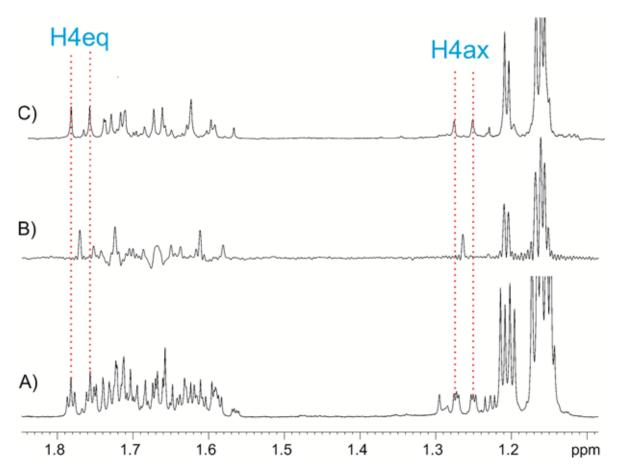


Figure S11: Expanded area between 1.1-1.8 ppm comparing the experimental sensitivity, multiplet simplification and line widths achieved in B) PSYCHE and C) HOBS spectra of Figure S9. As shown in Figure S9 and S10, the 1D HOBS spectrum shows a sensitivity enhancement by two orders of magnitude. Note the partial multiplet simplification of diastereotopic CH₂ protons, exemplified with the H4 protons of isomers IIa/IIb, where the geminal ²J(HH) splitting remains. In addition, also note how the PSYCHE experiment fails to homodecouple all strongly-coupled geminal protons resonating around 1.6-1.8 ppm.

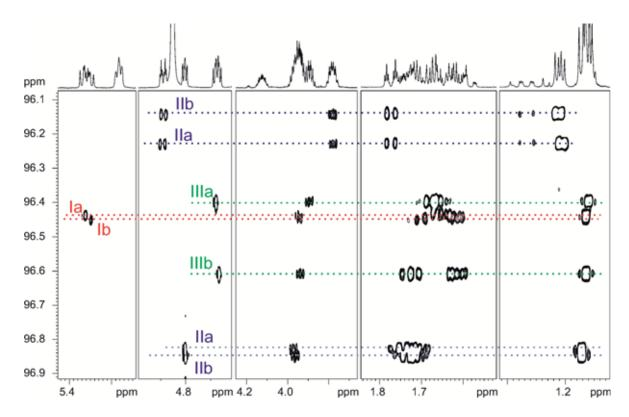


Figure S12: Expansion of the spectral aliased HSQC-TOCSY of Figure 4A. Note how eight different spin systems can be distinguished and assigned.

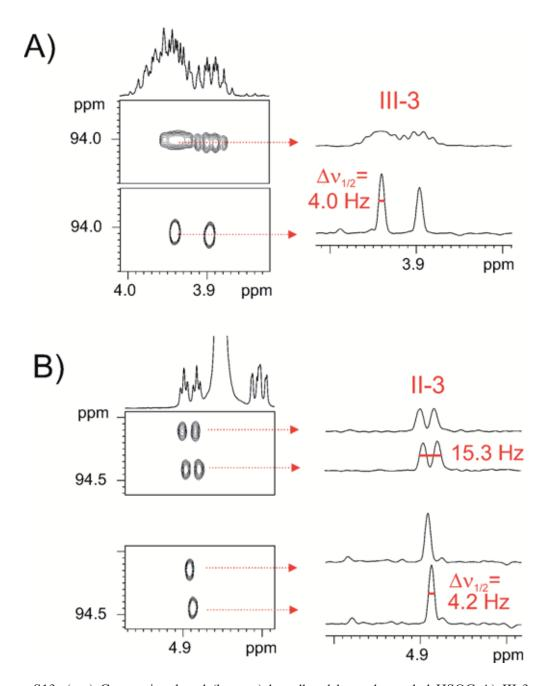


Figure S13: (top) Conventional and (bottom) broadband homodecoupled HSQC A) III-3 and B) II-3 cross peaks. 1D slices on the right allow to compare the relative sensitivity, the multiplet simplification and the experimental line widths achieved in both experiments.

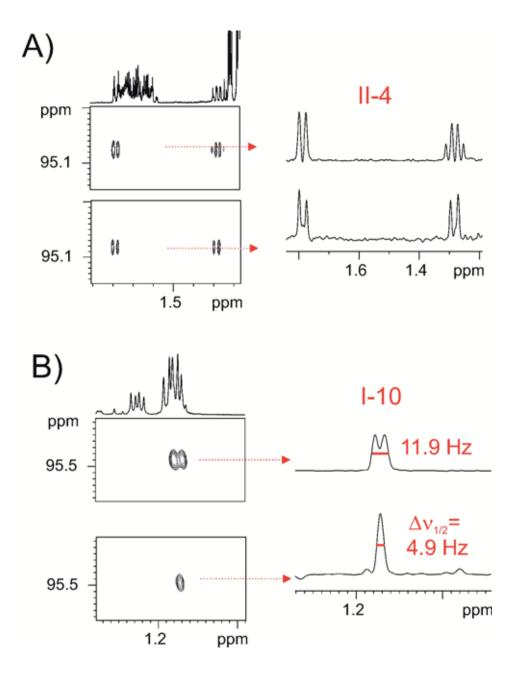


Figure S14: (top) Conventional and (bottom) broadband homodecoupled HSQC A) II-4 (diastereotopic CH_2) and B) I-10 (CH_3) cross peaks. 1D slices on the right allow to compare the relative sensitivity, the multiplet simplification and the experimental line widths achieved in both experiments.